

STRATEGIES FOR STRATIFIED CARTILAGE BIOPRINTING

Wouter Schuurman

Strategies for stratified cartilage bioprinting
Wouter Schuurman
PhD thesis, Utrecht University, the Netherlands

ISBN: 978-94-6182-129-4

Layout & printing: Off Page, www.offpage.nl

Cover design: Vincent Bos, Nymus3D

Copyright © 2012 W. Schuurman, All rights reserved. No part of
this thesis may be reproduced or transmitted in any form or by
any means, without the prior permission in writing of the author.

STRATEGIES FOR STRATIFIED CARTILAGE BIOPRINTING

**Strategieën voor het gelaagd bioprinten van kraakbeen
(met een samenvatting in het Nederlands)**

Proefschrift

ter verkrijging van de graad van doctor aan de Universiteit Utrecht,
op gezag van de rector magnificus, prof. dr. G.J. van der Zwaan,
ingevolge het besluit van het college voor promoties
in het openbaar te verdedigen op vrijdag
6 juli 2012 des middags te 4.15 uur

door

Wouter Schuurman
geboren op 20 september 1979 te 's Gravenhage

Promotoren: Prof. dr. P.R. van Weeren
Prof. dr. W.J.A. Dhert

Co-promotoren: Dr. ir. J. Malda
Dr. T.J Klein

Dit proefschrift werd (mede) mogelijk gemaakt
met financiële steun van

Anna Fonds
ChipSoft BV
Fonds Beter voor Gewrichten
Hippo Zorg
J.E. Jurriaanse Stichting
MRI centrum
Nederlandse Vereniging voor Biomaterialen en Tissue Engineering
Nederlandse Vereniging voor Matrix Biologie
Reumafonds

TABLE OF CONTENTS

INTRODUCTION	9
Chapter 1 General background and outline of the thesis	11
ZONAL DIFFERENCES IN VITRO AND THE ROLE OF IMPOSED ORGANIZATION	21
Chapter 2 Zonal chondrocyte subpopulations reacquire zone-specific characteristics during in vitro redifferentiation	23
Chapter 3 Layered Zonal Chondrocyte Pellets in Tissue Engineered Constructs Result in Cartilaginous Tissue Formation without Retainment of Zonal Characteristics	39
INSIGHT IN GROWTH MECHANISMS	57
Chapter 4 Mathematical modelling of tissue formation in chondrocyte filter cultures	59
THE DEVELOPMENT OF THE CONCEPT OF BIOPRINTING	81
Chapter 5 Biofabrication of osteochondral tissue equivalents by printing topologically defined, cell-laden hydrogel scaffolds	83
Chapter 6 Hyaluronic acid and Dextran based Semi-IPN Hydrogels as Biomaterials for Bioprinting	107
Chapter 7 Printable Photopolymerizable Thermosensitive p(HPMA-lactate)-PEG Hydrogel for Tissue Engineering	127
Chapter 8 Thermoresponsive Gelatin-Methacrylamide Hydrogels for Bioprinting of Cartilaginous Tissue Engineering Constructs	151
Chapter 9 Bioprinting of hybrid tissue constructs with tailorable mechanical properties	167
SYNOPSIS, REVIEW AND DISCUSSION	181
Chapter 10 Cartilage regeneration using zonal chondrocyte subpopulations: a promising approach or an overcomplicated strategy?	187
NEDERLANDSE SAMENVATTING	201
DANKWOORD	207
CURRICULUM VITAE AND LIST OF PUBLICATIONS	211



THIS THESIS IS BASED ON THE FOLLOWING PUBLICATIONS

- W. Schuurman, D. Gawlitta, T.J. Klein, W. ten Hoope, M.H.P van Rijen, W.J.A. Dhert, P.R. van Weeren, and J. Malda
Zonal Chondrocyte Subpopulations Reacquire Zone-specific Characteristics During *in vitro* Redifferentiation.
American Journal of Sports Medicine 2009
- W. Schuurman, E.B. Harimulyo, D. Gawlitta, T.B.F. Woodfield, W.J.A. Dhert, P.R. van Weeren, and J. Malda
Zonal Assembly of Chondrocyte Pellets in Tissue Engineered Constructs Results in Cartilaginous Tissue Formation without Retainment of Zonal Characteristics
Submitted for publication
- C.J. Catt, W. Schuurman, B. Sengers, C.P. Please, W.J.A. Dhert and J. Malda
Mathematical modelling of tissue formation in chondrocyte filter cultures.
European Cells and Materials 2011.
- W. Schuurman, N.E. Fedorovich, H.M. Wijnberg, H.J. Prins, P.R. van Weeren, J. Malda, J. Alblas, W.J.A. Dhert.
Biofabrication of Osteochondral Tissue Equivalents by Printing Topologically Defined, Cell-laden Hydrogel Scaffolds
Tissue Engineering part C 2012
- L. Pescosolido, W. Schuurman, J. Malda, P. Matricardi, F. Alhaique, T. Coviello, P.R. van Weeren, W.J.A. Dhert, W.E. Hennink, T. Vermonden.
Hyaluronic Acid and Dextran-Based Semi-IPN Hydrogels as Biomaterials for Bioprinting
Biomacromolecules 2011
- R. Censi, W. Schuurman, J. Malda, G. di Dato, P.E. Burgisser, W.J.A. Dhert, C.F. van Nostrum, P. di Martino, T. Vermonden, W.E. Hennink.
Printable Photopolymerizable Thermosensitive p(HPMA-lactate)-PEG Hydrogel as Scaffold for Tissue Engineering
Advanced functional materials 2011
- W. Schuurman, P. Levett, M.W. Pot, P.R. van Weeren, W.J.A. Dhert, D.M. Hutmacher, F. Melchels, T.J. Klein, and J. Malda,
Thermoresponsive Gelatin-Methacrylamide Hydrogels for Bioprinting of Cartilaginous Tissue Engineering Constructs
In preparation
- W. Schuurman, V. Khristov, M.W. Pot, P.R. van Weeren, W.J.A. Dhert, and J. Malda.
Bioprinting of Hybrid Tissue Constructs with Tailorable Mechanical Properties.
Biofabrication 2011
- W. Schuurman, T.J. Klein, W.J.A. Dhert, P.R. van Weeren, D.W. Hutmacher, and J. Malda
Cartilage regeneration using zonal chondrocyte subpopulations: a promising approach or an overcomplicated strategy?
Submitted for publication

INTRODUCTION





chapter **ONE**

GENERAL BACKGROUND
AND OUTLINE OF THE THESIS



CARTILAGE DEFECTS: A COMMON CLINICAL PROBLEM

Every day, patients seek medical attention for symptoms caused by articular cartilage defects. These defects are frequently observed in young and otherwise healthy patients with an active lifestyle, who can suffer from pain and to a certain extent are limited in their activities of daily life (1). Apart from the impact on quality of life, these patients also are a considerable economic burden to society, both due to absenteeism and to medical consumption (2). Therapies, such as autologous chondrocyte implantation (ACI) (3) and microfracturing (MF) (4) are well-established surgical procedures for treatment of cartilage defects and are currently regarded as state-of-the-art (5). The outcome of these treatments is satisfactory in terms of patient pain scores and short- and medium-term functional outcomes, with the regenerative therapy of ACI having slightly better results than microfracture (3). However, ACI is costly and both therapies do not always lead to functional restoration of the tissue.

CARTILAGE: INHOMOGENEOUS TISSUE

Articular cartilage (Figure 1) is the tissue in joints that covers the end of the bones, providing shock absorption and ensuring smooth motion. It is avascular, aneural, and has low cell content. Once damaged, cartilage has limited intrinsic healing capacity and a cartilage defect ultimately can lead to the early development of osteoarthritis (6). The outer appearance of articular cartilage suggests a homogeneous composition, but in fact native cartilage tissue differs both topographically (7, 8) and depth-wise (9, 10) in architecture and in distribution of the extracellular matrix components, which provide articular cartilage with its biomechanical properties (11) and the heterogeneity in structure and function hence permits a differentiated response of the tissue to the also inhomogeneous loading patterns in joints.

Cartilage can be divided into three zones (Figure 2): the superficial (the top 10–20% of the cartilage), middle (the next 40–60%), and deep (the bottom 30–40%) zone. Cell morphology and cell size, amount of glycosaminoglycans (GAGs) (9), and biosynthetic activity (12) are different between these zones. Furthermore, alignment of the collagen fibers varies between zones, being parallel to the surface in the superficial zone, randomly orientated in the middle zone, and perpendicular to the articular surface in the deep zone (13). Native articular cartilage has depth-related differences in a number of proteins that are secreted: in the superficial zone, clusterin (14) and proteoglycan-4 (PRG4) (15) (also known as superficial zone protein (SZP)) are more prominent, while in the middle zone the concentration of cartilage intermediate layer protein (CILP) (16, 17) is highest; cartilage oligomeric matrix protein (COMP) (18, 19) is mainly seen in the middle and deep zone. Not all specific functional roles of these matrix proteins have been clarified thus far.

We hypothesize that the lack of zonal organisation is the reason that current therapies do not always fully restore the functionality of the native tissue, and that, if tissue-engineered cartilage constructs are to be successful, the zonal differences as found in native cartilage should be taken into account (20).

1

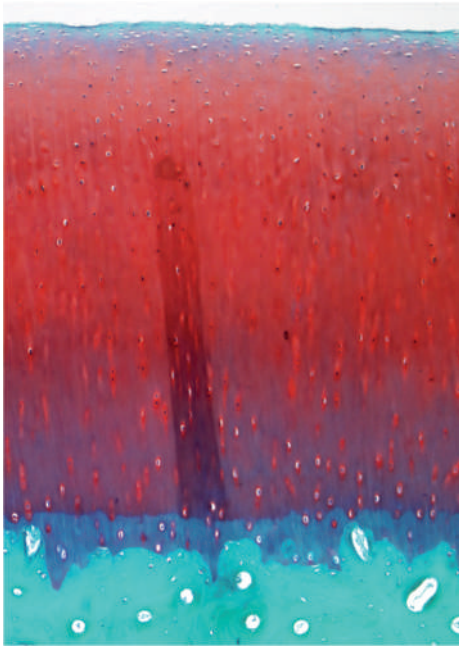


Figure 1. Histology of a cross-section of equine articular cartilage. Glycosamino-glycans are stained red and cell nuclei are stained blue in this safranin O staining. The underlying bone is stained blue. Scale bar represents 500 μm .

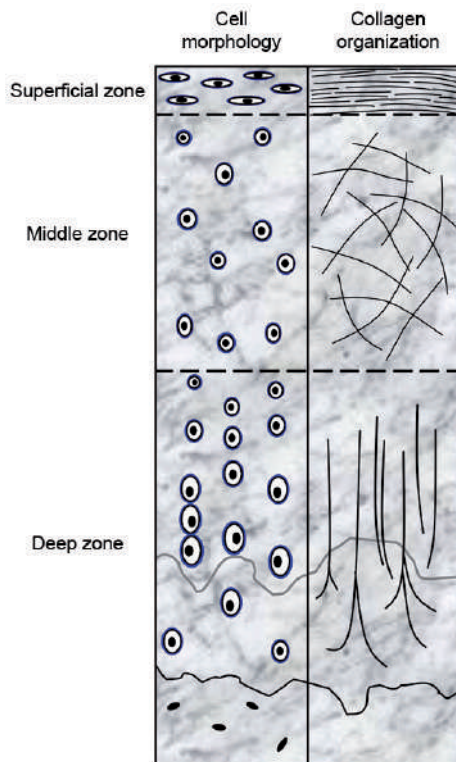


Figure 2. Schematic representation of articular cartilage. Cell morphology and cell density vary between superficial, middle and deep zone (left panel). Alignment of the collagen fibers is parallel to the surface in the superficial zone, randomly orientated in the middle zone, and perpendicular to the articular surface in the deep zone (right panel). Figure adapted from Hayes et al (37).

ZONAL CHONDROCYTE SUBPOPULATIONS FOR CARTILAGE REGENERATION

Differences between cartilage cells (chondrocytes) from the superficial, middle and deep zone of the tissue can be studied after isolation of the cells from the tissue of the respective zones (21). Typically, only a limited amount of chondrocytes is available, and multiplication of the cells is often needed. During expansion, chondrocytes will undergo dedifferentiation and hence lose both their chondrogenic and typical zonal phenotypic characteristics (22). With the use of growth factors basic fibroblast growth factor (basic FGF) and transforming growth factor- β (TGF- β) during expansion and redifferentiation, chondrocytes can reacquire, at least part of, their zonal characteristics (23). It has been shown that in three-dimensional culture systems chondrocytes from the deep zone produce more GAGs *in vitro* than those from the superficial zone (21, 24-26), and that zonal cells will start producing (part of) their specific proteins.

Combining zonal chondrocytes in a stratified manner using hydrogels can result in constructs with a higher shear and compressive strength (27), and a deep layer in which more GAGs (27, 28) and collagen (27) are produced as compared to the superficial layer. Values for collagen, GAG and mechanical properties were found to be comparable to, or higher than, for constructs containing populations of chondrocytes harvested from full thickness cartilage (27, 29). These data seem very promising, but it should be noted that for these studies primary chondrocytes from immature donors were used, which is not compatible with clinical application. The behaviour of expanded, redifferentiated, mature zonal cells in stratified cultures, which would be more relevant, has not yet been studied.

BIOPRINTING: THE TECHNICAL SOLUTION FOR A ZONAL APPROACH?

As mentioned before, there is a need for therapies that deliver prolonged functionality. This could possibly be provided by modern regenerative medicine techniques, which can potentially more accurately replicate the characteristics of native cartilage. Regenerative medicine aims to improve, restore or replace damaged tissues or organs using a combination of cells, materials and/or growth factors. A wide spectrum of approaches is available, ranging from cell-free approaches in which cells are attached to the affected site, to complex cell-laden approaches which use multiple cell types and biomaterials.

A recent regenerative medicine innovation is the technology of bioprinting (Figure 3). Cells, biomaterials, or both (30) are deposited layer by layer to form a porous, 3-dimensional construct with detailed specific spatial cellular architecture (30-34). Since the process of bioprinting is automated, construct properties such as size, shape and porosity, can easily be adjusted and tailored to specific demands. A highly reproducible architecture can be achieved, which is particularly interesting for the fabrication of multiple-material or multiple-cell type constructs. These characteristics may make bioprinting well suited for the fabrication of zonal constructs, allowing stratification of multiple types of cells and materials.

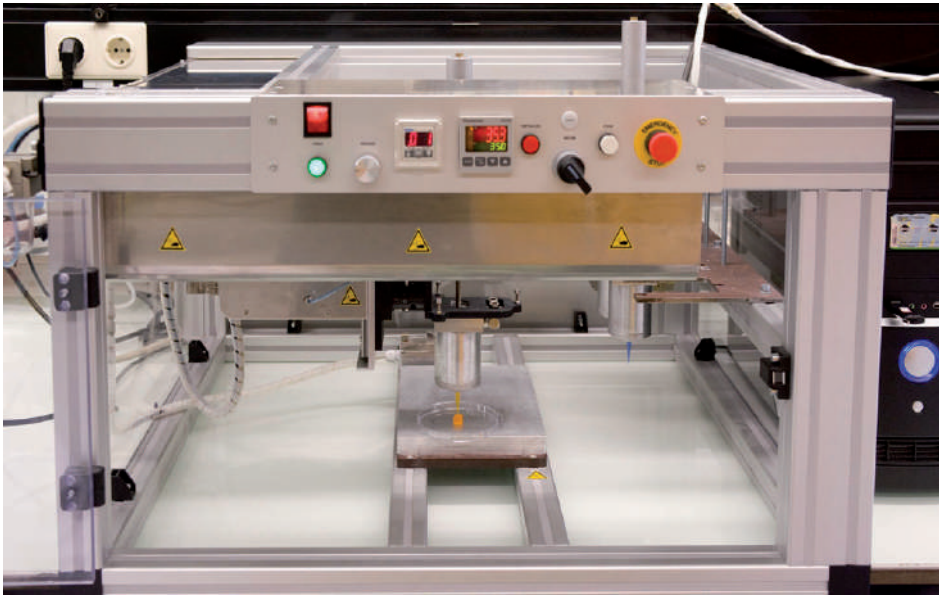


Figure 3. A bioprinter in the process of manufacturing a hydrogel construct. Photo: ZorginBeeld / Frank Muller.

However, although the approach is appealing and is potentially very promising, the technique is not without challenges. One of the most important items is the choice of biomaterial. Biomaterials for cell printing must promote cell survival and cell differentiation, and need to meet very specific requirements with regard to viscosity and gelling speed. These requirements limit the number of candidate materials that can be applied in bioprinting approaches (35, 36), with hydrogels being the most viable option. However, hydrogels themselves have their own limitations with respect to the fabrication of constructs with adequate mechanical characteristics and of clinically relevant size.

OUTLINE OF THE THESIS

This thesis aimed at further developing and investigating the concept of zonal organization of constructs for the treatment of cartilage and osteochondral defects. Zonal stratification is hypothesized to be a promising regenerative approach for improving long-term functionality of articular cartilage. To explore the potentiality of the zonal approach, both fundamental investigations concerning the behaviour of zonal cell populations and more applied experiments using a state-of-the-art bioprinting facility for construct manufacturing were carried out.

As referred to above, in earlier efforts zonal cell combinations have been used to replicate cartilaginous tissues, yielding neo-cartilage with depth-dependent differences. However, due to the nature of the cells – primary, and from an immature donor – these models cannot be translated to a clinical application. Therefore, in **chapter 2**, we explore whether mature, expanded zonal chondrocytes would retain or reacquire zonal characteristics when cultured

in either pellet culture or in alginate beads. In **chapter 3**, the influence of stratification of zonal chondrocyte pellets in a polymer scaffold on chondrogenesis and zonal characteristics is investigated. In **chapter 4**, experimental and mathematical methods are used to develop a model that can describe and predict *in vitro* tissue growth. Mathematical modeling can not only provide insight in the underlying mechanisms of growth, it can also be of great value for the design and fine-tuning of culture methods, as it permits large-scale *in silico* testing of culture circumstances.

In **chapter 5**, the use of a bioprinting technique, so-called 3-dimensional (3D) fiber deposition, is characterized, and the concept of bioprinting multi-cell type constructs is applied for the production of osteochondral grafts.

Since the applied biomaterial did not have optimal properties for bioprinting, in **chapters 6, 7 and 8**, we describe the use of three alternative thermosensitive and UV-crosslinkable biomaterials for cartilage 3D biofabrication: polyethylene glycol-hydroxypropylmethacrylamide (HPMA), hydroxyethyl-methacrylate-derivatized dextran (DEXHEMA) and gelatin methacrylamide (GelMA). In these chapters, the materials are characterized for their mechanical and swelling properties, degradation, biocompatibility and printability.

In **chapter 9**, a novel concept of bioprinting hybrid constructs is introduced by creating multiple-material constructs consisting of a thermoplastic polymer combined with a cell-laden hydrogel. The advantage of this type of constructs is that the mechanical characteristics of the construct can be improved without affecting the environmental conditions for the seeded cells. We investigated the mechanical properties of and cell survival in these hybrid constructs.

Finally, in **chapter 10**, we combine the conclusions from our own findings as documented in this thesis with a critical review of the literature on the use of zonal chondrocyte populations in regenerative approaches, and develop a new perspective on the potential value of this approach. We also present our view on the potential future significance of zonal chondrocyte populations in regenerative approaches for the treatment of cartilage defects.

REFERENCES

1. Minas T, Chondrocyte implantation in the repair of chondral lesions of the knee: economics and quality of life. *Am J Orthop (Belle Mead NJ)*, 1998. **27**(11): p. 739-44.
2. Lindahl A, Brittberg M, and Peterson L, Health economics benefits following autologous chondrocyte transplantation for patients with focal chondral lesions of the knee. *Knee Surg Sports Traumatol Arthrosc*, 2001. **9**(6): p. 358-63.
3. Saris DB, Vanlauwe J, Victor J, Almqvist KF, Verdonk R, Bellemans J, and Luyten FP, Treatment of symptomatic cartilage defects of the knee: characterized chondrocyte implantation results in better clinical outcome at 36 months in a randomized trial compared to microfracture. *Am J Sports Med*, 2009. **37 Suppl 1**: p. 105-195.
4. Hangody L, Vasarhelyi G, Hangody LR, Sukosd Z, Tibay G, Bartha L, and Bodo G, Autologous osteochondral grafting--technique and long-term results. *Injury*, 2008. **39 Suppl 1**: p. S32-9.
5. Bentley G and Minas T, Treating joint damage in young people. *Bmj*, 2000. **320**(7249): p. 1585-8.
6. Prakash D and Learmonth D, Natural progression of osteo-chondral defect in the femoral condyle. *Knee*, 2002. **9**(1): p. 7-10.
7. Brama PA, Tekoppele JM, Bank RA, Karssenbergh D, Barneveld A, and van Weeren PR, Topographical mapping of biochemical properties of articular cartilage in the equine fetlock joint. *Equine Vet J*, 2000. **32**(1): p. 19-26.
8. van der Harst MR, Brama PA, van de Lest CH, Kiers GH, DeGroot J, and van Weeren PR, An integral biochemical analysis of the main constituents of articular cartilage, subchondral and trabecular bone. *Osteoarthritis Cartilage*, 2004. **12**(9): p. 752-61.

9. Buckwalter JA and Mankin HJ, Articular cartilage: tissue design and chondrocyte-matrix interactions. Instr Course Lect, 1998. **47**: p. 477-86.
10. Schinagl RM, Gurskis D, Chen AC, and Sah RL, Depth-dependent confined compression modulus of full-thickness bovine articular cartilage. J Orthop Res, 1997. **15**(4): p. 499-506.
11. Benninghoff A, Form und Bau der Gelenkknorpel in Ihren Beziehungen zur Funktion. Z Zellforsch, 1925. **2**: p. 783-862.
12. Wong M, Wuethrich P, Eggli P, and Hunziker E, Zone-specific cell biosynthetic activity in mature bovine articular cartilage: a new method using confocal microscopic stereology and quantitative autoradiography. J Orthop Res, 1996. **14**(3): p. 424-32.
13. Benninghoff A, Form und Bau der Gelenkknorpel in Ihren Beziehungen zur Funktion. Z Zellforsch, 1925. **2**: p. 783-862.
14. Khan IM, Salter DM, Bayliss MT, Thomson BM, and Archer CW, Expression of clusterin in the superficial zone of bovine articular cartilage. Arthritis Rheum, 2001. **44**(8): p. 1795-9.
15. Flannery CR, Hughes CE, Schumacher BL, Tudor D, Aydelotte MB, Kuettner KE, and Caterson B, Articular cartilage superficial zone protein (SZP) is homologous to megakaryocyte stimulating factor precursor and is a multifunctional proteoglycan with potential growth-promoting, cytoprotective, and lubricating properties in cartilage metabolism. Biochem Biophys Res Commun, 1999. **254**(3): p. 535-41.
16. Bernardo BC, Belluoccio D, Rowley L, Little CB, Hansen U, and Bateman JF, Cartilage intermediate layer protein 2 (CILP-2) is expressed in articular and meniscal cartilage and down-regulated in experimental osteoarthritis. J Biol Chem, 2011. **286**(43): p. 37758-67.
17. Lorenzo P, Bayliss MT, and Heinegard D, A novel cartilage protein (CILP) present in the mid-zone of human articular cartilage increases with age. J Biol Chem, 1998. **273**(36): p. 23463-8.
18. DiCesare PE, Morgelin M, Carlson CS, Pasumarti S, and Paulsson M, Cartilage oligomeric matrix protein: isolation and characterization from human articular cartilage. J Orthop Res, 1995. **13**(3): p. 422-8.
19. Murray RC, Smith RK, Henson FM, and Goodship A, The distribution of cartilage oligomeric matrix protein (COMP) in equine carpal articular cartilage and its variation with exercise and cartilage deterioration. Vet J, 2001. **162**(2): p. 121-8.
20. Roberts S, McCall IW, Darby AJ, Menage J, Evans H, Harrison PE, and Richardson JB, Autologous chondrocyte implantation for cartilage repair: monitoring its success by magnetic resonance imaging and histology. Arthritis Res Ther, 2003. **5**(1): p. R60-73.
21. Aydelotte MB, Greenhill RR, and Kuettner KE, Differences between sub-populations of cultured bovine articular chondrocytes. II. Proteoglycan metabolism. Connect Tissue Res, 1988. **18**(3): p. 223-34.
22. Darling EM and Athanasiou KA, Rapid phenotypic changes in passaged articular chondrocyte subpopulations. J Orthop Res, 2005. **23**(2): p. 425-32.
23. Darling EM and Athanasiou KA, Growth factor impact on articular cartilage subpopulations. Cell Tissue Res, 2005. **322**(3): p. 463-73.
24. Hwang NS, Varghese S, Lee HJ, Theprungsirikul P, Canver A, Sharma B, and Elisseeff J, Response of zonal chondrocytes to extracellular matrix-hydrogels. FEBS Lett, 2007. **581**(22): p. 4172-8.
25. Lee DA, Noguchi T, Knight MM, O'Donnell L, Bentley G, and Bader DL, Response of chondrocyte subpopulations cultured within unloaded and loaded agarose. J Orthop Res, 1998. **16**(6): p. 726-33.
26. Cheng C, Conte E, Pleshko-Camacho N, and Hidaka C, Differences in matrix accumulation and hypertrophy in superficial and deep zone chondrocytes are controlled by bone morphogenetic protein. Matrix Biol, 2007. **26**(7): p. 541-53.
27. Sharma B, Williams CG, Kim TK, Sun D, Malik A, Khan M, Leong K, and Elisseeff JH, Designing zonal organization into tissue-engineered cartilage. Tissue Eng, 2007. **13**(2): p. 405-14.
28. Kim TK, Sharma B, Williams CG, Ruffner MA, Malik A, McFarland EG, and Elisseeff JH, Experimental model for cartilage tissue engineering to regenerate the zonal organization of articular cartilage. Osteoarthritis Cartilage, 2003. **11**(9): p. 653-64.
29. Ng KW, Ateshian GA, and Hung CT, Zonal chondrocytes seeded in a layered agarose hydrogel create engineered cartilage with depth-dependent cellular and mechanical inhomogeneity. Tissue Eng Part A, 2009. **15**(9): p. 2315-24.
30. Mironov V, Boland T, Trusk T, Forgacs G, and Markwald RR, Organ printing: computer-aided jet-based 3D tissue engineering. Trends Biotechnol, 2003. **21**(4): p. 157-61.
31. Arcaute K, Mann BK, and Wicker RB, Stereolithography of three-dimensional bioactive poly(ethylene glycol) constructs with encapsulated cells. Ann Biomed Eng, 2006. **34**(9): p. 1429-41.
32. Cohen DL, Malone E, Lipson H, and Bonassar LJ, Direct freeform fabrication of seeded hydrogels in arbitrary geometries. Tissue Eng, 2006. **12**(5): p. 1325-35.
33. Lee W, Debasitis JC, Lee VK, Lee JH, Fischer K, Edminster K, Park JK, and Yoo SS, Multi-layered culture of human skin fibroblasts and keratinocytes through three-dimensional freeform fabrication. Biomaterials, 2009. **30**(8): p. 1587-95.
34. Ovsianikov A, Gruene M, Pflaum M, Koch L, Maiorana F, Wilhelmi M, Haverich A, and Chichkov B, Laser printing of cells into 3D scaffolds. Biofabrication, 2010. **2**(1): p. 014104.
35. Fedorovich NE, De Wijn JR, Verbout AJ, Alblas J, and Dhert WJ, Three-dimensional fiber deposition of cell-

- laden, viable, patterned constructs for bone tissue printing. *Tissue Eng Part A*, 2008. **14**(1): p. 127-33.
36. Khalil S and Sun W, Bioprinting endothelial cells with alginate for 3D tissue constructs. *J Biomech Eng*, 2009. **131**(11): p. 111002.
37. Hayes AJ, Hall A, Brown L, Tubo R, and Caterson B, Macromolecular organization and in vitro growth characteristics of scaffold-free neocartilage grafts. *J Histochem Cytochem*, 2007. **55**(8): p. 853-66.

*ZONAL DIFFERENCES
IN VITRO AND THE ROLE
OF IMPOSED ORGANIZATION*





chapter **TWO**

ZONAL CHONDROCYTE SUBPOPULATIONS REACQUIRE ZONE-SPECIFIC CHARACTERISTICS DURING IN VITRO REDIFFERENTIATION

Wouter Schuurman, Debby Gawlitta, Travis J. Klein, Werner ten Hoope,
Mattie H. P. van Rijen, Wouter J. A. Dhert, P. René van Weeren, Jos Malda

ABSTRACT

Background: If chondrocytes from the superficial, middle and deep zones of articular cartilage zones could maintain or regain their characteristic properties during in vitro culture, it would be feasible to create constructs comprising these distinctive zones.

Hypothesis: Zone-specific characteristics of zonal cell populations will disappear during 2-dimensional expansion, but would reappear again after 3-dimensional redifferentiation, independent of the culture technique used (alginate beads versus pellet culture).

Study design: Controlled laboratory study.

Methods: Equine articular chondrocytes from the three zones were expanded in monolayer culture (8 donors) and subsequently redifferentiated in pellet and alginate bead cultures for up to 4 weeks. Glycosaminoglycans and DNA were quantified, along with immunohistochemical assessment of the expression of various zonal markers, including cartilage oligomeric protein (marking cells from the deeper zones), and clusterin (specifically expressed by superficial chondrocytes).

Results: Cell yield varied between zones, but proliferation rates did not show significant differences. Expression of all evaluated zonal markers was lost during expansion. Compared to alginate bead cultures, pellet cultures showed a higher amount of glycosaminoglycans produced per DNA after redifferentiation. In contrast to cells in pellet cultures, cells in alginate beads regained zonal differences, as evidenced by zone-specific reappearance of COMP and clusterin, as well as significantly higher glycosaminoglycan production by cells from the deep compared to the superficial zone.

Conclusions: Chondrocytes isolated from the three zones of equine cartilage can restore their zone-specific matrix expression when cultured in alginate after in vitro expansion.

Clinical relevance: Appreciation of the zonal differences can lead to important advances in cartilage tissue engineering. Findings support the use of hydrogels such as alginate for engineering zonal cartilage constructs.

Key Terms: cartilage, pellet culture, alginate culture, zonal chondrocytes.

INTRODUCTION

Articular cartilage is a highly organized tissue that under normal circumstances provides a low-friction, wear-resistant, and load-bearing surface for efficient joint movement. The tissue has limited intrinsic healing capacity; therefore, cartilage defects still remain a challenge for orthopedic surgeons world-wide. Regenerative approaches encompassing expanded autologous cells, such as autologous chondrocyte implantation (ACI) are well-established surgical procedures for treatment of cartilage defects (3;32). Although short- and medium-term functional outcomes regarding this procedure are satisfying and are superior to conservative techniques, such as microfracture (35), the neo-tissue that is formed lacks the structure and composition of the original cartilage. The native tissue is characterized by zonal differences in architecture and in distribution of the extracellular matrix components, which provide articular cartilage with its unique biomechanical properties, combining great compressive stiffness with a high degree of resilience (20). The lack of this zonal organization makes the repair tissue that is formed of insufficient functional quality (34;35) and there is growing insight that, if tissue-engineered cartilage constructs are to be successful, they must take into account the zonal differences found in native cartilage.

There are multiple differences between the superficial, middle and deep zones in articular cartilage, including variations in cell density and shape, biosynthetic activity, extracellular matrix composition and collagen fibril organization. Cell density is highest in the superficial zone (38;40;43). Furthermore, this zone has the lowest biosynthetic activity (43) and contains the lowest amount of glycosaminoglycans (GAG) (6) whilst it contains the highest amount of collagen type II (29). Collagen type I (18;19) and clusterin (22;30;44), are mainly present in the superficial zone, whereas cartilage oligomeric protein (COMP) (12;31), cartilage intermediate layer protein (CILP) (26;28) and collagen types IX (18) and X (18;19) are most abundant in the middle and deeper zones. These differences are thought to be essential for optimal functioning of the tissue and hence should be restored as much as possible in any construct that aims at replacing the native cartilage. For example, the lubricant molecule proteoglycan-4 (PRG-4) or lubricin (25;36) is secreted by the chondrocytes in the superficial zone. It is questionable if the low friction characteristics of the damaged cartilage could be restored using newly-synthesized tissue that lacks PRG-4. However, the presence of PRG-4 in the deeper zones of grafts might hamper integration with the surrounding tissue (14).

Constructs can closely mimic the characteristics of native cartilage by using cells of different zones of cartilage (7;19;23;24;37;41). If such constructs are to be used in a clinical setting, expansion of the cells is required. During expansion, chondrocytes typically acquire a fibroblast-like appearance and lose their chondrogenic phenotype during a process called dedifferentiation (4). Dedifferentiation is typically characterized by a shift in expression of matrix molecules from collagen type II to collagen type I and aggrecan to versican (4;9). In addition, gene expression of zonal markers, such as PRG-4 from superficial chondrocytes, is lost over the first few monolayer passages (10). In 3-dimensional culture, non-expanded chondrocyte populations derived from different zones of the cartilage show differences, such as zone-specific intensity of safranin-O and collagen type II staining (23) and zone-specific response to loading (40). In our opinion, it is crucial that cells maintain or regain their zonal characteristics after in vitro expansion.

It is still unclear if the inherent differences in protein expression and proteoglycan expression between zonal cell populations persist during expansion or, if not, whether these differences can be re-induced during in vitro culture. Therefore, we investigated zone-related differences between chondrocytes isolated from the superficial, middle and deep zones, during in vitro expansion and subsequent redifferentiation in both alginate bead and pellet cultures. We hypothesized that zone-specific characteristics of the cell populations would disappear during 2-dimensional expansion, but would reappear again after 3-dimensional redifferentiation, independent of the culture technique (alginate beads versus pellet culture) used. We elected to use equine chondrocytes because the horse model is gaining increasing attention for evaluation of potential orthopedic procedures (2;17;39).

MATERIALS AND METHODS

Tissue harvest and cell isolation

Full thickness healthy articular cartilage was obtained from the femoropatellar joints of fresh equine cadavers (n=8, age 6-17 years) under aseptic conditions. Adult equine chondrocytes were separately isolated from the superficial, middle, and deep zone tissue as previously described (1;37). Samples for histology were taken to confirm the correct separation of the zones. After overnight digestion using 0.15% type II collagenase (Worthington Biochemical, USA) at 37°C, the cell suspension was filtered (100 µm cell strainer) and washed three times in phosphate-buffered saline (PBS) (Invitrogen, USA). Cells were then resuspended in expansion medium (DMEM (Invitrogen, USA) supplemented with 10% Fetal Bovine Serum (FBS) (Biowhittaker, USA), 100 units/mL penicillin and 100 µg/mL streptomycin (Invitrogen, USA), and 10 ng/mL FGF-2 (R&D Systems, USA)) and counted using a hemacytometer.

Cell culture

Chondrocytes from the three zones were expanded for 10 days in monolayer cultures (5000 cells/cm²) in expansion medium. For evaluation of proliferation, the isolated cells were seeded in 6-well plates and total DNA (Quant-iT PicoGreen dsDNA kit (Molecular Probes, Invitrogen, USA)) was measured over time. Following expansion, cells were redifferentiated in alginate beads, as well as pellet cultures. For alginate bead cultures, a 2% alginate solution (Keltone HVCR, ISP, USA) containing 1.0×10^7 cells/mL was dripped into 102 mM calcium chloride solution using a 23G needle. Alginate beads were cultured in differentiation medium (DMEM supplemented with 0.2 mM ascorbic acid 2-phosphate (Sigma-Aldrich, USA), 0.5% human serum albumin (SeraCare Life Sciences, USA), 1x ITS-X (Invitrogen, USA), 100 units/mL penicillin and 100 µg/mL streptomycin and 5 ng/mL TGF-β2 (R&D Systems, USA)) for up to 4 weeks. For pellet cultures, 1 ml of differentiation medium containing 0.5×10^6 cells was centrifuged at 1500 rpm (415 x g) for 5 minutes. The resulting pellets were cultured in differentiation medium for up to 4 weeks. Medium was replaced every 2-3 days. Samples for histology and biochemical assays were taken weekly and cytopins for immunohistochemistry were made of freshly isolated, expanded and alginate redifferentiated chondrocytes.

Histology

Samples were fixed in formalin, dehydrated through graded ethanol series, cleared in xylene and embedded in paraffin. Embedded samples were sectioned to yield 5 mm sections. Sections were then stained with safranin-O for proteoglycans and with fast green and hematoxylin for cells. The sections were examined using a light microscope (Olympus BX51, United States).

Immunohistochemistry

Immunohistochemistry was performed to assess expression of various (zonal) markers. Prior to using the antibodies on the equine samples, cross-reactivity of all antibodies was confirmed using native equine, as well as native adult human or bovine articular cartilage. Briefly, samples were embedded in OCT compound (Tissue-Tek, Sakura Finetek, USA) or fixed in formalin and embedded in paraffin as described above, and sectioned to yield 5 μ m thick sections. Cryosections and cytopspins were fixed in formalin for 10 minutes. Subsequently, endogenous peroxidase was blocked using a 0.3% H₂O₂ solution for 10 minutes. Samples for clusterin staining were permeabilized with PBS/ Triton-X (0.2%) for 5 minutes. After blocking with 5% BSA in PBS for 30 minutes, the sections were incubated overnight with the monoclonal clusterin antibody (1:200, G7), a generous gift of Dr. Brendan Murphy, which has been described previously (30). Samples were then incubated for 60 minutes with the biotinylated goat anti-mouse antibody (1:200, GE Health Care, USA) followed by an additional 60-minute incubation period with HRP-conjugated avidin/streptavidin (Beckman Coulter, USA). Samples for COMP, and collagen types I, II, VI and IX staining were washed in PBS/Tween 20 (0.1%) for 5 minutes, blocked with 5% BSA in PBS for 30 minutes and incubated overnight with either anti-COMP (1:50, a kind gift from Anamar Medical AB, Goteborg, Sweden), anti-collagen type I (1:50, I-8H5, Calbiochem, USA), type II (1:100, II-6B3II, Developmental Studies Hybridoma Bank, USA), type VI (1:50, 5C6, Developmental Studies Hybridoma Bank, USA), or type IX (1:50, D1-9, Developmental Studies Hybridoma Bank, USA) antibodies. Samples were then incubated for 60 minutes with the secondary HRP-conjugated goat anti-mouse antibody (1:200, Dako, USA). Staining was visualized using DAB solution (Sigma-Aldrich, USA) for 10 minutes. Counterstaining was performed with hematoxylin. The sections were examined using a light microscope. Isotype controls were performed by using mouse isotype IgG1 monoclonal antibody at concentrations similar to those used for the stainings.

Biochemical assays

Alginate beads and pellets (n=3 for each condition and time point) were harvested. Alginate beads were dissolved using 55 mM sodium citrate/150mM sodium chloride buffer and all samples were digested overnight at 56°C in a solution containing 250 μ g/mL papain (Sigma-Aldrich, USA). Quantification of total DNA was performed by Quant-iT PicoGreen dsDNA kit (Molecular Probes, Invitrogen, USA) using a spectrofluorometer (Biorad, USA). The amount of GAGs was determined spectrophotometrically after reaction with dimethylmethylene blue dye (DMMB, Sigma-Aldrich, USA)(16), pH=3.0 for pellets and pH=1.75 for the alginate cultures (15). Intensity of color change was quantified immediately in a microplate reader (Biorad, USA) by measuring absorbance at 540 and 595 nm. The amount of GAG was calculated using a standard of chondroitin sulphate C (Sigma-Aldrich, USA) and by calculating the ratio of absorbances.

Statistics

Cell yield and proliferation rate are presented as mean \pm standard error of the mean. Differences in cell yield were analyzed by one-way ANOVA and corrected by a Tamhane posthoc test. Proteoglycan content of the alginate beads are presented as mean \pm standard deviation. Statistical differences were assessed by either one-way ANOVA and a Bonferroni posthoc test or a paired Student's t-test. $p < 0.05$ was considered a significant difference.

RESULTS

Zonal differences of native cells

Histologic analysis of osteochondral specimens from which zonal tissue was harvested confirmed the isolation of cartilage of the respective zones (Figure 1). Significant differences between the numbers of cells isolated per gram of tissue were observed. The superficial tissue had the highest yield, whilst the lowest number of cells was isolated from the deep zone (Figure 2).

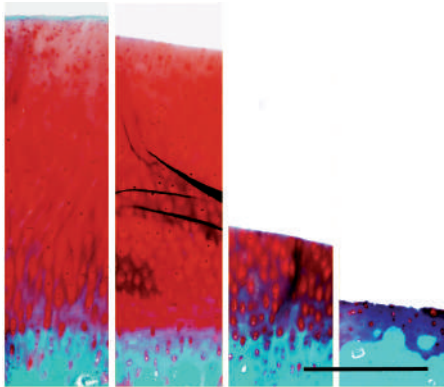


Figure 1. From left to right, safranin O staining of a full thickness osteochondral specimen and specimens from which, respectively, the superficial, middle, and deep zones have been removed, scale bar: 500 μ m.

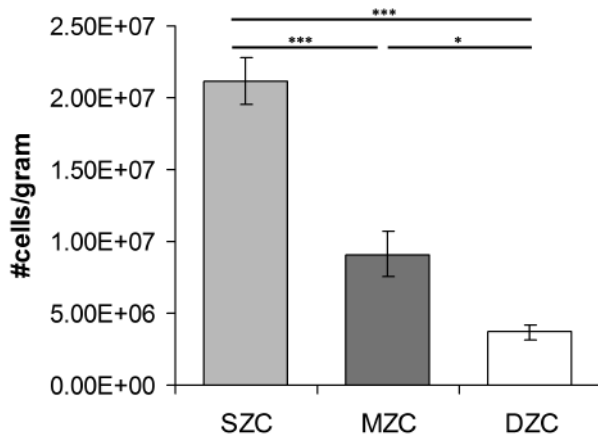


Figure 2. Cell yield per gram tissue for the 3 zones. SZC, superficial zone chondrocytes; MZC, middle zone chondrocytes; DZC, deep zone chondrocytes. Mean values \pm standard error of the mean. * $P < 0.05$; *** $P < 0.001$).

Cross-reactivity of the antibodies was confirmed using native equine cartilage tissue (Figure 3). Subsequently, the presence of collagen type VI was confirmed in cytopins of cells from all zones directly after isolation; collagen types II and IX were present in middle zone and deep zone chondrocytes; and collagen type I could not be detected (Table 1). Staining for clusterin, albeit faint, was limited to cytopins of superficial zone chondrocytes (Figure 4), whereas staining for COMP was observed only in cytopins of the middle and deep zone chondrocytes (Figure 5).

Behavior during expansion

During expansion, cells acquired a fibroblast-like spindle-shape, regardless of the zonal origin. Further, no significant differences between the proliferation rates of the zonal cells in expansion medium were observed during the first passage (4-4.5 population doublings; Figure 6). For all immunohistochemical markers examined (except collagen type I), staining decreased after 2-dimensional expansion, irrespective of the zone of origin (Table 1).

In pellet cultures, the amount of total GAG (Figure 7A), as well as GAG produced per cell was similar for the cultures derived from the cells of the superficial, middle and deep zones at any time point investigated (Figure 7B). In contrast, for chondrocytes cultured in alginate beads, significant differences among the zonal cultures were observed (Figure 7C). The GAG content per DNA was significantly higher after 7, 14 and 21 days ($p=0.047$, $p=0.019$, $p=0.029$, respectively) in beads containing deep zone chondrocytes compared to those with superficial zone chondrocytes. Furthermore, at 2 weeks, the amount of GAG per DNA was also significantly higher ($p=0.019$) in beads with middle zone chondrocytes compared to beads from the

Table 1. Staining intensity for clusterin, collagen types, cartilage oligomeric protein in cytopins of freshly isolated, expanded, and alginate cultured cells^a.

	Zone	P0	P1	t = 7	t = 28
Clusterin	Superficial	+	-	+	++
	Middle	-	-	+	+
	Deep	-	-	+	+
Collagen type I	Superficial	-	+	++	++
	Middle	-	+	++	++
	Deep	-	+	++	++
Collagen type II	Superficial	-	-	+	++
	Middle	+	+/-	+	++
	Deep	+	+/-	+	++
Collagen type VI	Superficial	+	+/-	+	++
	Middle	+	+/-	+	++
	Deep	+	+/-	+	++
Collagen type IX	Superficial	-	-	+	++
	Middle	+	-	+	++
	Deep	+	-	+	++
Cartilage oligomeric protein	Superficial	-	-	-	-
	Middle	+/-	-	+	++
	Deep	+	-	+	++

^aStaining intensity: -, none; +/-, weak; +, moderate; ++, strong. Cells: P0, freshly isolated; P1, expanded; t = 7, cultured for 7 days; t = 28, cultured for 28 days.

superficial zone. Nevertheless, the total amount of GAG per DNA in alginate was lower than that in pellets.

With respect to the immunohistochemical markers, their positive staining gradually re-appeared with redifferentiation (Table 1). Staining for collagen types II, VI and IX became positive after 7 days, and the intensity increased with culture time both in pellet and alginate cultures from all zones. In addition, the zonal differences, as observed directly after isolation of the cells, reappeared in the alginate cultures. Zone-specific expression patterns of COMP and clusterin resembled those in the native zones. Staining for clusterin was observed in all cultures after 7 days and increased up to day 28. At that time point, staining was most distinct in superficial zone alginate cultures, where it stained clusters of cells (Figure 4). Staining for COMP also increased with culture time but was observed only in cultures derived from the deep and middle zones (Figure 5).

In contrast to the alginate cultures, in the pellet cultures demonstrated no zonal differences. Pellets stained positive for both clusterin and COMP (Figure 8), regardless of the zonal origin of the chondrocytes. The intensity of staining for clusterin varied between donors, whereas staining for COMP was most pronounced in the outer periphery of the pellets.

DISCUSSION

In this study we investigated whether inherent differences between chondrocytes derived from the superficial zone, middle zone and deep zone persist or can be re-induced during expansion and redifferentiation using 2 different 3-dimensional culture modalities.

We did not detect significant differences in proliferation of the cells during 2-dimensional culture in our expansion medium. This corresponds with previous findings using mature chondrocytes (38), whilst for immature cartilage differences in proliferation have been observed (8;23;37). These contrasting results may be related to the age difference, but donor variation and differences in medium composition may also have played a role. For example, it

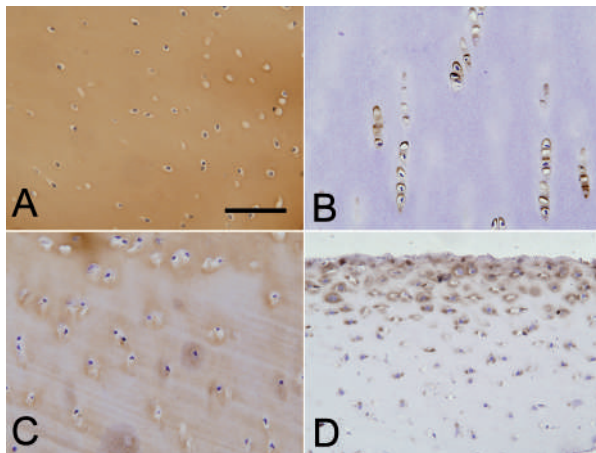


Figure 3. Cross-reactivity of antibodies against chick collagen type II (A), human collagen type VI (B), human cartilage oligomeric protein (C) and human clusterin (D) with equine articular cartilage. Slides were counterstained with hematoxylin. Scale bar: 100 μ m.

Figure 4. Immunolocalization of clusterin in cytopins of superficial zone (A and B), middle zone (C and D) and deep zone (E and F) chondrocytes, either primary (A, C, E) or embedded in alginate and cultured for 28 days in vitro (B, D, F). All sections were lightly counterstained with hematoxylin. Scale bar: 20 μ m.

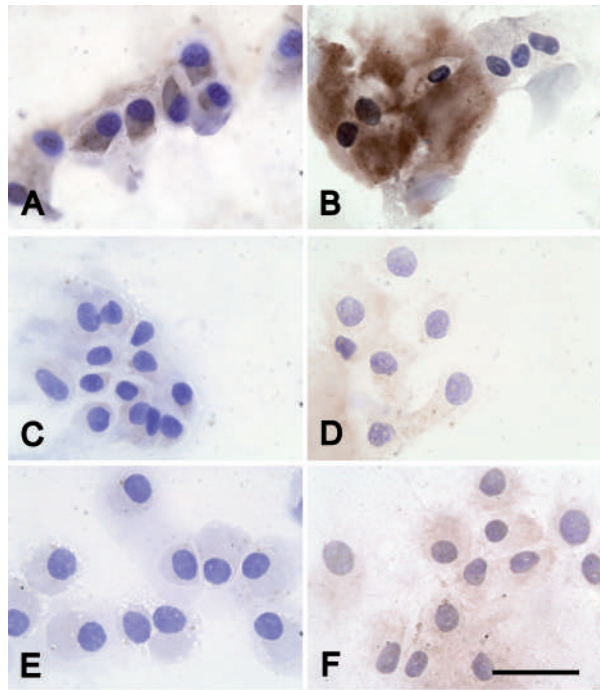
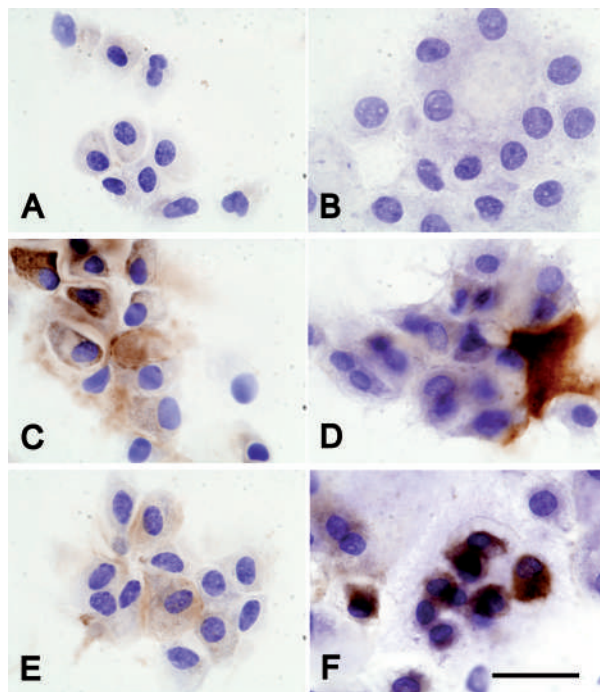


Figure 5. Immunolocalization of cartilage oligomeric protein of superficial zone (A and B), middle zone (C and D) and deep zone (E and F) chondrocytes, either primary (A, C, E) or embedded in alginate and cultured for 28 days in vitro (B, D, F). All sections were lightly counterstained with hematoxylin. Scale bar: 20 μ m.



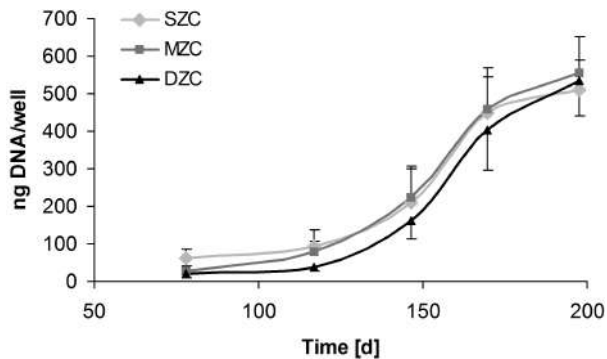


Figure 6. Proliferation rate during the first passage of cells isolated from the three zones: SZC, superficial zone chondrocytes; MZC, middle zone chondrocytes; DZC, deep zone chondrocytes. Values +/- standard error of the mean.

has been demonstrated that the presence of certain growth factors, such as insulin-like growth factor-1, has a differential effect on chondrocytes from the different zones (8). In addition, the fact that in our study the expansion medium was supplemented with fibroblast growth factor-2, which might have contributed to this phenomenon (fibroblast growth factor-2 increases proliferation and temporarily enhances dedifferentiation (21)).

The cartilage zones were dissected using a surgical technique that has been used to harvest zonal cartilage tissue (1;11;25;37). Indeed, the histologic analysis of the osteochondral specimens from which the subsequent zonal layers had been removed demonstrated the adequacy of this technique. Further support for the correct separation of the zones comes from the ratio of cell yield of the different zones, which was similar to the cell distribution in native tissue (33). Nevertheless, owing to the lack of specific zonal cell-surface markers to differentiate between cell populations, we cannot exclude small impurities; therefore, we consider the obtained cell populations as enriched zonal populations.

Redifferentiation of the enriched zonal populations resulted, at least in part, in the differential re-expression of characteristic zonal markers such as COMP and clusterin, as well as differential GAG production, thus confirming our first hypothesis. In line with previous observations (4;10;27), we showed that dedifferentiation of the zonal chondrocytes is associated with loss of their cartilage specific markers, including collagen types II, VI and IX, COMP, and clusterin, as well as up-regulation of collagen type I. During 3-dimensional culture, staining for collagen types II, VI and IX reappeared in all zones, indicative of redifferentiation. In native cartilage, these collagens are present in all zones.

In alginate beads, a significantly higher amount of GAG was produced by deep zone chondrocytes when compared to superficial zone chondrocytes, reflecting the zonal differences in native cartilage (6;43). In contrast to the alginate bead cultures, redifferentiation of the enriched zonal populations in pellets did not result in the distinct differential re-expression of zonal markers, rejecting our second hypothesis and demonstrating that for a given experiment, the selected culture method will have a major impact on outcome. The total amount of GAG per DNA in pellets was higher than in alginate beads, but no significant differences between zones were found. Furthermore, we observed a relatively high donor variation in both the amount of GAG and the amount of DNA in pellets. The higher biosynthetic

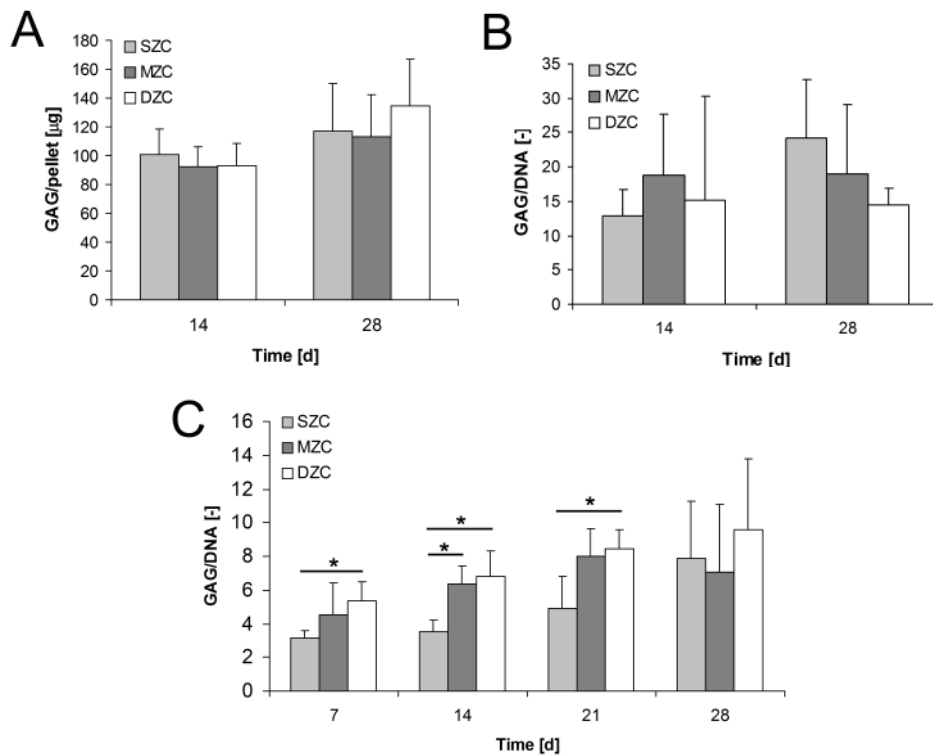


Figure 7. The amount of glycosaminoglycans per pellet (A). The ratio of glycosaminoglycans to DNA for pellet (B) and for alginate culture (C). SZC, superficial zone chondrocytes; MZC, middle zone chondrocytes; DZC, deep zone chondrocytes. * $P < 0.05$.

activity in pellets compared to alginate beads might be related to the difference in cell-cell contact between the culture modalities. Close cell-cell contact, as well as the initial lack of matrix, may stimulate the chondrocytes to produce high amounts of GAG, a major constituent of the extracellular matrix (42).

Overall, we showed better return of zonal differences in extracellular matrix synthesis and composition for chondrocytes cultured in alginate. The configuration of an alginate bead, as an artificial matrix, more closely mimics the natural *in vivo* environment of mature cartilage, compared with the pellet culture: cells in alginate are spaced apart from each other, cell-cell contact is minimal; and the hydrogel provides an extracellular matrix-like environment. This resemblance in surroundings may explain resurgence after expansion of the zonal differences in GAG production per cell and the restoration of characteristic zonal differences shown in immunohistochemistry. Although previous studies have compared pellet and alginate culture for short-term culture of immature chondrocytes (13) and chondrogenic differentiation of mesenchymal stem cells (45), the 2 culture modalities have never been compared for the longer term culture of mature chondrocytes. Further refinement of the culture methods might lead to even better preservation of zonal characteristics - for instance by influencing the dedifferentiation speed (10).

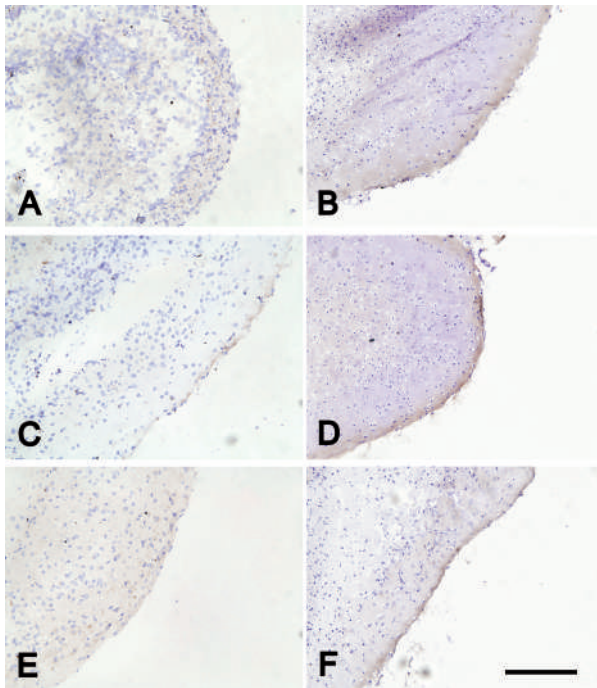


Figure 8. Immunolocalization of clusterin (**A, C, E**) and COMP (**B, D, F**) in pellets for superficial zone (**A and B**), middle zone (**C and D**) and deep zone (**E and F**) chondrocytes, after 28 days in vitro. All sections were lightly counterstained with hematoxylin. Scale bar: 200 μ m.

We have shown that zonal characteristics of chondrocytes can be re-induced after expansion. This knowledge is useful for the future development of biomimetic cartilage constructs. Note, however, that we studied only the enriched populations and did not focus on the co-culture of these populations. Previous studies have shown interaction between chondrocytes from the different zones. For instance, the amount of GAG produced per DNA and the amount of collagen produced per DNA increased significantly in the presence of superficial zone cells (37) when cultured in hydrogel. Also, the amount of proteoglycans increased when middle zone cells were combined with cells from the deep zone, leading to improvement of compressive mechanical properties (41). Furthermore, the amount of PRG-4 secreted by superficial zone chondrocytes is upregulated in the presence of middle zone chondrocytes (5). Future experiments will show whether combinations of expanded and redifferentiated zonal chondrocytes show similar interactions.

We demonstrated that it is feasible to harvest an enriched population of chondrocytes from the superficial, middle and deep zones of the articular cartilage. These enriched chondrocyte populations expressed zone-specific proteins and different amounts of GAG comparable to the situation in native articular cartilage when cultured in alginate after prior expansion, but not when pellet culture is used for re-differentiation. These observations support the use of alginate-based hydrogels for engineering zonal cartilage constructs.

REFERENCES

- Aydelotte MB, Kuettner KE. Differences between sub-populations of cultured bovine articular chondrocytes. I. Morphology and cartilage matrix production. *Connect Tissue Res* 1988;18(3):205-22.
- Barnewitz D, Endres M, Kruger I, Becker A, Zimmermann J, Wilke I, et al. Treatment of articular cartilage defects in horses with polymer-based cartilage tissue engineering grafts. *Biomaterials* 2006 May;27(14):2882-9.
- Bentley G, Minas T. Treating joint damage in young people. *BMJ* 2000 Jun 10;320(7249):1585-8.
- Benya PD, Shaffer JD. Dedifferentiated chondrocytes reexpress the differentiated collagen phenotype when cultured in agarose gels. *Cell* 1982 Aug;30(1):215-24.
- Blewis ME, Schumacher BL, Klein TJ, Schmidt TA, Voegtline MS, Sah RL. Microenvironment regulation of PRG4 phenotype of chondrocytes. *J Orthop Res* 2007 May;25(5):685-95.
- Buckwalter JA, Mankin HJ. Articular cartilage: tissue design and chondrocyte-matrix interactions. *Instr Course Lect* 1998;47:477-86.
- Chawla K, Klein TJ, Schumacher BL, Jadin KD, Shah BH, Nakagawa K, et al. Short-term retention of labeled chondrocyte subpopulations in stratified tissue-engineered cartilaginous constructs implanted in vivo in mini-pigs. *Tissue Eng* 2007 Jul;13(7):1525-37.
- Darling EM, Athanasiou KA. Growth factor impact on articular cartilage subpopulations. *Cell Tissue Res* 2005 Dec;322(3):463-73.
- Darling EM, Athanasiou KA. Rapid phenotypic changes in passaged articular chondrocyte subpopulations. *J Orthop Res* 2005 Mar;23(2):425-32.
- Darling EM, Athanasiou KA. Retaining zonal chondrocyte phenotype by means of novel growth environments. *Tissue Eng* 2005 Mar;11(3-4):395-403.
- Darling EM, Hu JC, Athanasiou KA. Zonal and topographical differences in articular cartilage gene expression. *J Orthop Res* 2004 Nov;22(6):1182-7.
- Dicesare PE, Morgelin M, Carlson CS, Pasumarti S, Paulsson M. Cartilage oligomeric matrix protein: isolation and characterization from human articular cartilage. *J Orthop Res* 1995 May;13(3):422-8.
- Elder SH, Sanders SW, McCulley WR, Marr ML, Shim JW, Hasty KA. Chondrocyte response to cyclic hydrostatic pressure in alginate versus pellet culture. *J Orthop Res* 2006 Apr;24(4):740-7.
- Englert C, McGowan KB, Klein TJ, Giurea A, Schumacher BL, Sah RL. Inhibition of integrative cartilage repair by proteoglycan 4 in synovial fluid. *Arthritis Rheum* 2005 Apr;52(4):1091-9.
- Enobakhare BO, Bader DL, Lee DA. Quantification of sulfated glycosaminoglycans in chondrocyte/alginate cultures, by use of 1,9-dimethylmethylene blue. *Anal Biochem* 1996 Dec 1;243(1):189-91.
- Farndale RW, Buttle DJ, Barrett AJ. Improved quantitation and discrimination of sulphated glycosaminoglycans by use of dimethylmethylene blue. *Biochim Biophys Acta* 1986 Sep 4;883(2):173-7.
- Frisbie DD, Bowman SM, Colhoun HA, Dicarlo EF, Kawcak CE, McIlwraith CW. Evaluation of autologous chondrocyte transplantation via a collagen membrane in equine articular defects: results at 12 and 18 months. *Osteoarthritis Cartilage* 2008 Jun;16(6):667-79.
- Fukui N, Miyamoto Y, Nakajima M, Ikeda Y, Hikita A, Furukawa H, et al. Zonal gene expression of chondrocytes in osteoarthritic cartilage. *Arthritis Rheum* 2008 Dec;58(12):3843-53.
- Hayes AJ, Hall A, Brown S, Tubo R, Caterson B. Macromolecular organization and in vitro growth characteristics of scaffold-free neocartilage grafts. *J Histochem Cytochem* 2007 Aug;55(8):853-66.
- Herzog W, Federico S. Considerations on joint and articular cartilage mechanics. *Biomech Model Mechanobiol* 2006 Jun;5(2-3):64-81.
- Jakob M, Demarteau O, Schafer D, Hintermann B, Dick W, Heberer M, et al. Specific growth factors during the expansion and redifferentiation of adult human articular chondrocytes enhance chondrogenesis and cartilaginous tissue formation in vitro. *J Cell Biochem* 2001 Mar 26;81(2):368-77.
- Khan IM, Salter DM, Bayliss MT, Thomson BM, Archer CW. Expression of clusterin in the superficial zone of bovine articular cartilage. *Arthritis Rheum* 2001 Aug;44(8):1795-9.
- Kim TK, Sharma B, Williams CG, Ruffner MA, Malik A, McFarland EG, et al. Experimental model for cartilage tissue engineering to regenerate the zonal organization of articular cartilage. *Osteoarthritis Cartilage* 2003 Sep;11(9):653-64.
- Klein TJ, Schumacher BL, Schmidt TA, Li KW, Voegtline MS, Masuda K, et al. Tissue engineering of stratified articular cartilage from chondrocyte subpopulations. *Osteoarthritis Cartilage* 2003 Aug;11(8):595-602.
- Li Z, Yao S, Alini M, Grad S. Different response of articular chondrocyte subpopulations to surface motion. *Osteoarthritis Cartilage* 2007 Sep;15(9):1034-41.
- Lorenzo P, Bayliss MT, Heinigard D. A novel cartilage protein (CILP) present in the mid-zone of human articular cartilage increases with age. *J Biol Chem* 1998 Sep 4;273(36):23463-8.
- Martin I, Obradovic B, Treppo S, Grodzinsky AJ, Langer R, Freed LE, et al. Modulation of the mechanical properties of tissue engineered cartilage. *Biorheology* 2000;37(1-2):141-7.
- Masuda I, Iyama KI, Halligan BD, Barbieri JT, Haas AL, McCarty DJ, et al. Variations in site and levels of expression of chondrocyte nucleotide pyrophosphohydrolase with aging. *J Bone Miner Res* 2001 May;16(5):868-75.
- Muir H, Bullough P, Maroudas A. The distribution of collagen in human articular cartilage with some of its

- physiological implications. *J Bone Joint Surg Br* 1970 Aug;52(3):554-63.
30. Murphy BF, Kirszbaum L, Walker ID, d'Apice AJ. SP-40,40, a newly identified normal human serum protein found in the SCSb-9 complex of complement and in the immune deposits in glomerulonephritis. *J Clin Invest* 1988 Jun;81(6):1858-64.
 31. Murray RC, Smith RK, Henson FMD, Goodship A. The Distribution of Cartilage Oligomeric Matrix Protein (COMP) in Equine Carpal Articular Cartilage and its Variation with Exercise and Cartilage Deterioration. *Vet J* 2001 Sep;162(2):121-8.
 32. Niemeyer P, Pestka JM, Kreuz PC, Erggelet C, Schmal H, Suedkamp NP, et al. Characteristic complications after autologous chondrocyte implantation for cartilage defects of the knee joint. *Am J Sports Med* 2008 Nov;36(11):2091-9.
 33. Quinn TM, Hunziker EB, Hauselmann HJ. Variation of cell and matrix morphologies in articular cartilage among locations in the adult human knee. *Osteoarthritis Cartilage* 2005 Aug;13(8):672-8.
 34. Roberts S, McCall IW, Darby AJ, Menage J, Evans H, Harrison PE, et al. Autologous chondrocyte implantation for cartilage repair: monitoring its success by magnetic resonance imaging and histology. *Arthritis Res Ther* 2003;5(1):R60-R73.
 35. Saris DB, Vanlauwe J, Victor J, Haspl M, Bohnsack M, Fortems Y, et al. Characterized chondrocyte implantation results in better structural repair when treating symptomatic cartilage defects of the knee in a randomized controlled trial versus microfracture. *Am J Sports Med* 2008 Feb;36(2):235-46.
 36. Schumacher BL, Hughes CE, Kuettner KE, Caterson B, Aydelotte MB. Immunodetection and partial cDNA sequence of the proteoglycan, superficial zone protein, synthesized by cells lining synovial joints. *J Orthop Res* 1999 Jan;17(1):110-20.
 37. Sharma B, Williams CG, Kim TK, Sun D, Malik A, Khan M, et al. Designing zonal organization into tissue-engineered cartilage. *Tissue Eng* 2007 Feb;13(2):405-14.
 38. Siczkowski M, Watt FM. Subpopulations of chondrocytes from different zones of pig articular cartilage. Isolation, growth and proteoglycan synthesis in culture. *J Cell Sci* 1990 Oct;97 (Pt 2):349-60.
 39. van Loon CJ, de Waal Malefijt MC, Buma P, Stolk T, Verdonschot N, Tromp AM, et al. Autologous morsellised bone grafting restores uncontained femoral bone defects in knee arthroplasty. An in vivo study in horses. *J Bone Joint Surg Br* 2000 Apr;82(3):436-44.
 40. Vanderploeg EJ, Wilson CG, Levenston ME. Articular chondrocytes derived from distinct tissue zones differentially respond to in vitro oscillatory tensile loading. *Osteoarthritis Cartilage* 2008 Apr 7.
 41. Waldman SD, Grynblas MD, Pilliar RM, Kandel RA. The use of specific chondrocyte populations to modulate the properties of tissue-engineered cartilage. *J Orthop Res* 2003 Jan;21(1):132-8.
 42. Wolf F, Candrian C, Wendt D, Farhadi J, Heberer M, Martin I, et al. Cartilage tissue engineering using pre-aggregated human articular chondrocytes. *Eur Cell Mater* 2008;16:92-9.
 43. Wong M, Wuethrich P, Egli P, Hunziker E. Zone-specific cell biosynthetic activity in mature bovine articular cartilage: a new method using confocal microscopic stereology and quantitative autoradiography. *J Orthop Res* 1996 May;14(3):424-32.
 44. Yamane S, Cheng E, You Z, Reddi AH. Gene expression profiling of mouse articular and growth plate cartilage. *Tissue Eng* 2007 Sep;13(9):2163-73.
 45. Yang IH, Kim SH, Kim YH, Sun HJ, Kim SJ, Lee JW. Comparison of phenotypic characterization between "alginate bead" and "pellet" culture systems as chondrogenic differentiation models for human mesenchymal stem cells. *Yonsei Med J* 2004 Oct 31;45(5):891-900.





chapter **THREE**

LAYERED ZONAL CHONDROCYTE PELLETS IN TISSUE ENGINEERED CONSTRUCTS RESULT IN CARTILAGINOUS TISSUE FORMATION WITHOUT RETAINMENT OF ZONAL CHARACTERISTICS

Wouter Schuurman, Eko B. Harimulyo, Debby Gawlitta, Tim B. F. Woodfield,
Wouter J. A. Dhert, P. René van Weeren, and Jos Malda

ABSTRACT

Articular cartilage has limited regenerative capabilities. Chondrocytes from different layers of cartilage have specific properties, and regenerative approaches using zonal chondrocytes may yield better replication of the architecture of native cartilage than when using a single cell population. To obtain high seeding efficiency while still mimicking zonal architecture, cell pellets of expanded deep zone and superficial zone equine chondrocytes were seeded and cultured in two layers on poly(ethylene glycol)-terephthalate/poly(butylene terephthalate) scaffolds. Scaffolds seeded with cell pellets consisting of a 1:1 mixture of both cell sources served as controls. Parallel to this, pellets of superficial or deep zone chondrocytes, and combinations of the two cell populations, were cultured without the scaffold.

Pellet cultures of zonal chondrocytes in scaffolds (constructs) resulted in a high seeding efficiency and abundant cartilaginous tissue formation, containing collagen type II and glycosaminoglycans (GAGs) in all groups, irrespective of the donor (n=3), zonal population used or of (stratified) seeding on the scaffolds. However, whereas total GAG production was similar, the constructs retained significantly more GAG than pellet cultures, from which a high percentage of the produced GAGs was secreted into the culture medium. Immunohistochemistry for zonal markers did not show any differences between the conditions.

We conclude that spatially defined pellet culture in 3D scaffolds is associated with high seeding efficiency and supports cartilaginous tissue formation, but did not result in the maintenance or restoration of the original zonal phenotype. The use of pellet-loaded constructs leads to a better retainment of newly produced GAGs than the use of pellet cultures.

INTRODUCTION

Cartilage is a tissue that mainly consists of extracellular matrix (proteoglycans and collagen fibers) and few cells. Once articular cartilage is damaged, it has very limited regenerative capacity. A number of treatments for focal cartilage defects are available, such as microfracture (1) and regenerative approaches such as autologous chondrocyte implantation (ACI) (2). Although clinical results are quite satisfactory (3), further developments are needed to more closely replicate the long-term functional restoration of the native tissue with the corresponding zonal architecture.

Although articular cartilage may appear as a homogeneous tissue, considerable differences exist throughout the depth of the tissue. Cartilage can be classified into different zones, of which the cells differ in size and morphology, and the extracellular matrix shows differences in glycosaminoglycan (GAG) content (4), collagen fiber orientation (5), gene expression patterns (6), and secreted protein profiles. For example, proteoglycan 4 (PRG4) or superficial zone protein (7) and clusterin (8, 9) are predominantly found in the superficial zone, while cartilage oligomeric matrix protein (COMP) (10, 11) and cartilage intermediate layer protein (CILP) (12) are important components of the middle and deep zones. Even after isolation from the native tissue, chondrocytes and their produced cartilaginous matrix display characteristic differences (13-16).

Combining zonal chondrocytes in a stratified manner has shown promise to enhance functional properties of the tissue engineered cartilage. A number of approaches have been used to mimic the zonal architecture of native cartilage, ranging from scaffold-free culture methods (14, 17) to scaffold-based methods using decellularized cartilage (18), and a range of hydrogels (19-21). An important drawback, however, of the use of hydrogels is their low intrinsic mechanical strength. Albeit there are several ways to increase the mechanical strength of hydrogels (22, 23), it still falls short of matching the natural mechanical properties of cartilage and bone (24).

In regenerative medicine, cells and/or biomaterials are combined: cells are seeded on a carrier material or scaffold and then cultured *in vitro* and/or (subsequently) implanted *in vivo*. A range of different materials, designs (24) and cell sources can be conjoined. Rapid prototyping techniques allow for the fabrication of polymer scaffolds with controlled porosity, pore size, and mechanical properties (25), which thus may overcome the mechanical deficiencies of the hydrogels mentioned earlier. However, although it is feasible to influence the distribution of cells in scaffolds, for instance by modulating pore size (26), the spatially defined placement of cell populations into polymer scaffolds is still a challenge. Furthermore, seeding efficiencies for polymer scaffolds are generally low (27, 28), especially with static seeding methods (29, 30). Therefore, there is a need for a combination of stiff scaffolds and high efficiency techniques for cell seeding.

Spherical pellet culture is a commonly applied chondrocyte redifferentiation model with high seeding efficiency, which supports the general chondrocyte phenotype and the formation of an extracellular matrix that is rich in collagen type II (31, 32). Although in our previous work pellet culture of zonal subpopulations did not show zonal differences for GAG content or specific zonal proteins (16), the interaction between zonal subpopulations in pellets was not examined. Incorporating zonal chondrocyte pellets in a 3D polymer scaffold provides a construct that might combine stratified zonal architecture with a high seeding efficiency and

enhanced mechanical stiffness (33). Therefore, we hypothesized that pellet seeding of zonal chondrocyte populations in poly(ethylene glycol)-terephthalate/poly(butylene terephthalate) (PEGT/PBT) copolymer scaffolds would feature a high seeding efficiency and restore native zonal differences.

MATERIALS AND METHODS

Materials

PEGT/PBT co-polymer (PolyActive™, IsoTis OrthoBiologics, Bilthoven, The Netherlands) with polymer compositions of 1000/70/30 (PEG molecular weight/weight percentage PEGT/weight percentage PBT) was used to create scaffolds. Using a BioScaffolder 3-dimensional fiber deposition machine (SYS+ENG, Salzgitter-Bad, Germany), scaffolds with a strand thickness of 0.17 mm and a fiber spacing of 1 mm were created in a 0–90 degrees alternating pattern, with 100% interconnecting pores. Scaffolds were cut into blocks of approximately 3.5x2.5x1.5 mm to fit two layers of 4 pellets each. The top of the scaffold was marked with a polypropylene suture (Prolene, Ethicon, Somerville, New Jersey, USA), to distinguish between the top and bottom layer.

Cells

Superficial and deep zone articular cartilage was dissected from knees of fresh equine cadavers (age: 2-8 years) under aseptic conditions, as described previously (16). The tissue was digested overnight by 0.15% type II collagenase (Worthington Biochemical Corporation, Lakewood, New Jersey, USA) at 37 degrees Celsius. Afterwards, the cell suspension was filtered through a 100 µm cell strainer (Falcon, BD Biosciences, Franklin Lakes, New Jersey, USA) and washed 3 times in phosphate buffered saline (Invitrogen, Carlsbad, California, USA). Cells were re-suspended in expansion medium consisting of DMEM (Dulbecco's Modified Eagle Medium, Invitrogen), supplemented with 10% fetal bovine serum (Biowhittaker, Walkersville, Maryland, USA), 100 units/mL penicillin-streptomycin (Invitrogen) and 10 ng/mL FGF-2 (R&D Systems, Minneapolis, Minnesota, USA).

Cell culture and scaffold seeding

Chondrocytes were expanded for 10 days in monolayer culture (5,000 cells/cm²) in expansion medium. After expansion, three groups of cells and cell mixtures were formed: superficial zone cells only (SZ), deep zone cells only (DZ) and a mixture (1:1) of superficial cell and deep zone cells (SZ+DZ). For all groups, cell suspensions of 0.25 x 10⁶ cells were centrifuged at 1500 rpm (300 x g) for 5 minutes. The resulting pellets were cultured in differentiation medium (DMEM (Invitrogen) supplemented with 1x Insuline Transferase Selenium-X (Invitrogen), 0.2 mM ascorbic acid 2-phosphate (Sigma-Aldrich, St Louis, Missouri), 0.5% human serum albumin (Cealb, Sanquin, Utrecht, The Netherlands), 100 units/mL penicillin-streptomycin (Invitrogen) and 5 ng/mL TGF-β2 (R&D Systems)) for 1 week in U-bottom ultra low attachment 96-well plates (Corning, Lowell, Massachusetts, USA), as previously described by (33).

After 1 week of culture, pellets were either seeded into the scaffolds or maintained in differentiation medium as controls. For scaffold seeding, 8 pellets were seeded into the pores

of the scaffolds, in two layers. Two groups were created: scaffolds were either seeded using 4 superficial zone pellets and 4 deep zone pellets, in which superficial zone pellets were seeded on top of deep zone pellets (zonal constructs) or seeded with pellets that contained both the superficial and deep zone cells (mixed constructs) (Figure 1). The resulting constructs were cultured in differentiation medium. Medium was refreshed and medium samples for biochemical analysis were taken twice a week. Samples for histology were taken after 31 days and for biochemical assays of the pellets and constructs after 7 and 31 days.

Histology and immunohistochemistry

Histology

Samples were fixed in formalin, dehydrated through graded ethanol series, cleared in xylene and embedded in paraffin. Embedded samples were sectioned to yield 5 μm sections. Sections were then stained with safranin-O for proteoglycans and with fast green and hematoxylin to detect collagenous matrix and cell nuclei. Further, samples were stained with a triple staining of alcian blue, hematoxylin, and picosirius red to visualize collagen fiber orientation. The sections were examined and photographed using a light microscope (Olympus BX51 microscope, Olympus DP70 camera, Hamburg, Germany). For visualization of the picosirius red staining, a light polarizing filter was used.

Immunohistochemistry

Immunohistochemistry was performed to assess expression of various (zonal) markers as previously described (16). Briefly, all samples were cultured in differentiation medium supplemented with 0.1 μM Monensin (18) overnight (to trap PRG4 intracellularly (34)), and subsequently either embedded in OCT compound at -20 degrees Celsius (Tissue-Tek, Sakura Finetek, USA) or fixed in formalin, embedded in paraffin and sectioned as described above. Cryosamples were cut to yield 10 μm sections, and were fixed in formalin for 10 minutes. Subsequently, endogenous peroxidase was blocked using a 0.3% H_2O_2 solution for 10 minutes. Samples for clusterin staining were permeabilized with PBS/ Triton-X (0.2%) for 5 minutes,

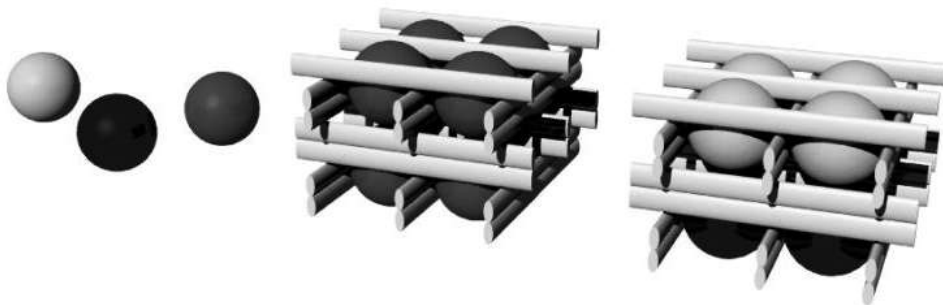


Figure 1. Schematic representation of zonal chondrocyte pellets (left) and scaffolds seeded with chondrocytes (center and right). In white, the superficial zone cell pellets, in black, the deep zone cell pellets, in grey, the pellets composed of superficial and deep zone cells (combined pellet). On the right, the PEGT/PBT scaffold seeded with the cell pellets of the superficial zone and deep zone are shown. The scaffold in the center is loaded with combined pellets.

while samples for CILP, COMP, collagen type II, collagen type VI and PRG4 were washed with PBS/Tween (0.1%). For the PRG4 staining, antigen retrieval was performed using proteinase XIV (Sigma-Aldrich), while for CILP, COMP, clusterin, and collagen type II and collagen type VI, hyaluronidase and pronase antigen retrieval was used. For all antibodies, samples were blocked with 5% BSA in PBS for 30 minutes. The sections were incubated overnight with the monoclonal clusterin antibody (35) (1:200, G7, a generous gift of Dr Brendan Murphy), anti-COMP (1:50, a kind gift from Professor R.K. Smith, Royal Veterinary College, London, UK), anti-collagen type II (1:100, II-6B3II, Developmental Studies Hybridoma Bank, USA), type VI (1:50, 5C6, Developmental Studies Hybridoma Bank, USA), anti-CILP (1:50, HPA3195, Atlas Antibodies, Sigma-Aldrich), anti-PRG4 (1:50, Ab28484, Abcam, Cambridge, UK). Samples were then incubated for 60 minutes with either goat anti-mouse HRP antibody (for collagen type II and type VI and for COMP, 1:200, Dako, Glostrup, Denmark), biotinylated anti-rabbit IgG (for CILP and PRG4, 1:200, Vector Laboratories, Burlingame, California, USA), or biotinylated anti-mouse IgG (for clusterin, 1:200, GE Health Care, Buckinghamshire, UK). Samples for CILP, clusterin and PRG4 were then incubated for 60 minutes with the tertiary HRP-conjugated streptavidin antibody (1:500, Immunotech, Beckman Coulter, Marseille, France). Staining was visualized using DAB solution (3,3'-diaminobenzidine tetrahydrochloride hydrate, Sigma-Aldrich) for 10 minutes. Counterstaining was performed with hematoxylin. The sections were examined using a light microscope. Isotype controls were performed by replacing the primary antibody with mouse or rabbit isotype IgG1 monoclonal antibody at concentrations similar to those of the primary antibodies.

Biochemical assays

Constructs and pellets (n=4 for each condition and time point) were harvested. For pellets, samples were taken after 7 and 31 days and for constructs after 31 days. All pellets and constructs were digested overnight at 56°C in a solution containing 250 mg/mL papain (Sigma-Aldrich, USA). The amount of GAGs of the digests and the media was determined spectrophotometrically after reaction with dimethylmethylene blue dye (DMMB, Sigma-Aldrich, USA) (36). Intensity of color change was quantified immediately in a microplate reader (Biorad) by measuring absorbance at 540 and 595 nm. The amount of GAG was calculated using a standard of chondroitin sulphate C (Sigma-Aldrich) and by calculating the ratio of absorbances. The production of GAG was normalized to the DNA content. Quantification of total DNA was performed by Quant-iT PicoGreen dsDNA kit (Molecular Probes, Invitrogen) using a spectrofluorometer (Biorad, Hercules, California, USA).

Statistics

Values for proteoglycan content of pellets, constructs, and media are presented as mean \pm standard deviation. Statistical differences were assessed by a repeated measurement ANOVA for comparing the differences for GAG, DNA or GAG per DNA in time, or by a one-way ANOVA and a Bonferroni posthoc test for the comparison of GAG, DNA and GAG per DNA between different pellet groups. For the comparison of construct groups and for the comparison between the grouped pellets and grouped constructs, an independent samples t-test was used. $p < 0.05$ was considered a significant difference.

RESULTS

Cell culture and scaffold seeding

Pellets were successfully seeded into the polymer scaffolds and cultured for up to 31 days. Macroscopically, no differences were seen between the pellets of different conditions, nor between the zonal constructs and the control constructs during the course of culture. For the pellets in the scaffolds, fusion between the different pellets could be observed macroscopically.

Histology and immunohistochemistry

Pellets

The safranin-O staining showed that glycosaminoglycan (GAG) formation was present for all conditions, and all samples stained positive for cartilage marker collagen type II at similar intensity after 31 days of culture (Figure 2). No differences were observed for gross tissue

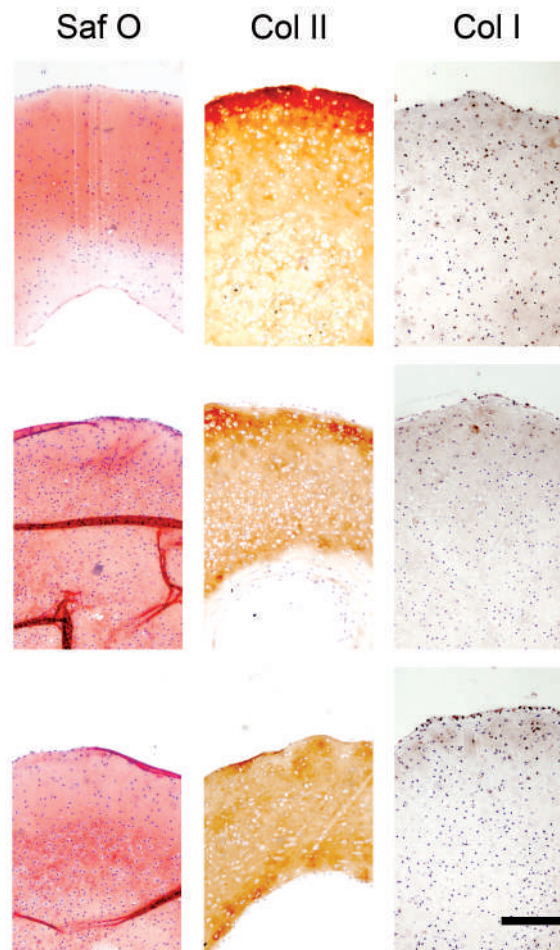


Figure 2. Histology and immunohistochemistry for collagen type II and I for the separately cultured chondrocyte pellets for the superficial zone (top row) and deep zone cells (middle row) and a combination of the two cell types (bottom row) at day 31. The safranin-O (Saf O) staining shows the presence of glycosaminoglycans for all conditions. Collagen type II (Col II) was detected in all conditions, while all conditions stain faintly positive for collagen type I (Col I). Scale bar represents 200 μ m.

morphology between the superficial zone pellets, the deep zone pellets, and the combined pellets. For all histological and immunohistochemical stainings, no differences between the different pellets were observed (Figures 2 and 3). Collagen type I staining was present for all conditions (Figure 2), but was low compared to positive controls. For the zonal markers CILP, clusterin, COMP and PRG4, no differences between cell pellet groups were seen (Figure 3). CILP immunolocalization was negative for all pellets that were cultured separately, while all pellet samples were positive for clusterin, COMP and PRG4. All pellet samples that exhibited positive immunostainings, showed the highest intensity in the outer shell of the cell pellets.

Zonal constructs

For the constructs, no differences in gross morphology were observed between the stratified zonal constructs and the mixed control constructs as shown by safranin-O staining (Figure 4). The different pellets in each construct had fused and had formed a continuous layer of neo-tissue around the PEGT/PBT copolymer fibers. Those fibers dissolve during the processing for histology, and leave holes, as illustrated by Figure 4. The cartilage marker collagen type II was present in both the zonal and mixed scaffolds, while the intensity of staining for the dedifferentiation marker collagen type I was comparably low in both. This is in line with the observations for the separately cultured pellets.

No differences were detected in zonal marker expression between the two construct types (not shown). Immunolocalization for CILP was negative for both conditions, while the positive staining for clusterin, COMP and PRG4 was most prominent in the outer rim of the constructs.

Biochemical assays

Pellets

The amount of GAG in the cell pellets of all conditions together showed a significant increase in time ($p=0.007$, Figure 5a), but for the separate zonal pellet groups, this increase was not statistically significant ($p=0.225$, $p=0.091$ and $p=0.209$ for SZ, DZ and SZ+DZ pellet, respectively), although there was a trend for increase for the DZ pellets. The amount of DNA did not significantly differ between time points, neither for the zonal pellets, nor for the pellet group as a whole ($p=0.250$, $p=0.761$, $p=0.374$, $p=0.168$, for SZ, DZ, SZ+DZ and whole pellet group, respectively). The values for glycosaminoglycans produced per DNA were similar for both time points, with average values ranging from 10 to 27 (Figure 5b). In line with these observations for the pellet cultures, no differences were detected for the amount of GAG (Figure 6a) or GAG per DNA (Figure 6b) between the experimental (zonal) and control constructs at day 31. The amount of GAG that was released into the medium and the total amount of GAGs produced did not differ either between zonal pellet groups (Figure 7a,b).

Zonal constructs

In the construct groups the amount of GAG released and total amount of GAG produced was, as in the pellets, not significantly different between zonal and combined conditions (Figure 8a). This was also true for GAG per DNA (data not shown).

Zonal constructs versus pellets

Pellet cultures and zonal constructs appeared to differ in the dynamics of GAG production and retention. Whereas GAG per DNA was not significantly different between the two culture techniques ($p=0.905$), the percentage of GAG that was incorporated per total amount of GAG was substantially higher for constructs than for pellets, $p=0.031$ (Figure 8b).

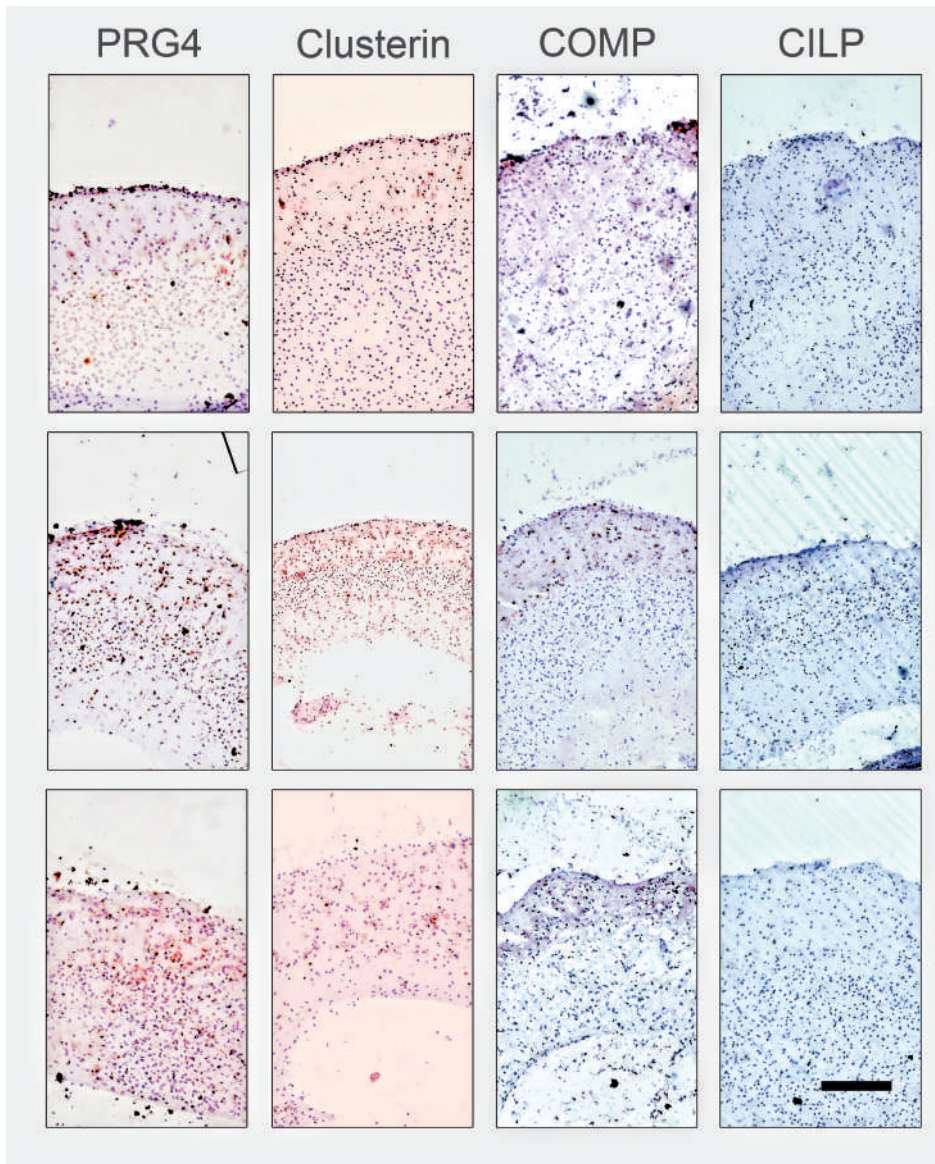


Figure 3. Immunolocalization of zonal markers for the separately cultured chondrocyte pellets for the superficial zone (top row) and deep zone cells (middle row) and a combination of the two cell types (bottom row) at day 31. Superficial zone markers PRG4 and clusterin were detected in pellets from all conditions. Staining for middle zone marker COMP is also (faintly) positive in pellets from all conditions, while samples of all conditions were negative for middle zone marker CILP. Scale bar represents 200 μ m.

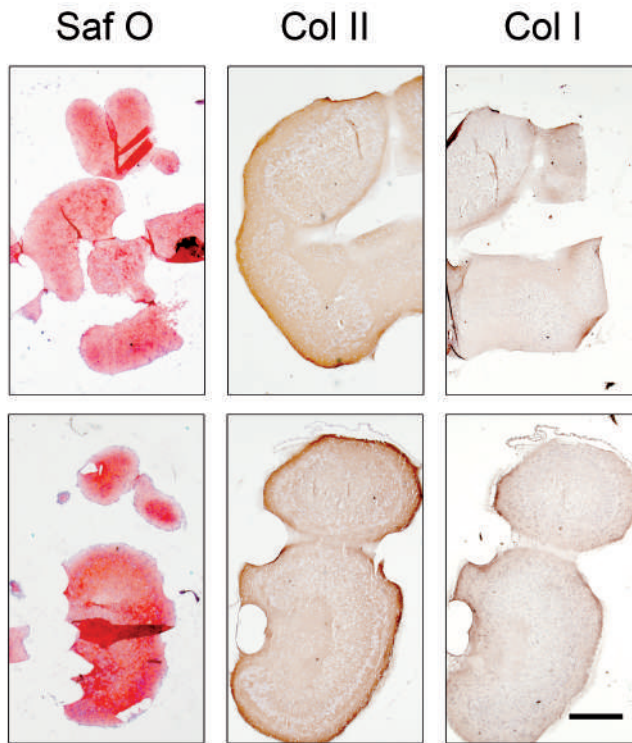


Figure 4. Cartilaginous markers for zonal (top row) and combined constructs (bottom row) at day 31. The top of the construct is in the top of the picture. Immunolocalization of collagen type II is positive for all conditions, while all conditions stain faintly positive for collagen type I. The safranin-O staining shows the presence of glycosaminoglycans for all conditions. Scale bar represents 500 μm .

DISCUSSION

In this study, we successfully seeded pellets of zonal and mixed chondrocytes into PEGT/PBT scaffolds. The pellets were cultured separately for 7 days after which they were put into the scaffolds and subsequently cultured for another 24 days. In parallel, separate pellets of superficial zone, deep zone and combined cells were cultured. All samples showed cartilaginous tissue formation as evidenced by the presence of collagen type II and the formation of glycosaminoglycans. This is in line with previous findings using a similar method (33).

No significant differences were detected with respect to cartilage markers or zonal cartilage markers, neither when cultured separately, nor when cultured combined or combined in a stratified manner.

Previous reports about high cell density culture of zonal chondrocytes are conflicting; in some studies the cells are shown to retain some of their zonal phenotypic characteristics, even after expansion (37, 38). In the latter study, however, the observed differences between zonal subpopulations were only present in pellets that were cultured under low oxygen tension. For chondrocytes that are expanded and thus dedifferentiated, we previously found no differences in terms of GAG content or (zonal) cartilage markers following redifferentiation in pellet culture (16). Our current data are in line with this previous work, showing similar results for pellet cultures in constructs that contain combinations of zonal chondrocyte subpopulations.

Figure 5. The amount of glycosaminoglycans (GAG) (a) and GAG per DNA (b) for pellet cultures of superficial zone (SZ), deep zone (DZ) and mixed cell pellets (SZ+DZ) for 7 and 31 days. For the amount of DNA in time, no differences were observed. Data are presented as mean \pm standard deviation. * represents a significant difference ($p < 0.05$).

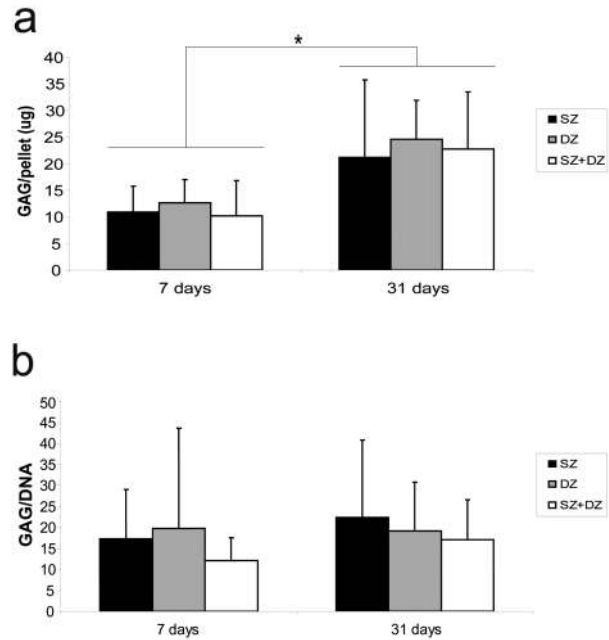
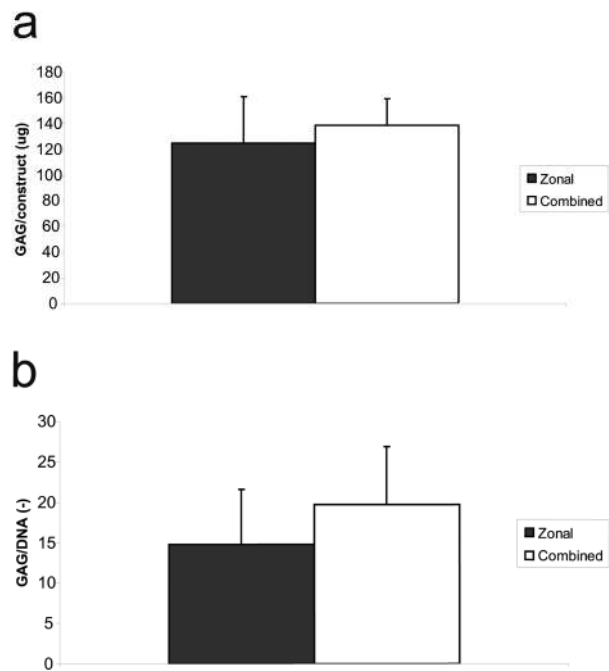


Figure 6. The amount of glycosaminoglycans (GAG) (a) and GAG per DNA (b) for zonal and combined constructs after 31 days of culture. Data are presented as mean \pm standard deviation. The results show no significant differences between conditions.



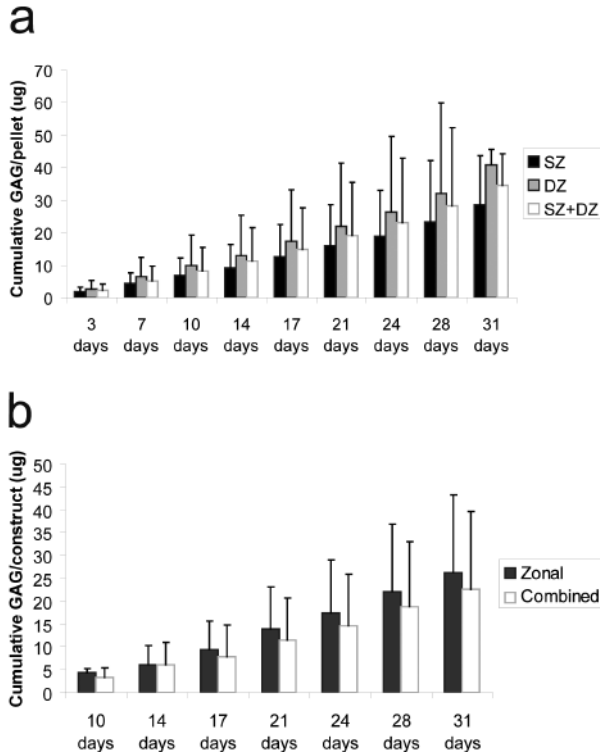


Figure 7. The cumulative amount of glycosaminoglycans (GAG) in the culture medium for superficial zone (SZ), deep zone (DZ) and mixed cell pellets (SZ+DZ) (a); and for zonal and combined constructs (b).

We used two supplemental immunohistochemical markers that also did not appear to differ between the zonal cell populations: CILP and PRG4. CILP is an identifier of the middle zone of articular cartilage (12, 39), which is also present in muscle and heart tissue (39), in meniscal cartilage (39) and the intervertebral disc (40). Proteoglycan 4 (PRG4) or superficial zone protein (SZP) is predominantly synthesized in the superficial zone of articular cartilage, and is thought to play a role in cell proliferation and lubrication of the joint (41). It has been suggested that transplanting or implanting cells or tissues that can secrete SZP may restore functional lubrication when this is hampered (18). In the present experiment, immunolocalization of PRG4 was seen for all conditions, as was the case for clusterin and COMP. The outer rims of both scaffolds and pellets stained most intense for all positive immunostainings. The increased secretion of proteins that are not zone-specific suggests a certain plasticity of chondrocytes during pellet culture. The mechanism behind this is unclear, and might depend on cell-cell interactions, or on the direct environment of the cells. For mesenchymal stromal cell (MSC) pellets, for instance, it is known that cell-cell and cell-matrix interactions play a pivotal role in early chondrogenic differentiation (42). Early condensation is modulated by the transient expression of cell-adhesion molecules (43), which are down-regulated when the cells become separated by extracellular matrix (44). This process may be not as well orchestrated in the pellet culture of dedifferentiated mature chondrocytes, in which a more basal chondrocyte phenotype is observed, without the more subtle zonal differences. Culture circumstances can

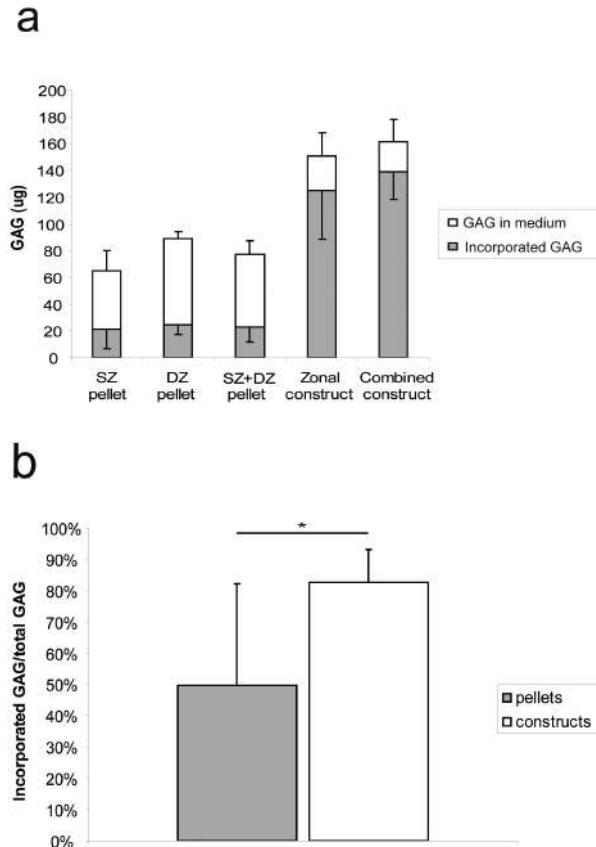


Figure 8. Total amount of GAGs produced and ratio of incorporated GAG per total GAG, (a) the total amount of GAG that was incorporated and secreted during the complete culture period for all conditions, (b) the ratio incorporated GAG per total produced GAG for pellets as a group and constructs as a group. Data are presented as mean \pm standard deviation. * represents a significant difference ($p < 0.05$).

also be of great influence: low oxygen tension can direct chondrocyte (zonal) phenotype, resulting in differences in GAG content, and more PRG4 gene expression and protein secretion for superficial zone chondrocyte pellets, and for the early time points, for clusterin (38). Furthermore, the addition of TGF- β to our culture medium can affect protein secretion: it is known that TGF- β can promote the levels of both PRG4 gene expression (41) and clusterin gene expression (45, 46) and protein secretion (46). However, when zonal chondrocytes are cultured in hydrogels or in filter culture in the presence of TGF- β , the production of PRG4 (14, 20) and clusterin (16) is predominantly seen in the superficial zone cells.

No differences were observed in GAG content and GAG/DNA between zonal and mixed constructs, indicating that the amount of glycosaminoglycans produced is not influenced by the stratified architecture. We observed large donor-dependent differences in all pellet and construct types for glycosaminoglycan content. The absence of zonal differences in glycosaminoglycan production is in contrast to previous studies, which show a higher amount of GAGs produced by deep zone cells than by superficial zone cells (21, 47, 48). However, these studies use hydrogels, and primary cells. Interestingly, the ratio of incorporated glycosaminoglycans to total amount of GAG production is significantly lower in the separately

cultured pellets. Typically, in the pellets that were loaded into a scaffold, the outer surface is relatively small compared to the separately cultured pellets, since in the constructs, the pellets fused together into one large mass. This phenomenon was also seen by previous authors (33). A smaller outer surface of a construct may hence lead to less loss of glycosaminoglycans and consequently a higher ratio of incorporation.

This study shows that high-density culture of expanded zonal chondrocytes in 3D scaffolds yields cartilaginous tissue, and circumvents the problem of low seeding efficiency that is usually seen when cells are seeded directly onto scaffolds. High contents of glycosaminoglycans were shown in the cultures, and constructs contained collagen type II. Pellet culture of chondrocytes has previously shown promise for the treatment of osteochondral defects (49) and chondrocyte pellet culture has been suggested as an intermediate culture step in cartilage tissue biofabrication (50). Nevertheless, no replication of zonal cartilage differences occurred, neither when pellets were cultured separately, nor when a stratified combination of pellets was used. Culturing the constructs at low oxygen levels might improve their zonal characteristics, especially for the superficial chondrocytes. Furthermore, the use of a mechanical loading regimen could be considered, since cells from the zonal subpopulations respond differently to mechanical loading (48, 51).

To improve the approach we used in this study, a 3-dimensional deposition machine could be used (25), which would enable examining several slight alterations to the applied protocols. That way, pellet placement within scaffolds could be automated. Alternatively, it might be beneficial to employ approaches in which more complex biofabrication techniques are used, which would provide the opportunity to better mimic a number of characteristics of native articular cartilage, such as curvature and variability of thickness of tissue layers and cell densities. Hydrogels are then probably preferable to pellet cultures. For bioprinting techniques and other computer-aided manufacturing techniques, hydrogels are already widely used (52-54), in some cases combined with other biomaterials to enhance mechanical characteristics of the construct (55-57).

CONCLUSION

In the present study, (stratified) seeding of pellets in PEGT/PBT copolymer scaffold resulted in organized constructs. In time, abundant cartilaginous tissue formation was observed, irrespective of the zonal population used or whether (stratified) seeding was employed. Incorporation of the pellets in the construct is an efficient way of seeding the polymer scaffolds. As such, subsequent culture leads to constructs with a high GAG content. However, analysis of glycosaminoglycans and DNA, and immunolocalization of zonal markers did not reveal any differences related to the zone the chondrocytes originated from. The substantially improved retainment of newly produced GAG in constructs compared to pellet cultures is a potentially interesting observation. In addition, the described method might hold promise for generating constructs containing multiple tissue types, in order to further recapitulate tissue organization in engineered tissues.

ACKNOWLEDGMENTS

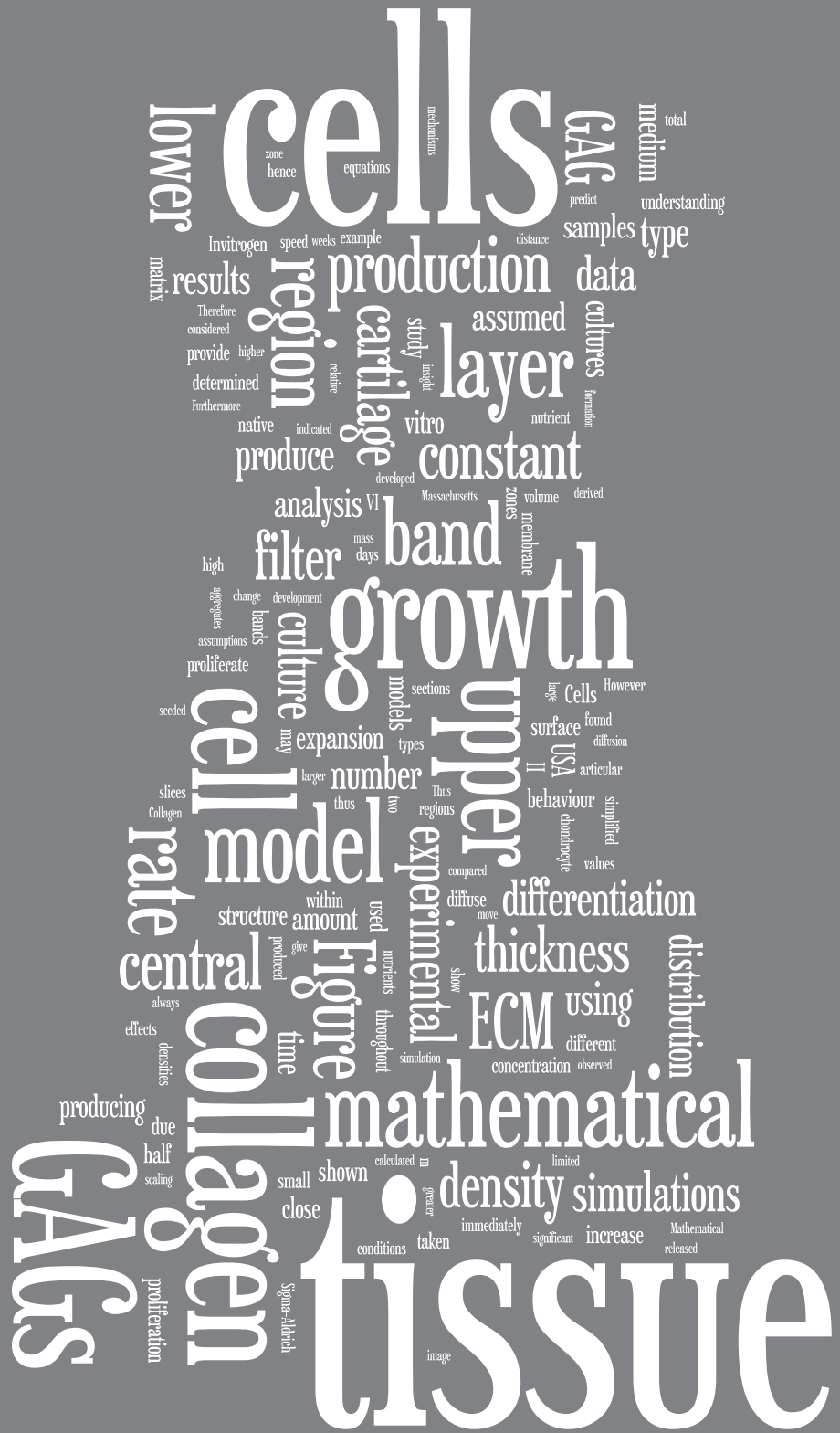
The collagen type II monoclonal antibody (developed by T. F. Linsenmayer) was obtained from the Developmental Studies Hybridoma Bank. TW and JM are supported by a starting grant from the AO Foundation. DG is supported by a VENI fellowship from the Dutch Technology Foundation STW.

REFERENCES

1. Steadman JR, Rodkey WG, Briggs KK, and Rodrigo JJ, [The microfracture technic in the management of complete cartilage defects in the knee joint]. *Orthopade*, 1999. **28**(1): p. 26-32.
2. Peterson L, Brittberg M, Kiviranta I, Akerlund EL, and Lindahl A, Autologous chondrocyte transplantation. Biomechanics and long-term durability. *Am J Sports Med*, 2002. **30**(1): p. 2-12.
3. Saris DB, Vanlauwe J, Victor J, Almqvist KF, Verdonk R, Bellemans J, and Luyten FP, Treatment of symptomatic cartilage defects of the knee: characterized chondrocyte implantation results in better clinical outcome at 36 months in a randomized trial compared to microfracture. *Am J Sports Med*, 2009. **37** Suppl 1: p. 10S-19S.
4. Bhosale AM and Richardson JB, Articular cartilage: structure, injuries and review of management. *Br Med Bull*, 2008. **87**: p. 77-95.
5. Buckwalter JA and Mankin HJ, Articular cartilage: tissue design and chondrocyte-matrix interactions. *Instr Course Lect*, 1998. **47**: p. 477-86.
6. Fukui N, Miyamoto Y, Nakajima M, Ikeda Y, Hikita A, Furukawa H, Mitomi H, Tanaka N, Katsuragawa Y, Yamamoto S, Sawabe M, et al., Zonal gene expression of chondrocytes in osteoarthritic cartilage. *Arthritis Rheum*, 2008. **58**(12): p. 3843-53.
7. Schumacher BL, Block JA, Schmid TM, Aydelotte MB, and Kuettner KE, A novel proteoglycan synthesized and secreted by chondrocytes of the superficial zone of articular cartilage. *Arch Biochem Biophys*, 1994. **311**(1): p. 144-52.
8. Khan IM, Salter DM, Bayliss MT, Thomson BM, and Archer CW, Expression of clusterin in the superficial zone of bovine articular cartilage. *Arthritis Rheum*, 2001. **44**(8): p. 1795-9.
9. Malda J, ten Hoope W, Schuurman W, van Osch GJ, van Weeren PR, and Dhert WJ, Localization of the potential zonal marker clusterin in native cartilage and in tissue-engineered constructs. *Tissue Eng Part A*, 2010. **16**(3): p. 897-904.
10. DiCesare PE, Morgelin M, Carlson CS, Pasmarti S, and Paulsson M, Cartilage oligomeric matrix protein: isolation and characterization from human articular cartilage. *J Orthop Res*, 1995. **13**(3): p. 422-8.
11. Murray RC, Smith RK, Henson FM, and Goodship A, The distribution of cartilage oligomeric matrix protein (COMP) in equine carpal articular cartilage and its variation with exercise and cartilage deterioration. *Vet J*, 2001. **162**(2): p. 121-8.
12. Lorenzo P, Bayliss MT, and Heinegard D, A novel cartilage protein (CILP) present in the mid-zone of human articular cartilage increases with age. *J Biol Chem*, 1998. **273**(36): p. 23463-8.
13. Darling EM and Athanasiou KA, Retaining zonal chondrocyte phenotype by means of novel growth environments. *Tissue Eng*, 2005. **11**(3-4): p. 395-403.
14. Hayes AJ, Hall A, Brown L, Tubo R, and Caterson B, Macromolecular organization and in vitro growth characteristics of scaffold-free neocartilage grafts. *J Histochem Cytochem*, 2007. **55**(8): p. 853-66.
15. Klein TJ, Schumacher BL, Blewis ME, Schmidt TA, Voegtline MS, Thonar EJ, Masuda K, and Sah RL, Tailoring secretion of proteoglycan 4 (PRG4) in tissue-engineered cartilage. *Tissue Eng*, 2006. **12**(6): p. 1429-39.
16. Schuurman W, Gawlitta D, Klein TJ, ten Hoope W, van Rijen MH, Dhert WJ, van Weeren PR, and Malda J, Zonal chondrocyte subpopulations reacquire zone-specific characteristics during in vitro redifferentiation. *Am J Sports Med*, 2009. **37** Suppl 1: p. 97S-104S.
17. Chawla K, Klein TJ, Schumacher BL, Jadin KD, Shah BH, Nakagawa K, Wong VW, Chen AC, Masuda K, and Sah RL, Short-term retention of labeled chondrocyte subpopulations in stratified tissue-engineered cartilaginous constructs implanted in vivo in minipigs. *Tissue Eng*, 2007. **13**(7): p. 1525-37.
18. Schmidt TA, Schumacher BL, Klein TJ, Voegtline MS, and Sah RL, Synthesis of proteoglycan 4 by chondrocyte subpopulations in cartilage explants, monolayer cultures, and resurfaced cartilage cultures. *Arthritis Rheum*, 2004. **50**(9): p. 2849-57.
19. Kim TK, Sharma B, Williams CG, Ruffner MA, Malik A, McFarland EG, and Elisseff JH, Experimental model for cartilage tissue engineering to regenerate the zonal organization of articular cartilage. *Osteoarthritis Cartilage*, 2003. **11**(9): p. 653-64.
20. Ng KW, Ateshian GA, and Hung CT, Zonal chondrocytes seeded in a layered agarose hydrogel create engineered cartilage with depth-dependent cellular and mechanical inhomogeneity. *Tissue Eng Part A*, 2009. **15**(9): p. 2315-24.

21. Sharma B, Williams CG, Kim TK, Sun D, Malik A, Khan M, Leong K, and Elisseeff JH, Designing zonal organization into tissue-engineered cartilage. *Tissue Eng*, 2007. **13**(2): p. 405-14.
22. Fedorovich NE, Alblas J, de Wijn JR, Hennink WE, Verbout AJ, and Dhert WJ, Hydrogels as extracellular matrices for skeletal tissue engineering: state-of-the-art and novel application in organ printing. *Tissue Eng*, 2007. **13**(8): p. 1905-25.
23. Jia X and Kiick KL, Hybrid multicomponent hydrogels for tissue engineering. *Macromol Biosci*, 2009. **9**(2): p. 140-56.
24. Hutmacher DW, Scaffolds in tissue engineering bone and cartilage. *Biomaterials*, 2000. **21**(24): p. 2529-43.
25. Woodfield TB, Malda J, de Wijn J, Peters F, Riesle J, and van Blitterswijk CA, Design of porous scaffolds for cartilage tissue engineering using a three-dimensional fiber-deposition technique. *Biomaterials*, 2004. **25**(18): p. 4149-61.
26. Woodfield TB, Van Blitterswijk CA, De Wijn J, Sims TJ, Hollander AP, and Riesle J, Polymer scaffolds fabricated with pore-size gradients as a model for studying the zonal organization within tissue-engineered cartilage constructs. *Tissue Eng*, 2005. **11**(9-10): p. 1297-311.
27. Roh JD, Nelson GN, Udelsman BV, Brennan MP, Lockhart B, Fong PM, Lopez-Soler RI, Saltzman WM, and Breuer CK, Centrifugal seeding increases seeding efficiency and cellular distribution of bone marrow stromal cells in porous biodegradable scaffolds. *Tissue Eng*, 2007. **13**(11): p. 2743-9.
28. Xiao YL, Riesle J, and Van Blitterswijk CA, Static and dynamic fibroblast seeding and cultivation in porous PEO/PBT scaffolds. *J Mater Sci Mater Med*, 1999. **10**(12): p. 773-7.
29. Shahin K and Doran PM, Improved seeding of chondrocytes into polyglycolic acid scaffolds using semi-static and alginate loading methods. *Biotechnol Prog*, 2011. **27**(1): p. 191-200.
30. Sobral JM, Caridade SC, Sousa RA, Mano JF, and Reis RL, Three-dimensional plotted scaffolds with controlled pore size gradients: Effect of scaffold geometry on mechanical performance and cell seeding efficiency. *Acta Biomater*, 2011. **7**(3): p. 1009-18.
31. Larson CM, Kelley SS, Blackwood AD, Baner AJ, and Lee GM, Retention of the native chondrocyte pericellular matrix results in significantly improved matrix production. *Matrix Biol*, 2002. **21**(4): p. 349-59.
32. Tallheden T, Bengtsson C, Brantsing C, Sjogren-Jansson E, Carlsson L, Pettersson L, Brittberg M, and Lindahl A, Proliferation and differentiation potential of chondrocytes from osteoarthritic patients. *Arthritis Res Ther*, 2005. **7**(3): p. R560-8.
33. Schon BS, Schrobback K, van der Ven M, Stroebel S, Hooper CJ, and Woodfield TB, Validation of a high-throughput microtissue fabrication process for 3D assembly of tissue engineered cartilage constructs. *Cell Tissue Res*, 2012. **[Epub ahead of print]**.
34. Schumacher BL, Hughes CE, Kuettner KE, Caterson B, and Aydelotte MB, Immunodetection and partial cDNA sequence of the proteoglycan, superficial zone protein, synthesized by cells lining synovial joints. *J Orthop Res*, 1999. **17**(1): p. 110-20.
35. Murphy BF, Kirszbaum L, Walker ID, and d'Apice AJ, SP-40,40, a newly identified normal human serum protein found in the SCSb-9 complex of complement and in the immune deposits in glomerulonephritis. *J Clin Invest*, 1988. **81**(6): p. 1858-64.
36. Farndale RW, Buttle DJ, and Barrett AJ, Improved quantitation and discrimination of sulphated glycosaminoglycans by use of dimethylmethylene blue. *Biochim Biophys Acta*, 1986. **883**(2): p. 173-7.
37. Hu JC and Athanasiou KA, Chondrocytes from different zones exhibit characteristic differences in high density culture. *Connect Tissue Res*, 2006. **47**(3): p. 133-40.
38. Schrobback K, Malda J, Crawford R, Upton Z, Leavesley D, and Klein TJ, Effects of Oxygen on Zonal Marker Expression in Human Articular Chondrocytes. *Tissue Eng Part A*, 2012. **[Epub ahead of print]**.
39. Bernardo BC, Belluoccio D, Rowley L, Little CB, Hansen U, and Bateman JF, Cartilage intermediate layer protein 2 (CILP-2) is expressed in articular and meniscal cartilage and down-regulated in experimental osteoarthritis. *J Biol Chem*, 2011. **286**(43): p. 37758-67.
40. Wang Z, Kim JH, Higashino K, Kim SS, Wang S, Seki S, Hutton WC, and Yoon ST, Cartilage Intermediate Layer Protein (CILP) Regulation in Intervertebral Discs: The Effect of Age, Degeneration, and BMP-2. *Spine (Phila Pa 1976)*, 2011. **[Epub ahead of print]**.
41. Flannery CR, Hughes CE, Schumacher BL, Tudor D, Aydelotte MB, Kuettner KE, and Caterson B, Articular cartilage superficial zone protein (SZP) is homologous to megakaryocyte stimulating factor precursor and is a multifunctional proteoglycan with potential growth-promoting, cytoprotective, and lubricating properties in cartilage metabolism. *Biochem Biophys Res Commun*, 1999. **254**(3): p. 535-41.
42. Goessler UR, Bugert P, Bieback K, Stern-Straeter J, Bran G, Hormann K, and Riedel F, Integrin expression in stem cells from bone marrow and adipose tissue during chondrogenic differentiation. *Int J Mol Med*, 2008. **21**(3): p. 271-9.
43. Tuan RS, Cellular signaling in developmental chondrogenesis: N-cadherin, Wnts, and BMP-2. *J Bone Joint Surg Am*, 2003. **85-A Suppl 2**: p. 137-41.
44. Gao L, McBeath R, and Chen CS, Stem cell shape regulates a chondrogenic versus myogenic fate through Rac1 and N-cadherin. *Stem Cells*. **28**(3): p. 564-72.
45. Jin G and Howe PH, Regulation of clusterin gene expression by transforming growth factor beta. *J Biol Chem*, 1997. **272**(42): p. 26620-6.
46. Reddy KB, Jin G, Karode MC, Harmony JA, and Howe PH, Transforming growth factor beta (TGF beta)-induced nuclear localization of apolipoprotein J/clusterin in epithelial cells. *Biochemistry*, 1996. **35**(19): p. 6157-63.

47. Hwang NS, Varghese S, Lee HJ, Theprungsirikul P, Canver A, Sharma B, and Elisseff J, Response of zonal chondrocytes to extracellular matrix-hydrogels. *FEBS Lett*, 2007. **581**(22): p. 4172-8.
48. Lee DA, Noguchi T, Knight MM, O'Donnell L, Bentley G, and Bader DL, Response of chondrocyte subpopulations cultured within unloaded and loaded agarose. *J Orthop Res*, 1998. **16**(6): p. 726-33.
49. Cheuk YC, Wong MW, Lee KM, and Fu SC, Use of allogeneic scaffold-free chondrocyte pellet in repair of osteochondral defect in a rabbit model. *J Orthop Res*, 2011. **29**(9): p. 1343-50.
50. Wolf F, Candrian C, Wendt D, Farhadi J, Heberer M, Martin I, and Barbero A, Cartilage tissue engineering using pre-aggregated human articular chondrocytes. *Eur Cell Mater*, 2008. **16**: p. 92-9.
51. Vanderploeg EJ, Wilson CG, and Levenston ME, Articular chondrocytes derived from distinct tissue zones differentially respond to in vitro oscillatory tensile loading. *Osteoarthritis Cartilage*, 2008. **16**(10): p. 1228-36.
52. Cohen DL, Malone E, Lipson H, and Bonassar LJ, Direct freeform fabrication of seeded hydrogels in arbitrary geometries. *Tissue Eng*, 2006. **12**(5): p. 1325-35.
53. Guillotin B, Souquet A, Catros S, Duocastella M, Pippenger B, Bellance S, Bareille R, Remy M, Bordenave L, Amedee J, and Guillemot F, Laser assisted bioprinting of engineered tissue with high cell density and microscale organization. *Biomaterials*, 2010. **31**(28): p. 7250-6.
54. Mironov V, Boland T, Trusk T, Forgacs G, and Markwald RR, Organ printing: computer-aided jet-based 3D tissue engineering. *Trends Biotechnol*, 2003. **21**(4): p. 157-61.
55. Lee CH, Cook JL, Mendelson A, Moioli EK, Yao H, and Mao JJ, Regeneration of the articular surface of the rabbit synovial joint by cell homing: a proof of concept study. *Lancet*, 2010. **376**(9739): p. 440-8.
56. Schagemann JC, Chung HW, Mrosek EH, Stone JJ, Fitzsimmons JS, O'Driscoll SW, and Reinholz GG, Poly-epsilon-caprolactone/gel hybrid scaffolds for cartilage tissue engineering. *J Biomed Mater Res A*, 2010. **93**(2): p. 454-63.
57. Schuurman W, Khristov V, Pot MW, van Weeren PR, Dhert WJ, and Malda J, Bioprinting of hybrid tissue constructs with tailorable mechanical properties. *Biofabrication*, 2011. **3**(2): p. 021001.



*INSIGHT IN GROWTH
MECHANISMS*





chapter **FOUR**

MATHEMATICAL MODELLING OF TISSUE FORMATION IN CHONDROCYTE FILTER CULTURES

Chris J. Catt, Wouter Schuurman, Bram G. Sengers, P. René van Weeren,
Wouter J. A. Dhert, Colin P. Please and Jos Malda*

ABSTRACT

In the field of cartilage tissue engineering, filter cultures are a frequently used three-dimensional differentiation model. However, understanding of the governing processes of *in vitro* growth and development of tissue in these models is limited. Therefore, this study aimed to further characterise these processes by means of an approach combining both experimental and applied mathematical methods.

A mathematical model was constructed, consisting of partial differential equations predicting the distribution of cells and glycosaminoglycans (GAGs), as well as the overall thickness of the tissue. Experimental data was collected to allow comparison with the predictions of the simulation and refinement of the initial models. Healthy mature equine chondrocytes were expanded and subsequently seeded on collagen-coated filters and cultured for up to 7 weeks. Resulting samples were characterised biochemically, as well as histologically.

The simulations showed a good representation of the experimentally obtained cell and matrix distribution within the cultures. The mathematical results indicate that the experimental GAG and cell distribution is critically dependent on the rate at which the cell differentiation process takes place, which has important implications for interpreting experimental results. This study demonstrates that large regions of the tissue are inactive in terms of proliferation and growth of the layer. In particular, this would imply that higher seeding densities will not significantly affect the growth rate. A simple mathematical model was developed to predict the observed experimental data and enable interpretation of the principal underlying mechanisms controlling growth-related changes in tissue composition.

INTRODUCTION

The limited self-healing capacity of articular cartilage has made the restoration of cartilage defects an important target in the field of regenerative medicine. However, despite many years of dedicated research, few regenerative approaches have successfully been translated to the clinic thus far (1). Natural articular cartilage tissue is organised in characteristic depth-related zones, each with distinct physicochemical and biological properties and functions, that work together to impart low-friction, wear-resistant behaviour that is characteristic of articular cartilage in diarthrodial joints (2-4). One of the likely reasons for the limited clinical success of regenerative approaches is our current lack of understanding of this specific spatial organization and our inability to induce it in tissue constructs.

During the growth of native articular cartilage cell proliferation and differentiation occur simultaneously (5, 6). The differentiated cells produce collagen and glycosaminoglycans (GAGs), which give structure and body to the tissue. The production of GAGs has been shown to follow the production of early phase collagen, especially of collagen type VI (5), suggesting the long collagen fibres provide the scaffold to the tissue whilst the GAGs provide the bulk to the structure.

In furthering our knowledge about cellular responses and behaviour, *in vitro* models play a significant role. However, two-dimensional (2D) *in vitro* models have limitations with respect to phenotypic cell changes, and most 3D models are poorly understood and generally lack the true native 3D environment (7). Common 3D *in vitro* models for cartilage tissue engineering research include a) the alginate bead culture in which cells are suspended in hydrogel beads (8), b) the aggregate or pellet culture (9), which allows direct cell-cell interactions to further enhance chondrogenic differentiation, and c) the filter culture, in which cells are grown on a permeable filter. Chondrocytes cultured in the last culture system have been demonstrated to synthesise neo-tissue that mimics the extracellular matrix (ECM) found in native cartilage (10). This method has been used to investigate the effects of culture conditions, such as co-cultures of different cell (sub) types or passages (2, 11), or the effect of synovial fluid factors on chondrogenesis (12).

Mathematical simulations can be used to predict biological growth for tissue engineered cartilage (13) and could provide improved understanding of *in vitro* growth in chondrocyte filter cultures and insight into the processes by which it is governed. For example, nutrient uptake and diffusion in cartilage tissue engineering have been extensively studied, using a range of mathematical models (for a review see (14)). These simulations have been extended to account for ECM production on seeded scaffolds (15, 16) or in explants (3). In this paper, we examine the effects of ECM production on the growth of chondrocytes in filter culture and compare the predictions of the mathematical simulations with experimental data. Results demonstrate that cell differentiation rates play a more significant role than nutrient transport.

MATERIALS AND METHODS

Cell isolation and culture

Full thickness healthy articular cartilage was harvested from the condyles and patellofemoral groove of a fresh equine cadaver (age 3 years) under aseptic conditions. After overnight digestion using 0.15% type II collagenase (Worthington Biochemical corporation, Lakewood,

New Jersey, USA) at 37°C, the cell suspension was filtered (100 µm cell strainer, BD Falcon, Bedford, Massachusetts, USA) and washed three times in phosphate-buffered saline (PBS, Invitrogen, Carlsbad, California, USA). Cells were then resuspended in chondrocyte expansion medium (DMEM (Invitrogen) supplemented with 10% Fetal Bovine Serum (FBS, Biowhittaker, Walkersville, Maryland, USA), 100 units/mL penicillin and 100 µg/mL streptomycin (both Invitrogen), and 10 ng/mL FGF-2 (R&D Systems, Minneapolis, Minnesota, USA)) and counted using a hemacytometer.

Chondrocytes were expanded for 10 days in monolayer cultures (5000 cells/cm²) in expansion medium. After expansion, cells were detached using trypsin 0.25% (Invitrogen), washed with PBS, and seeded at a density of 1x10⁶ cells/cm² on Millicell filters (Millipore, Bedford, Massachusetts, USA) (2, 10, 11) that were pre-coated with collagen type I (Sigma-Aldrich, St. Louis, Missouri, USA), and cultured for up to 7 weeks (49 days) in chondrocyte differentiation medium (DMEM supplemented with 0.2 mM ascorbic acid 2-phosphate (Sigma-Aldrich), 0.5% human serum albumin (SeraCare Life Sciences, Milford, Massachusetts, USA), 1x ITS-X (Invitrogen), 100 units/mL penicillin and 100 µg/mL streptomycin, and 5 ng/mL TGF-β2 (R&D Systems). Medium was refreshed twice a week and medium samples were taken and stored for further analysis. Samples of the filter cultures were taken weekly, and then cut in half; one half was processed for histology whilst the other half was used for quantitative assays.

Histological and biochemical analyses

For histology, samples were fixed in formalin, processed through graded alcohol series and embedded in paraffin. Embedded sections were cut to yield 5 µm sections. Sections were stained with Weigert's hematoxylin (Klinipath, Duiven, The Netherlands) and fast green (Merck, Darmstadt, Germany) for cells and with Safranin-O (Merck) for proteoglycans. For biochemical analysis, samples were digested overnight at 56°C in a solution containing 250 µg/mL papain (Sigma-Aldrich). Quantification of total DNA was performed by Quant-iT PicoGreen dsDNA kit (Molecular Probes, Invitrogen) using a spectrofluorometer (Biorad, Hercules, California, USA). The amount of GAGs was determined spectrophotometrically after reaction with dimethylmethylene blue dye (DMMB, Sigma-Aldrich) (17), pH=3.0. Intensity of color change was quantified immediately in a microplate reader (Biorad) by measuring absorbance at 540 and 595 nm. The amount of GAGs was calculated using a standard of chondroitin sulphate C (Sigma-Aldrich) and by calculating the ratio of absorbances.

The tissue sections were examined using a light microscope (Olympus BX51, Hamburg, Germany) to assess the tissue thickness, the distribution of cells and GAGs. Photographs of all samples were then taken using an Olympus DP70 camera.

Image and data analysis

The distribution of cells was derived using image analysis software written for this study in MATLAB (MATLAB V7.9.0.529, MathWorks Inc, Massachusetts, United States). The tissue samples did not grow as perfectly uniform layers, nor did the shape of the membrane remain flat during processing. Throughout the duration of the experiment the width of the cell layer is always at least two orders of magnitude greater than the thickness. Therefore, an appropriate approximation is to study the growth as a flat (one dimensional) layer, expanding in the vertical

direction. Based on this assumption the tissue slices were scaled so that the cell position was taken relative to the vertical distance from the membrane at that point (Figure 1). To do so the images were adjusted so that the lower and upper edges of the tissue were horizontal, assuring no information was lost (as could occur if part of the picture was cut off). The position of each cell was then defined in relation to the adjusted image.

For all time points the pictures of the slices were divided in horizontal bands of approximately $15\ \mu\text{m}$. The number of cells in each band was determined and divided by the averaged volume of the band to determine the density of cells and hence the density distribution through the tissue. The total number of cells through the layer of tissue was also calculated at each time point.

During histological analysis a cell could be included in multiple slices and corrupt the data. To correct for this the observed cell densities were multiplied by a scaling factor, ζ (Table 1). This scaling factor was derived from the analysis of vertical sections of photographed tissue samples with a width equal to the section thickness ($5\ \mu\text{m}$). The number of cells observed was compared to the number of cells whose centre resided in the section to give the ratio ζ . This value is similar to that computed using the approach of (18) and has the advantage of being independent of nucleus diameter.

The intensity of safranin-O staining was measured using image analysis software written for this study in MATLAB (MATLAB V7.9.0.529, MathWorks Inc). The relative distribution of GAGs was determined for each slice and these distributions were averaged to give a single value at each time. Assessing the relationship between the relative distribution of GAGs (as shown by the Safranin-O staining) and the absolute density of GAGs within the tissue is a common problem in biological analysis. We assumed that the concentration of GAGs and intensity of staining are linearly related (19). However, the scaling for this relationship may vary between experiments. Thus, the experimental results for the distribution of GAGs were only compared to the mathematical simulations at the end of the culture period at 49 days and the light intensity to mass of GAG scaling was determined from the weight of GAGs in the tissue from samples taken at that same moment.

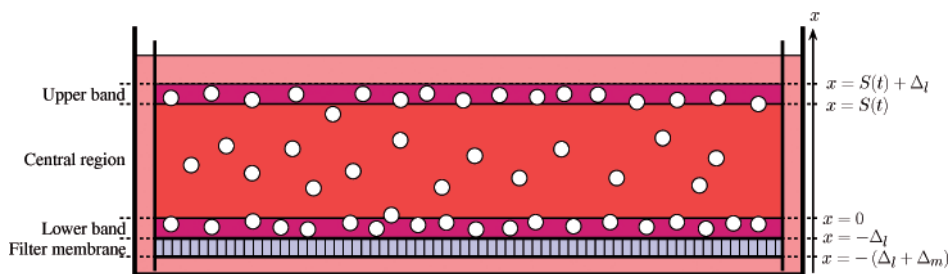


Figure 1. Schematic representation of the idealised model and modelling notation. The tissue layer is broken up into three regions, the lower layer, the central layer and the upper layer. Both the lower and upper layers have constant thickness, Δl . The central layer lies in between these two layers and the thickness of the central layer, $S(t)$, increases over time, t , due to growth. We shall therefore define the position where the lower layer and central layer meet to be at $x = 0$ and the position where the central layer and upper layer meet to be at $x = S(t)$. Beneath the lower layer is a fourth region, the filter membrane, which has thickness Δm . Cells in the upper layer are proliferating whilst those in the lower layer are quiescent. The central layer contains cells producing collagen and GAGs and increases in thickness over time. There are no cells in the filter membrane. The constant thicknesses Δl and Δm are given in Table 1.

Cartilage layer mathematical model

Both our experimental findings and information regarding the growth of cartilage from literature were used as a basis for the mechanistic assumptions used in the mathematical simulation to describe cell movement, cell differentiation and ECM production within the growing tissue structure.

The central assumption of the mathematical model is that the cells are separated by the ECM components that are produced. The ECM found in native cartilage tissue is a complex structure consisting of mainly collagen type II and GAGs in terms of volume, but there are various other components that are found in minor quantities, for instance collagen type VI which is found in the matrix directly around the cells in mature tissue, and throughout the matrix in early *in vitro* tissue formation (5). In this model, we assumed a bimodal ECM composition of collagen (irrespective of type) and GAGs. Therefore, in our simulation, collagen consists of either collagen type II or VI, as a fibrous material that acts to provide strength to the cartilage structure (20). Consequently, collagen was thought of as forming a scaffold in which the cells and GAGs are interspersed.

Histological sections indicated that it was appropriate to construct a model with three distinct layers: the lower band, central region and upper band (Figure 1). Measurements

Table 1. Values of parameters required for mathematical modelling. The values not from the literature are either directly measured or determined by fitting to the experimental results.

Parameter		Value	Units
D_{agg}	Diffusion coefficient of aggregate GAGs (22)	1×10^{-14}	$m^2 s^{-1}$
D_{gag}	Diffusion coefficient of GAGs (16)	1×10^{-11}	$m^2 s^{-1}$
N_{low}	Density of cells in lower band	3.32×10^{14}	cell m^{-3}
N_{up}	Density of cells in upper band	2.66×10^{14}	cell m^{-3}
R_{agg}	Aggregation rate of GAGs	2.05×10^{-2}	s^{-1}
R_{col}	Rate of collagen synthesis	9.75×10^{-15}	$g \text{ cell}^{-1} s^{-1}$
R_{dif}	Rate of cell differentiation (30)	7.10×10^{-6}	s^{-1}
R_{gag}	Rate of GAGs synthesis (30)	3.78×10^{-16}	$g \text{ cell}^{-1} s^{-1}$
F_N	Rate at which cells are added to the central region	3.31×10^3	cell $m^{-2} s^{-1}$
ζ	Cell over count ratio	0.283	
F_N	Flux of cells from upper band	3.31×10^3	cell $m^{-2} s^{-1}$
Col_o	Concentration of collagen (31)	1.23×10^4	$g m^{-3}$
Φ_m	Filter filtration fraction (32)	0.5305	
Δ_l	Height of lower and upper bands	1.5×10^{-5}	m
Δ_m	Height filter membrane	3×10^{-5}	m
N_o	Initial cell density	3.12×10^{14}	cell m^{-3}
C_{aggo}	Initial concentration of GAGs	7.45×10^{-5}	$g m^{-3}$
S_o	Initial height of central region	3.6×10^{-5}	m
α_{cg}	Initial ratio of cell types	0.059	
r	Radius of a cell	7.5×10^{-6}	m

Table 2. Variables used in the mathematical model.

Variable	Description
x	Distance from the bottom of the central region
t	Time
C_{agg}	Concentration of aggregate GAGs
C_{col}	Concentration of collagen
C_{gag}	Concentration of GAGs
N_{col}	Density of cells producing collagen
N_{gag}	Density of cells producing GAGs
U	Velocity of the tissue
Φ	Extracellular volume fraction

indicated that the number of cells in the lower and upper bands was constant and close to the expected density of confluence, hence both were considered to be a single cell (15 μm) thick and have constant cell density, while the central region grows to make up the remaining thickness. The lower band consists of a thin layer of densely packed cells that are situated directly on top of the filter membrane. It was assumed that inhibitory factors prevent these cells from proliferating and creating ECM. Thus, these cells are essentially quiescent, remaining at constant density. Above this is the central region in which the cells are solely focused on ECM production and do not proliferate. Although it is recognised that cells can simultaneously produce collagen and GAGs, to simplify the model we considered separate populations of cells that at any one time can either produce collagen or produce GAGs (5). Thus, the cell population was broken down into collagen producing cells and cells producing GAGs. Furthermore, it was assumed that the fibrous framework for the tissue structure (collagen) must be constructed before it is filled with the ground substance (GAGs). Cells were therefore initially defined as collagen producing cells before differentiating to GAG producing cells, as proposed by (5). Collagen was assumed to be the principal material that determined the distance between cells, while the GAGs were taken to be more passive. Collagen will move with the tissue as the layer expands, while the GAGs will move with the cells and will also be allowed to diffuse through the layer. Mathematical simulations with a single type of GAG were inadequate in predicting both the spatial distribution of GAG in the tissue and the amount of GAG in the surrounding medium. In reality, after secretion by the cell GAGs undergo a self-assembly process to form large aggregates. This has been modelled previously by considering separate mobile and immobilized (*i.e.* bound) GAG (15, 21). Extending the model to include two types of GAG, one smaller that diffuses easily and the other consisting of larger aggregates, which diffuse much slower, gave much better predictions. This simple model assumed that the small GAG would bind to the larger aggregates at a constant rate. In this scenario, growth of the central region will be due to the production of collagen and the GAGs are deemed to adhere to the collagen rather than contribute to the expansion of the layer. Finally, there is an upper band of cells lying on top of the central region. The data indicated that there was only a small but steady increase in the total number of cells in the tissue and for the model it was assumed that this occurred due to constant proliferation in the upper band.

As the upper band has a constant number of cells, the newly formed cells are assumed to immediately migrate into the central region where they will initially produce collagen. This implies that, since the proliferation rate in the upper band is unrestrained and hence constant, the resulting flux of cells into the central region from the upper band is constant and denoted by $F_{N\text{ Pro}}$ (for all other relevant equations and continuity conditions see Figure 9). The regular refreshing of the medium will result in the GAGs being washed away from the upper surface and diffusing out through the filter membrane.

Throughout the whole structure the effect of cell death, due either to necrosis or apoptosis was neglected. The surrounding medium is rich in nutrients and is replaced regularly and hence is assumed to have constant properties. In addition, the size of the tissue remains relatively small throughout the experiment and thus the nutrient concentrations throughout the tissue will be always be high. Therefore, we assumed that the cells will always be able to obtain the energy they require for respiration and the raw materials necessary for ECM production.

The growth of tissue is a complicated process involving, for example, production of ECM constituents, generation of forces between cells, movement of cells through the ECM matrix and remodelling of the ECM. For example, GAG induced swelling forces could contribute to tissue expansion (15). However, in the mathematical model developed here a highly idealised behaviour was assumed with collagen providing the framework that determines the distance between cells. As collagen is produced by cells, the cells will move apart such that the density of collagen within the ECM remains constant. Alternative approaches with far greater mechanistic detail, such as for instance including the forces that develop during growth, would have complicated the model, but were expected not to significantly increase the insight into the general mechanisms involved.

Immediately after being seeded, the cells go through a settling period in which their characteristics greatly differ from those during the later stages of growth. This settling period was not modelled and the modelling simulations began at day seven.

In summary, the assumptions the mathematical model was based on were the following (including the mathematical modelling notation):

- The diameter of the filter is much greater than the thickness of the tissue layer; therefore the mathematical model needs to consider only variations through the thickness of the layer.
- The concentration of nutrients is high and uniform throughout the tissue layer.
- The lower and upper bands remain at a fixed thickness of 15 μm .
- The density of cells in the lower and upper bands is constant, at densities N_{low} and N_{up} respectively.
- Cells in the lower band are quiescent, thus not proliferating or producing ECM.
- Cells in the upper band do not produce ECM, but do proliferate, releasing the newly formed daughter cells into the central region at a constant rate, $F_{N\text{ Pro}}$.
- Cells in the central region do not proliferate or undergo necrosis or apoptosis.
- In the central region newly produced cells first produce collagen and then differentiate at a rate R_{dif} into cells that produce GAGs.
- Collagen and GAGs will be synthesized by a cell at constant rates R_{col} and R_{gag} .

- GAGs will diffuse at a rate D_{gag} and bind to other GAGs at a rate R_{agg} . Once bound GAG will diffuse at a rate D_{agg} .
- The volume growth rate of the tissue at any point is directly proportional to the rate of collagen production.
- Collagen does not diffuse through the tissue.
- Cells will, because of the small size of the neo-tissue, always have sufficient supply of nutrients.

The values of parameters described above are given in Table 1. The diffusion coefficients are representative values based on (22) which shows a range of the order $10^{-10} - 10^{-14} \text{ m}^2\text{sec}^{-1}$ for proteoglycan aggregates. The remaining values were derived from the experimental results.

RESULTS

Experimental results

The averaged thickness of the tissue slices (example shown in Figure 2a) was calculated from the image analysis data and showed a linear increase over time (Figure 2b). Similarly, the adjusted tissue slices (Figure 3a), show a linear increase in the number of cells per slice over time (Figure 3b). Interestingly, this is not the case in both the lower and upper bands, where the cell number is stable. Proliferation occurs solely in the upper band, with cells then migrating to the central region, which leads to an increase in cell numbers in that area (Figure 3c). Furthermore, the total number of cells in the central region of the synthesised tissue increases (Figure 3c), but the expansion of the tissue layer causes a decrease in the relative density of cells in the central region. After 14 days of culture, cell densities (which were calculated using the experimental cell numbers) in the lower $90 \mu\text{m}$ of the tissue, formed on the filter, do not change (Figure 4).

The accumulated mass of GAGs produced and retained by the tissue structure increased linearly with time (Figure 5a). The same was true for the accumulated mass of GAGs released from the tissue in the culture medium (Figure 5b).

Comparison of mathematical model with experimental results

The mathematical model that was developed is described in detail in Appendix A. Initially, the tissue has a high density of cells that produce collagen and GAGs and cause the tissue to expand rapidly, and consequently the cell density decreases within the central region. Cell differentiation then creates a zone of predominantly GAG producing cells in the lower part of the central region of the tissue (Figure 6a). Within this zone collagen production is low and therefore the growth of the tissue is negligible. In the central region above this zone the flux of cells into the central region from the upper band results in a population of cells that predominantly produce collagen (Figure 6b). Thus, close to the upper band the tissue continues to expand (Figure 7) and the cell density continues to drop. Consequently, the sole contributor to the growth of the tissue layer is the region immediately beneath the upper band. Growth is determined by the rate at which cells proliferate to be released into the central region, the differentiation rate of cells and the rate at which cells produce collagen.

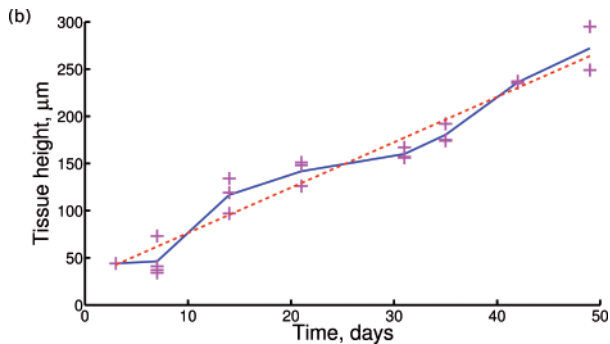
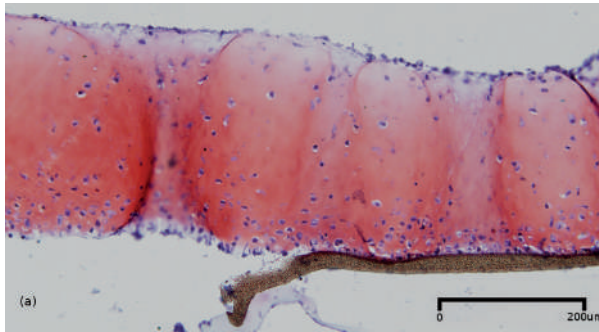


Figure 2. (a) Safranin O staining of the tissue sample at 49 days. The red staining indicates the presence of GAGs. The cells can be seen as darker dots, distributed throughout the tissue but with highest density at the surface of the filter membrane and at the surface of the tissue. The darker strip at the bottom is a remnant of the membrane. (b) Thickness of the tissue slices over time. The experimental data (+), averaged data (—) and a linear fit to the averaged data (- - -) are given. The average thickness of the tissue increases linearly with time ($R^2 = 0.9675$).

The cells in the lower band and central region of the tissue have fully differentiated to cells that produce GAGs (Figure 6a). This results in a high concentration of GAGs accumulating in the lower half of the tissue (Figure 8a) and an even larger amount of GAGs being excreted from the tissue (Figure 5b). GAGs are excreted from the tissue through both upper and lower boundaries. Due to the higher concentration of GAGs close to the filter membrane (Figure 8a), the amount of GAGs diffusing out of the upper surface is similar to that diffusing from the lower surface through the filter membrane (Figure 5b), despite the fact that some inhibition of GAG diffusion by the filter may occur. By implementing the appropriate parameter values the mathematical simulations can generate data that comply with the experimental measurements for both GAG production and the amount of GAGs retained by the tissue construct (Figure 5a). The experimental results show that GAG concentration is highest in the lower half of the tissue and less at the upper and lower boundaries of the tissue. The mathematical simulations confirm this trend, but show a lower value of GAG concentration near the lower boundary (Figure 8b). According to the mathematical model, the overall rate of collagen synthesis, which facilitates separation of the cells, varies through the tissue layer. The cells near the tissue boundaries do not produce any substantial amount of ECM.

The mathematical simulations replicate the experimental data with respect to the distribution of cells (Figure 4). Both show the lower band with a constant density of cells and a central region above this area that expands at a nearly constant rate. To more fully explore the resulting trends in the model behaviour a highly simplified version of the mathematical model

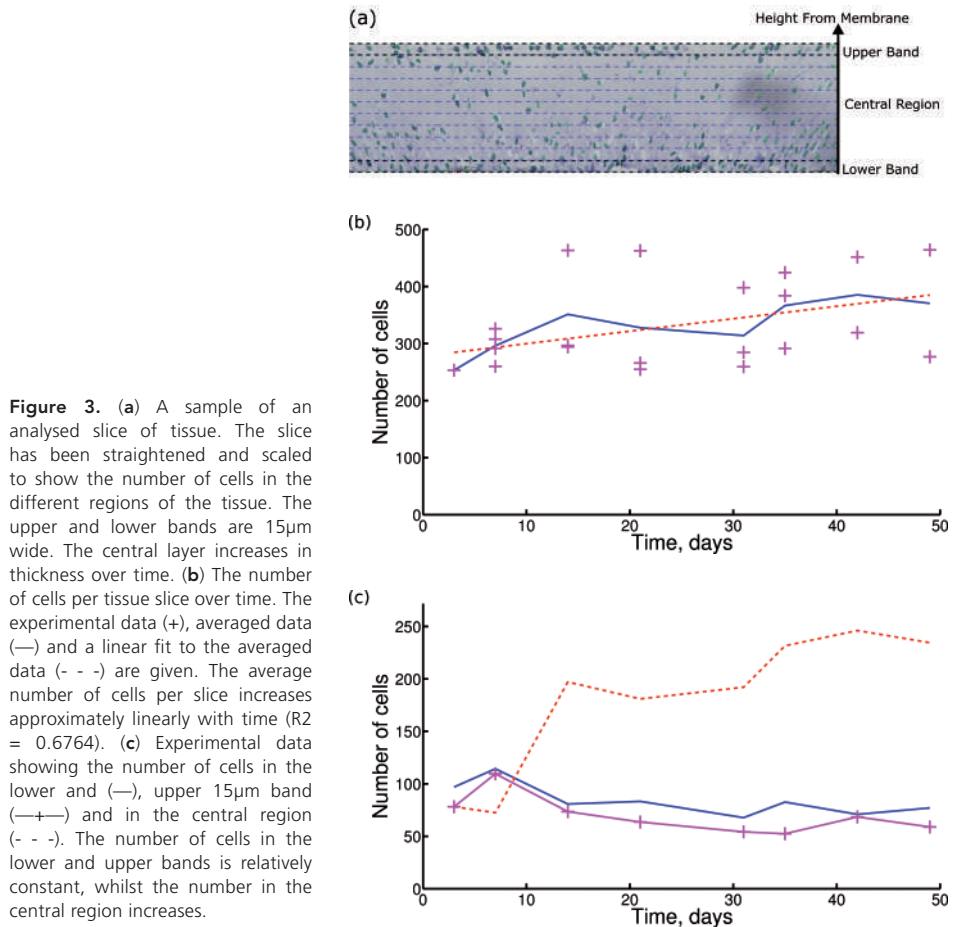


Figure 3. (a) A sample of an analysed slice of tissue. The slice has been straightened and scaled to show the number of cells in the different regions of the tissue. The upper and lower bands are 15μm wide. The central layer increases in thickness over time. (b) The number of cells per tissue slice over time. The experimental data (+), averaged data (—) and a linear fit to the averaged data (- - -) are given. The average number of cells per slice increases approximately linearly with time ($R^2 = 0.6764$). (c) Experimental data showing the number of cells in the lower and (—), upper 15μm band (—+) and in the central region (- - -). The number of cells in the lower and upper bands is relatively constant, whilst the number in the central region increases.

was considered where a very narrow layer immediately below the upper band was considered to travel at constant speed. This travelling wave analysis neglects the GAG and is shown in Figure 10. The solution to this model can be found analytically by changing to coordinates travelling at the constant speed and solving the resulting ordinary differential equations on the infinite region, as indicated on the left of Figure 10. From this simplified model we find that the thickness grows at a speed given by

$$\dot{S} \approx \frac{F_{NPrm}}{N_{up}} \left(1 + \frac{N_{up} R_{col}}{Co_0 R_{diff}} \right) \quad \dot{S} \approx \frac{F_{NPre} R_{col}}{Co_0 R_{diff}}$$

and the growth is primarily in a layer immediately under the upper band of thickness

$$\frac{\dot{S}}{R_{diff}} \approx \frac{F_{NPre} R_{col}}{Co_0 R_{diff}^2}$$

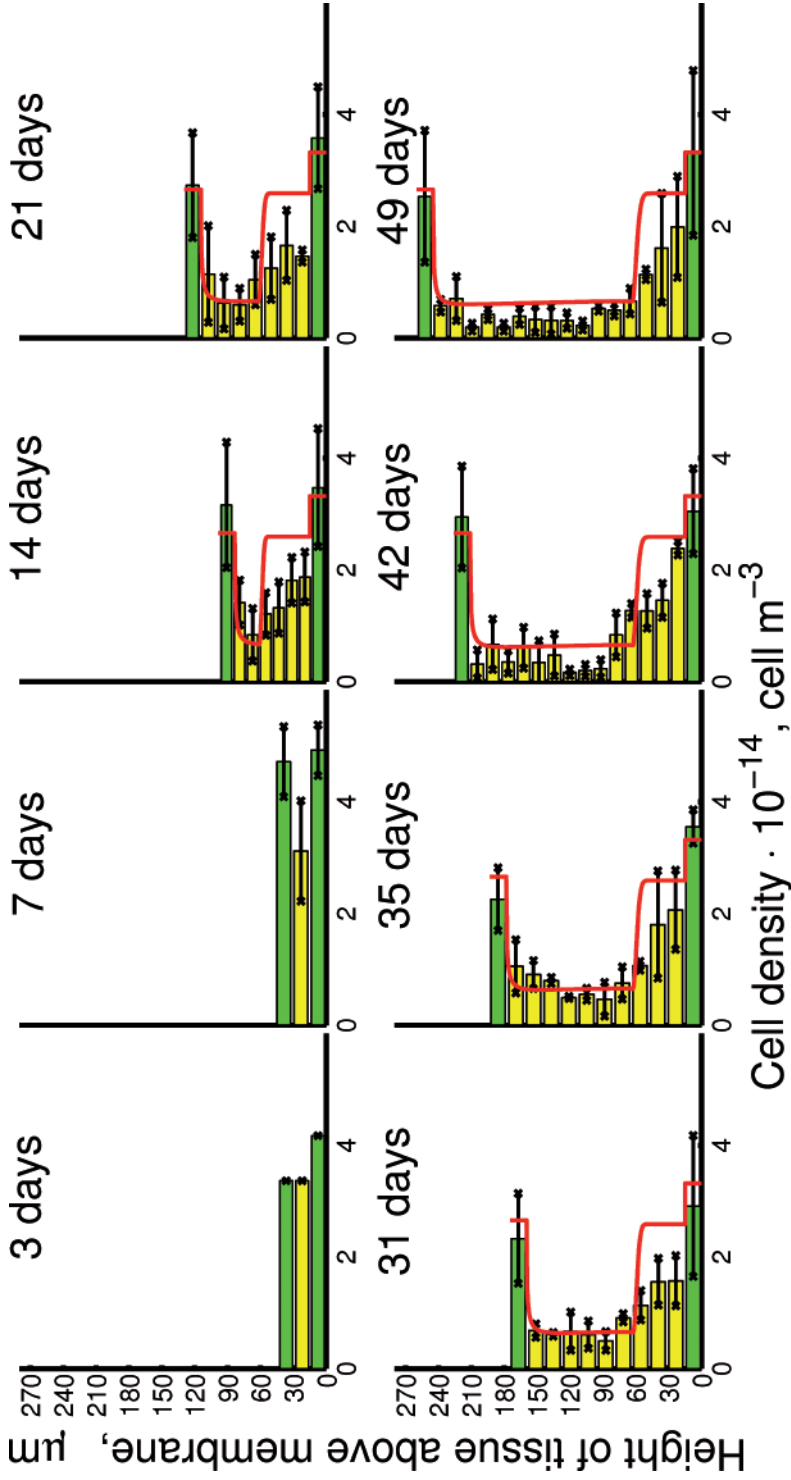
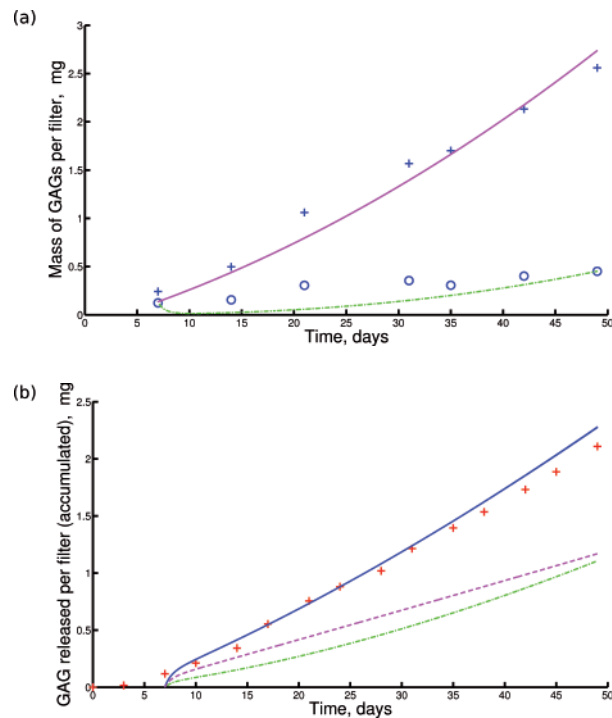


Figure 4. Density of cells within the tissue samples over time. The histograms show the averaged experimental data with the standard deviations (note there is only a single data point for day 3); the continuous line represents the results of the mathematical model. The lowest bar of each histogram represents the cell density next to the membrane in the lower $15\mu\text{m}$ layer. The highest bar represents the cell density in the upper $15\mu\text{m}$ layer next to the tissue surface. The bars in between represent the cell density in the central layer. The thickness of each band in the histograms is approximately $15\mu\text{m}$. After 14 days the cell densities are approximately constant. The mathematical simulations match the experimental results well and show that growth is confined to a region close to the upper band.

Figure 5. (a) Accumulated amount of GAGs produced by the filter (+) and the accumulated mass of GAGs that is retained in the tissue construct (o). Experimental data and results of the mathematical simulations (—, - -) are shown. The increase in the mass of GAGs produced and retained by the tissue construct is approximately linear. (b) Accumulated mass of GAGs released from the tissue layer. Experimental results (+) and results of the mathematical simulation (—) are shown. The mathematical simulations for GAGs released through the filter membrane (- -) and upper surface (-•-) are also shown. The accumulated mass of GAGs released increased approximately linearly with time.



Using the same data as the full model, these simplified results give a speed of $4.3 \mu\text{m}/\text{day}$ and a narrow growth layer of $7 \mu\text{m}$ thick. Here the two parts of the equation for the speed represent growth due to the additional tissue volume created by proliferating cells and the second part by the volume created by production of collagen to move cells apart. The approximations in the subsequent equations are based on the fact that growth due to cell division is negligible compared to the ECM production.

DISCUSSION

We present a mathematical simulation that can accurately predict essential parameters of *in vitro* cartilage tissue growth on filter cultures. Photographs of experimental samples were analysed to determine the distribution and density of cells, thickness of the tissue layer, and distribution of GAGs in the tissue. In addition, GAG content and GAGs released into the culture medium were measured. Based on these values and on existing data from the literature regarding tissue formation, a mathematical model was formulated that could predict the density of cells, production of collagen, production of GAGs and the growth of the tissue layer, taking into account the effects of cell metabolism, cell differentiation, ECM production, and structural growth.

Some interesting observations were made. The density of cells at both the lower and upper surfaces of the tissue remained constant and the amount of cells in the lower band of the tissue did not change after 14 days. The thickness of the tissue, the average cell density and the

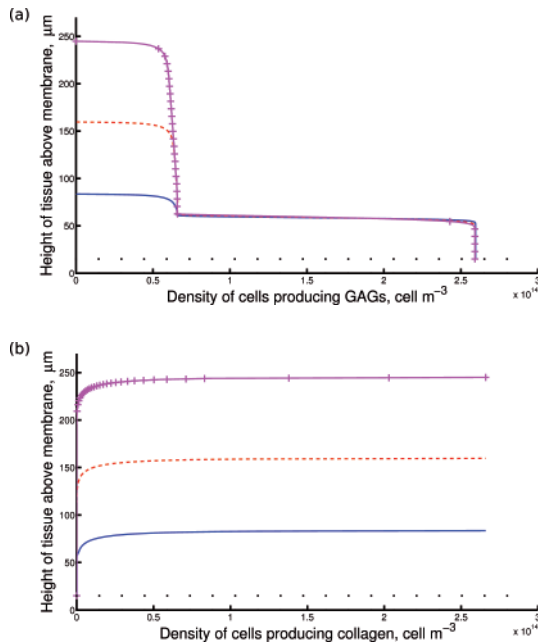


Figure 6. (a) The density of GAG producing cells over the thickness of the central layer, as predicted by the mathematical model, at 14 (—), 31 (---) and 49 days (—+—). The newly formed cells quickly differentiate into cells that produce GAGs, leaving only a low density of GAG producing cells close to the upper layer of the tissue. The left hand section of the graph shows that the density of GAG producing cells in the upper layer of the tissue is relatively low. Subsequently, over a large segment of the tissue (60 μm and above) the density of GAG producing cells is relatively constant. In the middle part the lines are almost horizontal, indicating a very steep increase in GAG producing cells between 50 and 60 μm. In the far right hand section of the graph, it is shown that the density of GAG producing cells, in samples at all time points, is constant within the lowest 50 μm. (b) The density of cells producing collagen, as predicted by the mathematical model, through the central region, at 14 (—), 31 (---) and 49 days (—+—). The cells rapidly differentiate so that only a small region of collagen producing cells is left close to the upper layer, where the maximum density of cells is equal to that in the upper layer, $2.66 \times 10^{14} \text{ cells m}^{-3}$. In both graphs the lower layer is denoted by the horizontal dotted line.

accumulated mass of GAGs released all increased linearly over time. The absolute increase in thickness of the tissue was deemed insufficient to cause gradients in nutrient concentrations that could potentially affect the growth characteristics (23).

This mathematical model shows that the growth of the tissue layer is limited to behaviour in a small region close to the upper surface. The thickness of this “growth layer”, as can be seen from the simplified model, is defined by the differentiation rate of cells, the production rate of collagen and the proliferation rate in the upper band and is far less than the critical distance over which nutrients can diffuse. Furthermore, the mathematical model did not take into account confounding factors such as cell death and ECM degradation. The equations have, however, the potential to be modified to incorporate these effects and thus to study larger tissue structures.

Neither the cells in the lower band nor in the upper band produced ECM, whilst the cells in the lower band were also shown not to proliferate. It is unlikely that this is a result of inefficient nutrient transport, as these two bands are very close to the culture medium that was replenished regularly.

The mathematical simulations confirm that large regions of the tissue are inactive with regard to proliferation and growth of the tissue layer. Cells in the lower half of the layer did not proliferate and ceased collagen production even at high concentrations of nutrients. Only a relatively small region close to the upper surface contributes to the expansion of the tissue and the increase in cell number. Interestingly, a similar phenomenon is observed during cartilage

Figure 7. The velocity of growth of the tissue layer, as predicted by the mathematical model, through the central region at 14 (—), 31 (- -) and 49 days (—+—). Growth is a consequence of collagen production in this model, thus the only region that is expanding is close to the upper layer. The lower layer is denoted by a horizontal dotted line.

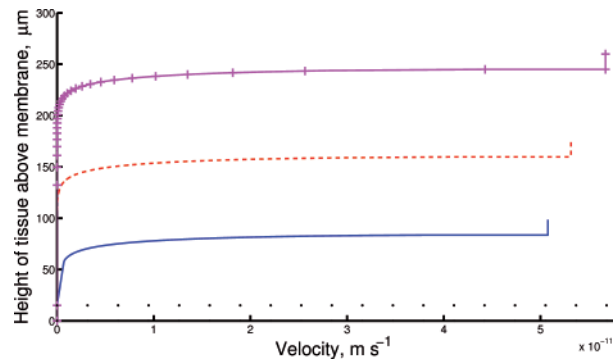
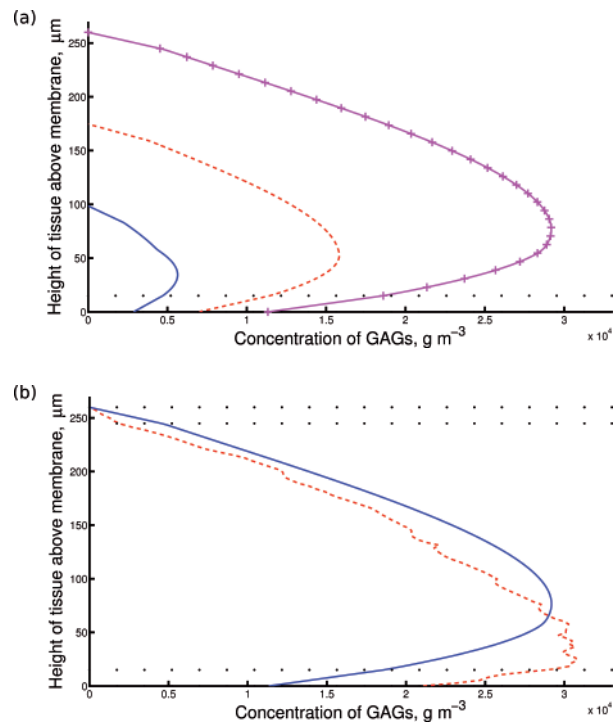


Figure 8. (a) The concentration of unbound and aggregate GAGs through the tissue layer, as predicted by the mathematical model. Results are shown at 14 (—), 31 (- -) and 49 days (—+—). The filter membrane impedes the diffusion of GAGs from the tissue, thus the highest concentration of GAGs is found in the lower regions of the tissue, where the density of cells producing GAGs is also highest. (b) The distribution of GAGs through the tissue layer. A representative of the experimental results (- -) and results of the mathematical simulation are shown at 49 days (—). The filter membrane is resisting the diffusion of GAGs from the lower boundary layer, whilst the GAGs on the top are 'washed' away by the medium. In both graphs the upper and lower bands are denoted by horizontal dotted lines.



growth *in vivo*. In immature tissue, a pool of slowly dividing stem-like cells in the upper layers of the tissue (24) supplies the rapidly dividing daughter-cell pool that feeds the transitional and upper radial zones during the appositional growth of cartilage (25, 26). In mature tissue there are indications that the cells in the upper zones are better suited for the reorganisation of the zonal architecture of the native tissue compared to cells from the deeper zones (27). Based on these observations and given the current efforts to regenerate the zonal architecture of the tissue (28), it can be concluded that the analysis of the temporal tissue development in filter cultures by cells derived from the different zones may be very helpful in generating

$$N_{col} U = N_{col} \dot{S} - F_{N_{pro}}$$

$$N_{gas} = 0$$

$$N_{col} = N_{up}$$

$$C_{gas} = 0$$

$$[F_{gas}] = [F_{ogg}] = 0$$

$$C_{ogg} = 0$$

$$U = 0$$

$$[F_{ogg}] = [F_{ogg}] = 0$$

$$C_{ogg} = 0$$

$$\frac{\partial}{\partial t} (N_{col}) + \frac{\partial}{\partial x} (N_{col} U) = -N_{col} R_{diff}$$

$$\frac{\partial}{\partial t} (N_{gas}) + \frac{\partial}{\partial x} (N_{gas} U) = N_{col} R_{diff}$$

$$\frac{\partial}{\partial t} (\Phi C_{ogg}) + \frac{\partial}{\partial x} (F_{ogg}) = N_{gas} R_{ogg} - C_{ogg} R_{ogg}$$

$$\frac{\partial}{\partial t} (\Phi C_{col}) + \frac{\partial}{\partial x} (F_{col}) = C_{ogg} R_{ogg}$$

$$\frac{\partial U}{\partial x} = \frac{N_{col} R_{col}}{C_{col}}$$

$$C_{col} = Col_0$$

$$\Phi = 1 - \frac{4}{3} \pi r^3 (N_{col} + N_{gas})$$

$$\frac{\partial}{\partial x} (F_{gas}) = 0$$

$$\frac{\partial}{\partial x} (F_{ogg}) = 0$$

$$U = \dot{S}$$

$$C_{col} = Col_0$$

$$\Phi = 1 - \frac{4}{3} \pi r^3 N_{up}$$

Membrane

Lower band

Central region

Upper band

$$-(\Delta_m + \Delta_l)$$

$$-\Delta_l$$

$$0$$

$$S(t)$$

$$S(t) + \Delta_l$$

x

Figure 9. Mathematical model of the four separate regions showing the relevant equations and continuity conditions between regions. Here the brackets [] represent the jump in the quantity across a boundary. The fluxes in each region are given by

$$F_i = \Phi (C_i U - D_i \frac{\partial C_i}{\partial x})$$

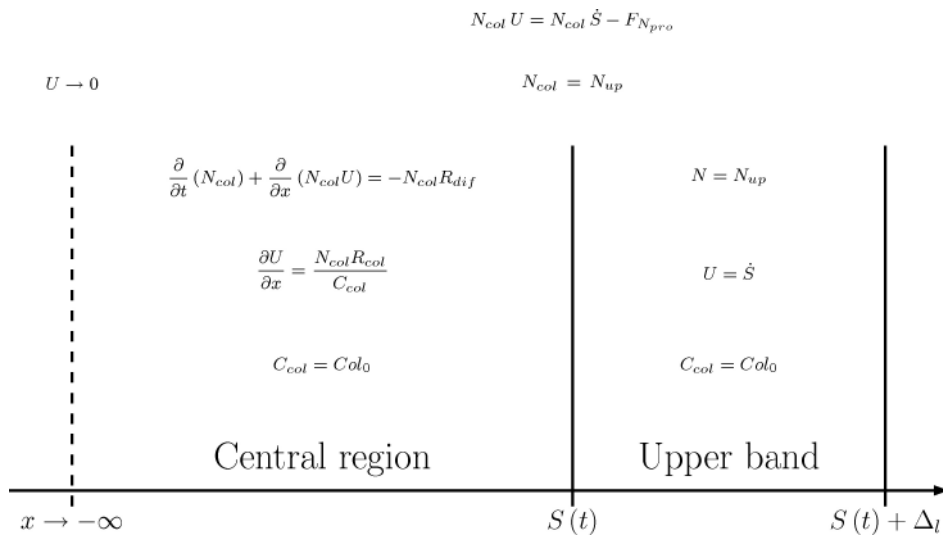


Figure 10. Simplified mathematical model of the very narrow region just below the upper band showing the relevant equations and continuity conditions between regions.

greater insight into the differences between these cell populations. Apart from the behaviour of the different cell types, investigations could target the effects of different culture conditions, including varying glucose concentrations, different oxygen tensions and growth factor levels, which will most likely affect tissue architecture and development. This would further enhance our understanding of the mechanisms involved in the growth of cartilaginous tissue and the mathematical simulations might in the future provide a means for the quick and efficient comparison and optimisation of different culture conditions.

During the first weeks of *in vitro* cartilaginous tissue neo-formation, collagen type VI is the main collagen, and is present throughout the matrix (5). With time, it is replaced by collagen type II, and after 4 weeks, it is basically restricted to the pericellular area. Furthermore, the total amount of collagen decreases with time (5). Because of these two characteristics, we chose not to differentiate between collagen types in our mathematical model, but instead to consider the combined content of collagen types VI and II as the scaffold in which GAGs could spread. Gradually, the balance between collagen type VI and II in the scaffold shifts towards collagen type II.

Both the experimental results and the mathematical simulations contribute to the understanding of *in vitro* tissue growth. The characteristic distributions of cells and GAGs shown in this work have not been described previously. Further, the fact that growth of neocartilage apparently takes place in the upper half of the tissue, while the underlying regions remain relatively inactive, suggests an appositional growth rather than an interstitial growth. It has hitherto been presumed that in native cartilage growth occurs *via* a combination of appositional and interstitial growth (1). Our data show that cell behaviour in the superficial zones is most critical to growth, which has important implications for the engineering of tissue growth. This would indicate that higher seeding densities in filter culture may not result in

significant benefits, in line with observations by Hayes and colleagues (29). In addition, the model indicates directions for future experiments to provide further validation for example, by using biochemical stimulation to modulate the differentiation rate to investigate how this affects growth. The simplified model shows clearly that a faster differentiation rate from collagen producing phenotypes to GAG producing phenotypes will result in a smaller zone where collagen is created just below the upper region and that this will reduce the growth rate of the layer. Similarly reducing the proliferation rate in the upper layer will reduce the number of collagen producing cells and reduce the growth rate.

For the mathematical model used in this study several assumptions were made. These assumptions may need refining in future simulations as more experimental data becomes available, in particular with respect to the mechanisms of collagen production, cell differentiation and ECM construction, thus providing further insight into the natural development of the tissue layer.

CONCLUSION

The mathematical simulations developed in this study showed a good correlation with the results from the tissue cultures. It was shown that the thickness of the tissue increases at a constant rate due to the local expansion of the tissue close to the upper tissue surface, as opposed to uniform growth throughout. The restriction of growth to regions close to the tissue surface is governed by the rate at which cells change from a state dominated by the production of matrix components allowing rapid tissue expansion (e.g. collagen), to a state characterised by slower growth and higher production of GAGs. It was shown that GAGs were excreted at a constant rate due to diffusion and dependent on the aggregation rate. There are large regions within the tissue that are quiescent and where growth is negligible. It is concluded that the use of mathematical models can closely replicate experimental data and hence are useful for the interpretation and understanding of culture systems. Mathematical modelling may offer significant potential for the optimisation of cartilage regeneration strategies.

REFERENCES

1. Williams GM, Klisch SM, and Sah RL, Bioengineering cartilage growth, maturation, and form. *Pediatric Research*, 2008. **63**(5): p. 527-534.
2. Hayes AJ, Hall A, Brown L, Tubo R, and Caterson B, Macromolecular organization and in vitro growth characteristics of scaffold-free neocartilage grafts. *Journal of Histochemistry and Cytochemistry*, 2007. **55**(8): p. 853-866.
3. Klisch SM, Asanbaeva A, Oungouljian SR, Masuda K, Eugene JMAT, Davol A, and Sah RL, A cartilage growth mixture model with collagen remodeling: validation protocols. *Journal of Biomechanical Engineering*, 2008. **130**: p. 031006.
4. Schinagl RM, Gurskis D, Chen AC, and Sah RL, Depth-dependent confined compression modulus of full-thickness bovine articular cartilage. *Journal of Orthopaedic Research*, 1997. **15**(4): p. 499-506.
5. Ofek G, Revell CM, Hu JC, Allison DD, Grande-Allen KJ, and Athanasiou KA, Matrix development in self-assembly of articular cartilage. *PLoS ONE*, 2008. **3**(7): p. e2795.
6. Park K, Huang J, Azar F, Jin RL, Min BH, Han DK, and Hasty K, Scaffold-free, engineered porcine cartilage construct for cartilage defect repair in vitro and in vivo study. *Artificial Organs*, 2006. **30**(8): p. 586-596.
7. Rouwkema J, Gibbs S, Lutolf MP, Martin I, Vunjak-Novakovic G, and Malda J, In vitro platforms for tissue engineering: implications for basic research and clinical translation. *J Tissue Eng Regen Med*, 2011. **5**(8): p. e164-7.

8. Guo J, Jourdan GW, and Maccallum DK, Culture and growth characteristics of chondrocytes encapsulated in alginate beads. *Connective Tissue Research*, 1989. **19**(2): p. 277-297.
9. Kato Y, Iwamoto M, Koike T, Suzuki F, and Takano Y, Terminal differentiation and calcification in rabbit chondrocyte cultures grown in centrifuge tubes: regulation by transforming growth factor beta and serum factors. *Proceedings of the National Academy of Sciences of the United States of America*, 1988. **85**(24): p. 9552-9556.
10. Yang KGA, Saris DBF, Geuze RE, Helm YJMVD, Rijen MHPV, Verbout AJ, Dhert WJA, and Creemers LB, Impact of expansion and redifferentiation conditions on chondrogenic capacity of cultured chondrocytes. *Tissue Engineering*, 2006. **12**(9): p. 2435-2447.
11. Taylor DW, Ahmed N, Gan L, Gross AE, and Kandel RA, Proteoglycan and collagen accumulation by passaged chondrocytes can be enhanced through side-by-side culture with primary chondrocytes. *Tissue Engineering Part A*, 2009. **16**(2): p. 643-651.
12. Yang KGA, Saris D, Verbout A, Creemers L, and Dhert W, The effect of synovial fluid from injured knee joints on in vitro chondrogenesis. *Tissue Engineering*, 2006. **12**(10): p. 2957-2964.
13. Galban CJ and Locke BR, Analysis of cell-growth in a polymer scaffold using a moving boundary approach. *Biotechnology and Bioengineering*, 1997. **56**(4): p. 422-432.
14. Sengers BG, Taylor M, Please CP, and Oreffo ROC, Computational modelling of cell spreading and tissue regeneration in porous scaffolds. *Biomaterials*, 2007. **28**(10): p. 1926-1940.
15. Nikolaev NI, Obradovic B, Versteeg HK, Lemon G, and Williams DJ, A validated model of GAG deposition, cell distribution, and growth of tissue engineered cartilage cultured in a rotating bioreactor. *Biotechnol Bioeng*, 2010. **105**(4): p. 842-53.
16. Obradovic B, Meldon JH, Freed LE, and Vunjak-Novakovic G, Glycosaminoglycan deposition in engineered cartilage: experiments and mathematical model. *AIChE Journal*, 2000. **46**(9): p. 1860-1871.
17. Farndale RW, Buttle DJ, and Barrett AJ, Improved quantitation and discrimination of sulphated glycosaminoglycans by use of dimethylmethylene blue. *Biochimica et Biophysica Acta (BBA)-General Subjects*, 1986. **883**(2): p. 173-177.
18. Stockwell RA, The interrelationship of cell density and cartilage thickness in mammalian articular cartilage. *Journal of Anatomy*, 1971. **109**(3): p. 411.
19. Martin I, Obradovic B, Freed LE, and Vunjak-Novakovic G, Method for quantitative analysis of glycosaminoglycan distribution in cultured natural and engineered cartilage. *Annals of biomedical engineering*, 1999. **27**(5): p. 656-662.
20. Davies CdL, Berk DA, Pluen A, and Jain RK, Comparison of IgG diffusion and extracellular matrix composition in rhabdomyosarcomas grown in mice versus in vitro as spheroids reveals the role of host stromal cells. *British Journal of Cancer*, 2002. **86**(10): p. 1639-1644.
21. DiMicco M, A. and Sah RL, Dependence of cartilage matrix composition on biosynthesis, diffusion and reaction. *Transport Porous Med*, 2003. **50**: p. 57-73.
22. Comper WD and Williams RP, Hydrodynamics of concentrated proteoglycan solutions. *Journal of Biological Chemistry*, 1987. **262**(28): p. 13464-13471.
23. Malda J, Rouwkema J, Martens DE, Le Comte EP, Kooy FK, Tramper J, Van Blitterswijk CA, and Riesle J, Oxygen gradients in tissue-engineered PEGT/PBT cartilaginous constructs: measurement and modeling. *Biotechnology and Bioengineering*, 2004. **86**(1): p. 9-18.
24. Dowthwaite GP, Bishop JC, Redman SN, Khan IM, Rooney P, Evans D, Haughton L, Bayram Z, Boyer S, and Thomson B, The surface of articular cartilage contains a progenitor cell population. *Journal of cell science*, 2004. **117**(Pt 6): p. 889-897.
25. Hunziker EB, Kapfinger E, and Geiss J, The structural architecture of adult mammalian articular cartilage evolves by a synchronized process of tissue resorption and neof ormation during postnatal development. *Osteoarthritis and Cartilage*, 2007. **15**(4): p. 403-413.
26. Hayes AJ, MacPherson S, Morrison H, Dowthwaite G, and Archer CW, The development of articular cartilage: evidence for an appositional growth mechanism. *Anatomy and embryology*, 2001. **203**(6): p. 469-479.
27. Hayes AJ, Hall A, Cheung I, Brown L, Tubo R, and Catterson B, Surface zone but not deep zone chondrocytes reorganize zonal architecture of articular cartilage grafts grown in vitro. *Transactions Orthopaedic Research Society*, 2005. **30**.
28. Klein TJ, Malda J, Sah RL, and Huttmacher DW, Tissue engineering of articular cartilage with biomimetic zones. *Tissue Engineering Part B: Reviews*, 2009. **15**(2): p. 143-157.
29. Hayes AJ, Hall A, Brown L, Tubo R, and Catterson B, Macromolecular organization and in vitro growth characteristics of scaffold-free neocartilage grafts. *Journal of Histochemistry and Cytochemistry*, 2007. **55**(8): p. 853-66.
30. Sengers BG, Modeling the development of tissue engineered cartilage. 2005, Technische Universiteit Eindhoven; the Netherlands.
31. Freed L, Hollander A, Martin I, Barry J, Langer R, and Vunjak-Novakovic G, Chondrogenesis in a cell-polymer-bioreactor system. *Exp Cell Res*, 1998. **240**(1): p. 58-65.
32. Millipore, Millicell cell culture insert. <http://www.millipore.com/catalogue/item/picm01250>, 2009.

APPENDIX A

The full system of equations used to mathematically model the tissue is shown in Figure 9 with the physical description of the variables given in Table 2. The initial conditions used to solve the model are that at $t = 0$,

4

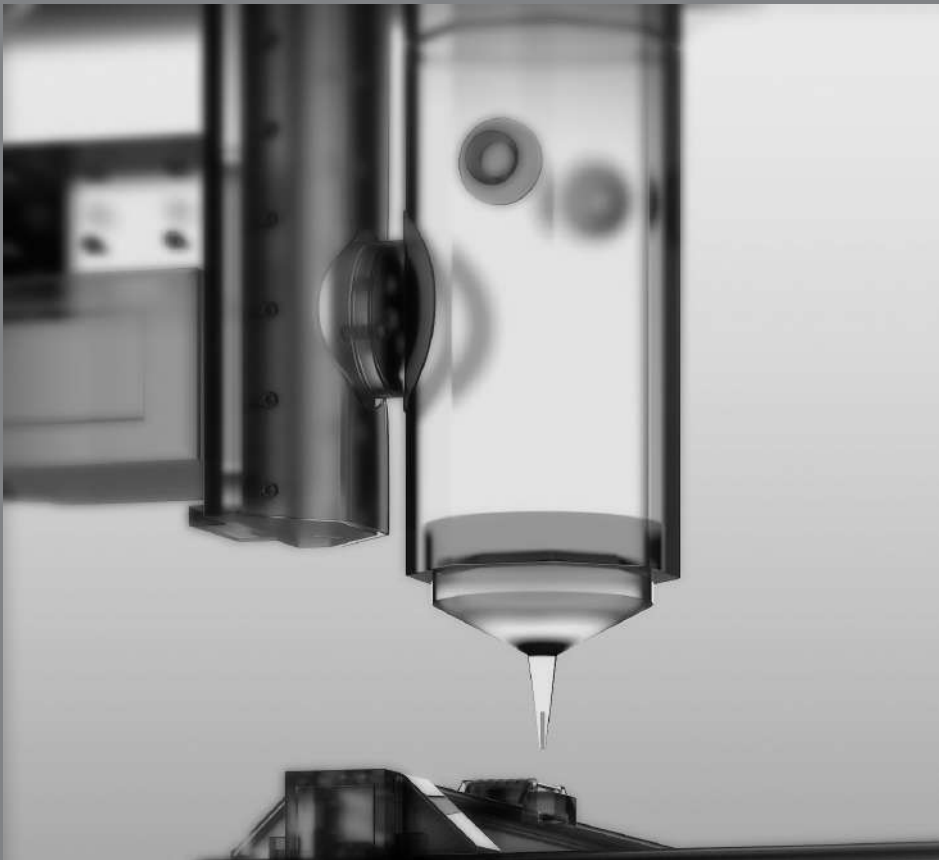
$$N_{col} = \alpha_{cg} N_{o'}, \quad N_{gag} = (1 - \alpha_{cg}) N_{o'}, \quad C_{gag} = 0, \quad C_{agg} = C_{agg0} \quad \text{and} \quad S = S_0.$$

All parameters used in the simulations are given in Table 1.

The system of equations, with corresponding boundary condition, defined in the filter membrane, the lower band and in the upper band can be solved analytically. The system of modelling equations for the central region were solved numerically in MATLAB (The MathWorks, 2009). To incorporate the moving boundary the equations were transformed from the original expanding domain $x \in [0, S(t)]$ to a stationary coordinate frame, $\eta \in [0, 1)$, using the transformation $x = \eta S(t)$ and $t = \tau$. The transformed system of equations was then rearranged into conservation form. Using a finite difference method the system of partial differential equations was discretised centrally in space. The backward Euler method was then used to discretise in time before solving at each time step using Newton's method. At each iteration the Jacobian was updated using Broyden's method.



*THE DEVELOPMENT
OF THE CONCEPT
OF BIOPRINTING*





chapter **FIVE**

BIOFABRICATION OF OSTEOCHONDRAL TISSUE EQUIVALENTS BY PRINTING TOPOLOGICALLY DEFINED, CELL-LADEN HYDROGEL SCAFFOLDS

Wouter Schuurman, Natalja E. Fedorovich, Hans M. Wijnberg, Henk-Jan Prins,
P. René van Weeren, Jos Malda, Jacqueline Alblas, Wouter J. A. Dhert

Wouter Schuurman, Natalja Fedorovich contributed equally to the work described

ABSTRACT

Osteochondral defects are prone to induce osteoarthritic degenerative changes. Many tissue-engineering approaches that aim to generate osteochondral implants suffer from poor tissue formation and compromised integration. This illustrates the need for further improvement of heterogeneous tissue constructs. Engineering of these structures is expected to profit from strategies addressing the complexity of tissue organization and the simultaneous use of multiple cell types. Moreover, this enables the investigation of the effects of three-dimensional (3D) organization and architecture on tissue function.

In the present study, we characterize the use of a 3D fiber deposition (3DF) technique for the fabrication of cell-laden, heterogeneous hydrogel constructs for potential use as osteochondral grafts. Changing fiber spacing or angle of fiber deposition, yielded scaffolds of varying porosity and elastic modulus. We encapsulated and printed fluorescently labeled human chondrocytes and osteogenic progenitors in alginate hydrogel yielding scaffolds of 1x2cm with different parts for both cell types. Cell viability remained high throughout the printing process, and cells remained in their compartment of the printed scaffold for the whole culture period. Moreover, distinctive tissue formation was observed, both *in vitro* after 3 weeks and *in vivo* (6 weeks subcutaneously in immunodeficient mice), at different locations within one construct. These results demonstrate the possibility of manufacturing viable cm-scaled structured tissues by the 3D fiber deposition technique, which could potentially be used for the repair of osteochondral defects.

INTRODUCTION

Osteochondral defects, affecting both articular cartilage and the underlying subchondral bone, are prone to induce osteoarthritic degenerative changes over time (1). Current strategies to restore the biological and mechanical functionality of the joint include microfracture and mosaicplasty (autologous osteochondral grafting) (2-5), but their clinical use suffers from several limitations, including compromised cartilage tissue formation and donor site morbidity (6). Furthermore, in mosaicplasty it is difficult to match the shape of the injured site (6). Current approaches for the engineering of osteochondral grafts suffer from poor tissue formation and compromised integration at the interface between the cartilage and bone layers (7-9), and between osteochondral graft and host tissue (10), advocating the need for further improvement of these techniques.

An important focus in current cell-based tissue engineering lies on the development of engineered osteochondral tissues with design strategies that closely mimic the complex structure of matrix, cells and bioactive factors assorted in a distinct spatiotemporal order inside native tissue (11-13). Engineered (osteochondral) tissues can profit from the synergistic effects of combined growth factor delivery and heterotypic cell interactions on extracellular matrix (ECM) formation both *in vitro* and *in vivo* (14-16). This bio-mimicking approach is expected to enhance graft functionality, render suitable mechanical properties to the engineered tissue (17, 18), and enhance the regenerative process. This was previously illustrated by the use of bilayered (hydrogel) scaffolds laden with multipotent stromal cells (MSC) and chondrocytes, which supports the integration between the two layers (14-16, 19, 20). For a further review of the literature on osteochondral implants, see Martin et al. (6) and O'Shea et al. (21).

Organ- or tissue printing by 3D fiber deposition (3DF) is an innovative approach in regenerative medicine, based on layered deposition of cell-laden hydrogel strands and is derived from rapid-prototyping (RP) technology. With RP, 3D scaffolds with highly reproducible architecture (size, shape, porosity, interconnectivity, pore-geometry and orientation) and compositional variation can be created (22). The porosity of the implants is easily tailored, which is important for mechanical and cell/tissue conductive properties. Interconnected porosity is of particular importance since it facilitates nutrient supply and waste product removal (23) and allows ingrowth of blood vessels (24). Using 3DF, living cells can be incorporated into the printed construct, creating grafts that further recapitulate the intricate 3D structure of cells and matrix in natural tissues (25).

The aim of the present study is to build and characterize 3D structures for application in osteochondral tissue engineering and to validate organized cell placement inside printed grafts *in vitro* and *in vivo*. By combining human chondrocytes and human osteogenic progenitors with alginate hydrogel - a widely-used polysaccharide that supports both chondrogenic and osteogenic differentiation (26) - we printed porous, heterogeneous constructs. We tested the design of various heterogeneous scaffolds, and tailored the porosity and elastic modulus of grafts by modulating the distance between the strands and their configuration. The ensuing hybrid grafts were characterized for cell performance *in vitro* and for tissue development *in vivo*.

MATERIALS AND METHODS

Hydrogel preparation and viscosity measurements

High-viscosity alginate powder (International Specialty Products, ISP, Memmingen, Germany) was autoclaved and subsequently mixed (10% (w/v)) overnight at 37°C either with MSC expansion medium ((α MEM (Invitrogen) supplemented with 10% FBS (Lonza, Basel, Switzerland), 0.1 mM ascorbic acid 2-phosphate (AsAP; Sigma-Aldrich, Zwijndrecht, The Netherlands), 2 mM L-glutamine (Glutamax, Invitrogen), and 100 U/ml penicillin, 100 mg/ml streptomycin (Invitrogen)), or osteogenic differentiation medium (MSC expansion medium supplemented with 10⁻⁸ M dexamethasone (Sigma-Aldrich) and 10 mM β -glycerophosphate (Sigma-Aldrich)), or chondrogenic differentiation medium (DMEM (Invitrogen) supplemented with 0.2 mM AsAP (Sigma-Aldrich), 0.5% human serum albumin (SeraCare Life Sciences, Milford, USA), 1% (v/v) insulin-transferrin-selenium mixture (ITS-X, Invitrogen), 100 U/ml penicillin, 100 μ g/ml streptomycin and 5 ng/ml TGF- β 2 (R&D Systems, Abingdon, United Kingdom)). Alginate was crosslinked with 102 mM aqueous CaCl₂ solution supplemented with 10 mM HEPES (pH 7.4, Invitrogen, Carlsbad, USA) for 15 minutes.

To determine the viscosity of the 10% (w/v) alginate, rheology analysis was performed on an ARG2 1000N rheometer (TA Instruments, New Castle, USA) using a cone-plate geometry (steel, 40 mm diameter with an angle of 2°) at 4°C. Shear rates between 1/s and 1500/s were applied for ten minutes.

3D fiber deposition presets

The BioScaffolder pneumatic dispensing system (SYS+ENG, Germany) was used for 3D printing of hydrogel scaffolds. The prototype of this system is described in more detail elsewhere (25, 27). Briefly, the BioScaffolder is a three-axis dispensing machine, which builds 3D constructs by coordinating the motion of a pneumatic syringe dispenser (Supplementary Figure 1). The dispenser deposits extrudate consisting of hydrogel either or not supplemented with cells on a stationary platform. Models of the scaffolds are loaded via computer-aided design/computer-aided manufacturing (CAD/CAM) software, and translated for layer-by-layer fiber deposition by the machine (Figure 1).

Effect of nozzle diameter, deposition speed and pressure, and fiber orientation

The inner nozzle diameter, deposition speed and pressure were varied between, respectively, 210-1610 μ m, 100 and 300 mm/min and 0.1 and 0.2 MPa in order to assess their influence on strand size. Ten-layer rectangular 3D scaffolds of 10x10 mm with spacing between fibers of 0.8- 2.5 mm and a layer thickness of 100 μ m were constructed and subsequently crosslinked in CaCl₂ solution as indicated.

Fiber orientation was changed by plotting fibers with 45° or 90° angle steps between two successive layers (strand orientation (SO)45 and (SO)90, respectively). Flow rate of the hydrogel through a 210 μ m inner nozzle diameter needle was determined for pressures of 0.15 - 0.6 MPa, by measuring the amount of extruded material per second (flow rate in ml/s). Shear stress was then determined according to the formula below, in which Q is flow rate (mm³/s), r is radius of the needle (mm) and h is the viscosity (Pa*s): $(4Q / \pi r^3) h = \text{shear stress}$.

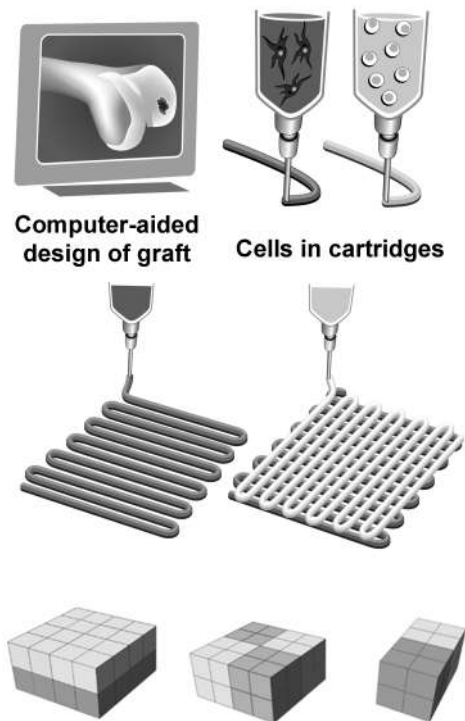


Figure 1. Three-dimensional fiber deposition and characterization of the printing parameters. Schematic representation of tissue printing using various cell types; the design of a construct is translated to a robot arm that drives a cartridge loaded with a cell-hydrogel mixture and extrudes fibers in a layered fashion; the bottom panel represents various scaffold designs used in this study.

Mechanical analysis of printed scaffolds of different porosity and strand orientation

Alginate scaffolds of 7x7x0.8 mm (w_xl_xh) were prepared by varying the strand distance (0.8 mm, 1.5 mm, 2 mm and 2.5 mm at (SO)90), i.e. 90° relative to the underlying strand) and (SO)90 and (SO) 45 at 2 mm strand diameter). Subsequently, the scaffolds were crosslinked as described above.

Porosity was estimated by comparing the weight of the porous scaffolds to the weight of non-porous controls. The stiffness of the scaffolds was measured at room temperature using a dynamic mechanical analyzer (DMA 2980, TA Instruments) in controlled force mode. Scaffolds were placed between the parallel plates and a static force was applied between 0 and 1 N, and varied at a rate of 0.1 N/min. The Young's modulus (E) was determined as described previously (28), by measuring the variation of stress/strain ratio.

Deposition of acellular heterogeneous scaffolds

Heterogeneous scaffolds consisting of two different materials were designed, as illustrated in Figure 1. Alginate hydrogel was left translucent or stained with fast green, methylene blue or basic fuchsin (pink) for illustration purposes and loaded into the BioScaffolder. Unless stated otherwise, an inner nozzle diameter of 420 μm was used, the speed of deposition was set at 300 mm/min and the pneumatic pressure was set at 0.175 MPa to yield uniform, continuous extrusion of strands.

Cells

Human multipotent stromal cells (MSCs) were isolated from bone marrow aspirates, obtained from donors undergoing hip arthroplasty after informed consent with approval of the local medical ethical committee, and culture-expanded as described previously (29). Briefly, aspirates were resuspended by using 20-gauge needles, plated at a density of 5×10^5 cells per square centimeter and cultured in MSC expansion medium supplemented with 1 ng/ml recombinant human basic fibroblast growth factor ((rhFGF2), 233-FB, R&D Systems). Medium was refreshed twice a week and cells were used for further subculturing. MSCs passage 3-4 were used in these experiments.

Human articular chondrocytes (Chs) were isolated from cartilage, after informed consent with approval of the local medical ethical committee, from patients undergoing total knee arthroplasty. Cartilage was digested overnight using 0.15% collagenase type II (Worthington Biochemical, Lakewood, USA) at 37°C. The cell suspension was filtered through a 100 mm cell strainer and washed in phosphate buffered saline (PBS) (Invitrogen). Cells were resuspended in chondrocyte expansion medium (DMEM (Invitrogen), supplemented with 10% FBS (Biowhittaker), 100 U/ml penicillin, 100 µg/mL streptomycin (Invitrogen) and 10 ng mL rhFGF2 (R&D Systems). Cells were then counted and seeded at a density of 5000 cells/cm² in expansion medium. For chondrocyte redifferentiation (30) after ten days, the chondrocytes were detached using 0.25% trypsin (Invitrogen) and stored in liquid nitrogen until further use. Expanded chondrocytes were combined with alginate (2% (w/w) in differentiation medium) (31) at a density of 1×10^7 cells/ml. To create alginate beads, this solution was dripped with a 23G needle into 102 mM CaCl₂ solution supplemented with 10 mM HEPES pH 7.4 (Invitrogen). The beads were then cultured in chondrogenic differentiation medium for five days and subsequently, cells were retrieved from the beads using sterile citrate buffer (150 mM sodium chloride, 55 mM sodium citrate, pH = 7.4) for 15 minutes.

Viability analysis

To test the effect of shear stresses during the printing process on cell viability, hydrogel-embedded MSCs (5×10^6 cells/ml gel) were extruded through a needle with an inner nozzle diameter of 210 µm at various pressure settings (0.175-0.5 MPa). Unprinted cell-laden alginate was used as a control. The samples (n=5 per group) were incubated in CaCl₂ solution and cultured for five or 24 hours in expansion medium. The viability of the cells was determined by a LIVE/DEAD assay (Molecular Probes MP03224, Eugene, USA) according to the manufacturer's recommendations. For this, five samples per condition were measured using a microscope equipped with an epifluorescence set-up, excitation/emission setting of 488/530 nm to detect green fluorescence and 530/580 nm to detect red cells (Leica DM IRBE, Germany). Three randomly selected fields per sample were taken and cell viability was calculated as the average ratio of vital over total cells in a sample, determined from four randomly chosen fields per sample.

Fluorescent labeling and tracing of cells

Cells were fluorescently labeled for spatial distribution-analysis. For this, Chs were incubated with PKH26 (20 µM, red; Sigma-Aldrich) and MSCs with CFSE (1 µM, green; Molecular Probes, Leiden, The Netherlands). The presence of fluorescent cells was analyzed directly after printing and after 14 and 21 days under a fluorescence microscope (Olympus BX51 microscope, Olympus

DP70 camera, Hamburg, Germany) equipped with an epifluorescence set-up, excitation/emission setting of 488/530 nm to detect green-fluorescent MSCs or 530/580 nm to detect red Chs (Leica DM IRBE, Solms, Germany).

Deposition of cell-laden scaffolds

To develop dual, heterogeneous scaffolds for *in vitro* use, fluorescently labeled MSCs and Chs were separately mixed with alginate at 5×10^6 cells/ml and 3×10^6 cells/ml respectively. A rectangular (1x2cm), ten-layer scaffold was designed, and consisted of two parts (1x1cm) directly adjacent to each other. The BioScaffolder interchanged the cooled cartridges (4°C) with the loaded syringes every two layers. The scaffolds were subsequently crosslinked in CaCl₂ solution.

For building heterogeneous scaffolds for *in vivo* implantation, an analogous protocol was followed: Chs (1×10^7 cells/ml) were mixed with alginate, and MSCs (1×10^7 cells/ml) were mixed with alginate supplemented with 10% (w/v) osteoinductive biphasic calcium phosphate particles (BCPs, 80 ± 5 % (w/v) hydroxyapatite and 20 ± 5 % (w/v) β -tricalciumphosphate; total porosity 70 ± 5 %, macroporosity 55 ± 5 % and microporosity 20 ± 5 %). Irregularly shaped BCP particles (kindly provided by Progentix Orthobiology BV, Bilthoven, the Netherlands) were sintered at 1150°C and ranged from 106 to 212 μ m in size. Acellular printed grafts served as negative controls. After printing, the constructs were cultured overnight and subcutaneously implanted in mice (see section on *in vivo* implantation).

Heterogeneous scaffold culture and embedding

Heterogeneous scaffolds were cultured in a 1:1 mixture of osteogenic and chondrogenic differentiation medium for a period of 7 and 21 days ($n=4$ scaffolds for each time point). Scaffolds were maintained in a humidified incubator at 5% CO₂ and 37°C, and the medium was changed every 3 days. Additionally, the scaffolds were incubated for 15 minutes in 102 mM CaCl₂ once a week to prevent gel weakening (unpublished observation, WS). Upon termination of the experiment, half of the experimental set of scaffolds was embedded in Tissue-Tek® (Sakura Finetek, Alphen aan den Rijn, The Netherlands) and the others were dehydrated through graded ethanol series and embedded in paraffin. Samples were cut to yield 5 mm sections.

In vivo implantation

For *in vivo* assessment, printed Ch/MSC-laden grafts ($n=6$) and acellular constructs consisting of an alginate part and an alginate/BCP part ($n=4$) were cultured in proliferation medium for 24 hours prior to implantation. Female nude mice (NMRI-Foxnu, Charles River, Brussels, Belgium), 6-weeks old, were anaesthetized with 1.5% isoflurane, after which the implants were placed in separate subcutaneous dorsal pockets. The incisions were closed using a Vicryl 5-0 suture. The animals were postoperatively treated with the analgesic buprenorphine (0.05 mg/kg, sc; Temgesic, Schering-Plough, Kenilworth, USA) and housed in groups at the Central Laboratory Animal Institute, Utrecht University. Experiments were conducted with the permission of the local Ethical Committee for Animal Experimentation and in compliance with the Institutional Guidelines on the use of laboratory animals. After 6 weeks, the mice were killed and the constructs were harvested, fixed in 4% buffered formalin, decalcified in Luthra's solution (0.35 M HCl, 2.65 M formic acid in distilled water) for 24 h and processed for sections.

Analysis of differentiation of MSCs and Chs in vitro

Osteogenic differentiation of embedded cells was assessed by alkaline phosphatase (ALP) staining, collagen type I and osteonectin immunohistochemistry, and Alizarin red staining.

For the evaluation of ALP activity of encapsulated cells, cryosections were air-dried, fixed with 100% acetone for 10 minutes and incubated in 0.2% (v/v) Triton-X100 in TBS for 10 minutes. The activity of ALP was determined by 30 minute staining with the Fuchsin Substrate-Chromogen system (Dako, Carpinteria, USA). The presence of ALP positive cells was analyzed with a light microscope and equipped with an Olympus DP70 camera. For immunocytochemical analysis, the paraffin sections were rehydrated and blocked in 0.3% (v/v) H₂O₂ in TBS for 10 minutes followed by antigen retrieval in pronase (1 mg/ml, 10165921001 Roche Diagnostics, Mannheim, Germany) for 30 minutes at 37°C and hyaluronidase type II (10 mg/ml, H2126; Sigma-Aldrich) for 30 minutes at 37°C. The sections were then blocked in 5% (w/v) bovine serum albumin fraction V (BSA, Roche, Almere, the Netherlands) in TBS for 30 min and incubated overnight at 4°C with either mouse anti-collagen type I antibody (2 µg/ml in 5% (w/v) BSA in TBS, clone I-8H5, Calbiochem, Darmstadt, Germany) or mouse anti-onectin antibody (1/50 in 5% (w/v) BSA in TBS, clone AON-1, Developmental Studies Hybridoma Bank (DSHB, Iowa City, USA). A biotinylated secondary antibody was applied (1/200 in 5% (w/v) BSA in TBS, biotinylated sheep anti-mouse, RPN1001V1, GE Healthcare, Diegem, Belgium) for one hour and the staining was enhanced by incubation with streptavidine-peroxidase for an additional hour (2 µg/ml, PN IM0309, Immunotec, Montreal, Canada).

Chondrogenesis of encapsulated cells was assessed by Safranin-O staining and collagen type II and VI immunohistochemistry. To demonstrate proteoglycan production, alginate was removed from the sections by 10-minute incubation in citrate buffer and the sections were stained with Weigert's hematoxylin (Klinipath, Duiven, The Netherlands) and fast green (Merck, Darmstadt, Germany) for cells and with Safranin-O (Merck) for proteoglycans. Immunohistochemical analysis of collagens was performed using a rabbit polyclonal antibody against collagen type II (10 µg/ml in 5% (w/v) BSA/PBS; Abcam 53047) and mouse anti-collagen type VI antibody (1/10 in 5% (w/v) BSA in TBS, clone 5C6, DSHB). Incubation with rabbit IgG or mouse isotype-matched control IgG (Dako) served as negative controls for the stainings. Subsequently the secondary antibody was applied for one hour, respectively goat-anti-rabbit Powervision (DPVR-55HRP, Immunologic, Duiven, the Netherlands) and goat anti-mouse HRP, 10 µg/ml in 5% (w/v) BSA in TBS). All immunohistochemical stainings were developed with DAB and counterstained with Mayer's hematoxylin.

Analysis of printed tissue formed in vivo

Sections were stained with hematoxylin and eosin (HE) and Goldner's trichrome for general visualization of tissue development. To demonstrate formation of cartilaginous tissue, collagen types II and VI were immunolocalized, as indicated above.

To determine the presence of the osteogenic marker osteocalcin, immunohistochemical analysis was performed on rehydrated sections that were blocked in 5% (w/v) BSA in TBS for 30 minutes and incubated with rabbit polyclonal antibody to osteocalcin (2 µg/ml in 5% BSA/TBS; Alexis ALX-210-333, Enzo Life Sciences, Farmingdale, NY, USA) overnight at 4 °C. As secondary antibody goat anti-rabbit HRP (1.6 µg/ml in 5% BSA/TBS; Dako) was applied for one hour.

For osteogenic marker collagen type I, immunohistochemical analysis was performed on rehydrated sections that were pre-incubated in 0.3 % H₂O₂ for 10 minutes, followed by antigen retrieval with 10 mM sodium citrate buffer, pH 6.0 for 30 minutes at 95°C. The sections were then blocked in 5% (w/v) BSA in PBS for 30 minutes and incubated with rabbit polyclonal antibody to collagen type I (3.3 µg/ml in 5% BSA/PBS; Abcam 34710) overnight at 4°C. Incubation with rabbit IgG (Dako) served as negative control for the staining. As secondary antibody we used goat anti-rabbit HRP (2.5 µg/ml in 5% BSA/PBS; DAKO) for 1 hour. The stainings were developed with DAB and counterstained with Mayer's hematoxylin.

Statistical analysis

Statistical analysis was performed with SPSS 12.0.1 software. A Mann-Whitney U-test was used to evaluate the viability data in printed and unprinted samples (n=5). This statistical test was chosen because of the small number of samples. A one-way ANOVA with Bonferroni post-hoc test was used to analyze the viability data at different pressures and for the comparison of the Young's modulus of the different constructs. P-values of less than 0.05 were considered statistically significant. Values are reported as mean ± standard deviation.

RESULTS

3D fiber deposition of structured hydrogel scaffolds

Defined, 3D hydrogel scaffolds consisting for up to ten layers (0.8 mm) were printed by the BioScaffolder machine (Supplementary Figure 1). Vertical pores were regular throughout the samples, while transversal pores fused due to the relative softness of the material. Strand size was tailored by adjusting the speed of deposition and the extrusion pressure (Figure 2a-c). The shear-thinning effect that occurred in the system resulted in a fall in shear stress at higher extrusion pressures (Figure 2d, e). The values calculated for the shear stress experienced by the (cell-laden) hydrogel inside the printer cartridge corresponded to those obtained using rheometer analysis (Figure 2f).

Modulating the strand distance during printing resulted in formation of scaffolds with different porosities, while the resulting pore architecture of the printed scaffolds followed the imposed strand orientation (Figure 3a). To illustrate the effect of strand orientation (SO) and strand distance (SD) on overall porosity and mechanical properties of the printed hydrogel scaffolds, SO and SD were varied between two successive layers. Increasing the strand distance from 0.8 mm to 1.5, 2.0 and 2.5 mm resulted in formation of scaffolds with 0, 35±3%, 48±7% and 66±4% porosity, respectively (Figure 3a). Porosity in turn influences the elastic modulus of the scaffolds (Table 1). Increased scaffold porosities corresponded with a decrease in the elastic modulus of the scaffolds (Table 1). Changing strand orientation relative to the underlying layer from (SO)₉₀ to (SO)₄₅ produced scaffolds with comparable porosity, but higher elastic modulus (Table 1).

Heterogeneous scaffolds, consisting of two differently stained hydrogels were printed according to the CAD/CAM design (Figure 3b). The adjacent compartments, here indicated by different colors, interacted well without visible signs of delamination (Figure 3b).

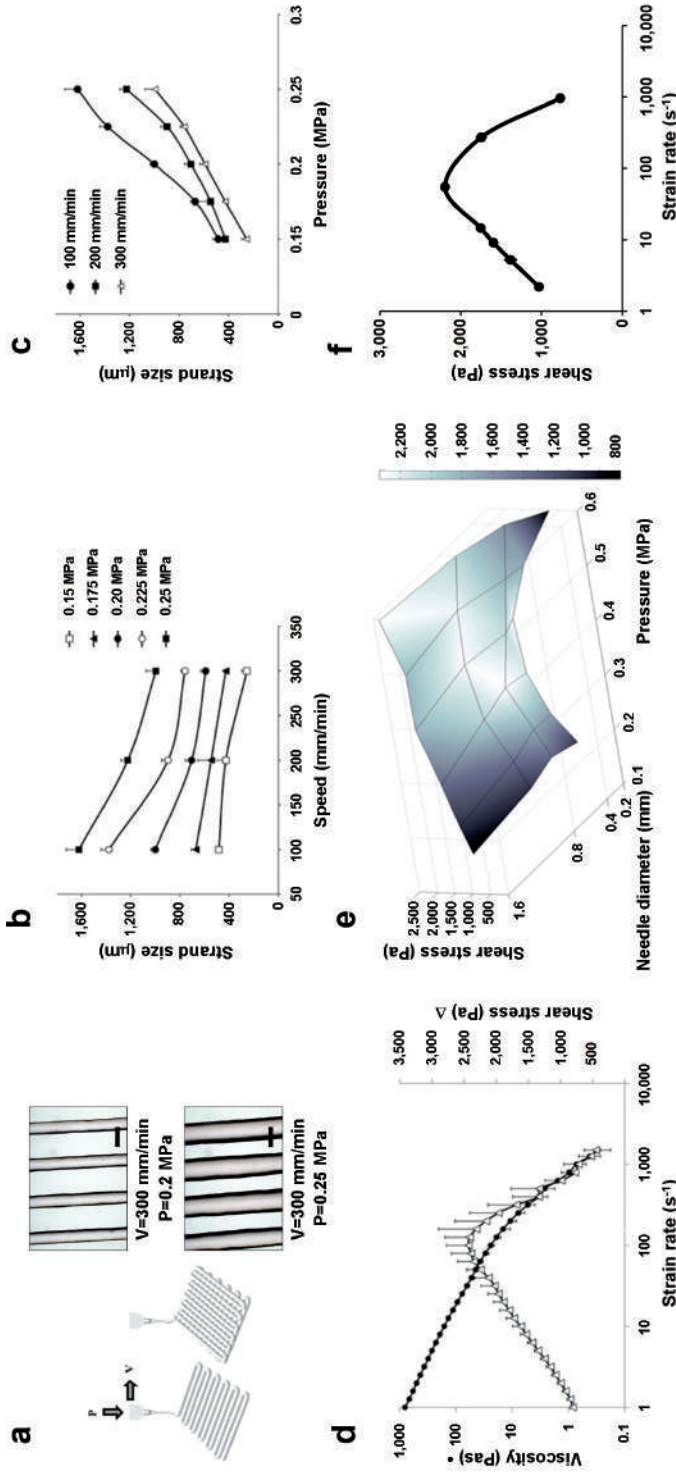


Figure 2. The effect of printing parameters on strand size, strain rate and shear stress. **(a)** The effect of speed of deposition (V) and pressure (P) on strand size, scale bars: 500 μm . Strand size as function of speed **(b)** and pressure **(c)**, shows that strand size is increased by decreasing printing speed or by increasing printing pressure. Data presented as mean \pm standard deviation ($n=8$). **(d)** Viscosity (circles) and shear stress (triangles) of the hydrogel as a function of shear rate measured by rheometer ($n=6$). **(e)** Shear stress as a function of needle diameter and pressure ($n=4$), showing a shear-thinning effect at higher extrusion pressures, resulting in a fall in shear stress. **(f)** Shear stress in the BioScaffold, calculated values for shear stress correspond to those obtained using rheometer analysis; values given as mean \pm standard deviation ($n=4$).

Table 1. Scaffold strength as a function of porosity. Porosity (%), Young's modulus (kPa) and strand distance of the printed scaffolds (solid: n=2; porous: n=4) are given. Strand distance is the distance between the middle of two consecutive strands. A deposited strand distance of 0.8 mm yields solid constructs. (SO)90 and (SO)45 indicate a difference in (SO) relative to the underlying layer of 90° and 45°, respectively. Data are presented as mean \pm standard deviation, *: significantly different from solid construct ($p < 0.05$), **: significantly different ($p < 0.05$) from construct (SO)90 with strand distance of 2.5 mm. (SO), strand orientation

	<i>Solid</i>	<i>Porous; SO90</i>	<i>Porous; SO90</i>	<i>Porous; SO90</i>	<i>Porous; SO45</i>
<i>Porosity (%)</i>	0	35 (3)	48 (7)	66 (4)	48 (2)
<i>Modulus (kPa)</i>	14.8 (3.6)	7.6 (0.6)* **	5.6 (0.6)*	4.5 (0.1)*	6.4 (0.2)*
<i>Strand distance</i>	0.8 mm	1.5 mm	2.0 mm	2.5 mm	2.0 mm

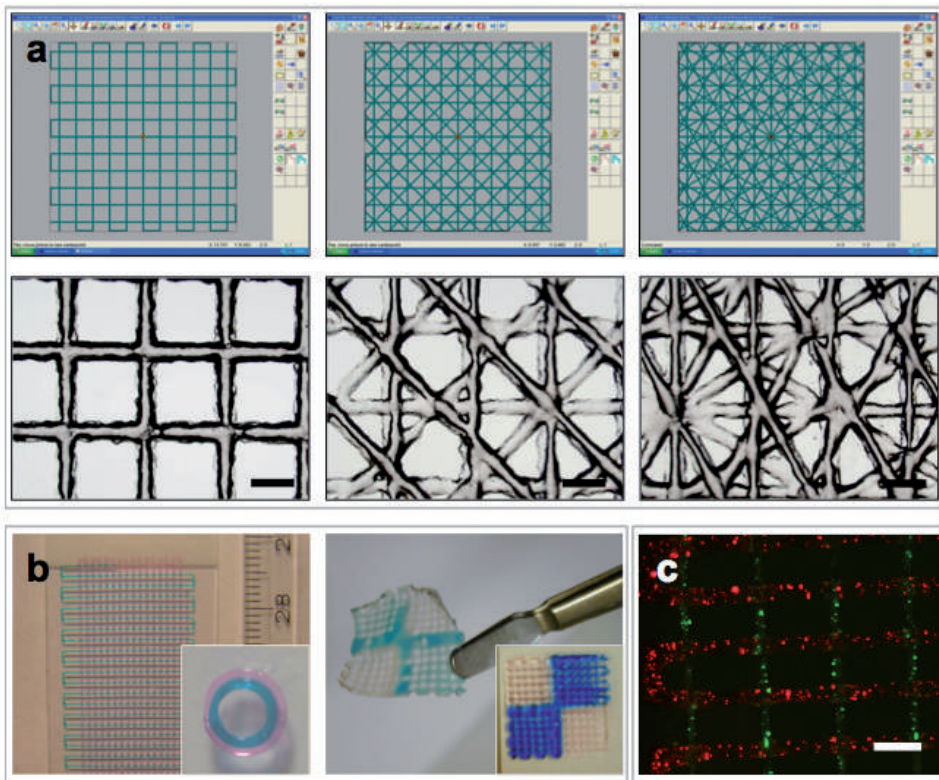


Figure 3. Scaffold architecture. (a) A computer blueprint is used to construct scaffolds with variable strand orientation; computer-aided design/computer-aided manufacturing software design is shown in the top panels and light microscope images of resultant scaffolds in lower panels. Scale bar: 1 mm. Strand orientations of any layer in a design relative to the underlying layer from left to right is 90, 45, 30 (in degrees°). (b) Examples of heterogeneous acellular scaffolds (left: multilayer and a circular construct with a diameter of 5 mm (inset); right: a chess-board construct, blue dye is used for illustration purposes; right: no delamination between the printed alginate compartments). (c) Encapsulated cells (fluorescently labeled red and green) in a heterogeneous scaffold, (SO)90. Scale bar: 1mm.

Printing of viable and heterogeneous cell-laden constructs

In the design of viable cell-laden structures, survival of the printed cells (Figure 4a,b) is a crucial factor, while homogeneous cell dispersion allows uniform cell distribution throughout the construct. There were no statistically significant differences in cell survival five hours after printing ($89\pm 2\%$ viable cells in printed gels ($n=5$) versus $89\pm 3\%$ in unprinted controls ($n=5$), $p=0.94$), indicating that the printing process did not induce immediate cell death in this system (Figure 4c). We analyzed the effect of shear stress on the viability of printed MSCs, showing that 3DF printing sustains high viability of MSCs after 24 hours in culture (viability of $88\pm 6\%$ and $89\pm 7\%$ in printed group (≈ 210 mm; 0.2 MPa) and unprinted control, respectively). Furthermore, the viability of MSCs extruded at different pressures, and at different shear stresses, follows the inverse pattern of shear stress values (Figure 4d).

An attractive feature of the 3DF approach is its ability to controllably place cells encapsulated in hydrogels and to combine different cell types. To illustrate the feasibility of printing cell-laden constructs with organizational diversity, different cell types were organized in layered configuration (Figure 3c). Fluorescent detection of the cells demonstrates that the designed scaffold geometry is sustained by the entrapped cellular patterns *in vitro* (Figure 6b).

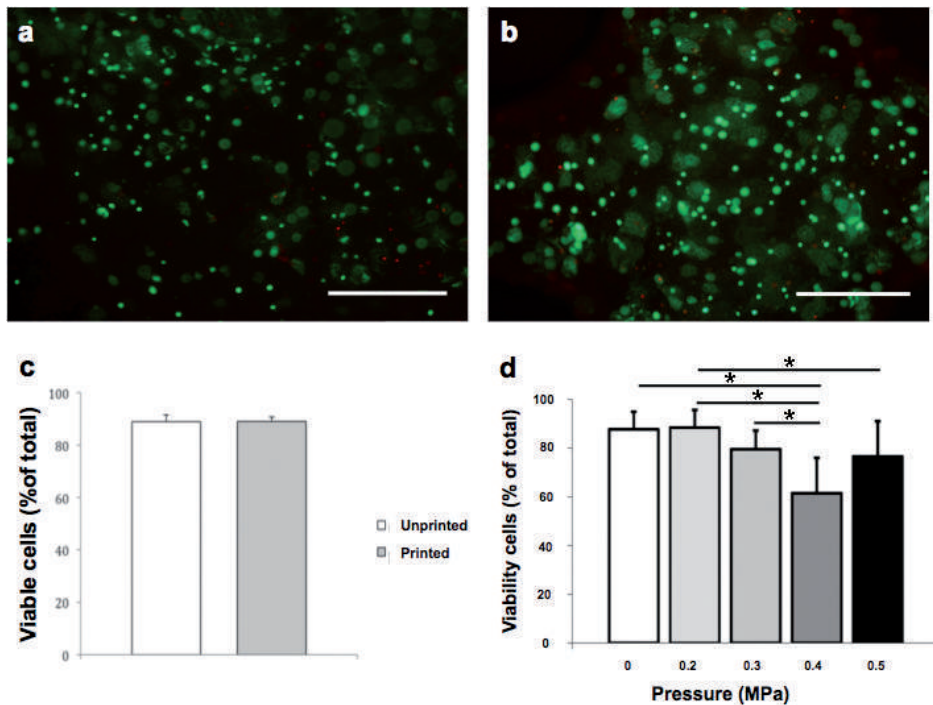


Figure 4. The effect of the printing process on MSCs survival. (a) MSCs in unprinted control; red: dead cells, green: live cells. (b): MSCs in alginate 5 hours after printing; (c) Viability in unprinted (white) and printed (grey) samples ($n=5$) 5 hours after printing the pneumatic pressure was set at 0.175 MPa.; no significant differences between printed and unprinted samples were found ($p=0.94$). (d) Viability at 24 hours after printing at various pressures ($n=4$), controls (0 MPa) are non-printed. * $p<0.05$. MSCs, multipotent stromal cells.

Tissue formation by heterogeneous cell-laden constructs *in vitro*

To demonstrate the biological potential of 3DF using multiple cell types, we investigated cellular organization *in vitro*. Cell distribution differences in ECM formation were followed in time. For this, 10-layer alginate constructs were built, containing two adjacent regions with either MSCs or chondrocytes (Figure 5a). Gross appearance of the implants indicated formation of two distinctive compartments starting two weeks after printing. The chondrocyte region exhibited thickening and increased opacity of the scaffold structure (Figure 5a, lower panel), which was attributed to ECM deposition. In the MSC part, tissue formation was more subtle, as described below. The distribution of cell types was assessed for up to three weeks in culture by fluorescence labeling and showed strict containment of the printed population to either scaffold compartment, indicating a good retention of organization *in vitro* (Figure 6a, b). General histology of the composite scaffolds demonstrated appearance of cell-clusters confined to the chondrocyte compartment, rich in cartilage-specific markers collagen VI and II (Figure 5e and Figure 6e). Concurrently in the osteogenic part, the cells remained homogeneously dispersed and stained positive for osteogenic markers alkaline phosphatase, collagen type I, osteonectin and Alizarin red (Figure 5d and Figure 6). Together these findings illustrate heterogeneous extracellular matrix formation *in vitro* analogous to the deposited cell type.

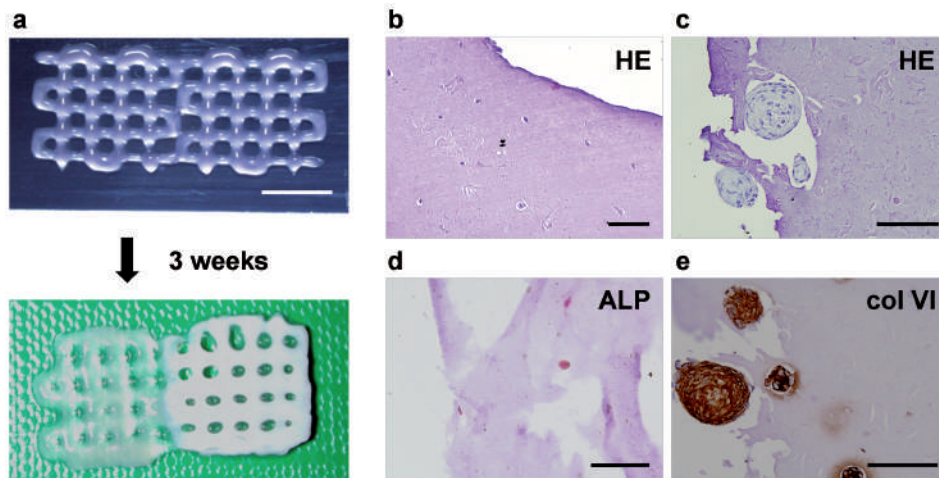


Figure 5: Appearance and cell function in printed grafts *in vitro*. (a) Macroscopic appearance of printed composite constructs with a MSC-laden compartment on the left and a chondrocyte-laden compartment on the right, directly after printing (top) and after three weeks of culture (bottom), showing differences on a macroscopic level. Scale bar: 500 μm . HE-staining after 21 days in osteogenic part (b) and chondrogenic part (c) illustrates clusters inside the alginate fiber in the chondrocyte-part of the construct, while cells are dispersed in the MSCs-compartment. Cells: dark blue, alginate: light blue. (d) ALP-staining (red) after 7 days demonstrates positive cells in MSC-compartment of the construct; (e) Immunolocalization of collagen type VI (brown) at 21 days in the chondrocyte-laden part of the scaffold. Scale bars: 100 μm . HE, hematoxylin and eosin; ALP alkaline phosphatase.

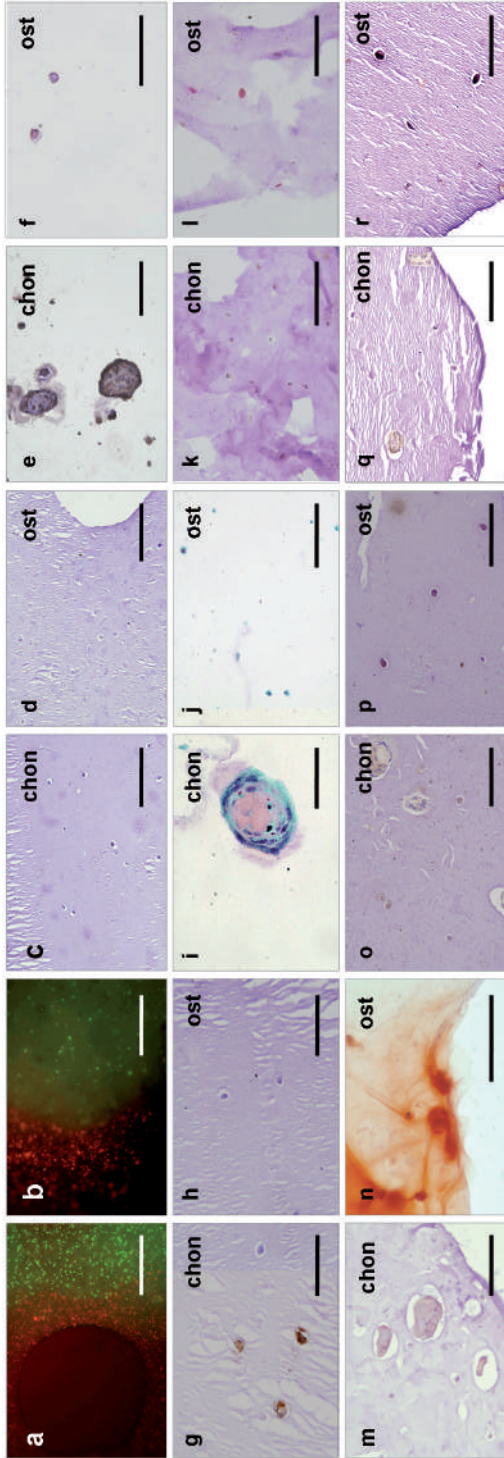


Figure 6. Analysis of extracellular matrix formation in printed grafts *in vitro*. The MSC-laden osteogenic part is indicated with "ost", while the chondrocyte-laden part is indicated with "chon". (a, b) Fluorescently labeled cells, MSC in green and chondrocytes in red, directly after printing (a) and after three weeks (b). Scale bars: 500 μ m. (c, d) HE-staining after 7 days demonstrates homogeneous dispersion of cells in both regions of the scaffold, in chondrogenic part (c) and in osteogenic part (d). Scale bars: 200 μ m. (e, f) Immunolocalization of collagen type II (brown) after 21 days, in chondrogenic part (e) and in osteogenic part (f), the surrounding alginate has been washed away. Scale bars: 100 μ m. (g, h) Immunolocalization of collagen type VI (brown) after 7 days, in chondrogenic part (g) and in osteogenic part (h). Scale bars: 100 μ m. (i, j) Safranin-O staining at 21 days indicates presence of proteoglycans (pink) in chondrocyte region (i), and not in osteogenic part (j), the surrounding alginate has been washed away. Scale bar in i: 50 μ m, in j: 100 μ m. (k, l) ALP-staining after 7 days demonstrates positive cells (red) in the osteogenic compartment of the construct (l) and not in chondrogenic part (k). Scale bars: 100 μ m. (m, n) Alizarin red staining for calcium deposits (orange-red) after 21 days, in chondrogenic part (m) and in osteogenic part (n). Scale bars: 100 μ m. (o, p) Collagen type I immunostaining (brown) at 21 days, in chondrogenic part (o) and in osteogenic part (p). Scale bars: 100 μ m. (q, r) Osteonectin immunostaining (brown) at 21 days, in chondrogenic part (q) and in osteogenic part (r). Scale bars: 100 μ m.

Tissue formation by heterogeneous cell-laden grafts *in vivo*

To validate the retention of heterogeneous tissue organization *in vivo*, we investigated the effect of 3DF-defined cell placement on osteochondral tissue formation in mice. Grafts were composed of a chondrocyte-laden compartment and an MSC-laden compartment, which included osteoinductive ceramic particles. Constructs exhibited heterogeneous tissue formation corresponding to the deposited cell type (Figure 7) after six weeks. Extracellular matrix formation was evidenced by Goldner's trichrome staining, while almost no matrix developed in acellular control gels (Figure 7b, inset), signifying that embedded cells contribute substantially to formation of ECM in these grafts. Osteocalcin- (Figure 7d) and collagen type I (not shown)-positive matrix enveloped the BCP particles, suggesting the onset of osteogenic differentiation in this part of the construct.

In the chondrocyte-laden region of the construct we observed dense matrix accumulations in alginate and formation of cell clusters positive for cartilage-specific markers collagen type II and VI (Figure 7c and Figure 8). The latter marker is specific for human collagen VI and does not cross-react with mouse tissue, indicating that the newly formed collagenous matrix is derived from the transplanted cells.

DISCUSSION

In the present study, for the first time the feasibility of 3DF to fabricate porous heterogeneous osteochondral constructs that encompass living chondrocytes and osteogenic progenitors is demonstrated. Printed cell-hydrogel constructs revealed differential lineage commitment and extracellular matrix formation. This study addresses recent development in the field of regenerative medicine that aims to recapitulate the complexity of natural biological tissues, consisting of different cell types with a specific organization and matrix composition.

Previously, 3DF has been developed as a rapid prototyping method to create 3D porous shapes of a range of materials, including thermoplastics (22, 32) and hydrogels (27) and the adapted technology used by us can comply with several important prerequisites of tissue-engineered grafts, including tailorable mechanical properties, the introduction of sufficient interconnected porosity, the introduction of living (progenitor) cells, and the possibility to investigate organizational aspects in tissue regeneration. Moreover, 3DF is a robust dispensing technology, resulting in constructs that easily reach relevant (cm-scale) sizes for tissue replacement. Addition of cells to the process of hydrogel fiber deposition facilitates formation of cell-laden, viable printed scaffolds for tissue engineering purposes (25, 33), while local cell densities can be modulated and various types of cells can be deposited in tissue-like architectures.

When adding cells to the materials before printing, we demonstrated that human primary stem cells survive the shear stresses imposed on them during the deposition process, which is in line with previous reports (25, 34). A relatively high cell survival was observed at higher dispensing pressures, which is explained by shear thinning of the hydrogel resulting in a drop in shear stress. This phenomenon of shear-thinning is common behavior for (natural) polymers (35) and has been described in detail for minimal invasive material delivery (36). As matrix stiffness is a known factor in cell differentiation (37), modulating biomechanical

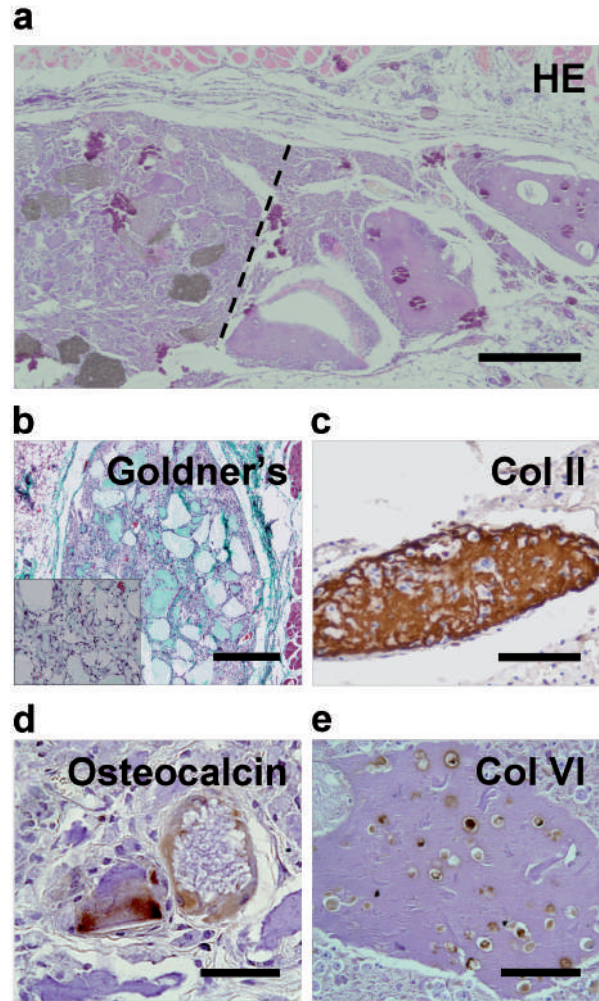


Figure 7. Tissue development in printed scaffolds *in vivo*. (a) General histology (HE staining) of the graft illustrates heterogeneous tissue formation, alginate appears purple (dashed line represents the interface between MSC-laden region with BCP particles (grey, left) and Ch-laden alginate (right)). Scale bar: 500 μ m. (b) Goldner's trichrome staining in MSC-laden part demonstrates ECM formation in the cell-laden grafts, and limited tissue formation in acellular scaffolds (inset). Scale bar: 500 μ m. (c, e) Immunostaining for cartilage-specific markers collagen types II (c) and VI (e) is positive in the chondrocyte-laden part of the grafts, alginate appears purple. Scale bars: 100 μ m. (d) Immunostaining for osteocalcin (brown) demonstrates osteogenic differentiation in MSC-laden part of the grafts. Scale bar: 50 μ m.

properties by using various depositing configurations and materials is likely to influence tissue formation *in vitro* and *in vivo*.

The concurrent printing of different hydrogels illustrated the ability of the system to reproducibly print heterogeneous 3D structures comprising different matrices. The results show adequate integration between the adjacent layers of separately printed gels. As a following step we demonstrated the design of cell-laden heterogeneous scaffolds (*i.e.* printed with different cell types at different locations). In the heterogeneous grafts *in vitro* studies revealed that the cells remained located specifically in their original deposited position during the entire culture period. This limited interaction between the cells of the adjacent layers can be explained by the hydrogel matrix employed for the encapsulation of the cells. Due to the non-interactive nature of alginate, the cells are unable to adhere or degrade the surrounding gel matrix (38), and will remain confined.

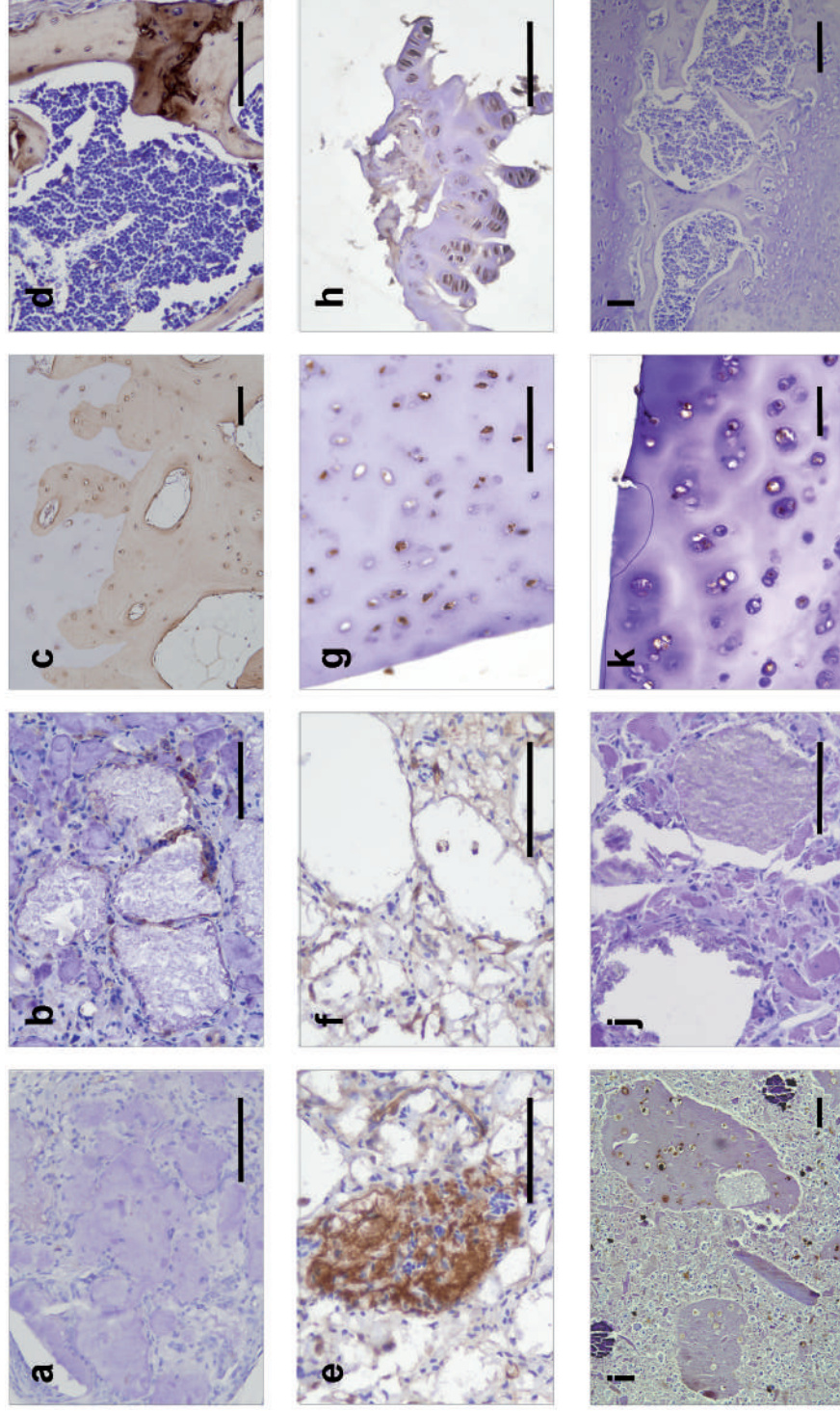


Figure 8. Collagen production in printed scaffolds in vivo. (a-d) Collagen type I immunohistochemistry (brown) performed on explanted tissue after 6 weeks; in chondrocyte-laden region (a), MSC-laden region (b), human osteochondral control tissue (c), and a murine bone control (d). (e-h) Collagen type II immunohistochemistry (brown) and (f-i) collagen type VI immunostaining (brown) on chondrocyte-laden region (e, f), MSC-laden region (f, j), human cartilage (g, k) and murine cartilage (h, i). Scale bars: 100 μ m.

Our *in vivo* study demonstrated that in printed osteochondral grafts, specific structural arrangements imposed by 3DF may induce heterogeneous tissue formation and can lead to a stable cellular architecture, which is an important factor in the success of 3D constructs (39). Another important characteristic for tissue engineering purposes is maintenance of the required phenotype (40). Our printed osteochondral grafts exhibited heterogeneous extracellular matrix formation at defined locations within one scaffold, corresponding to the deposited cell type. The transplanted human cells contributed to extracellular matrix formation, as evidenced by detection of substantial amounts of human collagen matrix in the cellular grafts and absence of ECM in acellular gels. The lack of abundant osteogenic tissue formation in the osteochondral printed grafts may be explained by the use of low interactive alginate matrix with a relatively high polymer concentration. Extracellular matrix formation deposition could be improved by optimizing pre-culture and perfusion regimes (41) or using hydrogels with lower viscosity combined with stiffer materials, which would also broaden the range of hydrogels that can be used (42). The issue of vascularization of the bone grafts needs to be addressed in future studies in order to bring the scale-up of constructs to clinically relevant sizes within reach.

In order to design better cartilage implants, and larger bone grafts, design-strategies should mimic anatomical and biochemical organization of cells, matrix and growth factors found in the native tissue (17, 18, 43). Various other cell printing approaches, including 3D ink-jet printing (44) and 3D robotic dispensing (34), have previously been applied for precise patterning of various cell populations. Similarly, micropatterning approaches, such as microfluidic patterning (45) and microcontact printing (46), allow the study of cellular interactions between various populations and at different ratios. Each of these technologies copes with specific challenges, like material choice, precision of the deposition, combining multiple components and cell types, stability of the construct and, depending on the application, the realization of relevant sized constructs. While most of these technologies are very precise and reach high resolutions, the attained scale of the constructs is at maximum mm-size. The 3DF technology presented in the current study is powerful in that respect, as cm-scale scaffolds are easily printed, making the technology an interesting option in tissue replacement therapies. Nevertheless, several important issues in 3DF still have to be addressed. First, the use of materials that possess the mechanical properties to enable printing and endure the forces acting on tissues, especially on cartilage and bone, and at the same time are biocompatible (47) should be considered. The materials so far used for 3DF, result in variable cell viability and tissue responses (48, 49), the seemingly best performers being natural hydrogels. However, using model alginate gels in this study, only a limited height of the construct could be achieved. The limitations of alginate with respect to its low mechanical strength could be alleviated by the use of thermo- and photo-curable hydrogels (50, 51), or by the use of combination of hydrogels with biomaterials that possess higher mechanical strength (42, 52, 53). Further modulations of mechanical properties of these hydrogel scaffolds with 3DF can potentially meet the mechanical requirements needed for tailored tissue engineering applications. Future advances in biomaterial sciences may provide more sophisticated and tailored materials that meet the 3DF requirements better. An additional challenge will be the *in vivo* implantation of heterogeneous printed grafts at orthotopic locations, at the same time maintaining the external shape and internal organization of the printed constructs and ensuring good integration with the surrounding host tissue. With

respect to the biology of self-organization, organ printing with 3DF is a powerful tool to study the relevance of biomimicking, i.e. to address the question whether anatomical tissue design is an important prerequisite for the development of functional tissues.

CONCLUSIONS

In the present study, we demonstrate the possibility of manufacturing viable heterogeneous tissue constructs consisting of bone and cartilage matrix by a 3D fiber deposition technique. We printed cm-scale intricate hydrogel scaffolds with high cell viability. By encapsulating osteogenic progenitors and chondrocytes in different parts of a construct, the formation of distinctive ECM regions *in vitro* and *in vivo* according to the anticipated tissue type was attained.

ACKNOWLEDGEMENTS

The collagen type VI antibody (developed by E. Engvall) and the osteonectin antibody (developed by J.D. Termine) were obtained from the Developmental Studies Hybridoma Bank. We thank Dr. T. Vermonden from the Department of Pharmaceutics, Utrecht University for the help with rheometry measurements. We acknowledge the financial support by the Anna Foundation, the Netherlands Organization for Scientific Research (NWO; grant number: 017.001.181), the Smart Mix Program of the Netherlands Ministry of Economic Affairs and the Netherlands Ministry of Education, Culture and Science and the Dutch Technology Foundation STW.

AUTHOR DISCLOSURE STATEMENT

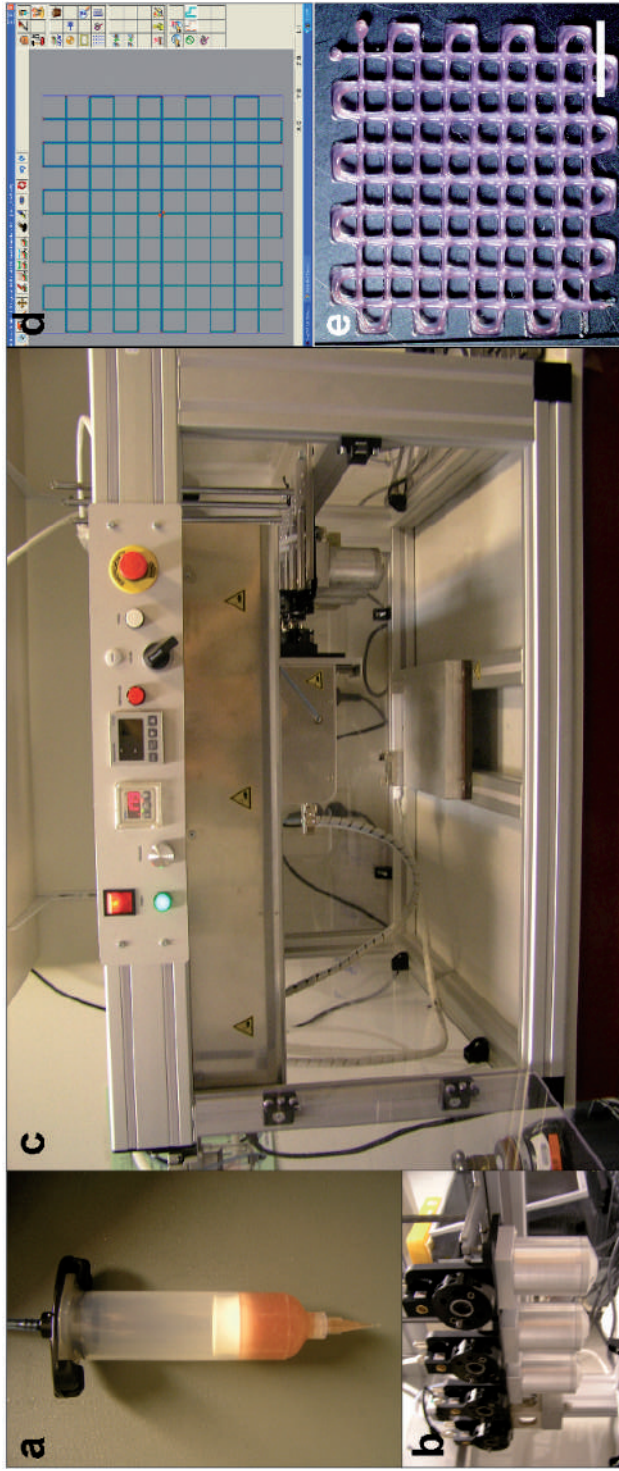
No competing financial interests exist.

REFERENCES

1. Prakash D and Learmonth D, Natural progression of osteo-chondral defect in the femoral condyle. *Knee*, 2002. **9**(1): p. 7-10.
2. Hangody L, Vasarhelyi G, Hangody LR, Sukosd Z, Tibay G, Bartha L, and Bodo G, Autologous osteochondral grafting--technique and long-term results. *Injury*, 2008. **39 Suppl 1**: p. S32-9.
3. Kon E, Gobbi A, Filardo G, Delcogliano M, Zaffagnini S, and Marcacci M, Arthroscopic second-generation autologous chondrocyte implantation compared with microfracture for chondral lesions of the knee: prospective nonrandomized study at 5 years. *Am. J. Sports Med.*, 2009. **37**(1): p. 33-41.
4. Marcacci M, Kon E, Delcogliano M, Filardo G, Busacca M, and Zaffagnini S, Arthroscopic autologous osteochondral grafting for cartilage defects of the knee: prospective study results at a minimum 7-year follow-up. *Am. J. Sports Med.*, 2007. **35**(12): p. 2014-21.
5. Lane JG, Healey RM, Chen AC, Sah RL, and Amiel D, Can osteochondral grafting be augmented with microfracture in an extended-size lesion of articular cartilage? *Am J Sports Med*, 2010. **38**(7): p. 1316-23.
6. Martin I, Miot S, Barbero A, Jakob M, and Wendt D, Osteochondral tissue engineering. *J. Biomech.*, 2007. **40**(4): p. 750-65.
7. Gao J, Dennis JE, Solchaga LA, Awadallah AS, Goldberg VM, and Caplan AI, Tissue-engineered fabrication of an osteochondral composite graft using rat bone marrow-derived mesenchymal stem cells. *Tissue Eng.*, 2001. **7**(4): p. 363-71.
8. Schaefer D, Martin I, Jundt G, Seidel J, Heberer M, Grodzinsky A, Bergin I, Vunjak-Novakovic G, and Freed LE, Tissue-engineered composites for the repair of large osteochondral defects. *Arthritis Rheum.*, 2002. **46**(9): p. 2524-34.
9. Schaefer D, Martin I, Shastri P, Padera RF, Langer R, Freed LE, and Vunjak-Novakovic G, In vitro generation of osteochondral composites. *Biomaterials*, 2000. **21**(24): p. 2599-606.

10. Theodoropoulos JS, De Croos JN, Park SS, Pilliar R, and Kandel RA, Integration of tissue-engineered cartilage with host cartilage: an in vitro model. *Clin Orthop Relat Res*, 2011. **469**(10): p. 2785-95.
11. Abrahamsson CK, Yang F, Park H, Brunger JM, Valonen PK, Langer R, Welter JF, Caplan AI, Guilak F, and Freed LE, Chondrogenesis and mineralization during in vitro culture of human mesenchymal stem cells on three-dimensional woven scaffolds. *Tissue Eng Part A*, 2010. **16**(12): p. 3709-18.
12. Allan KS, Pilliar RM, Wang J, Grynblas MD, and Kandel RA, Formation of biphasic constructs containing cartilage with a calcified zone interface. *Tissue Eng*, 2007. **13**(1): p. 167-77.
13. Guo X, Park H, Young S, Kretlow JD, van den Beucken JJ, Baggett LS, Tabata Y, Kasper FK, Mikos AG, and Jansen JA, Repair of osteochondral defects with biodegradable hydrogel composites encapsulating marrow mesenchymal stem cells in a rabbit model. *Acta Biomater*, 2010. **6**(1): p. 39-47.
14. Alhadlaq A and Mao JJ, Tissue-engineered osteochondral constructs in the shape of an articular condyle. *J. Bone Joint Surg. Am.*, 2005. **87**(5): p. 936-44.
15. Elisseeff J, Puleo C, Yang F, and Sharma B, Advances in skeletal tissue engineering with hydrogels. *Orthod. Craniofac. Res.*, 2005. **8**(3): p. 150-61.
16. Isogai N, Landis W, Kim TH, Gerstenfeld LC, Upton J, and Vacanti JP, Formation of phalanges and small joints by tissue-engineering. *J. Bone Joint Surg. Am.*, 1999. **81**(3): p. 306-16.
17. Klein TJ, Malda J, Sah RL, and Huttmacher DW, Tissue Engineering of Articular Cartilage with Biomimetic Zones. *Tissue Eng. Part B Rev.*, 2009.
18. Sharma B and Elisseeff JH, Engineering structurally organized cartilage and bone tissues. *Ann. Biomed. Eng.*, 2004. **32**(1): p. 148-59.
19. Alhadlaq A, Elisseeff JH, Hong L, Williams CG, Caplan AI, Sharma B, Kopher RA, Tomkoria S, Lennon DP, Lopez A, and Mao JJ, Adult stem cell driven genesis of human-shaped articular condyle. *Ann. Biomed. Eng.*, 2004. **32**(7): p. 911-23.
20. Alhadlaq A and Mao JJ, Tissue-engineered neogenesis of human-shaped mandibular condyle from rat mesenchymal stem cells. *J. Dent. Res.*, 2003. **82**(12): p. 951-6.
21. O'Shea TM and Miao X, Bilayered scaffolds for osteochondral tissue engineering. *Tissue Eng Part B Rev*, 2008. **14**(4): p. 447-64.
22. Woodfield TB, Malda J, de Wijn J, Peters F, Riesle J, and van Blitterswijk CA, Design of porous scaffolds for cartilage tissue engineering using a three-dimensional fiber-deposition technique. *Biomaterials*, 2004. **25**(18): p. 4149-61.
23. Malda J, Woodfield TB, van der Vloodt F, Kooy FK, Martens DE, Trumper J, van Blitterswijk CA, and Riesle J, The effect of PEGT/PBT scaffold architecture on oxygen gradients in tissue engineered cartilaginous constructs. *Biomaterials*, 2004. **25**(26): p. 5773-80.
24. Karageorgiou V and Kaplan D, Porosity of 3D biomaterial scaffolds and osteogenesis. *Biomaterials*, 2005. **26**(27): p. 5474-91.
25. Fedorovich NE, De Wijn JR, Verbout AJ, Alblas J, and Dhert WJ, Three-dimensional fiber deposition of cell-laden, viable, patterned constructs for bone tissue printing. *Tissue Eng. Part A*, 2008. **14**(1): p. 127-33.
26. Tuli R, Nandi S, Li WJ, Tuli S, Huang X, Manner PA, Laquerriere P, Noth U, Hall DJ, and Tuan RS, Human mesenchymal progenitor cell-based tissue engineering of a single-unit osteochondral construct. *Tissue Eng.*, 2004. **10**(7-8): p. 1169-79.
27. Landers R, Hubner U, Schmelzeisen R, and Mulhaupt R, Rapid prototyping of scaffolds derived from thermoreversible hydrogels and tailored for applications in tissue engineering. *Biomaterials*, 2002. **23**(23): p. 4437-47.
28. Meyvis TK, Stubbe BG, Van Steenberghe MJ, Hennink WE, De Smedt SC, and Demeester J, A comparison between the use of dynamic mechanical analysis and oscillatory shear rheometry for the characterisation of hydrogels. *Int. J. Pharm.*, 2002. **244**(1-2): p. 163-8.
29. Siddappa R, Martens A, Doorn J, Leusink A, Olivo C, Licht R, van Rijn L, Gaspar C, Fodde R, Janssen F, van Blitterswijk C, et al., cAMP/PKA pathway activation in human mesenchymal stem cells in vitro results in robust bone formation in vivo. *Proc. Natl. Acad. Sci. U S A*, 2008. **105**(20): p. 7281-6.
30. Masuda K, Sah RL, Hejna MJ, and Thonar EJ, A novel two-step method for the formation of tissue-engineered cartilage by mature bovine chondrocytes: the alginate-recovered-chondrocyte (ARC) method. *J Orthop Res*, 2003. **21**(1): p. 139-48.
31. Guo JF, Jourdan GW, and MacCallum DK, Culture and growth characteristics of chondrocytes encapsulated in alginate beads. *Connect. Tissue Res.*, 1989. **19**(2-4): p. 277-97.
32. Moroni L, de Wijn JR, and van Blitterswijk CA, Integrating novel technologies to fabricate smart scaffolds. *J Biomater Sci Polym Ed*, 2008. **19**(5): p. 543-72.
33. Cohen DL, Malone E, Lipson H, and Bonassar LJ, Direct freeform fabrication of seeded hydrogels in arbitrary geometries. *Tissue. Eng.*, 2006. **12**(5): p. 1325-35.
34. Lee W, Debasitis JC, Lee VK, Lee JH, Fischer K, Edminster K, Park JK, and Yoo SS, Multi-layered culture of human skin fibroblasts and keratinocytes through three-dimensional freeform fabrication. *Biomaterials*, 2009. **30**(8): p. 1587-95.
35. Song F, Zhang LM, Li NN, and Shi JF, In situ crosslinkable hydrogel formed from a polysaccharide-based hydrogelator. *Biomacromolecules*, 2009. **10**(4): p. 959-65.
36. Haines-Butterick L, Rajagopal K, Branco M, Salick D, Rughani R, Pilarz M, Lamm MS, Pochan DJ, and Schneider JP, Controlling hydrogelation kinetics by peptide design for three-dimensional encapsulation and injectable delivery of cells. *Proc. Natl. Acad. Sci. U S A*, 2007. **104**(19): p. 7791-6.

37. Engler AJ, Sen S, Sweeney HL, and Discher DE, Matrix elasticity directs stem cell lineage specification. *Cell*, 2006. **126**(4): p. 677-89.
38. Fedorovich NE, Alblas J, de Wijn JR, Hennink WE, Verboort AJ, and Dhert WJ, Hydrogels as extracellular matrices for skeletal tissue engineering: state-of-the-art and novel application in organ printing. *Tissue Eng.*, 2007. **13**(8): p. 1905-25.
39. Koike N, Fukumura D, Gralla O, Au P, Schechner JS, and Jain RK, Tissue engineering: creation of long-lasting blood vessels. *Nature*, 2004. **428**(6979): p. 138-9.
40. Mironov V, Reis N, and Derby B, Review: bioprinting: a beginning. *Tissue Eng*, 2006. **12**(4): p. 631-4.
41. Grayson WL, Bhumiratana S, Grace Chao PH, Hung CT, and Vunjak-Novakovic G, Spatial regulation of human mesenchymal stem cell differentiation in engineered osteochondral constructs: effects of pre-differentiation, soluble factors and medium perfusion. *Osteoarthritis Cartilage*, 2010. **18**(5): p. 714-23.
42. Schuurman W, Khristov V, Pot MW, van Weeren PR, Dhert WJ, and Malda J, Bioprinting of hybrid tissue constructs with tailorable mechanical properties. *Biofabrication*, 2011. **3**(2): p. 021001.
43. Kim TK, Sharma B, Williams CG, Ruffner MA, Malik A, McFarland EG, and Elisseeff JH, Experimental model for cartilage tissue engineering to regenerate the zonal organization of articular cartilage. *Osteoarthritis Cartilage*, 2003. **11**(9): p. 653-64.
44. Mironov V, Boland T, Trusk T, Forgacs G, and Markwald RR, Organ printing: computer-aided jet-based 3D tissue engineering. *Trends Biotechnol*, 2003. **21**(4): p. 157-61.
45. Lee MC, Choi S, and Park JK, Three-dimensional hydrodynamic focusing with a single sheath flow in a single-layer microfluidic device. *Lab Chip*, 2009. **9**(21): p. 3155-60.
46. Elloumi Hannachi I, Itoga K, Kumashiro Y, Kobayashi J, Yamato M, and Okano T, Fabrication of transferable micropatterned-co-cultured cell sheets with microcontact printing. *Biomaterials*, 2009. **30**(29): p. 5427-32.
47. Williams DF, On the mechanisms of biocompatibility. *Biomaterials*, 2008. **29**(20): p. 2941-53.
48. Khattak SF, Bhatia SR, and Roberts SC, Pluronic F127 as a cell encapsulation material: utilization of membrane-stabilizing agents. *Tissue Eng*, 2005. **11**(5-6): p. 974-83.
49. Thonhoff JR, Lou DI, Jordan PM, Zhao X, and Wu P, Compatibility of human fetal neural stem cells with hydrogel biomaterials in vitro. *Brain Res*, 2008. **1187**: p. 42-51.
50. Fedorovich NE, Swennen I, Girones J, Moroni L, van Blitterswijk CA, Schacht E, Alblas J, and Dhert WJ, Evaluation of Photocrosslinked Lutrol Hydrogel for Tissue Printing Applications. *Biomacromolecules*, 2009.
51. Vermonden T, Fedorovich NE, van Geemen D, Alblas J, van Nostrum CF, Dhert WJ, and Hennink WE, Photopolymerized thermosensitive hydrogels: synthesis, degradation, and cytocompatibility. *Biomacromolecules*, 2008. **9**(3): p. 919-26.
52. Endres M, Huttmacher DW, Salgado AJ, Kaps C, Ringe J, Reis RL, Sittinger M, Brandwood A, and Schantz JT, Osteogenic induction of human bone marrow-derived mesenchymal progenitor cells in novel synthetic polymer-hydrogel matrices. *Tissue Eng*, 2003. **9**(4): p. 689-702.
53. Schagemann JC, Chung HW, Mrosek EH, Stone JJ, Fitzsimmons JS, O'Driscoll SW, and Reinholz GG, Poly-epsilon-caprolactone/gel hybrid scaffolds for cartilage tissue engineering. *J Biomed Mater Res A*, 2010. **93**(2): p. 454-63.



Supplemental figure 1. The components of the 3D fiber deposition technology. Hydrogel is loaded into the syringe (a), which is placed in one of the cartridges (b) on the BioScaffold (c). Hydrogel fibers are deposited according to a model for a scaffold that is designed by the CAD/CAM software (d). Pressure-driven extrusion in a layered fashion yields porous 3D constructs (e), scale bar: 500 mm.





chapter **SIX**

HYALURONIC ACID AND DEXTRAN BASED SEMI-IPN HYDROGELS AS BIOMATERIALS FOR BIOPRINTING

Laura Pescosolido, Wouter Schuurman, Jos Malda, Pietro Matricardi, Franco Alhaique,
Tommasina Coviello, P. René van Weeren, Wouter J. A. Dhert, Wim E. Hennink,
Tina Vermonden

ABSTRACT

Bioprinting is a recent technology in tissue engineering used for the design of porous constructs through layer-by-layer deposition of cell-laden material. This technology would benefit new biomaterials that can fulfill specific requirements for the fabrication of well-defined three-dimensional (3D) constructs, such as the preservation of cell viability and adequate mechanical properties.

We evaluated the suitability of novel semi-interpenetrating network (semi-IPN), based on hyaluronic acid and hydroxyethyl-methacrylate-derivatized dextran (dex-HEMA), to form 3D hydrogel bioprinted constructs. The rheological properties of the solutions allowed proper handling during bioprinting while photopolymerization led to stable constructs of which their mechanical properties matched the wide range of mechanical strengths of natural tissues. Importantly, excellent viability was observed for encapsulated chondrocytes. The results demonstrate the suitability of hyaluronic acid/dex-HEMA semi-IPNs to manufacture bioprinted constructs for tissue engineering.

INTRODUCTION

The aim of tissue engineering is to support and promote the biological and functional regeneration of damaged or diseased tissues using a combination of cells and bioactive molecules seeded into a supporting material or scaffold (1-3). A scaffold defines the initial architecture of the construct by providing a three-dimensional mechanical support in which cells, together with the formed extracellular matrix and bioactive compounds, such as drugs or growth factors, can fulfill their specific functions and lead to new tissue formation (4-7).

An ideal scaffold combines appropriate mechanical properties to withstand the forces imposed *in vivo* with a high porosity allowing for easy diffusion of nutrients and waste products. Moreover, the construct should be biocompatible, biodegradable and ideally provides signals that aid cellular function (3, 8). There is an increasing demand for three-dimensional (3D) organized tissue structures which can be used for implantation, as well as for *in vitro* screening systems for cell's studies and basic research. Several technologies have been developed in the last decades for the manufacturing of cell-laden constructs for tissue engineering, such as lithography (9-11), fused deposition (12) and 3D printing (13, 14). Bioprinting differs from these approaches by allowing the generation of constructs that mimic the native tissue organization through the simultaneous deposition of both cells and bioactive biomaterials at predefined locations.(15) Bioprinting also builds 3D constructs with spatial variations along multiple axes and heterogeneous cell distributions. These characteristics make bioprinting very suitable for the regeneration of several tissues such as bone(14), nervous tissue(16) and cartilage (17). Commonly used materials for tissue regeneration are biodegradable polymers (18), ceramics composites(19) and hydrogels (20). Hydrogels (hydrophilic polymer networks) in particular offer characteristics that ensure a suitable environment for living cells both during and after scaffold fabrication. In general, these materials show excellent biocompatibility and mimic the extracellular matrix with their high equilibrium water contents.

In the present study, a new polysaccharidic semi-IPN (semi-Interpenetrating Polymer Network) hydrogel was studied for the development of a 3D printed construct suitable for tissue engineering. A suitable hydrogel for this 3D printing technique should fulfill several requirements. Firstly, the cell viability and function should be preserved during fabrication and secondly, the mechanical properties of the hydrogel construct should be suitable to withstand the implantation procedure and ideally mimic that of the natural tissue in which the scaffold is placed and degrade while simultaneous new tissue is formed. To tackle these demands, we propose a new semi-IPN hydrogel based on hyaluronic acid (HA) and a dextran derivate (dex-HEMA), a photocrosslinkable polymer able to form a stable hydrogel after UV irradiation (21). The mechanical properties and the degradation time of this hydrogel can be tuned by varying the degree of substitution and the concentration of dex-HEMA (22, 23). Hyaluronic acid (HA) is a natural linear polysaccharide composed of β -1,4-linked D- glucuronic acid (β -1,3) *N*-acetyl-D-glucosamine disaccharide units and it is the only non-sulfated glycosaminoglycan (GAG) in the extracellular matrix (ECM). HA based materials offer great advantages, including an excellent biocompatibility, biodegradability and versatility in producing materials with a broad range of properties for the design of tissue engineering scaffolds. However, one drawback of unmodified HA for 3D printing is the low stability of the resulting construct, due to its high water solubility. In literature, some strategies have been

reported aimed to reduce the hydrophilicity of the HA, i.e. derivatizing the polysaccharidic chains with hydrophobic moieties or with crosslinkable groups (24, 25).

In this study, to overcome the problem of the instability of the HA scaffold, we combined the viscoelastic and bioactive properties of HA with the photo-crosslinkable dextran derivate. The aim of this study was to assess the applicability of the polysaccharidic semi-IPN based on hyaluronic acid and dex-HEMA (chemical structures shown in Figure 1) as a scaffolding material. The mechanical properties and the printability of the material, together with the degradation kinetics of the construct were studied. Moreover, the cell viability of chondrocytes encapsulated in this hydrogel system was evaluated.

MATERIALS AND METHODS

Materials

Dextran (dex) from *Leuconostoc* ssp. with M_w 4×10^4 Da, hyaluronic acid sodium salt (HA) from *streptococcus equi* sp with M_w 160×10^4 Da, and 4-*N,N*-dimethylaminopyridine (4-DMAP), hydroxyethyl methacrylate (HEMA) were sourced from Fluka. Irgacure 2959 (2-hydroxy-4 β -(2-hydroxyethoxy)-2-methyl-propiophenone) was obtained by Ciba Specialty Chemicals Inc. Carbonyldiimidazole (CDI), (4-(2-hydroxyethyl)-1-piperazineethanesulfonic acid (HEPES) buffer, dimethylmethylene blue dye, chondroitin sulphate C, papain penicillin-streptomycin, ascorbic acid 2-phosphate and hyaluronidase from bovine testes (801U/mg) were provided by Sigma-Aldrich, USA. Dulbecco's Modified Eagle Medium (DMEM) and Insuline Transferase Selenium-X were obtained from Invitrogen (Carlsbad, California, USA). TGF- β 2 and FGF-2 were purchased from R&D Systems (Minneapolis, Minnesota, USA). Type II collagenase was obtained from Worthington Biochemical Corporation (Lakewood, New Jersey, USA), fetal bovine serum was supplied from Biowhittaker (Walkersville, Maryland, USA), human serum albumin from Cealb (Sanquin, Utrecht, The Netherlands) was used.

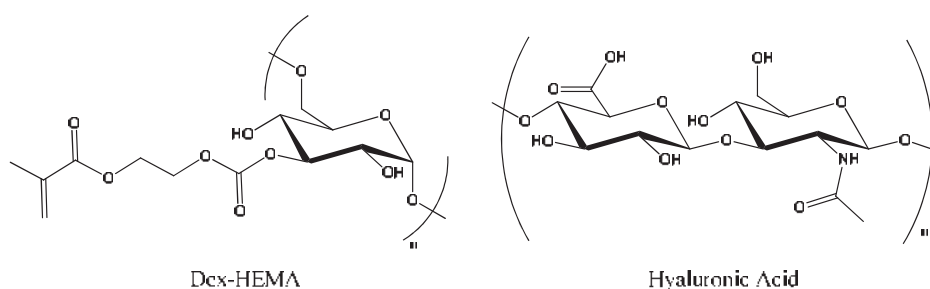


Figure 1. Chemical structures of hydroxyethyl methacrylate derivatized dextran (Dex-HEMA) and hyaluronic acid (HA).

Synthesis and Characterization of Dex-HEMA

Dex-HEMA was prepared by functionalizing dextran according to a previously described method comprising two steps.⁽²¹⁾ The first step concerns the activation of HEMA with CDI (resulting in HEMA-Cl); the second step couples HEMA-Cl to the hydroxyl groups of dextran. ¹H NMR in D₂O using a Gemini 300 MHz spectrometer (Varian Associates Inc., NMR instruments, Palo Alto, CA) was used to determine the degree of substitution (DS, i.e., the number of HEMA groups per 100 glucopyranose residues of dextran). The dex-HEMA used in this study had a DS of 18.

Hydrogel Preparation

Dex-HEMA (10% w/v) was dissolved in HEPES buffer (100 mM, pH 7.4) or chondrocyte culture medium (DMEM supplemented with 0.2 mM ascorbic acid 2-phosphate, 0.5% human serum albumin, 1x ITS-X, 100 units/mL penicillin-streptomycin, and 5 ng/mL TGF-β2) before adding photoinitiator Irgacure 2959 (final concentration of 1% w/v). Hyaluronic acid was added slowly to the solution under vigorous stirring (final concentrations of 2%, 4% or 6% (w/v)). The mixtures were mechanically stirred and vortexed overnight in order to allow complete dissolution of HA. For cyto-compatibility tests, HA (powder) was sterilized in an autoclave (30 minutes, 121 °C) and then added in the dex-HEMA solution, which was previously sterilized by filtration (0.2 μm - polycarbonate). Intrinsic viscosity data confirmed that HA did not degrade in the experimental conditions adopted. For the preparation of the semi-IPN, 1 mL of HA/dex-HEMA solution was transferred into a glass vial (diameter 12 mm) and irradiated with a mercury lamp (λ range 350-450 nm, light intensity of 20mW/cm²) for 10 minutes allowing the photopolymerization of dex-HEMA resulting in the formation of the semi-IPN.

For scaffold preparation, the polymer solutions were transferred into the dispenser of the Bioscaffolder (see below). Table 1 summarizes the compositions of the different polymer solutions used for scaffold preparation.

Capillary Viscometry

Intrinsic viscosity measurements were performed at 25 °C using a Haake automatic viscometer equipped with an Ubbelohde capillary (d = 0.53 mm) and a water thermostatted bath. HA was dissolved in 0.1 M NaCl solution (polymer concentration of 0.2 g/dL) whereas dextran or dex-HEMA were dissolved in distilled water (polymer concentration of 1 g/dL). NaCl solution and distilled water were filtered with 0.22 μm Millipore filters (polycarbonate), and used for further dilutions, while the polymer solutions were passed through 0.45 μm Millipore filters.

Table 1. Polymer compositions used for scaffold preparation.

Sample	hyaluronic acid (w/v)	dex-HEMA (w/v)
HA ₂ D ₁₀	2%	10%
HA ₄ D ₁₀	4%	10%
HA ₆ D ₁₀	6%	10%
HA ₆	6%	-
D ₁₀	-	10%

Mechanical Characterization

Rheology

A controlled stress Haake RheoStress 300 Rotational Rheometer equipped with a Haake DC10 thermostat, using a cone-plate geometry (Haake CP60Ti: diameter = 60 mm; cone = 1°) was used to obtain flow curves of the samples. In order to assess the linear viscoelastic region, stress sweep experiments were performed in the range 0.1 Pa - 200 Pa at 1 Hz. Frequency sweeps of the solutions were undertaken using an AR-G2 Rheometer (TA-Instruments) with a cone-plate geometry (diameter = 20 mm; cone = 1°) (range 0.005 to 10 Hz) in the linear viscoelastic region. A solvent trap prevented evaporation of water. The photopolymerization kinetics were measured using a AR-G2 Rheometer (TA-Instruments) equipped with a UHP device connected to a BluePoint 4 mercury lamp (Honle UV technology, λ range 230-500 nm, intensity of 50 mW/cm²), setting the gap to 300 μ m and starting irradiation 120 s after application of the sample on the geometry. G' (storage modulus) and G'' (loss modulus) were monitored during the polymerization of dex-HEMA at a strain of 0.1% and a frequency of 1 Hz. The frequency-dependent rheological properties of the formed semi-IPN hydrogels were recorded in the range of 0.01 to 10 Hz, applying a constant deformation in the linear regime (1%). All measurements were performed in duplicate at 25 °C.

Texture Analysis

Gel samples were mechanically characterized (26, 27) by a software-controlled dynamometer, TA-XT2i Texture Analyzer (Stable Micro Systems, UK), with a 5 kg load cell, a force measurement accuracy of 0.0025% and a distance resolution of 0.0025 mm (according to the instrument specifications).

Compression tests were performed by recording the resistance of cylindrical samples (diameter 12 mm, height 10 mm) to the compression of an aluminum cylinder probe with a diameter of 35 mm. The pre-test, test, and post-test speeds were 2.0 mm/s, 1.0 mm/s, 1.0 mm/s respectively, with an acquisition rate of 10 points/s. The stress σ was obtained by the following equation: $\sigma(t) = F(t) / A$, where $F(t)$ is the applied force and A is the surface of the specimen at the beginning of the experiment. The strain γ was obtained using $\gamma(t) = D(t) \times 100 / h$, where $D(t)$ is the sample displacement during compression and h is the sample height. The end point of the test was determined by rupture of the hydrogel and the values of stress and strain at rupture were monitored and referred to as ultimate compressive stress, σ , and ultimate compressive deformation, γ , respectively. The Young modulus (E) was calculated as the slope of the stress-versus-strain curve, in the range of strain from 0 to 10%. The experiments were carried out at room temperature and performed in triplicate.

Hydrogel Swelling and Degradation

Semi-IPN hydrogels of HA and dex-HEMA, prepared as described in section 2.3, were weighed (1 g) and transferred into pre-weighed glass vials. HEPES buffer (6mL, 100mM, pH 7.4, supplemented with 0.02% NaN₃ to prevent bacterial growth), with or without hyaluronidase, (200 U/mL) was added before incubating the hydrogels at 37 °C. At regular time intervals, excess buffer was removed and the swollen hydrogels were weighed before the addition of fresh buffer (6mL). The hydrogel swelling is defined as the ratio W_t/W_0 , where W_0 and W_t are the hydrogel weight immediately after preparation and in the swollen state at time t , respectively. The same

procedure was applied to the printed scaffold, prepared as described below (section 2.7). The swelling/degradation experiments were performed in duplicate.

Calculation of hydrogel mesh size

The hydrogel mesh size, ξ , in the swollen state was calculated using the following equation (28):

$$\xi = (v_{2,s})^{-1/3} \sqrt{r_0^2} \quad (1)$$

where $\sqrt{r_0^2}$ is the average distance between two adjacent crosslinks in the solvent free state and $v_{2,s}$ is the polymer volume fraction. $\sqrt{r_0^2}$ is related to the molecular weight between crosslinks M_c . For dextran it has been reported that (29):

$$\sqrt{r_0^2} = 0.0071 \sqrt{M_c} \quad (2)$$

M_c for an hydrogel material can be calculated as follows (30):

$$G = \frac{\rho RT}{M_c} \quad (3)$$

where ρ is the polymer concentration [g/m^3], R is the molar gas constant and T is the absolute temperature.

Printing of Semi IPN Scaffolds

Three dimensional printing of the hyaluronic acid/dex-HEMA semi-IPNs scaffolds was achieved using the Bioscaffolder pneumatic dispensing system (Syseng, Salzgitter-Bad, Germany). This is a three-axis dispensing machine, provided with a pneumatic syringe dispenser (13, 31). The bioscaffolder CAD/CAM software translates a three dimensional scaffold model into a layer-by-layer fiber deposition protocol, and the material is subsequently extruded on a stationary platform. In the present study, the pneumatic syringe dispenser was loaded with the polymer solutions as reported in Table 1 and rectangular 3D scaffolds of 20 layers were printed with 0/90° configuration at room temperature. After deposition, the scaffolds were photopolymerized for 10 minutes using a Superlite S-UV 2001AV lamp (Lumatec, Munchen, Germany), which emits UVA and blue light (320–500 nm, intensity of 6 mW/cm² at 365 nm). Pictures of the scaffolds were captured using a Canon D450 camera equipped with a 18-55mm objective.

Conversion of Methacrylic Groups upon UV irradiation

Semi-IPN scaffolds, prepared with the Bioscaffolder system as previously, were added to NaOH (1 mL, 0.02 M) in a vial and incubated at 37 °C to hydrolyze unreacted methacrylic groups (32), before adding acetic acid (0.2mL, 2M) to convert the methacrylate anion into methacrylic acid. The same procedure was applied to dex-HEMA samples (without UV irradiation) as control. Methacrylic acid concentrations were measured using an Acquity UPLC (Ultra Performance Liquid Chromatography) trade, equipped with a UV detector operating at 210 nm, utilizing a BEH C18 1.7 μm , 2.1 x 50 mm column and mobile phase: H₂O/ acetonitrile/ perchloric acid (95/ 5/ 0.1%)

at a flow rate of 1 mL/min. The methacrylate conversion is defined as $(1 - (\text{moles of unreacted methacrylate groups} / \text{moles of methacrylate groups originally coupled to dextran}) \times 100)$.

Cell Encapsulation and Cell Viability

Healthy, full-thickness articular cartilage was obtained under aseptic conditions from the femoral condyles and femoropatellar groove of fresh equine cadavers ($n = 3$; age, 2-10 years). Tissue was digested overnight using 0.15% type II collagenase at 37 °C and the cell suspension was filtered (100- μm cell strainer) and washed 3 times in phosphate-buffered saline. Cells were then resuspended in expansion medium (DMEM, Dulbecco's Modified Eagle Medium) supplemented with 10% fetal bovine serum, 100 units/mL penicillin-streptomycin and 10 ng/mL FGF-2 and counted using a hemacytometer. Chondrocytes were cultered (5000 cells/ cm^2) in expansion medium until 90% confluency. Cells were then suspended in sterile HA_6D_{10} solution containing Irgacure 2959, at a density of 5.0×10^6 cells/mL. Constructs of 100 μL were fabricated using two sterilized glass slides separated by two PVC spacers of 2 mm height. The cell-laden solution was then irradiated using a Superlite S-UV 2001AV lamp (Lumatec, Munchen, Germany), which emits UVA and blue light (320–500 nm) at an intensity of 6 mW/cm^2 , measured at 365 nm. The obtained semi-IPN hydrogels were cultured in chondrocyte medium (DMEM supplemented with 0.2 mM ascorbic acid 2-phosphate, 0.5% human serum albumin, 1x ITS-X, 100 units/mL penicillin-streptomycin, and 5 ng/mL TGF- β 2 for up to 3 days. Medium was replaced and collected for biochemical analysis. Samples were taken after 1 and 3 days.

The LIVE/DEAD Viability Assay (Molecular Probes MP03224, Eugene, Oregon, USA) was used to assess cell viability according to the manufacturer's instructions. Briefly, samples were examined and photographed using a BX51 light microscope (Olympus, Center Valley, Pennsylvania, USA) equipped with a DP 70 camera (Olympus, USA) with excitation/emission filters set at 488/530 nm to observe living cells (33) and at 530/580 nm to detect dead (red) cells. Live and dead cells were counted for 4 samples per time point, at 4 locations within each construct.

RESULTS AND DISCUSSION

Physico-Chemical Characterization of the Polymer Solutions and Semi-IPNs

A suitable biomaterial for 3D fiber deposition should have an appropriate viscosity (with a maximum of 100 Pa.s) allowing extrusion through a syringe system (34). The biomaterial also has to retain its plotted shape during deposition implying that the solution should not have a too low viscosity. In order to evaluate the suitability of the described systems for this technology, rheological measurements of the solutions and the corresponding semi-IPNs were performed.

The used Dex-HEMA and HA have an intrinsic viscosity $[\eta]$ of 0.18 dL/g and 20.4 dL/g, respectively. Consequently, the polymer concentrations used to prepare the samples (compositions given in Table 1) were above their critical coil overlap concentration (C^*) (C^* is inversely proportional to $[\eta]$) (35), which is around 5.5 g/dL and 0.05 g/dL, for dex-HEMA and HA, respectively. Just above C^* , soluble polymers are in a semi-diluted regime and their chains start to overlap. Particularly, the used HA concentrations were over four times C^* and under these conditions the HA polymer chains were completely entangled.

The viscosity of the prepared samples (Table 1) was evaluated as a function of the shear rate. HA is a high molecular weight polysaccharide forming very viscous solutions in water already at relatively low concentrations. As shown in Figure 2, at low shear rate (between 10^{-3} and 0.03 s^{-1}) HA and HA/dex-HEMA blends behave as Newtonian fluids. The blend viscosities in that range of shear increase as the hyaluronic acid concentration increases; e.g., at 0.1 s^{-1} , η is about $70 \text{ Pa}\cdot\text{s}$ for HA_2D_{10} , $800 \text{ Pa}\cdot\text{s}$ for HA_4D_{10} and $3500 \text{ Pa}\cdot\text{s}$ for HA_6D_{10} . When increasing the shear rate above 0.05 s^{-1} , shear thinning was observed and at high shear rates the blend viscosities decrease below $10 \text{ Pa}\cdot\text{s}$. The results of Figure 2 further show that it is possible to tune the viscosity for bioprinting by the blend composition. During extrusion through the used needle shear rates above 100 s^{-1} are obtained (36) yielding, due to the shear thinning character of the hyaluronic acid/dex-HEMA solutions, suitable viscosities for extrusion. On the other hand, the high viscosity of the blend solutions at low shear is favorable as the deposited fibers will retain their structural dimensions for some time after the printing.

The shear rate/viscosity profile of D_{10} and HA_6 solutions are also reported in Figure 2. The insert shows the flow curve of the dex-HEMA (D_{10}) solution that exhibits Newtonian behavior in the studied shear rate range, meaning that its viscosity ($10^{-2} \text{ Pa}\cdot\text{s}$) is independent of the applied stress. Comparing the flow curves of the HA_6 and HA_6D_{10} it is evident that the rheological behavior of the blend solutions is dominated by hyaluronic acid as could be expected from its high molecular weight and high intrinsic viscosity.

The viscoelastic properties of the polymer blend solutions were also characterized in oscillatory experiments. The frequency-dependent storage (G') and loss (G'') moduli of the HA_2D_{10} , HA_4D_{10} and HA_6D_{10} solutions are shown in Figure 3a.

The blend solutions showed, as expected, curves typical of entangled networks: both G' and G'' increased with frequency (but with different slopes), and cross-over points (G' equals G'') are clearly present. At frequencies higher than the cross-over point, the solutions show more elastic behavior, whereas at frequencies lower than the cross-over point the viscous behavior prevails ($G' < G''$).

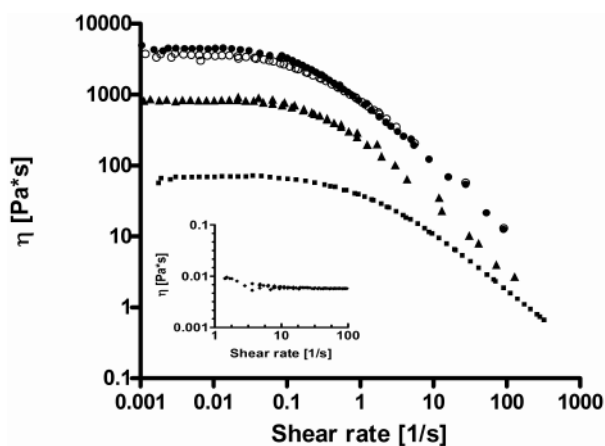


Figure 2. Flow curves of the solutions: (■) HA_2D_{10} ; (▲) HA_4D_{10} ; (●) HA_6D_{10} and (○) HA_6 ; the insert shows the flow curve of the (◆) D_{10} solution. Compositions of the solutions: see table 1.

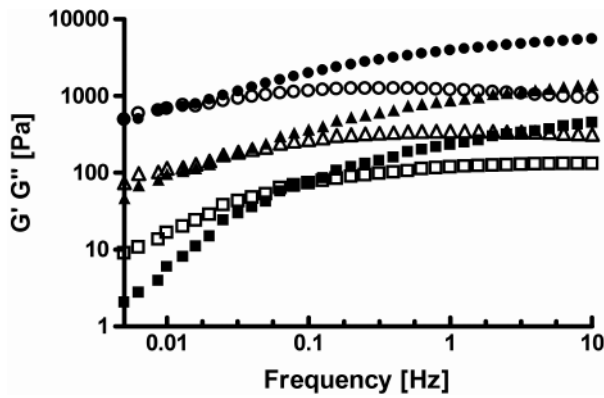


Figure 3a. Storage modulus G' (closed symbols) and loss modulus G'' (open symbols) of the blend solutions as a function of frequency for: (■) HA_2D_{10} ; (▲) HA_4D_{10} ; (●) HA_6D_{10} .

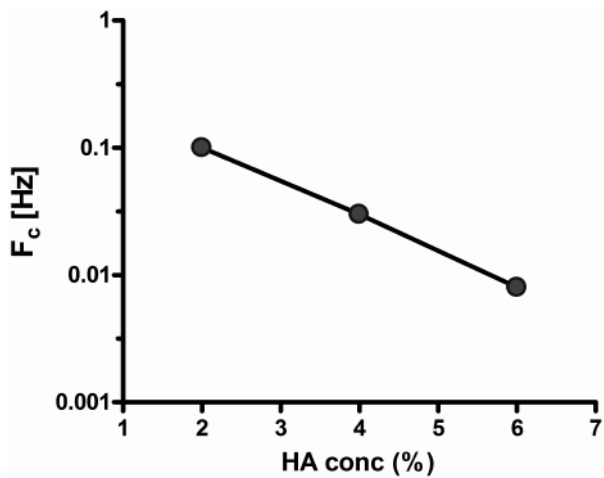


Figure 3b. The cross over frequency (F_c) as a function of the HA concentration for HA/Dex-HEMA blends.

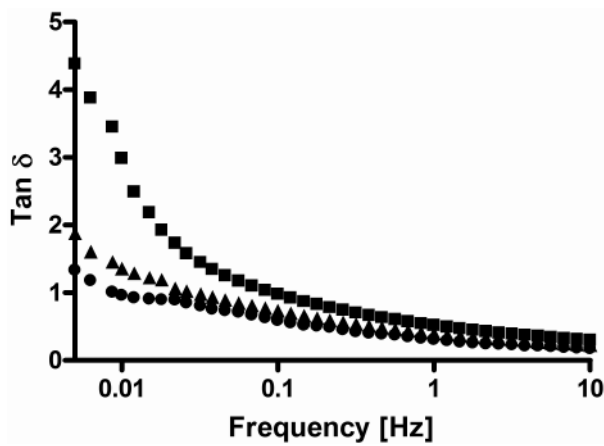


Figure 3c. $\tan \delta$ of the blend solutions as a function of frequency for: (■) HA_2D_{10} ; (▲) HA_4D_{10} ; (●) HA_6D_{10} . Compositions of the solution are given in Table 1.

The frequency at which cross-over occurs is dependent on the HA concentration in the polymer blend solutions (Figure 3b) and it is observed that with increasing HA concentration, the cross-over shifts towards lower frequency values, indicating, that the elastic character of the polymer blends increases with increasing of HA concentration (35, 37). In this respect, it should be pointed out that HA solutions showed similar solution profiles (data not shown), displaying cross-over of the moduli (e.g. HA₆ displayed a F_c at 0.01 Hz). Also dex-HEMA solutions showed a typical solution profile but with G' ($10^{-2} - 10^{-3}$ Pa) lower than G'' in the range $10^{-3} - 10$ Hz; these values are negligible compared to those of HA₆, confirming the above depicted model.

Figure 3c shows that $\tan \delta$, defined as G''/G' , is very low for all the samples at high frequencies values, while it increases at lower frequencies. In particular, the HA₄D₁₀ and HA₆D₁₀ solutions exhibit an overall solid-like character, since their $\tan \delta$ is below 2 over the whole frequency range analyzed, while for the sample with the lowest HA content, HA₂D₁₀, more viscous behavior is found as at low frequencies $\tan \delta$ is above 2.

The overall rheological behavior of the blend solution is dominated by HA because of the high molecular weight and the stiffness of the polymer chains, reflected by the a parameter of the Mark Houwink equation, which is 0.8 for the HA in this solvent (38): if a is between 0.5 and 0.7, the polymer chains are flexible; when a is greater than 0.7 the chains are stiff (39).

When HA/dex-HEMA solutions containing a photoinitiator were exposed to UV light, the HEMA groups linked to the dextran chains polymerized, leading to a chemically crosslinked dex-HEMA network, in which the HA chains are entangled (semi-IPN). The kinetics of the crosslinking process are shown in Figure 4 in which the G' values of the samples with different concentrations of HA are plotted as a function of time. This figure shows that upon UV irradiation, the storage moduli G' rapidly increased and reached a plateau level within 10 seconds, meaning that polymerization occurred instantaneously, as found previously for another polysaccharide system (23). Figure 4 also shows that after UV irradiation, the storage moduli of the obtained hydrogel networks are almost equal for all the samples analyzed (G' of ~ 10 kPa) and independent of the HA concentration. This means that in contrast to the blends solution of which the rheological properties are dominated by hyaluronic acid, G' of the semi-IPNs is governed by the formed dex-HEMA network. The HA-independent G' values

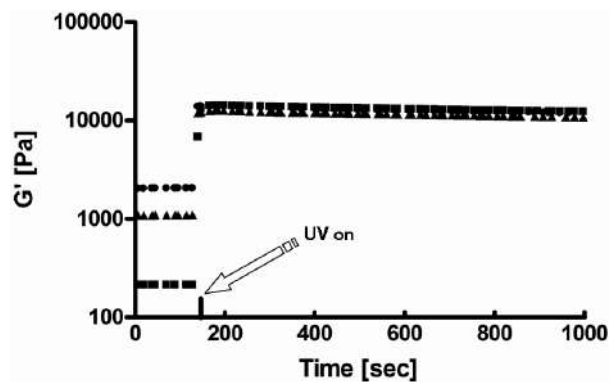


Figure 4. Storage modulus, G' , at 1 Hz, of the systems: (■) HA2D10; (▲) HA4D10; (●) HA6D10 as a function of time. UV irradiation was started at 120 seconds, as indicated by the arrow.

of the semi-IPNs demonstrate that this polymer does not hamper the polymerization of the HEMA moieties and the network formation.

To further investigate the properties of the obtained hydrogels, frequency sweeps of the semi-IPNs were recorded and compared with that of a dex-HEMA gel (Figure 5). All hydrogels behave typically as fully elastic gels, with G' independent of the applied frequency and with G'' values more than one order of magnitude smaller than G' . In line with the data of Figure 4, the semi-IPNs possessed the same storage modulus as the dex-HEMA hydrogel, regardless of the HA concentration, again confirming that the elasticity of the system is dictated by the cross linked dex-HEMA network. Figure 5 also shows that G'' of the semi-IPNs increases with increasing HA concentration which can be ascribed to an increased ability to dissipate the mechanical energy when a stress is applied.

Since natural tissues, and also implanted scaffolds, are subjected *in vivo* to shear as well as compressive stresses, the behavior of the semi-IPNs in compression was also investigated. Figure 6 shows that the different semi-IPNs have the same Young's modulus (E) as that of the dex-HEMA

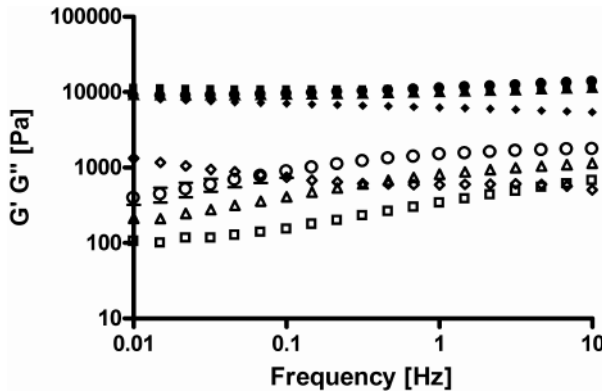


Figure 5. Storage modulus G' (filled symbols) and loss modulus G'' (open symbols) of the semi-IPNs and the dex-HEMA gel as a function of frequency for: (■) HA₂D₁₀; (▲) HA₄D₁₀; (●) HA₆D₁₀; (◆) D₁₀.

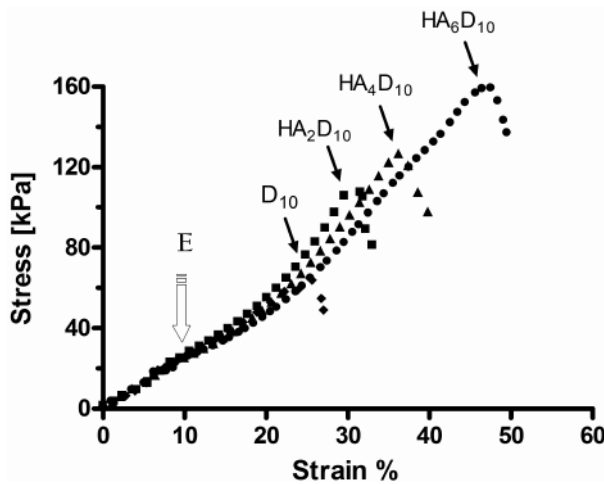


Figure 6. Stress-strain plot of: (◆) D₁₀; (■) HA₂D₁₀; (▲) HA₄D₁₀; (●) HA₆D₁₀. The arrows indicate the corresponding ultimate compressive stress (σ) and strain (γ).

hydrogel. The constant value of approximately 26 kPa again demonstrates that the dex-HEMA chemical network determines the elasticity of the semi-IPNs with no significant contribution of the free HA chains. It should be noted that theoretically the E value is three times the storage modulus value (35), which is approximately true for our system ($G' \sim 10$ kPa and $E \sim 26$ kPa).

In Figure 6, the stress-strain curves of the semi-IPNs as well as the dex-HEMA hydrogel are shown and the ultimate compressive stresses and strains are indicated by the arrows. The fracture of the D_{10} hydrogel occurred at 25% of deformation, while the semi-IPNs possessed higher ultimate compressive strain γ , that increases as the HA content increases ($30 \pm 4\%$, $38 \pm 2\%$ and $50 \pm 4\%$ for HA_2D_{10} , HA_4D_{10} and HA_6D_{10} , respectively). Also, the ultimate compressive σ of these semi-IPNs depends on the HA content (100, 120, 160 kPa for HA_2D_{10} , HA_4D_{10} and HA_6D_{10} , respectively).

The results show that, also in the non-linear viscoelastic region, HA influenced the energy dissipation ability of the semi-IPNs. HA chains entangled into the network are able to dissipate the deformation energy more efficiently and in that way retard network collapse. Consequently, hydrogels are obtained that can be deformed more easily before breaking, thereby mimicking viscoelastic behavior of natural tissues.

Hydrogel Swelling, Degradation and Cytocompatibility

The swelling and degradation behavior of the semi-IPNs was studied by incubating them in HEPES buffer at 37 °C. Figure 7 shows the swelling behavior of the HA_6D_{10} semi-IPN in comparison to that of the hydrogel based on dex-HEMA. We selected the semi-IPN with HA_6D_{10} composition for these studies as it showed better rheological properties for printing applications than the semi-IPNs with lower HA content. The dex-HEMA hydrogel swelled almost two times its original weight within 20 days, in agreement with previous results (29). The HA_6D_{10} semi-IPN hydrogel showed a 7-fold increase in weight within 40 days. It should be mentioned that even with this considerable increase in weight the semi-IPNs preserved their structural integrity during the swelling phase. This high swelling is likely due to the presence of HA which is a very hydrophilic and thus a high water-absorbing polymer. It can be expected that the HA chains remained entangled in the network because of its very high molecular weight (mesh size of Dex-HEMA network (ξ) ~ 25 nm). The M_w of HA (160×10^4 Da) is approximately 100 times larger

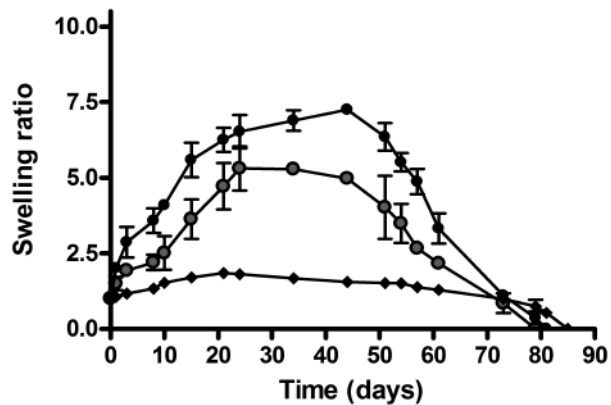


Figure 7. Swelling and degradation curves at 37°C, pH 7.4 for: (●) HA_6D_{10} semi-IPN and (◆) D_{10} hydrogel in 100 mM HEPES buffer (◼) HA_6D_{10} semi-IPNs in 100 mM HEPES buffer supplemented with hyaluronidase (200 U/mL).

than the molar weight between effective crosslinks (40) of the dex-HEMA network which is 2×10^4 Da as calculated using eq. 3. Although the HA₆D₁₀ semi-IPN and dex-HEMA hydrogel show remarkable differences in swelling, both systems show the same overall degradation rate (80-85 days), demonstrating that degradation is dictated by the hydrolysis of carbonate ester bonds present in the crosslinks of the dex-HEMA network.

The degradation of the semi-IPNs was also studied in the presence of 200 U/mL of hyaluronidase in the medium. This enzyme concentration was chosen in order to assure a complete degradation of the polysaccharide in these conditions (41). The presence of the hydrolytic enzyme only slightly influenced the ability of the semi-IPN to swell (Figure 7, grey symbol) as compared to the IPN in the absence of enzyme. Likely, the penetration of hyaluronidase into the semi-IPN gel is highly restricted because of the entangled network and consequently hyaluronidase was only active on the edges of the hydrogel. In this hypothesis, the enzymatic action of hyaluronidase led to the cleavage of HA into smaller fragments, enabling HA to diffuse out of the hydrogel. As a consequence, the HA content in the hydrogel is lowered, and thereby reducing the swelling ability of the hydrogel.

A high extent of survival of chondrocytes was shown using LIVE/DEAD assays after 1 and 3 days ($94 \pm 4\%$ and $75 \pm 19\%$, respectively) which is comparable with cell survival numbers described previously for other hydrogels (42, 43). In figure 8, the viability of the cells after three days of seeding into the HA₆D₁₀ semi-IPN hydrogel is reported. These results show that the IPN has a good cytocompatibility and therefore excellent candidate material for tissue engineering and specifically, bioprinting.

3D Printed Scaffold based on Hyaluronic acid/Dex-HEMA Semi-IPNs.

The rheological characterization described in section 3.1. demonstrated that the HA₆D₁₀ formulation had the best viscoelastic properties suitable for printing of a 3D construct. To explain, the HA₆D₁₀ solution could be easily injected through the dispenser needle because of its low viscosity at high shear rates. This solution also had, at low shear, both high viscosity (3500 Pa.s) and

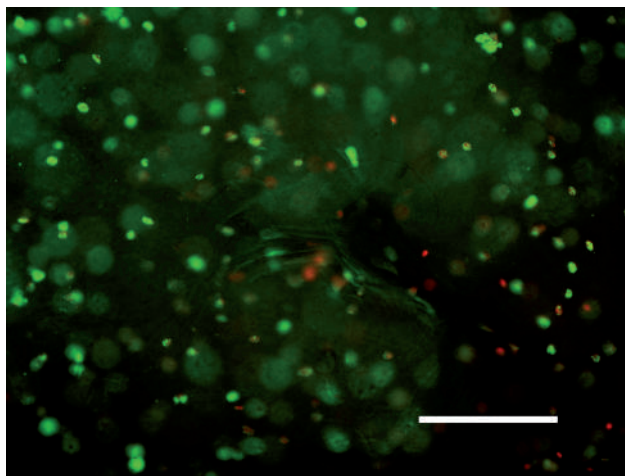


Figure 8. Chondrocyte viability after 3 days of seeding into the HA₆D₁₀ semi-IPN hydrogel. Scale bar represents 200 μ m.

high elasticity ($\tan \delta < 1$) that can prevent flow after deposition, and thus allowing the preservation of the macroporous structure. Moreover, the formed semi-IPN construct, after UV curing, had good elasticity (E modulus 26 kPa) and also showed large resistance to the fracture.

Multiple layers of the HA₆D₁₀ polymer solution were deposited resulting in macroporous constructs with dimensions of 100 × 100 × 2 mm (length × width × height). The deposition was followed by UV stabilization of the construct (shown in figure 9).

Clearly, the shear thinning properties of the hyaluronic acid/dex-HEMA polysaccharidic solution allowed the preservation of the shape and, more importantly, the porosity of the designed construct. The samples showed a slight distortion of the printed perimeter but the entire printed construct had a reproducible internal structure with a channels of dimensions of $730 \pm 28 \mu\text{m}$ (in the x and y direction). UPLC analysis showed that the $83 \pm 9\%$ of the methacrylic groups had reacted after 5 minutes of UV light exposure, confirming the good efficiency of the photopolymerization of the dex-HEMA polymer under experimental conditions (23). These data underline the effective capability of the dex-HEMA to form a stable hydrogel irrespective of the volume, the porosity and total polymer concentration.

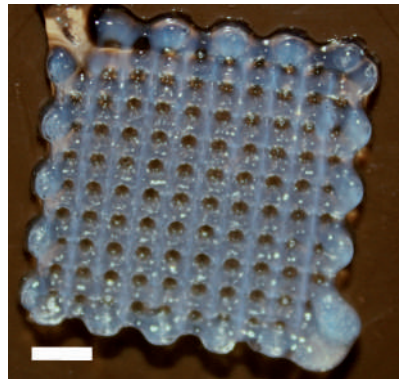


Figure 9. Photograph (top view) of 3D printed HA₆D₁₀ hydrogel. Scale bar indicates 25 mm.

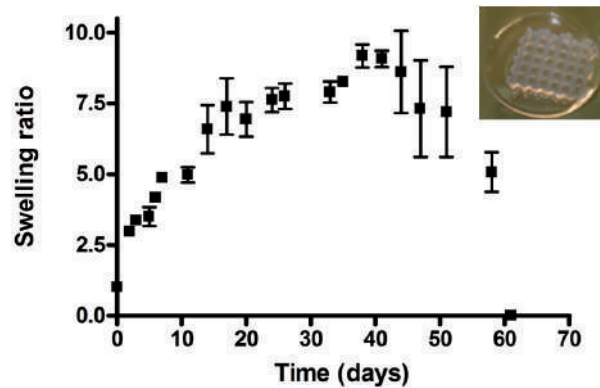


Figure 10. Swelling and degradation of the printed construct based on HA₆D₁₀ hydrogel in 100 mM HEPES buffer at 37 °C, pH 7.4. The insert shows the hydrogel after 30 days of incubation.

CONCLUSIONS

The pseudoplastic behavior of hyaluronic acid/dex-HEMA solutions and their viscoelastic properties met the requirements of the bioprinting process. The solutions have sufficient viscosity at high shear to allow extrusion and have high viscosity at low shear to retain its plotted shape during deposition. The photo-polymerization of the dex-HEMA chains led to strong and biodegradable interpenetrating hydrogels with mechanical properties that can be tuned to suit tissue engineering applications. The polysaccharide semi-IPNs hydrogels showed good cytocompatibility. The system with highest hyaluronic acid content investigated (HA_6D_{10}) was successfully printed by deposition of fibers, which were subsequently stabilized by photo-curing. The resulting 3D construct showed high porosity and had well defined strand spacing. Construct architecture can be easily tuned by controlling the process parameters such as fiber spacing and orientation. The results presented in this paper demonstrate the suitability of the HA/dex-HEMA systems for bioprinting applications in tissue engineering.

REFERENCES

1. Langer R and Vacanti JP, Tissue engineering. *Science*, 1993. **260**(5110): p. 920-6.
2. Saltzman WM and Olbricht WL, Building drug delivery into tissue engineering. *Nat Rev Drug Discov*, 2002. **1**(3): p. 177-86.
3. Sokolsky-Papkov M, Agashi K, Olaye A, Shakesheff K, and Domb AJ, Polymer carriers for drug delivery in tissue engineering. *Adv Drug Deliv Rev*, 2007. **59**(4-5): p. 187-206.
4. Dawson JI, Wahl DA, Lanham SA, Kanczler JM, Czernuszka JT, and Oreffo RO, Development of specific collagen scaffolds to support the osteogenic and chondrogenic differentiation of human bone marrow stromal cells. *Biomaterials*, 2008. **29**(21): p. 3105-16.
5. Kolambkar YM, Dupont KM, Boerckel JD, Huebsch N, Mooney DJ, Huttmacher DW, and Guldberg RE, An alginate-based hybrid system for growth factor delivery in the functional repair of large bone defects. *Biomaterials*, 2011. **32**(1): p. 65-74.
6. Lee J, Cuddihy MJ, and Kotov NA, Three-dimensional cell culture matrices: state of the art. *Tissue Eng Part B Rev*, 2008. **14**(1): p. 61-86.
7. Shoichet MS, Polymer Scaffolds for Biomaterials Applications. *Macromolecules*, 2010. **43**(2): p. 581-591.
8. Kim BS, Park IK, Hoshiba T, Jiang HL, Choi YJ, Akaike T, and Cho CS, Design of artificial extracellular matrices for tissue engineering. *Prog Polym Sci*, 2011. **36**: p. 238-268.
9. Arcaute K, Mann B, and Wicker R, Stereolithography of spatially controlled multi-material bioactive poly(ethylene glycol) scaffolds. *Acta Biomater*, 2010. **6**(3): p. 1047-54.
10. Gallego D, Ferrell N, Sun Y, and Hansford DJ, Multilayer micromolding of degradable polymer tissue engineering scaffolds. *Mater Sci Eng C*, 2008. **28**(3): p. 353-358.
11. Melchels FP, Feijen J, and Grijpma DW, A review on stereolithography and its applications in biomedical engineering. *Biomaterials*, 2010. **31**(24): p. 6121-30.
12. Zein I, Huttmacher DW, Tan KC, and Teoh SH, Fused deposition modeling of novel scaffold architectures for tissue engineering applications. *Biomaterials*, 2002. **23**(4): p. 1169-1185.
13. Fedorovich NE, Swennen I, Girones J, Moroni L, van Blitterswijk CA, Schacht E, Alblas J, and Dhert WJ, Evaluation of photocrosslinked Lutrol hydrogel for tissue printing applications. *Biomacromolecules*, 2009. **10**(7): p. 1689-96.

14. Seitz H, Rieder W, Irsen S, Leukers B, and Tille C, Three-dimensional printing of porous ceramic scaffolds for bone tissue engineering. *Journal of Biomedical Materials Research Part B: Applied Biomaterials*, 2005. **74B**(2): p. 782-788.
15. Klein TJ, Rizzi SC, Reichert JC, Georgi N, Malda J, Schuurman W, Crawford RW, and Huttmacher DW, Strategies for Zonal Cartilage Repair using Hydrogels. *Macromolecular Bioscience*, 2009. **9**(11): p. 1049-1058.
16. Silva NA, Salgado AJ, Sousa RA, Oliveira JT, Pedro AJ, Leite-Almeida H, Cerqueira R, Almeida A, Mastrorardi F, Mano JoF, Neves NM, et al., Development and Characterization of a Novel Hybrid Tissue Engineering-based Scaffold for Spinal Cord Injury Repair. *Tissue Engineering Part A*, 2010. **16**(1): p. 45-54.
17. Woodfield TBF, Guggenheim M, Von Rechenberg B, Riesle J, Van Blitterswijk CA, and Wedler V, Rapid prototyping of anatomically shaped, tissue-engineered implants for restoring congruent articulating surfaces in small joints. *Cell Proliferation*, 2009. **42**(4): p. 485-497.
18. Barnewitz D, Endres M, Krüger I, Becker A, Zimmermann J, Wilke I, Ringe J, Sittner M, and Kaps C, Treatment of articular cartilage defects in horses with polymer-based cartilage tissue engineering grafts. *Biomaterials*, 2006. **27**(14): p. 2882-2889.
19. Tamai N, Myoui A, Hirao M, Kaito T, Ochi T, Tanaka J, Takaoka K, and Yoshikawa H, A new biotechnology for articular cartilage repair: subchondral implantation of a composite of interconnected porous hydroxyapatite, synthetic polymer (PLA-PEG), and bone morphogenetic protein-2 (rhBMP-2). *Osteoarthritis and Cartilage*, 2005. **13**(5): p. 405-417.
20. Pereira RC, Scaranari M, Castagnola P, Grandizio M, Azevedo HS, Reis RL, Cancedda R, and Gentili C, Novel injectable gel (system) as a vehicle for human articular chondrocytes in cartilage tissue regeneration. *Journal of Tissue Engineering and Regenerative Medicine*, 2009. **3**(2): p. 97-106.
21. van Dijk-Wolthuis WNE, Tsang SKY, and Kettenes-van den Bosch W.E. Hennink JJ, A new class of polymerizable dextrans with hydrolyzable groups: hydroxyethyl methacrylated dextran with and without oligolactate spacer. *Polymer*, 1997. **38**(25): p. 6235-6242.
22. Franssen O, Vandervennet L, Roders P, and Hennink WE, Degradable dextran hydrogels: controlled release of a model protein from cylinders and microspheres. *J Control Release*, 1999. **60**(2-3): p. 211-21.
23. Pescosolido L, Vermonden T, Malda J, Censi R, Dhert WJ, Alhaique F, Hennink WE, and Matricardi P, In situ forming IPN hydrogels of calcium alginate and dextran-HEMA for biomedical applications. *Acta Biomater*, 2011. **7**(4): p. 1627-33.
24. Palumbo FS, Pitarresi G, Mandracchia D, Tripodo G, and Giammona G, New graft copolymers of hyaluronic acid and polylactic acid: Synthesis and characterization. *Carbohydr Polym*, 2006. **66**(3): p. 379-385.
25. Oudshoorn MHM, Rissmann R, Bouwstra JA, and Hennink WE, Synthesis of methacrylated hyaluronic acid with tailored degree of substitution. *Polymer*, 2007. **48**(7): p. 1915-1920.
26. Alves MM, Antonov YA, and Goncalves MP, Phase equilibria and mechanical properties of gel-like water-gelatin-locust bean gum systems. *Int J Biol Macromol*, 2000. **27**(1): p. 41-7.
27. Tamburic S and Craig DQ, A comparison of different in vitro methods for measuring mucoadhesive performance. *Eur J Pharm Biopharm*, 1997. **44**(2): p. 158-167.
28. Peppas NA, Moynihan HJ, and Lucht LM, The structure of highly crosslinked poly(2-hydroxyethyl methacrylate) hydrogels. *Journal of Biomedical Materials Research*, 1985. **19**(4): p. 397-411.
29. Hennink WE, Talsma H, Borchert JCH, De Smedt SC, and Demeester J, Controlled release of proteins from dextran hydrogels. *Journal of Controlled Release*, 1996. **39**(1): p. 47-55.
30. Goodwin JW and Hughes RW, *Rheology for Chemists: An Introduction*. 1 edition ed. 2000: Royal Society of Chemistry.
31. Landers R, Hubner U, Schmelzeisen R, and Mulhaupt R, Rapid prototyping of scaffolds derived from thermoreversible hydrogels and tailored for applications in tissue engineering. *Biomaterials*, 2002. **23**(23): p. 4437-47.
32. Stenekes RJH and Hennink WE, Polymerization kinetics of dextran-bound methacrylate in an aqueous two phase system. *Polymer*, 2000. **41**(15): p. 5563-5569.
33. Zhang M, Efremov MY, Schiettekatte F, Olson EA, Kwan AT, Lai SL, Wisleder T, Greene JE, and Allen LH, Size-dependent melting point depression of nanostructures: Nanocalorimetric measurements. *Physical Review B*, 2000. **62**(15): p. 10548.
34. Rungsevijitprapa W and Bodmeier R, Injectability of biodegradable in situ forming microparticle systems (ISM). *European Journal of Pharmaceutical Sciences*, 2009. **36**(4-5): p. 524-531.
35. Flory PJ, *Principles of polymer chemistry*. 1953: Itahaca.
36. Li MG, Tian XY, and Chen XB, Modeling of flow rate, pore size, and porosity for the dispensing-based tissue scaffolds fabrication. *Journal of Manufacturing Science and Engineering, Transactions of the ASME*, 2009. **131**(3): p. 0345011-0345015.
37. Flory PJ, Molecular Size Distribution in Three Dimensional Polymers. III. Tetrafunctional Branching Units. *J Am Chem Soc*, 1941. **63**(11): p. 3096-3100.
38. Tadmor R, Chen N, and Israelachvili JN, Thin film rheology and lubricity of hyaluronic acid solutions at a normal physiological concentration. *J Biomed Mater Res*, 2002. **61**(4): p. 514-23.

39. Jones WM, *Viscoelastic Properties of Polymers*: by J.D. Ferry, John Wiley and Son, 1980, 3rd Edition. *Journal of Non-Newtonian Fluid Mechanics*, 1981. **8**(3-4): p. 369-369.
40. Erzurumlu R S JSTH and McKay RD, Target-derived influences on axon growth modes in cultures of trigeminal neurons. *Proc. Natl Acad. Sci. USA*, 1993. **90**(15): p. 7235.
41. Musoke-Zawedde P and Shoichet MS, Anisotropic three-dimensional peptide channels guide neurite outgrowth within a biodegradable hydrogel matrix. *Biomed Mater*, 2006. **1**(3): p. 162-9.
42. Fedorovich NE, De Wijn JR, Verbout AJ, Alblas J, and Dhert WJ, Three-dimensional fiber deposition of cell-laden, viable, patterned constructs for bone tissue printing. *Tissue Eng Part A*, 2008. **14**(1): p. 127-33.
43. Censi R, Schuurman W, Malda J, di Dato G, Burgisser PE, Dhert WJA, van Nostrum CF, di Martino P, Vermonden T, and Hennink WE, A Printable Photopolymerizable Thermosensitive p(HPMAM-lactate)-PEG Hydrogel for Tissue Engineering. *Adv Funct Mat*, 2012. **21**(10): p. 1833-1842.





chapter **SEVEN**

PRINTABLE PHOTOPOLYMERIZABLE THERMOSENSITIVE P(HPMA-LACTATE)-PEG HYDROGEL FOR TISSUE ENGINEERING

Roberta Censi, Wouter Schuurman, Jos Malda, Giorgio di Dato, Petra E. Burgisser,
Wouter J. A. Dhert, Cornelus F. van Nostrum, Piera di Martino, Tina Vermonden
and Wim E. Hennink

ABSTRACT

Bioprinting is a new technology in regenerative medicine that allows the engineering of tissues by specific placement of cells in biomaterials. Importantly, the porosity and the relatively small dimensions of the fibers allow rapid diffusion of nutrients and metabolites. This technology requires the availability of hydrogels that ensure viability of encapsulated cells and have adequate mechanical properties for the preparation of structurally stable and well-defined three-dimensional constructs. The aim of this study is

to evaluate the suitability of a biodegradable, photopolymerizable and thermosensitive A–B–A triblock copolymer hydrogel as a synthetic extracellular matrix for engineering tissues by means of three dimensional fiber deposition. The polymer is composed of poly(*N*-(2-hydroxypropyl)methacrylamide lactate) A-blocks, partly derivatized with methacrylate groups, and hydrophilic poly(ethylene glycol) B-blocks of a molecular weight of 10 kDa. Gels are obtained by thermal gelation and stabilized with additional chemical cross-links by photopolymerization of the methacrylate groups coupled to the polymer. A power law dependence of the storage plateau modulus of the studied hydrogels on polymer concentration is observed for both thermally and chemically cross-linked hydrogels. The hydrogels demonstrated mechanical characteristics similar to natural semi-flexible polymers, including collagen. Moreover, the hydrogel shows suitable mechanical properties for bioprinting, allowing subsequent layer-by-layer deposition of gel fibers to form stable constructs up to at least 0.6 cm (height) with different patterns and strand spacing. The resulting constructs have reproducible vertical porosity and the ability to maintain separate localization of encapsulated fluorescent microspheres. Moreover, the constructs show an elastic modulus of 119 kPa (25 wt% polymer content) and a degradation time of approximately 190 days. Furthermore, high viability is observed for encapsulated chondrocytes after 1 and 3 days of culture. In summary, we conclude that the evaluated hydrogel is an interesting candidate for bioprinting applications.

INTRODUCTION

The development of novel tissue engineering strategies using a manifold of three dimensional (3D) patterning techniques, such as fiber templating (1), lithography (2), or 3D fiber deposition (3DF) (3-5) (whereby cells are combined with a matrix and printed to yield a 3D construct for subsequent transplantation *in vivo*) offers a novel and potential route towards tissue regeneration (6-8).

Bioprinting is a novel approach in tissue engineering for scaffold preparation based on computer aided layer-by-layer or dropwise deposition of cell-laden hydrogels (3, 9-11). This rapid prototyping-derived technique allows the preparation of complex 3D cell laden constructs, with reproducible control over cell placement and highly porous structure, which allows easy diffusion of nutrients, oxygen, and metabolites (13-17).

The possibility to incorporate different types of living cells and to deposit different materials within a construct by using 3DF, allows the creation of grafts that closely resemble the hierarchy of cells natural tissues matrices (18). The success of this approach highly depends upon upon the availability of suitable biodegradable and biocompatible biomaterials, which can be processed into a suitable 3D structure (19-23). Furthermore, the final construct should have sufficient porosity to facilitate nutrients and oxygen supply and good resolution to allow fine-tuning of the 3D structure and precise reconstruction of the shape of the defect/organ to be regenerated.

Hydrogels are 3D networks of cross-linked hydrophilic polymers that fulfill some of these requirements. These materials are therefore extensively used as supportive matrices for tissue engineering. So far, both natural (alginate, chitosan, hyaluronic acid, collagen, fibrin)(12, 24, 25) and synthetic (poly(ethylene glycol) (PEG), poly(N-isopropylacrylamide), Pluronic) (26-29) hydrogels have been used *in vitro* as scaffolding material for tissue engineering. However, all these materials have some drawbacks. Natural polymers possess an inherent biocompatibility and often show positive cell interaction and modulation (30), but also have a large lot-to-lot variation, poor mechanical properties and lack of tailorability. On the other hand, synthetic polymers have well-defined structures with possibilities to fine-tune their properties, but biodegradability and biocompatibility often represent an issue. Therefore, there is a high need for novel biomaterials for tissue engineering.

In the present study, a biodegradable, synthetic, photopolymerizable and thermosensitive hydrogel, that exhibits an advantageous combination of properties, is used for the development of 3D printed constructs. The polymer has an A-B-A architecture consisting of thermosensitive poly(*N*-(2-hydroxypropyl)methacrylamide lactate) (31) (p(HPMAm-lac) A-blocks that are partly modified with methacrylate moieties, to allow chemical cross-linking using photopolymerization, and a B-block of poly(ethylene glycol) (PEG) (32-34). The p(HPMAm-lac) A-blocks exhibit thermosensitive behavior (22, 35, 36), having a cloud point (CP) that can be tuned by the average length of the lactate side chains (31).

Bioprinted hydrogel based constructs can potentially be used for the regeneration of a number of tissues such as bone, skin, liver, cartilage, replicating the hierarchical structures of natural tissues at an unprecedented level. In this paper, the potential of the developed p(HPMAm-lac)-PEG-p(HPMAm-lac) hydrogel for cartilage tissue engineering is investigated. The use of hydrogels for cartilage repair is particularly attractive as these materials possess several

characteristics of native cartilage, and allow homogeneous encapsulation of chondrocytes in a highly hydrated and structurally stable and 3D network.

Articular cartilage is an avascular supporting connective tissue, exhibiting a low metabolic rate and a low regenerative potential. It has a hydrogel-like structure consisting of 70% water, 20% collagen, responsible for the tensile properties, and 10% proteoglycans, providing compression resistance (37). The cell densities and types differ with depth in cartilage. The most superficial layer has a very high density, which decreases with depth (38). Because of lack of healing capacity of the tissue due to poor blood supply, local cartilage damage eventually leads to generalized cartilage degeneration and permanent loss of organization and functionality.

The treatment of choice for generalized cartilage damage is prosthetic joint replacement (39), whereas for focal lesions, either microfracture or cell-based therapy can be used (40, 41). However, although clinical outcomes are satisfactory for these methods, they have drawbacks: prostheses have a limited life span, whereas microfracture and chondrocyte implantation do not fully restore the organization and consequently the functionality of native cartilage. By using 3D printing techniques, ideally, patient-derived cells can be mixed with the hydrogel matrices and printed at defined locations within a single construct, reproducing hierarchical cell organization of native cartilage and potentially enhancing clinical outcomes (18, 42, 43).

The goal of this study was to evaluate the suitability of methacrylate bearing p(HPMAM-lac)-PEG-p(HPMAM-lac) based hydrogels for 3D fiber deposition. Upon printing, the construct is photopolymerized to provide the cells with long-term mechanical support and, in time, is expected to gradually degrade into biocompatible products. The printability, mechanical properties, degradation behavior, and chondrocyte compatibility were evaluated for this hydrogel.

MATERIALS AND METHODS

Materials

All chemicals were obtained from Sigma-Aldrich and used as received, unless stated otherwise. All solvents were purchased from Biosolve. Tetrahydrofuran (THF) was distilled from sodium/benzophenone and stored over 3 Å molecular sieves. Phosphate buffered saline (PBS) (8.2 g l⁻¹ NaCl; 3.1 g l⁻¹ NaH₂PO₄·12H₂O; 0.3 g l⁻¹ NaH₂PO₄) used to prepare the hydrogels for mechanical characterization and degradation studies was obtained from Braun (The Netherlands). HPMAM (hydroxypropylmethacrylamide) was obtained from Zentiva a.s. (Praha, Czech Republic), L-lactide from Purac Biochem BV (Gorinchem, The Netherlands) and 2-hydroxy-1-[4-(2-hydroxyethoxy)phenyl]-2-methyl-1-propanone (Irgacure 2959) from Ciba Specialty Chemicals Inc (Basel, Switzerland). DMAP (dimethylaminopyridine) and 4,4'-Azobis(4-cyanopentanoic acid) (ABCPA) were purchased from Fluka Chemie AG (Buchs, Switzerland). HPMAM-monolactate and HPMAM-dilactate were synthesized according to a previously reported method (31). The synthesis of triblock copolymers with PEG as middle block and polyHPMAM-lactate as outer blocks was described previously (44-46) and applied in this study for the preparation of a triblock copolymer having p(HPMAM-lac) A-blocks of 23.5 kDa, derivatized with 30% of methacrylate groups and PEG B-blocks of 10 kDa molecular

weight. Dye-Trak "F" fluorescent microspheres (fluorescent lemon and fluorescent orange) were purchased from Triton technology (San Diego, CA). Type II collagenase was obtained from Worthington Biochemical Corp (Lakewood, NJ). DMEM [Dulbecco's Modified Eagle Medium] insulin-transferrin-selenium mixture (ITS-X), penicillin and streptomycin were obtained from Invitrogen (Carlsbad, CA). Fetal bovine serum was obtained from Biowhittaker (Walkersville, MD) and FGF-2 and TGF- β 2 from R&D Systems (Minneapolis, MN). Human serum albumin from Cealb (Sanquin, Utrecht, The Netherlands) was used.

Synthesis of (PEG-ABCPA)_n Macroinitiator

(PEG-ABCPA)_n was synthesized slightly modifying the procedure described by Neradovic *et al* (47) and Vermonden *et al.* (45). In detail, 10 g (1 mmol) of PEG (number-average molar mass $M_n = 10000 \text{ g mol}^{-1}$), 280 mg (1 mmol) of ABCPA, 91.6 mg (0.3 mmol) of 4-(dimethylamino)pyridinium-4-toluenesulfonate (DPTS) and 618 mg (3 mmol) of *N,N'*-dicyclohexylcarbodiimide (DCC) were dissolved in 60 ml of a 1:1 mixture of dichloromethane and dry THF. The mixture was stirred at room temperature at 0°C for 1 hour and subsequently at room temperature for 24 h under nitrogen atmosphere. The formed dicyclourea (DCU) was filtered off, and the organic solvents were removed by rotary evaporation. The product was suspended in water, filtrated over hyflo and dialyzed for 48 hours at 4°C against water using a dialysis membrane with a cut-off of 12-14 kDa. The macroinitiator was obtained in a high yield (80%) after freeze-drying and characterized by ¹H NMR in CDCl₃ and gel permeation chromatography (GPC).

Synthesis of Methacrylated Triblock Copolymers

A thermosensitive triblock copolymer consisting of PEG 10 kDa as hydrophilic block and pHPMAM_{lac} as thermosensitive outer blocks with a HPMAm-mono lactate/HPMAm-dilactate ratio of 50/50 was synthesized by free radical polymerization using (PEG-ABCPA)_n macroinitiator according to a method described earlier.(45) The OH side groups of p(HPMAm lac) were partially methacrylated using the following procedure. The triblock copolymer (7 g, 21 mmol) was dissolved in dry THF under a N₂ atmosphere, DMAP (21 mg, 174 μmol) and triethylamine (TEA) (601 μl, 4.35 mmol) were added at 0°C. Finally, methacrylic anhydride (MA) (648 μl, 4.35 mmol) at 1:1 molar ratio with TEA was added. The reaction mixture was subsequently stirred for 24 hours at room temperature, followed by the addition of approximately 20 ml water. Next the reaction mixture was dialyzed (membrane with a cut-off of 12-14 kDa) against water for two days at 4 °C and isolated by freeze-drying. The synthesized polymers were characterized by ¹H NMR (300 MHz, DMSO-*d*₆, δ): 7.35 (b, 1H, NH), 6.15 & 5.80 (d, 2H, C=CH₂), 5.4 (d, 1H, CH-OH), 4.95 (d, CO-CH(CH₃)-O), 4.1 (d, 1H, CO-CH(CH₃)-OH), 3.60 (s, 904H, OCH₂CH₂ (PEG-protons)), 3.4 (s, 2H, NHCH₂), 2.2-0.6 (main chain protons and CH₃ of lactate groups). The degree of methacrylation (DM), defined as the percentage of OH groups derivatized with methacrylate moieties was calculated from the ratio of the average intensity of the peaks at 6.15 and 5.80 and intensity of the peak at 5.4 ppm as follows (46):

$$\left((I_{6.15} + I_{5.8}) / 2 \right) / \left((I_{6.15} + I_{5.8}) / 2 + I_{5.4} \right) \times 100\% \quad (2)$$

¹H NMR Spectroscopy

¹H NMR (300 MHz) spectra were recorded on a Gemini 300 MHz spectrometer (Varian Associates Inc., NMR Instruments, Palo Alto, CA) using DMSO-*d*₆ and CDCl₃ as solvents. Chemical shifts were referred to the solvent peak ($\delta = 2.49$ ppm and $\delta = 7.24$ ppm, for DMSO-*d*₆ and CDCl₃, respectively).

Gel Permeation Chromatography

The molecular weights of the polymers were determined by GPC using a Plgel 5 μ m MIXED-D column (Polymer Laboratories) with a column temperature of 40 °C. DMF containing 10 mM LiCl was used as eluent with an elution rate of 0.7 ml min⁻¹, and the sample concentration was 5 mg ml⁻¹ in the same eluent. Poly(ethylene glycols) with defined molecular weights were used as calibration standards (31).

Determination of the Cloud Point

The cloud point (CP) of the polymers was measured with static light scattering using a Horiba Fluorolog fluorometer (650 nm, 90° angle). The polymers were dissolved at a concentration of 3 mg ml⁻¹ in ammonium acetate buffer (pH 5.0, 120 mM). The heating rate was approximately 1 °C min⁻¹ and every 0.2 °C the scattering intensity was measured at 90° angle. The CP is defined as the onset of increasing scattering intensity (48).

Rheological Characterization

The rheological analysis of the (non)-photopolymerized hydrogels was performed on an AR-G2 rheometer (TA-Instruments). Triblock copolymer solutions at a concentration of 20, 25, 30 and 35 wt % were prepared in PBS pH 7.4 supplemented with 0.2 wt% NaN₃ at 4°C and Irgacure 2959 (0.05 wt %) was added. The thermal gels were prepared heating the polymer solutions from 5 to 45 °C at a rate of 1 °C min⁻¹. Non-photopolymerized gels were studied using a cone-plate geometry (steel, 20 mm diameter with an angle of 1°). A solvent trap was used to prevent evaporation of the solvent and 1% strain was applied (45).

To analyze the photopolymerized hydrogels the AR G-2 rheometer was equipped with a UV lightguide connected to a BluePoint lamp 4 (350-450 nm, Honle UV technology, light intensity of 50 mW/cm²). Gels were studied at 37 °C using a plate–plate geometry at 0.1% strain and 1 Hz frequency. The diameter of the geometry was 20 mm and the gap between the plates 300 μ m (44). Strain sweep experiments were performed at 37°C using a plate–plate geometry at 0.2 Hz frequency and a strain range between 0.001 and 10. The polymer solutions were measured as such or upon 5 min UV irradiation.

3D printing of methacrylated HPMAm-lac-PEG triblock copolymer constructs

A BioScaffolder dispensing system (Sys Eng, Salzgitter-Bad, Germany) was used for 3D printing of hydrogel constructs. The pneumatic syringe dispenser was loaded with the triblock copolymer solution (25 wt%), containing 0.05 wt% Irgacure 2959. The dispenser at room temperature extruded the hydrogel on a stationary platform preheated at 40°C according to a CAD/CAM aided pattern in a layer-by-layer deposition mode. Rectangular 3D constructs of 37 (0.6 cm) and 12 layers (0.19 cm), for DMA and degradation studies, respectively, were printed with 0/90° configuration, strand spacing of 1.5 mm and 25 μ m of fiber thickness. A Nikon D40 camera equipped with AF-S NIKKOR 18-55mm 1:3.5-5.6 GII ED objective was used to take pictures of

the constructs. After deposition, the constructs were photopolymerized using a Superlite S-UV 2001AV lamp (Lumatec, Munchen, Germany), which emits UVA and blue light (320–500 nm, intensity of 6 mW cm⁻² at 365 nm).

In a separate experiment, two polymer solutions were loaded with two different Dye-Trak “F” fluorescent microspheres (fluorescent lemon and fluorescent orange) of 15 μm diameter at a concentration of 1*10⁶ spheres per ml. The two microsphere containing polymer/Irgacure 2959 solutions were loaded into two separate extruding syringes and 2 or 3 layer constructs were printed using the settings described above resulting in alternating layers of different hydrogels and several patterns and strand spacing. Subsequently, the constructs were photopolymerized for 10 minutes using a Superlite S-UV 2001AV lamp (Lumatec, Munchen, Germany, blue light 320–500 nm, intensity of 6 mW cm⁻² at 365 nm) and imaged using an Olympus BX51 microscope (Olympus DP70 camera (Hamburg, Germany) equipped with an epifluorescence set-up).

Conversion of methacrylate groups after photopolymerization

To evaluate the conversion of methacrylate groups after photopolymerization, the resulting porous constructs were incubated in 5 ml of 0.2 M NaOH for 3 hours at 37 °C. The gels completely degraded during this incubation. Next, the solution was neutralized by addition of 2 ml of 2M acetic acid, prior to analysis of methacrylic acid. The methacrylate conversion was calculated by comparing the unreacted methacrylic acid of the degraded gels to the initial amount of methacrylic acid prior to photo-cross-linking. Methacrylic acid was detected by Acquity UPLC™, equipped with a BEH C18 1.7 μm, 2.1 x 50 mm column. The eluent used was 95/5/0.1% H₂O/acetonitrile/trifluoroacetic acid. A calibration curve was obtained by injecting different volumes (from 0.1 to 7.5 μl) of a 0.1 mM methacrylic acid solution (44, 46).

DMA Measurements

The elastic moduli (E) of the 3D printed and solid cylindrical constructs (both composed of 25 wt% polymer) were determined by dynamic mechanical analysis (DMA), performed with a DMA 2980 Dynamic Mechanical Analyzer (TA Instruments, New Castle, England) in the controlled force mode. Photopolymerized 3D printed constructs were cut in cylinders of approximately 5 x 6 mm (diameter x height) while the solid constructs were molded and photo-cross-linked in cylinders of 4.5 x 4 mm (diameter x height). These constructs were placed between the parallel plates (upper plate 6 mm, lower plate 45 mm) and a force ramp from 0.001 to 1.0 N at a rate of 0.1 N min⁻¹ was applied at 25 °C. The elastic modulus (E) was the slope of the linear range of the curve stress vs α , where α was calculated as follows:

$$\alpha = (h / \Delta h) + 1 \quad (3)$$

h represents the initial height and Δh is the dimensional change of the measured construct during compression.

Swelling and Degradation Studies

The degradation behavior of 3D constructs was studied in PBS pH 7.4, supplemented with 0.2 wt% NaN₃, at 37°C. Constructs consisting of 12 layers were prepared according to the above described procedure and placed in a 15 ml glass vial with screw cap. The initial weight of the constructs was measured (W₀) and upon addition of 5 ml PBS the vials were incubated at 37°C.

At regular intervals, the incubation buffer was removed and the weight of the constructs was measured (W_t) to calculate the swelling ratio:

$$SR = W_t/W_0 \quad (4)$$

Next, 5 ml PBS was added and the samples were further incubated at 37 °C (44).

Cell Encapsulation and Viability analysis

Full-thickness healthy articular cartilage was obtained from the femoral condyles and femoropatellar groove of fresh equine cadavers ($n = 2$; age, 2-10 years) under aseptic conditions. After overnight digestion using 0.15% type II collagenase at 37°C, the cell suspension was filtered (100- μ m cell strainer) and washed 3 times with phosphate-buffered saline. Cells were then resuspended in expansion medium (DMEM supplemented with 10% fetal bovine serum, 100 units ml^{-1} penicillin and 100 $\mu\text{g ml}^{-1}$ streptomycin and 10 ng ml^{-1} FGF-2) and counted using a hemacytometer. Chondrocytes were expanded in monolayer cultures (5000 cells cm^{-2}) in expansion medium until 90% confluency. After expansion, cells were mixed in 25 wt% pHPMAM-lac-PEG triblock copolymer solution at 4°C containing 0.05 wt% Irgacure 2959. Cells were encapsulated at a density of 5.0×10^6 cells ml^{-1} for LIVE/DEAD assays and at a density of 2.0×10^7 cells ml^{-1} gel for differentiation assays. Constructs of 100 μl were fabricated using two sterilized glass slides and two PVC spacers of 2 mm height. The hydrogel-cell solution at room temperature was put on a glass, the spacers were placed, and the second glass was put on top of the gel, yielding a cylindrical shaped construct. The previously mentioned Superlite S-UV 2001AV lamp (Lumatec) was used to cross-link the cell-laden hydrogel constructs.

Constructs were cultured in differentiation medium (DMEM supplemented with 0.2 mM ascorbic acid 2-phosphate, 0.5% human serum albumin, 1x ITS-X, 100 units/mL penicillin and 100 unit/mL streptomycin, and 5 ng/mL TGF-b2). Samples for LIVE/DEAD assays were taken after 1 and 3 days.

To visualize cell viability, LIVE/DEAD Viability Assay (Molecular Probes MP03224, Eugene, USA) was performed according to the manufacturer's recommendations. The samples were examined using a light microscope (Olympus, BX51, United States) and photomicrographs taken with an Olympus DP70 camera (United States). The excitation/emission filters were set at 488/530 nm to observe living (green) cells and at 530/580 nm to detect dead (red) cells. Live and dead cells were counted for 4 samples per time point, at four locations within each construct.

RESULTS AND DISCUSSION

Polymer Synthesis and Characterization

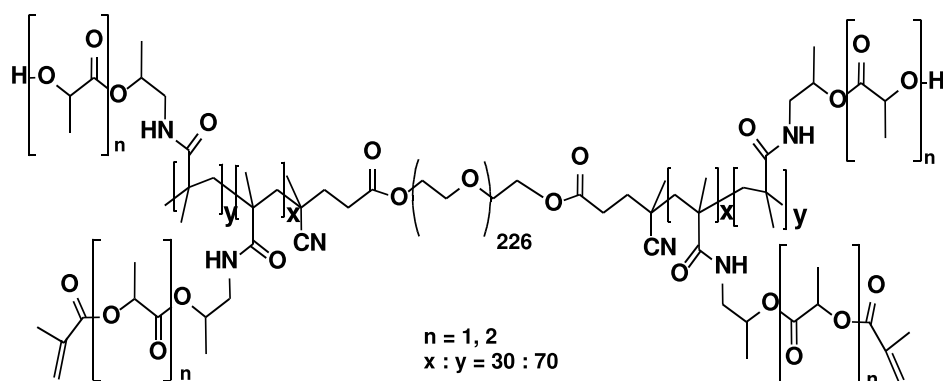
(PEG-ABCPA) $_n$ macroinitiator was synthesized by DCC coupling reaction of PEG (molecular weight (M_w) of 10 kDa) and ABCPA with a yield of 79% and characterized by GPC and $^1\text{H-NMR}$. GPC analysis showed that ~6 molecules of PEG 10 kDa were coupled, (number average molecular weight was 58 kDa with a polydispersity index (PDI) of 2.3). A small peak of unreacted free PEG was visible in the GPC chromatogram (Supporting information (SI) Figure 1), an observation also confirmed by $^1\text{H-NMR}$ (a ratio PEG/ABCPA of 1.2 was calculated by comparing PEG protons to those of ABCPA) (SI, Figure 2) (47). Removal of unreacted ABCPA, achieved by the purification

method used, prevented the formation of polymers of HPMAm-lactate without PEG chain during the subsequent radical copolymerization (SI, Figure 3).

A thermosensitive A-B-A triblock copolymer consisting of pHPMAm-lac A-blocks of approximately 23.5 kDa, as determined by $^1\text{H-NMR}$ and PEG B-block of a M_w of 10 kDa was synthesized by free radical copolymerization using a $(\text{PEG-ABCPA})_n$ macroinitiator and HPMAm mono and dilactate in a molar ratio of 1/1 with a yield of 73 %. The pendant OH groups on the lactate side chains of the polymer were then partly methacrylated in order to allow the formation of chemical cross-links by photopolymerization. The structure of the final polymer is depicted in scheme 1.

The synthesized products are abbreviated as MI, M_0P_{10} and $M_{30}P_{10}$, for macro-initiator, non-methacrylated and methacrylated triblock copolymers, respectively, and their characteristics are listed in Table 1.

The triblock copolymer M_0P_{10} was obtained with a yield of approximately 74% and a HPMAm-monomer/dilactate/HPMAm-dilactate ratio of 1, corresponding to the feed ratio and resulting in a CP



Scheme 1. Chemical structure of A-B-A triblock copolymer composed of methacrylated p(HPMAm-lac) A-blocks and PEG B-block. The hydroxyl groups on the poly(HPMAm) backbone of the thermosensitive block are modified with lactate side chains containing 1 or 2 lactate units ($n = 1, 2$). Thirty percent of the hydroxyl groups on the lactate side chains are derivatized with methacrylate moieties.

Table 1. Characteristics of PEG-ABCPA macroinitiator and A-B-A triblock copolymers composed of (methacrylated) p(HPMAm-lac) A-blocks and PEG B-block. The table lists the values of weight average molecular weight (M_w), number average molecular weight (M_n), polydispersity index (PDI), degree of methacrylation (DM) and cloud point (CP) for macroinitiator (MI), non methacrylated (M_0P_{10}), and methacrylated ($M_{30}P_{10}$) triblock copolymers.

Name	M_w (kDa)	M_n (kDa)	PDI	DM (%)	CP ($^{\circ}\text{C}$)
MI	136 ^b	58 ^b	2.3 ^b	N.A.	N.A.
M_0P_{10}	48 ^b	57 ^a 32 ^b	1.5 ^b	N.A.	29 ^c
$M_{30}P_{10}$	48 ^b	57 ^a 32 ^b	1.5 ^b	30 ^a	11 ^c

[a] Determined by $^1\text{H-NMR}$ [b] Determined by GPC [c] Determined by static light scattering (SLS)

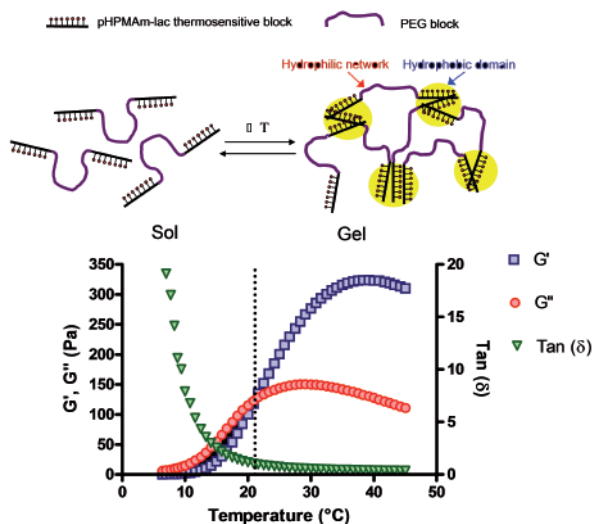


Figure 1. Effect of temperature on storage modulus (G'), loss modulus (G'') and $\tan(\delta)$ of a hydrogel of 25 wt% polymer concentration in PBS, pH 7.4. At temperature below the cloud point of the polymer the system is in the sol-state with $G'' > G'$. With increasing temperature, G' increases and equals G'' at 21 °C, referred to as gel temperature. Above this temperature, the network is in the gel-state with the thermosensitive blocks assembled in hydrophobic domains.

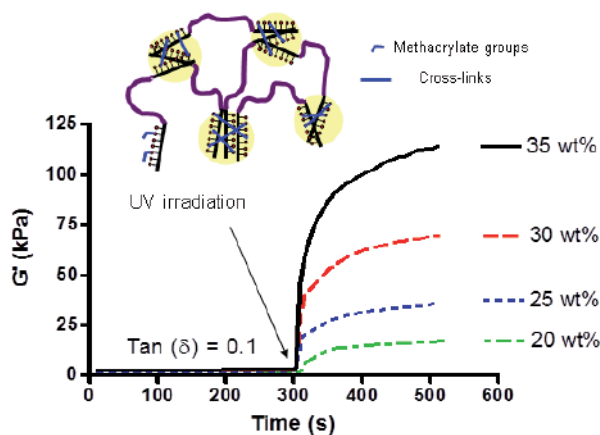


Figure 2. Effect of photopolymerization on mechanical properties of 20, 25, 30 and 35 wt% polymer hydrogels at 37°C. The storage modulus (G') is shown as a function of time. UV irradiation was applied after 300 sec. During UV curing chemical cross-links within the hydrophobic domains are formed, leading to an increase in G' and values of $\tan(\delta) < 0.1$ for all the studied concentrations.

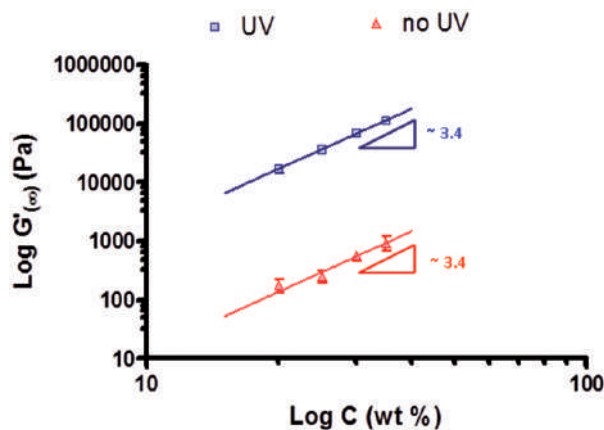


Figure 3. Power law dependence of the storage plateau modulus (G'_{∞}) of photopolymerized (squares) and thermal hydrogels (triangles) at 37 °C on polymer concentration (C). The solid lines represent the fit, calculated by power law. For both thermal and photopolymerized networks, a similar power law coefficient of approximately 3.4 was found. Data are shown as mean \pm standard deviation, $n = 3$.

of the polymer of 29 °C. Based on ^1H NMR, a M_n of 57 kDa was calculated. It appears that the M_n based on ^1H -NMR analysis exceeds that measured by GPC analysis (M_n 32 kDa). It was shown earlier that this discrepancy can be ascribed to the use of PEG homopolymers as GPC standards that display larger hydrodynamic volumes than the triblock copolymers in the used eluent (44, 45).

As expected, upon methacrylation, the $M_{30}P_{10}$ polymer displayed the same molecular weight as the non-methacrylated M_0P_{10} polymer. The yield was 88% and the polymer had a methacrylation degree of 30%, (calculated based on ^1H -NMR). Similarly to previously reported data, the introduction of methacrylate groups on the lactate side chains of the polymer led to an increase of hydrophobicity and consequently to a decrease in CP to 11 °C (44, 46).

Hydrogel Mechanical Properties

In order to be used in organ printing, the hydrogels must possess adequate mechanical properties, allow easy extrusion through the pneumatic dispensing system described earlier and maintain dimensional stability upon computer aided layer-by-layer fiber deposition. Besides processability requirements, the hydrogel must provide for encapsulated cells with long-term mechanical support and eventually degrade into biocompatible products when new tissue is formed (21). All the abovementioned requirements for organ printing were addressed in this study, starting with the characterization of the gelation kinetics of $M_{30}P_{10}$ triblock copolymer hydrogel.

A hydrogel composed of 25 wt% $M_{30}P_{10}$ triblock copolymer was prepared and characterized by rheological analysis. The hydrogel solid content was chosen based on good cell survival in these gels in a previous study performed by Vermonden et al (46). Figure 1 shows the effect of temperature on the visco-elastic properties of the hydrogel and demonstrates that at low temperatures (5 °C), $M_{30}P_{10}$ has a liquid-like behavior in aqueous solution with a storage modulus (G') close to zero (45). This behavior is particularly beneficial for the encapsulation of cells that can be easily and homogeneously mixed at high concentration with the cold polymer solution. The temperature controlled dispensing system can be then loaded with the polymer solution, in which the cells can be mixed, and the required viscosity can be tuned by adjusting the dispenser temperature. Figure 1 shows that G' increases from 0 to 350 Pa when increasing the temperature from 5 to 45 °C, with 21 °C often referred to as the gelation temperature (T_{gel}) where G' starts to dominate G'' .

Upon extrusion, the cell-laden hydrogel fibers are deposited layer-by-layer according to a computer-aided pattern on a fixed collector, pre-heated to 37 °C. A visco-elastic material, displaying a G' of 350 Pa and a $\tan(\delta)$ of 0.3, is formed at 40 °C (Figure 1), demonstrating that the thermosensitive character of the studied hydrogel is particularly beneficial for 3DF application as it ensures good resolution and dimensional stability of the hydrogel upon extrusion. However, the mechanical properties of the physically cross-linked hydrogel does not provide long-term stability, as the thermo-gel undergoes relatively rapid dissolution in culture, releasing the cells prematurely (46). Therefore, a chemical cross-linking strategy was employed to stabilize the hydrogel structure (46). Upon printing, the 3D construct was exposed to UV light (Superlite S-UV 2001AV lamp (Lumatec), which emits UVA and blue light (320–500 nm, intensity of 6 mW cm^{-2} at 365 nm)), which induces the formation of chemical cross-links within the hydrophobic domains. Figure 2 shows the effect of the photopolymerization on the rheological properties of

the hydrogels. As can be seen in Figure 2 and as demonstrated earlier (44), the storage modulus of the hydrogel remarkably increased upon UV irradiation (BluePoint lamp 4, 350–450 nm, Honle UV technology, light intensity of 50 mW cm⁻²), due to the stabilization of the hydrophobic domains via chemical cross-links. For example, G' increased approximately by a factor 100 for the 25 wt% $M_{30}P_{10}$ hydrogel after photopolymerization (from 0.35 to 36 kPa).

Figure 2 further shows that G' increased with increasing polymer concentration, demonstrating the possibility to tailor the stiffness of the hydrogel by changing the solid content. For all the tested polymer concentrations, the photopolymerized hydrogels exhibited $\tan(\delta)$ values of 0.1, meaning that almost fully elastic matrices were formed.

In Figure 3, it can be observed that for thermal hydrogels (triangles), the storage modulus (G') at 37 °C scaled with polymer concentration (C) according to a power law Equation (1). Chemically cross-linked hydrogels (squares in Figure 3), also displayed the same power law scaling between storage modulus at plateau level (G'_{∞}) and C:

$$G'_{\infty}(\text{Pa}) = A * C (\text{wt } \%)^K \quad (1)$$

where A is equal to 0.71 ± 0.19 and $5.3 \pm 0.60 * 10^{-3}$ and K is equal to 3.37 ± 0.08 and 3.40 ± 0.32 for photo-polymerized and thermal hydrogels, respectively.

This non-linear rheological behavior is typically found for semi-flexible polymers and can be ascribed to differences in hydrogel inner structure, at increasing polymer concentration, due to different self-assembly of the thermosensitive chains. At temperatures higher than the polymer cloud point, the thermosensitive chains arrange into hydrophobic domains that increase in size as well as density at increasing polymer concentration, resulting in power law dependence between G'_{∞} and C. Indeed, the formation of larger polymer-rich clusters at increasing concentration greatly contributes to the hydrogel strength even at limited increase in polymer fraction. The non-linear mechanical properties in thermally assembled p(HPMAM-lac-PEG-p(HPMAM-lac) based hydrogels was also observed earlier by Vermonden *et al.* (45).

Many biopolymers, such as DNA, collagen, actin display semi-flexible behavior (49-52), unlike ordinary flexible polymers, such as polystyrene, poly(methyl methacrylate) or polylactide-PEG-polylactide block copolymers, that show a linear dependence of G'_{∞} on concentration (53). Semi-flexible polymers based networks are of great technological interest because they exhibit a high modulus at relatively low polymer volume fraction (52). This property is particularly relevant for load bearing applications, such as cartilage tissue engineering. Although a considerable number of semi-flexible natural biomaterials is reported in literature, only a few synthetic polymers exhibit semi-flexible character (54, 55).

As compared to networks of natural biopolymers described in literature, a higher value of K was found for photopolymerized and thermal hydrogels. Rammensee *et al.* reported a $G'_{\infty} \sim C^2$ dependence of both cross-linked and non-cross-linked spider silk hydrogels. Similarly, MacKintosh *et al.* showed that for entangled solutions of actin, the plateau modulus scaled with concentration as $G'_{\infty} \sim C^{1/5}$ and predicted a stronger ($G'_{\infty} \sim C^{5/2}$) dependence for densely cross-linked hydrogels (52). In $M_{10}P_{30}$ based hydrogel, a value of K (3.4) higher than those reported above was found, demonstrating the possibility to increase the elastic modulus of the photo-crosslinked hydrogel to an even higher extent at low polymer volume fractions.

The value of 3.4 is similar to the one reported by Vader *et al.* for collagen type I networks, which showed $G'_{\infty} \sim C^3$ dependence (56). Because of the similarity of its rheological properties to those of collagen, the described M 10 P 30 hydrogel is a promising candidate for tissue regeneration purposes.

The rheological behavior and the dependence of storage modulus on polymer concentration can be tuned by the preparation procedure of the hydrogel, e.g. we previously demonstrated that the heating rate remarkably affects the hydrogel self-assembly (57). Particularly, it was shown that when the hydrogel self-assembles by heat shock (immediate temperature change from 4 to 37 °C), its inner structure shows a homogeneous distribution of nano/micro phase separated polymer assemblies. In contrast, at slower heating rate, a more extensive phase separation occurred, resulting in the formation of larger polymer-rich domains.

Non-linear mechanical behavior was also observed in (non)photo-polymerized hydrogels at 37 °C with increasing shear strain from 0.001 to 10 (Figure 4). In contrast to many biopolymers, exhibiting strain-stiffening, $M_{10}P_{30}$ hydrogels of different polymer concentrations, both thermally and chemically cross-linked (Figure 4a), showed strain-softening behavior, with substantial decrease of G' and predominance of loss modulus for strain values higher than 0.1. This behavior is often found in (permanently) cross-linked elastic networks and is attributed to the redistribution of internal stresses upon progressive slip of the cross-links with increasing shear strain and to the eventual breakage of the reversible cross-links or of the photopolymerized network at high strains (54, 58). As expected, the thermal hydrogels are disrupted at lower strain values as compared to chemical networks (Figure 4a), as their cross-links can be more easily destabilized by internal stresses. Interestingly, comparing photopolymerized hydrogels of different polymer concentration (Figure 4b), it can be noted that the networks of higher polymer concentration start to soften and break at lower strain as compared to their analogues of lower solid content, while the corresponding stress values at the failure strain were similar for both polymer concentrations. Matrices of higher polymer concentration, indeed, have a higher cross-link density that yield more rigid and brittle gels that break at lower shear strains as compared to more flexible networks of lower polymer content.

3D Printed Constructs

Figure 5 shows that computer controlled deposition of 25 wt% $M_{30}P_{10}$ hydrogels resulted in the formation of 3D porous hydrogels with a thickness up to a total height of approximately 0.6 cm (37 layers) and regular squared vertical pores of $1.2 \times 1.2 \times 6$ mm (length \times width \times height) throughout the printed matrix. The height of the printed scaffold was chosen arbitrarily and was dependent on the design of the STL file imported in the printing program. Potentially, higher scaffolds can be built. Clearly, the combination of thermosensitivity and photopolymerization allows the preparation of matrices with remarkable thickness, precise and reproducible internal design and porosity and good dimensional stability. Importantly, the dual cross-linking method (thermally and UV induced) yielded constructs of enhanced resolution as compared to bioprinted scaffolds that rely only on photopolymerization, as described for hyaluronan/gelatin hydrogels by Skardal *et al.* (59) or on physical cross-linking as studied by Cohen *et al.* for alginate hydrogels (60). Resolution is an important property as it allows the preparation of constructs with highly defined 3D structure and good geometrical fidelity to the shape of the

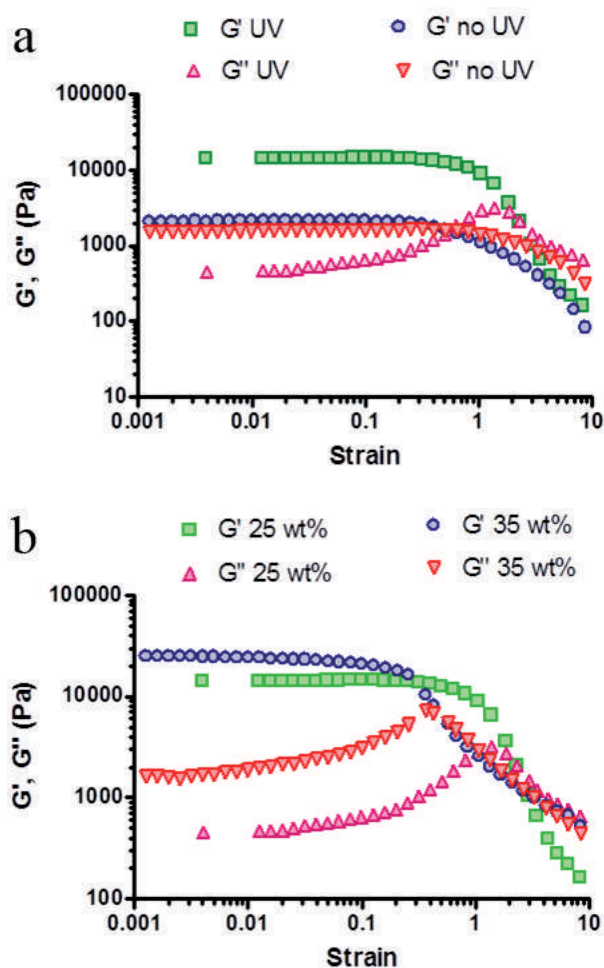


Figure 4. Strain-softening behavior of thermally and chemically assembled networks. The effect of increasing strain on storage (G') and loss (G'') moduli is studied for **a)** thermally assembled (no UV) and photopolymerized (UV) 25 wt% polymer hydrogels and for **b)** photopolymerized hydrogels of 25 and 35 wt% polymer concentration. The rheological analyses of the hydrogels were performed at 37 °C and at a frequency of 0.2 Hz.

defect in the organ to be regenerated. The weight of subsequent hydrogel layers caused the fusion of transversal pores during stacking of layers, as indicated by the white arrow in Figure 5b. The fusion of transversal pores, commonly found in 3DF of soft materials like hydrogels (61) can be a potential limitation of the current printing technology. However, the presence of vertical pores combined with the high diffusivity of the studied hydrogel matrix (57, 58), is sufficient to provide rapid diffusion of nutrients and metabolites (61).

Figure 6 shows microscopy images of layered and adjacent 25 wt% $M_{30}P_{10}$ hydrogel fibers loaded with fluorescent microspheres (fluorescent lemon and fluorescent orange). The microspheres are easy to handle and to detect by microscopy. Moreover, they can be easily incorporated in the hydrogel matrix and are used in this study as cell models. Several patterns were generated (straight layered fibers in Figure 6a, 6b and 6e and adjacent circular/squared fibers in Figure 6c and 6d). These pictures illustrate the printability of the studied hydrogel with highly defined patterning. By comparing Figures 6a and 6e, it can be observed that

Figure 5. Photographs of 3D printed 25 wt% $M_{30}P_{10}$ hydrogels (dimensions: 1 cm \times 1.5 cm \times 0.59 cm, strand spacing: 1.5 mm). a, Top vision, b, detail of vertical pores with fused transversal pores (white arrow).

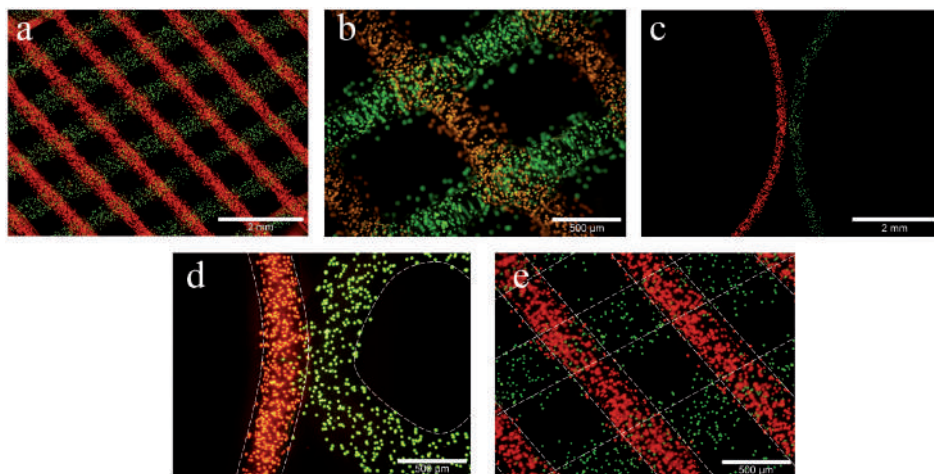
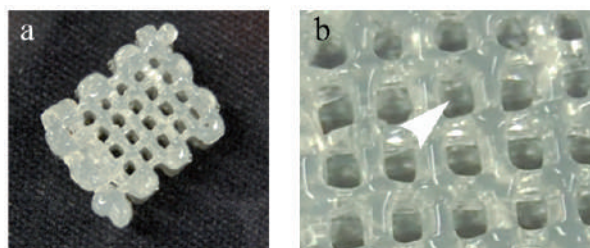


Figure 6. Microscopy pictures of subsequently printed layers of 25 wt% $M_{30}P_{10}$ hydrogels loaded with Dye-Trak “F” fluorescent microspheres, fluorescent lemon and fluorescent orange at the concentration of 1×10^6 spheres per ml. a, 2 and b, 3 layers angled construct (1.5 mm strand spacing) with distinct localization of fluorescent microspheres. c, d, printing of adjacent fibers with circular patterns with maintenance of distinct dye localization. e, 2 layers construct with 0.8 mm strand spacing.

the same layered design can be realized at different strand spacing (1.5 mm and 0.8 mm, for Figure 6a and 6e, respectively) and pore shape is maintained, demonstrating a good resolution for 3D printing of the studied thermosensitive material. Both the layered and the adjacent fluorescent microsphere loaded hydrogels (Figure 6) displayed excellent maintenance of distinct localization of the cell mimicking microspheres. The hydrogel can thus be potentially used for the construction of organized structures containing different cell types, as long as the hydrogel maintains integrity and supports survival of cells during and after the printing process.

Mechanical characterization and degradation behavior of 3D constructs

Porous constructs of 25 wt% $M_{30}P_{10}$ hydrogel (dimensions of 1 cm \times 1.5 cm \times 0.6 cm) with a strand spacing of 1.5 mm were printed and subsequently photopolymerized for 10 minutes. It was shown that $88 \pm 7\%$ of the available methacrylate groups had reacted (UPLC analysis), which is in line with previous data on the photopolymerization of solid constructs, where a methacrylate conversion of

90 ± 2% was found (44, 46). It is clear that regardless of the shape, porosity and hydrogel volume, the photopolymerization process is very efficient for hydrogels of 25 wt% $M_{30}P_{10}$ polymer concentration.

The chemical cross-links influenced the mechanical and degradation behavior of the (porous 3D printed) hydrogels. An elastic modulus (E) of 119 ± 4 kPa was obtained for 3D printed constructs of 0.6 cm. This value is comparable with that of a solid construct of equal polymer composition, which had elastic modulus of 108 ± 7 kPa (SI, Figure 4) but lower than that reported for native cartilage tissue (E of approximately 4 MPa) (62). The similarity found in elastic moduli of solid and porous constructs can be explained by the lack of transversal pores in the 3D constructs that made the compression resistance of the printed constructs similar to that of solid cylinders. Also, the constructs might suffer from water evaporation during the printing process, resulting in slightly higher polymer concentrations and stronger gels as compared to the solid constructs. We reported earlier E values of 40 to 70 kPa for solid constructs of 25 wt % p(HPMAM-lac)-PEG triblock copolymer with methacrylation degrees ranging from 4 to 9% (46), demonstrating the possibility to tailor the elastic modulus of the matrices by the methacrylation extent. Other photopolymerized PEG based solid hydrogels studied for cartilage engineering showed values of E from 60 to 500 kPa, a range that includes the elastic modulus found in the present study for 3D printed constructs (63).

The degradation rate of porous constructs composed of 12 layers of 25 wt% $M_{30}P_{10}$ hydrogel was studied by incubating them at pH 7.4 and 37 °C. Figure 7a shows that the constructs degraded completely in approximately 190 days upon a swelling phase of about 130 days, where the constructs doubled their weight (swelling ratio of 2), due to uptake of water. The swelling behavior of the photopolymerized hydrogels is a direct consequence of the degradation of the polymer. As described previously by Neradovic *et al.* (48), during incubation with buffer at pH 7.4, the lactate side chains of the polymer are hydrolyzed through a backbiting mechanism, resulting in increased hydrophilicity of the network and consequently higher water uptake. The weight loss of the hydrogel begins when the ester groups connecting the methacrylate moieties and the polymer backbone are also hydrolyzed. These connecting ester bonds are less sensitive for hydrolysis than those present in the non-derivatized units. Therefore, during its initial phase, the degradation translates into a gradual increase of the swelling ratio and only when the chemical cross-links are cleaved, the networks dissolves, resulting in weight loss (64).

The degradation time of the constructs relates very well to the degradation time of cylindrical gels of 100 mg weight based on 20 and 35 wt % $M_{30}P_{10}$ (Figure 7a) (58). Indeed, regardless of the weight of the (porous) matrix (100 and 750 mg for cylindrical gels and porous constructs, respectively), the degradation time scales linearly with polymer concentration (Figure 7b). This finding is supported and explained by previous studies, where it was shown that the degradation of the polymer is exclusively mediated by hydrolysis (48, 64). The degradation rate depends on the polymer concentration and consequently on the cross-linking density and it is not related to the amount or shape of the hydrogel.

The observed degradation time-scale of the constructs is suitable for cartilage regeneration purposes, for which long-term mechanical support is of importance and eventually complete degradation of the material is needed.

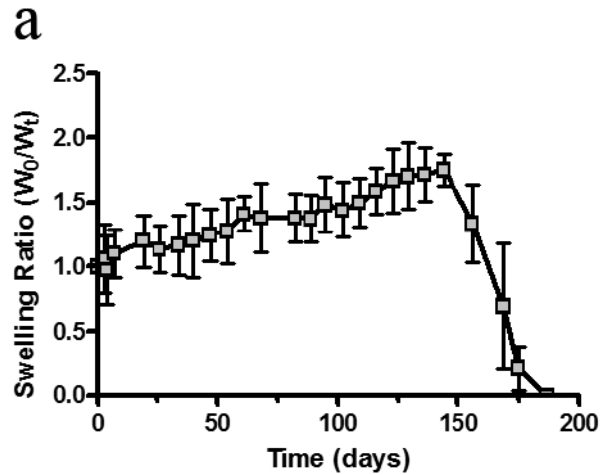
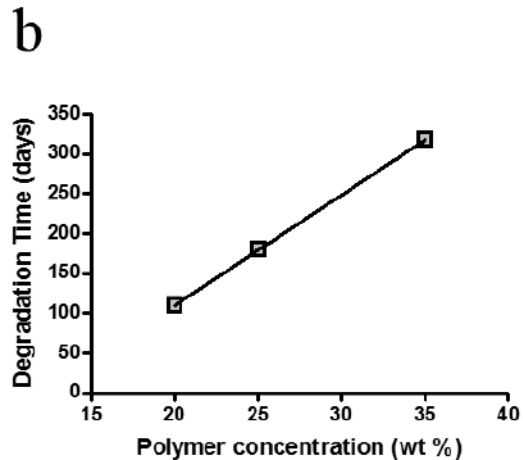


Figure 7. a, degradation profile of 12 layered 3D constructs of 25 wt% $M_{30}P_{10}$ hydrogel (dimensions: 1 cm \times 1.5 cm \times 0.6 cm, strand spacing: 1.5 mm) at 37 °C and pH 7.4. The swelling ratio, defined as ratio between the weight of the construct at different timepoints during exposure to degradation medium (W_t) and the initial weight of the construct (W_0), is shown as a function of time. Data are shown as mean \pm SD, $n = 3$. **b**, relationship between the degradation times of 20 and 35 wt% $M_{30}P_{10}$ solid cylindrically shaped photopolymerized hydrogels of 100 mg and 12 layered 3D constructs of 25 wt% $M_{30}P_{10}$ hydrogel (dimensions: 1 cm \times 1.5 cm \times 0.6 cm; strand spacing: 1.5 mm; 250 mg) at 37 °C and pH 7.4. Regardless of the shape and weight of the hydrogels, the degradation time scaled linearly with the polymer concentration.



Viability of Equine Articular Chondrocytes in Photopolymerized Hydrogels

To assess to which extent photopolymerized hydrogels affect the viability of encapsulated chondrocytes, their survival was studied in cylindrical solid constructs of 100 μ l volume after 1 and 3 days culture. Upon encapsulation of the chondrocytes in the 25 wt% hydrogel and subsequent photo-polymerization, a homogeneous distribution of cells throughout the hydrogel was observed (data not shown). Excellent viability ($94 \pm 3\%$) was observed after 1 day of culture and no significant decrease in cell survival was found after 3 days with a viability of $85 \pm 7\%$ (Pictures of chondrocytes stained for LIVE/DEAD assay are shown in SI, Figure 5). As shown earlier for human mesenchymal stromal cells (46), the investigated material also supports viability of chondrocytes, and no adverse effects due to the UV exposure were observed (65). These results establish the basis for further implementation of these materials in the field of cartilage tissue engineering.

CONCLUSIONS

In this paper, we reported on the feasibility of a photopolymerizable thermosensitive and biodegradable hydrogel based on PEG and HPMA-lactate for 3D fiber deposition. We demonstrated that the hydrogel mechanical properties adapt well to the process of 3D printing, as structurally stable 3D constructs with well defined vertical porosity and enhanced stability by photopolymerization were successfully printed by subsequent deposition of gel fibers up to at least 0.6 cm. Construct pattern and strand spacing could easily be tuned. Using layer-by-layer deposition of hydrogels, accurate and precise placement of different beads encapsulated in p(HPMAm-lac)-PEG-p(HPMAm-lac) was shown. The semi-flexible character of the studied polymer, demonstrated by the power law scaling of the hydrogel storage moduli with the polymer concentration, establishes similarities with many natural polymers, including collagen. These similarities make the studied biomaterial potentially suitable as synthetic extracellular matrix for cartilage tissue engineering. The good mechanical resistance and tunable degradation rate of the hydrogels offer potential long-term support to the encapsulated cells until the new tissue is formed. Importantly, high chondrocyte viability was observed after 1 and 3 days, further emphasized the suitability of the studied hydrogel as a promising candidate for bioprinting applications. Possible applications might not be limited to the described biofabrication technique, but might include other rapid prototyping techniques like laser assisted bioprinting (66), organ printing (11) and soft lithography (67).

Future studies will be addressed towards the design of complex 3D constructs with appropriate properties for engineering articular cartilage and long-term tissue formation both *in vitro* and *in vivo* will be investigated. The high tailorability of the hydrogels, in terms of mechanical properties, degradation behavior and diffusivity (44, 58, 68), as well as the possibility to regulate cell behavior by incorporating and releasing growth factors in a diffusion controlled and tailorable fashion (44) and the functionalization of polymer hydroxyl groups with adhesive peptides (69) hold great potential for a successful further development.

ACKNOWLEDGEMENTS

This research was supported by the Dutch Program for Tissue Engineering (DPTE) (project number 6731) and Dutch Technology Foundation STW, Applied Science Division of NWO and the Technology Program of the Ministry of Economic Affairs (Project number 07825).

REFERENCES

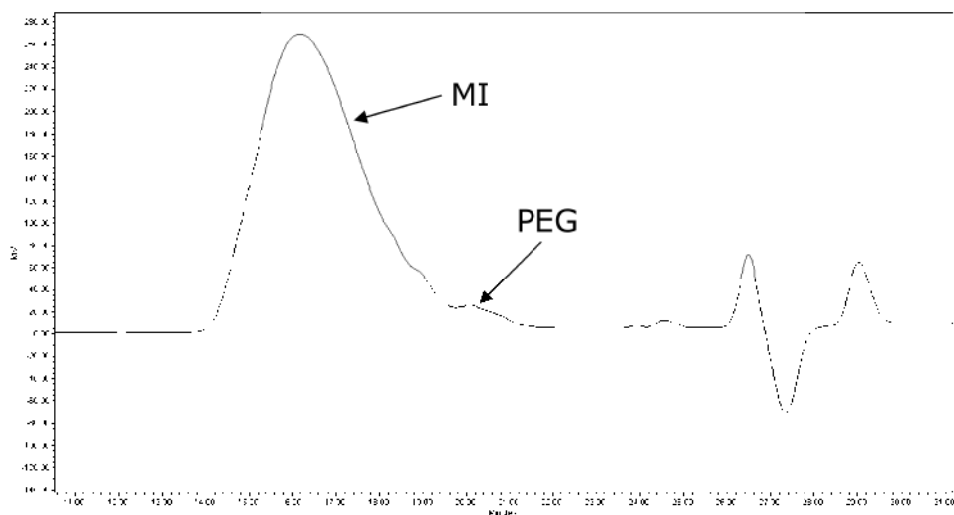
1. Yoshida H, Matsusaki M, and Akashi M, Scaffold-Mediated 2D Cellular Orientations for Construction of Three Dimensionally Engineered Tissues Composed of Oriented Cells and Extracellular Matrices. *Advanced Functional Materials*, 2009. **19**(7): p. 1001-1007.
2. Suh KY and Lee HH, Capillary Force Lithography: Large-Area Patterning, Self-Organization, and Anisotropic Dewetting. *Adv. Funct. Mat.*, 2002. **12**(6-7): p. 405-413.
3. Klein TJ, Rizzi SC, Reichert JC, Georgi N, Malda J, Schuurman W, Crawford RW, and Huttmacher DW, Strategies for zonal cartilage repair using hydrogels. *Macromol Biosci*, 2009. **9**(11): p. 1049-58.
4. Fedorovich NE, Alblas J, de Wijn JR, Hennink WE, Verboort AJ, and Dhert WJ, Hydrogels as extracellular matrices for skeletal tissue engineering: state-of-the-art and novel application in organ printing. *Tissue Eng*, 2007. **13**(8): p. 1905-25.

5. Hutmacher DW, Sittinger M, and Risbud MV, Scaffold-based tissue engineering: rationale for computer-aided design and solid free-form fabrication systems. *Trends Biotechnol*, 2004. **22**(7): p. 354-62.
6. Klein TJ, Malda J, Sah RL, and Hutmacher DW, Tissue engineering of articular cartilage with biomimetic zones. *Tissue Eng Part B Rev*, 2009. **15**(2): p. 143-57.
7. Klein TJ, Schumacher BL, Schmidt TA, Li KW, Voegtline MS, Masuda K, Thonar EJ, and Sah RL, Tissue engineering of stratified articular cartilage from chondrocyte subpopulations. *Osteoarthritis Cartilage*, 2003. **11**(8): p. 595-602.
8. Waldman SD, Grynspas MD, Pilliar RM, and Kandel RA, The use of specific chondrocyte populations to modulate the properties of tissue-engineered cartilage. *J Orthop Res*, 2003. **21**(1): p. 132-8.
9. Fedorovich NE, De Wijn JR, Verbout AJ, Alblas J, and Dhert WJ, Three-dimensional fiber deposition of cell-laden, viable, patterned constructs for bone tissue printing. *Tissue Eng Part A*, 2008. **14**(1): p. 127-33.
10. Fedorovich NE, Swennen I, Girones J, Moroni L, van Blitterswijk CA, Schacht E, Alblas J, and Dhert WJ, Evaluation of photocrosslinked Lutrol hydrogel for tissue printing applications. *Biomacromolecules*, 2009. **10**(7): p. 1689-96.
11. Mironov V, Visconti RP, Kasyanov V, Forgacs G, Drake CJ, and Markwald RR, Organ printing: tissue spheroids as building blocks. *Biomaterials*, 2009. **30**(12): p. 2164-74.
12. Suh JK and Matthew HW, Application of chitosan-based polysaccharide biomaterials in cartilage tissue engineering: a review. *Biomaterials*, 2000. **21**(24): p. 2589-98.
13. El-Ayoubi R, DeGrandpre C, DiRaddo R, Yousefi AM, and Lavigne P, Design and dynamic culture of 3D-scaffolds for cartilage tissue engineering. *J Biomater Appl*, 2009. **25**(5): p. 429-44.
14. Hollister SJ, Porous scaffold design for tissue engineering. *Nat Mater*, 2005. **4**(7): p. 518-24.
15. Masood SH, Singh JP, and Morsi Y, The design and manufacturing of porous scaffolds for tissue engineering using rapid prototyping. *Int J Adv Manuf Technol*, 2005. **27**: p. 415-420.
16. Moutos FT, Freed LE, and Guilak F, A biomimetic three-dimensional woven composite scaffold for functional tissue engineering of cartilage. *Nat Mater*, 2007. **6**(2): p. 162-7.
17. Woodfield TB, Malda J, de Wijn J, Peters F, Riesle J, and van Blitterswijk CA, Design of porous scaffolds for cartilage tissue engineering using a three-dimensional fiber-deposition technique. *Biomaterials*, 2004. **25**(18): p. 4149-61.
18. Fedorovich NE, De Wijn JR, Verbout AJ, Alblas J, and Dhert WJ, Three-dimensional fiber deposition of cell-laden, viable, patterned constructs for bone tissue printing. *Tissue Eng. Part A*, 2008. **14**(1): p. 127-33.
19. Stoop R, Smart biomaterials for tissue engineering of cartilage. *Injury*, 2008. **39** **Suppl 1**: p. S77-87.
20. Vinatier C, Guicheux J, Daculsi G, Layrolle P, and Weiss P, Cartilage and bone tissue engineering using hydrogels. *Biomed Mater Eng*, 2006. **16**(4 **Suppl**): p. S107-13.
21. Vinatier C, Mrugala D, Jorgensen C, Guicheux J, and Noel D, Cartilage engineering: a crucial combination of cells, biomaterials and biofactors. *Trends Biotechnol*, 2009. **27**(5): p. 307-14.
22. Van Tomme SR, Storm G, and Hennink WE, In situ gelling hydrogels for pharmaceutical and biomedical applications. *Int J Pharm*, 2008. **355**(1-2): p. 1-18.
23. Jeong B and Gutowska A, Lessons from nature: stimuli-responsive polymers and their biomedical applications. *Trends Biotechnol*, 2002. **20**(7): p. 305-11.
24. Grandolfo M, D'Andrea P, Paoletti S, Martina M, Silvestrini G, Bonucci E, and Vittur F, Culture and differentiation of chondrocytes entrapped in alginate gels. *Calcif Tissue Int*, 1993. **52**(1): p. 42-8.
25. Hauselmann HJ, Fernandes RJ, Mok SS, Schmid TM, Block JA, Aydelotte MB, Kuettner KE, and Thonar EJ, Phenotypic stability of bovine articular chondrocytes after long-term culture in alginate beads. *J Cell Sci*, 1994. **107** (**Pt 1**): p. 17-27.
26. Sims CD, Butler PE, Casanova R, Lee BT, Randolph MA, Lee WP, Vacanti CA, and Yaremchuk MJ, Injectable cartilage using polyethylene oxide polymer substrates. *Plast Reconstr Surg*, 1996. **98**(5): p. 843-50.
27. Ibusuki S, Iwamoto Y, and Matsuda T, System-engineered cartilage using poly(N-isopropylacrylamide)-grafted gelatin as in situ-formable scaffold: in vivo performance. *Tissue Eng*, 2003. **9**(6): p. 1133-42.
28. Nagahama K, Ouchi T, and Ohya Y, Temperature-Induced Hydrogels Through Self-Assembly of Cholesterol-Substituted Star PEG-b-PLLA Copolymers: An Injectable Scaffold for Tissue Engineering. *Adv Funct Mater*, 2008. **18**(8): p. 1220-1231.
29. Chaouat M, Le Visage C, Baille WE, Escoubet B, Chaubet F, Mateescu ME, and Letourneur D, A Novel Cross-linked Poly(vinyl alcohol) (PVA) for Vascular Grafts. *Adv Funct Mater*, 2008. **18**(19): p. 2855-2861.
30. Morra M, Cassinelli C, Cascardo G, Nagel M-D, Della Volpe C, Siboni S, Maniglio D, Brugnara M, Ceccone C, Schols HA, and Ulvskov P, Effects on Interfacial Properties and Cell Adhesion of Surface Modification by Pectic Hairy Regions. *Biomacromolecules*, 2004. **5**(6): p. 2094-2104.
31. Soga O, van Nostrum CF, and Hennink WE, Poly(N-(2-hydroxypropyl) methacrylamide mono/di lactate): a new class of biodegradable polymers with tuneable thermosensitivity. *Biomacromolecules*, 2004. **5**(3): p. 818-21.
32. Vermonden T, Besseling NAM, van Steenberghe MJ, and Hennink WE, Rheological studies of thermosensitive triblock copolymer hydrogels. *Langmuir*, 2006. **22**(24): p. 10180-4.
33. Vermonden T, Fedorovich NE, van Geemen D, Alblas J, van Nostrum CF, Dhert WJ, and Hennink

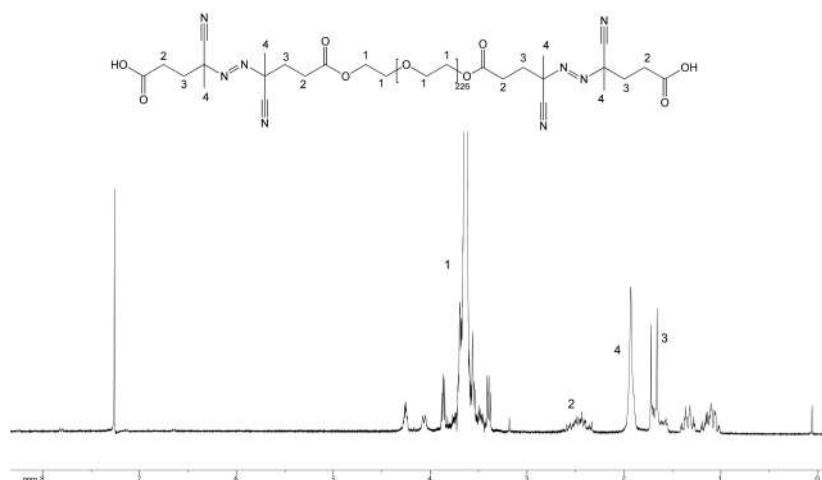
- WE, Photopolymerized thermosensitive hydrogels: synthesis, degradation, and cytocompatibility. *Biomacromolecules*, 2008. **9**(3): p. 919-26.
34. Censi R, Vermonden T, van Steenberg MJ, Deschout H, Braeckmans K, De Smedt SC, van Nostrum CF, di Martino P, and Hennink WE, Photopolymerized thermosensitive hydrogels for tailorable diffusion-controlled protein delivery. *J Control Release*, 2009. **140**(3): p. 230-6.
 35. Jeong B, Kim SW, and Bae YH, Thermosensitive sol-gel reversible hydrogels. *Adv Drug Deliv Rev*, 2002. **54**(1): p. 37-51.
 36. Klouda L and Mikos AG, Thermoresponsive hydrogels in biomedical applications. *Eur J Pharm Biopharm*, 2008. **68**(1): p. 34-45.
 37. Mow VC, *Structure and function of articular cartilage and meniscus*, in *Basic Orthopaedic Biomechanics*, Mow VC and Hayes WC, Editors. 1997, Lippincott-Raven Press: Philadelphia. p. 514.
 38. Vanderploeg EJ, Wilson CG, and Levenston ME, Articular chondrocytes derived from distinct tissue zones differentially respond to in vitro oscillatory tensile loading. *Osteoarthritis Cartilage*, 2008. **16**(10): p. 1228-36.
 39. Kim S, Changes in surgical loads and economic burden of hip and knee replacements in the US: 1997-2004. *Arthritis Care Res.*, 2008. **59**(4): p. 481-488.
 40. Saris DB, Vanlauwe J, Victor J, Almqvist KF, Verdonk R, Bellemans J, and Luyten FP, Treatment of symptomatic cartilage defects of the knee: characterized chondrocyte implantation results in better clinical outcome at 36 months in a randomized trial compared to microfracture. *Am J Sports Med*, 2009. **37 Suppl 1**: p. 10S-19S.
 41. Ochi M, Adachi N, Nobuto H, Yanada S, Ito Y, and Agung M, Articular cartilage repair using tissue engineering technique--novel approach with minimally invasive procedure. *Artif Organs*, 2004. **28**(1): p. 28-32.
 42. Boland T, Xu T, Damon B, and Cui X, Application of inkjet printing to tissue engineering. *Biotechnol J*, 2006. **1**(9): p. 910-7.
 43. Varghese D, Deshpande M, Xu T, Kesari P, Ohri S, and Boland T, Advances in tissue engineering: cell printing. *J Thorac Cardiovasc Surg*, 2005. **129**(2): p. 470-2.
 44. Censi R, Vermonden T, van Steenberg MJ, Deschout H, Braeckmans K, De Smedt SC, van Nostrum CF, di Martino P, and Hennink WE, Photopolymerized thermosensitive hydrogels for tailorable diffusion-controlled protein delivery. *Journal of Controlled Release*, 2009. **140**(3): p. 230-236.
 45. Vermonden T, Besseling NAM, van Steenberg MJ, and Hennink WE, Rheological Studies of Thermosensitive Triblock Copolymer Hydrogels. *Langmuir*, 2006. **22**(24): p. 10180-10184.
 46. Vermonden T, Fedorovich NE, van Geemen D, Alblas J, van Nostrum CF, Dhert WJA, and Hennink WE, Photopolymerized Thermosensitive Hydrogels: Synthesis, Degradation, and Cytocompatibility. *Biomacromolecules*, 2008. **9**(3): p. 919-926.
 47. Neradovic D, van Nostrum CF, and Hennink WE, Thermoresponsive Polymeric Micelles with Controlled Instability Based on Hydrolytically Sensitive N-Isopropylacrylamide Copolymers. *Macromolecules*, 2001. **34**(22): p. 7589-7591.
 48. Neradovic D, van Steenberg MJ, Vansteelant L, Meijer YJ, van Nostrum CF, and Hennink WE, Degradation Mechanism and Kinetics of Thermosensitive Polyacrylamides Containing Lactic Acid Side Chains. *Macromolecules*, 2003. **36**(20): p. 7491-7498.
 49. Narine SS and Marangoni AG, Mechanical and structural model of fractal networks of fat crystals at low deformations. *Phys Rev E Stat Phys Plasmas Fluids Relat Interdiscip Topics*, 1999. **60**(6 Pt B): p. 6991-7000.
 50. Yan H, Nykanen A, Ruokolainen J, Farrar D, Gough JE, Saiani A, and Miller AF, Thermo-reversible protein fibrillar hydrogels as cell scaffolds. *Faraday Discuss*, 2008. **139**: p. 71-84; discussion 105-28, 419-20.
 51. Rammensee S, Huennerich D, Hermanson KD, Scheibel T, and Bausch AR, Rheological characterization of hydrogels formed by recombinantly produced spider silk. *Appl Phys A-Mater Sci Process*, 2006. **82**: p. 261-264.
 52. MacKintosh FC, Kas J, and Janmey PA, Elasticity of semiflexible biopolymer networks. *Phys Rev Lett*, 1995. **75**(24): p. 4425-4428.
 53. Sanabria-DeLong N, Crosby AJ, and Tew GN, Photo-Cross-Linked PLA-PEO-PLA Hydrogels from Self-Assembled Physical Networks: Mechanical Properties and Influence of Assumed Constitutive Relationships. *Biomacromolecules*, 2008. **9**(10): p. 2784-2791.
 54. Erk KA, Henderson KJ, and Shull KR, Strain Stiffening in Synthetic and Biopolymer Networks. *Biomacromolecules*, 2010. **11**(5): p. 1358-1363.
 55. Pellens L, Corrales RG, and Mewis J, General Nonlinear Rheological Behavior of Associative Polymers. *J Rheol*, 2004. **48**: p. 379-393.
 56. Vader D, Kabla A, Weitz D, and Mahadevan L, Strain-Induced Alignment in Collagen Gels. *PLoS ONE*, 2009. **4**(6): p. e5902.
 57. Vermonden T, Jena SS, Barriet D, Censi R, van der Gucht J, Hennink WE, and Siegel RA, Macromolecular Diffusion in Self-Assembling Biodegradable Thermosensitive Hydrogels. *Macromolecules*, 2009. **43**(2): p. 782-789.
 58. Censi R, Vermonden T, Deschout H, Braeckmans K, di Martino P, De Smedt SC, van Nostrum CF, and Hennink WE, Photopolymerized thermosensitive poly(HPMA lactate)-PEG-based hydrogels: effect of network design on mechanical properties, degradation, and release behavior. *Biomacromolecules*, 2010. **11**(8): p. 2143-51.

59. Skardal A, Zhang J, McCoard L, Xu X, Oottamasathien S, and Prestwich GD, Photocrosslinkable hyaluronan-gelatin hydrogels for two-step bioprinting. *Tissue Eng Part A*, 2010. **16**(8): p. 2675-85.
60. Cohen DL, Malone E, Lipson H, and Bonassar LJ, Direct freeform fabrication of seeded hydrogels in arbitrary geometries. *Tissue Eng*, 2006. **12**(5): p. 1325-35.
61. Fedorovich NE, Swennen I, Girones J, Moroni L, van Blitterswijk CA, Schacht E, Alblas J, and Dhert WJA, Evaluation of Photocrosslinked Lutrol Hydrogel for Tissue Printing Applications. *Biomacromolecules*, 2009. **10**(7): p. 1689-1696.
62. Woodfield TB, Bezemer JM, Pieper JS, van Blitterswijk CA, and Riesle J, Scaffolds for tissue engineering of cartilage. *Crit Rev Eukaryot Gene Expr*, 2002. **12**(3): p. 209-36.
63. Bryant SJ, Bender RJ, Durand KL, and Anseth KS, Encapsulating chondrocytes in degrading PEG hydrogels with high modulus: Engineering gel structural changes to facilitate cartilaginous tissue production. *Biotechnol. Bioeng.*, 2004. **86**(7): p. 747-755.
64. Rijcken CJ, Snel CJ, Schiffelers RM, van Nostrum CF, and Hennink WE, Hydrolysable core-crosslinked thermosensitive polymeric micelles: synthesis, characterisation and in vivo studies. *Biomaterials*, 2007. **28**(36): p. 5581-93.
65. Fedorovich NE, Oudshoorn MH, van Geemen D, Hennink WE, Alblas J, and Dhert WJ, The effect of photopolymerization on stem cells embedded in hydrogels. *Biomaterials*, 2009. **30**(3): p. 344-53.
66. Guillotin B, Souquet A, Catros S, Duocastella M, Pippenger B, Bellance S, Bareille R, Remy M, Bordenave L, Amedee J, and Guillemot F, Laser assisted bioprinting of engineered tissue with high cell density and microscale organization. *Biomaterials*, 2010. **31**(28): p. 7250-6.
67. Qin D, Xia Y, and Whitesides GM, Soft lithography for micro- and nanoscale patterning. *Nat Protoc*, 2010. **5**(3): p. 491-502.
68. Tai H, Wang W, Vermonden T, Heath F, Hennink WE, Alexander C, Shakesheff KM, and Howdle SM, Thermoresponsive and photocrosslinkable PEG/EMA-PPGMA-EGDMA copolymers from a one-step ATRP synthesis. *Biomacromolecules*, 2009. **10**(4): p. 822-8.
69. Salinas CN and Anseth KS, Decorin moieties tethered into PEG networks induce chondrogenesis of human mesenchymal stem cells. *J Biomed. Mater. Res., Part A*, 2009. **90A**(2): p. 456-464.

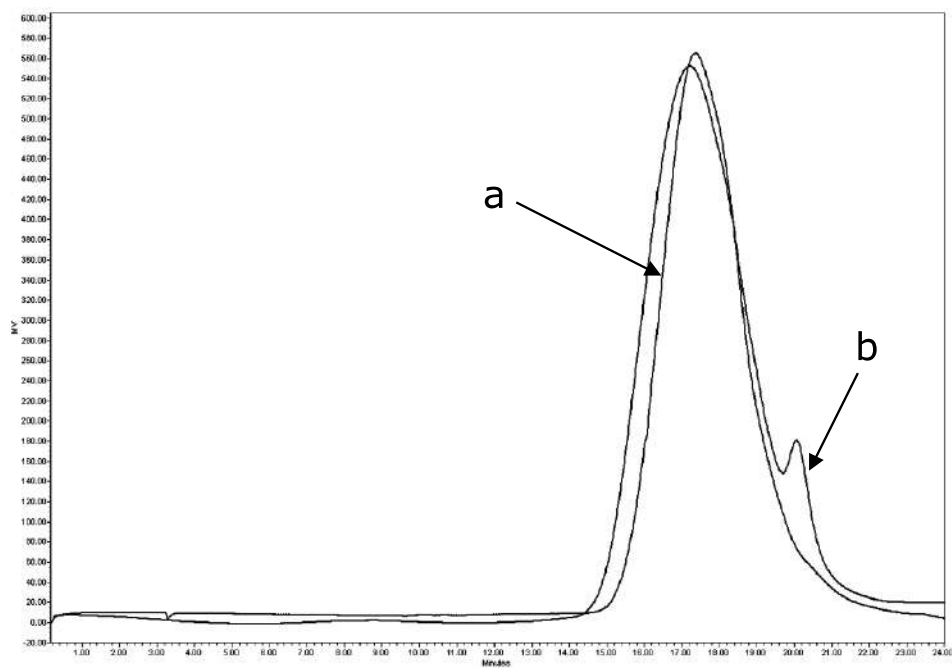
SUPPORTING INFORMATION



SI Figure 1. GPC chromatogram of $(\text{PEG-ABCPA})_n$ macroinitiator (MI); a trace amount of unreacted PEG (< 1 % based on AUC)



SI Figure 2. $^1\text{H-NMR}$ spectrum of $(\text{PEG-ABCPA})_n$ macroinitiator (MI) in CDCl_3 . By comparing the integration of PEG protons to those of ABCPA, a ratio PEG/ABCPA of 1.2 was calculated, demonstrating the presence of a small amount of unreacted PEG in the MI.



SI Figure 3. Comparison of GPC chromatograms of PEG-pHPMAm-lactate triblock copolymers ($M_{30}P_{10}$) synthesized using dialyzed (a) and non-dialyzed (b) $(\text{PEG-ABCPA})_n$ macroinitiator. The presence of unreacted ABCPA in the non-dialyzed macroinitiator leads to the formation of polymers of HPMAm-lactate without PEG chain during the radical copolymerization of PEG and HPMAm-lactate, visible as side peak in chromatogram (b). It appears that dialysis is an effective method to purify the unreacted ABCPA from the macroinitiator and prevent the formation of polymers of HPMAm-lactate without PEG chain, as shown in chromatogram (a).





chapter **EIGHT**

THERMORESPONSIVE GELATIN- METHACRYLAMIDE HYDROGELS FOR BIOPRINTING OF CARTILAGINOUS TISSUE ENGINEERING CONSTRUCTS

Wouter Schuurman, Peter Levett, Michiel W. Pot, P. René van Weeren, Wouter J. A. Dhert,
Dietmar W. Hutmacher, Ferry Melchels, Travis J. Klein, and Jos Malda

Wouter Schuurman, Peter Levett contributed equally to the work described

ABSTRACT

For regenerative medicine approaches, materials need to be biocompatible and biodegradable. The mechanical stability of the material is of particular importance for the tissue engineering of musculoskeletal tissues, which can be subjected to high mechanical forces. We therefore investigated the mechanical properties and swelling behavior of gelatin methacrylamide (gelMA) hydrogel.

The swelling and mechanical properties of gelMA hydrogel could be controlled by a number of means, allowing the swelling and mechanical properties to be modulated over large ranges. Increasing the photocrosslinking time from 5 to 30 minutes markedly increased the compressive modulus of the GelMA hydrogel and led to significant differences in swelling properties. By increasing the concentration of gelMA in the precursor solution from 5 to 20% and maintaining the photocrosslinking time at 30 minutes, the stiffness of hydrogels increased, with only minor variations in swelling. Swelling and mechanical properties can hence be controlled by manipulating these two simple parameters.

Moreover, the feasibility of the use of GelMA hydrogels in a 3-dimensional bioprinting technique was explored, and when this proved to be challenging, due to the low viscosity of the material, hyaluronic acid (HA) was added. The addition of HA to GelMA significantly improved bioprinting qualities of the hydrogel, both alone and in hybrid configuration. Further, the cell compatibility and differentiation of chondrocytes in gelMA with and without the addition of HA was investigated. High cell viability was shown for all groups, with values comparable to those described in literature for other hydrogel types. The addition of HA had a significant positive effect on cell viability at a 3 days time point. In both biomaterials, cartilaginous tissue formation was observed. In conclusion, gelatin methacrylamide is a suitable candidate for cartilage tissue engineering, and when combined with HA, the biomaterial is also an interesting candidate for bioprinting.

INTRODUCTION

Cartilage defects, for instance resulting from a sports trauma, do not heal spontaneously. A number of treatments are available for these defects, such as mosaicplasty, microfracture, and autologous chondrocyte implantation. Although the functional outcome of these treatments is generally satisfactory (1, 2), all techniques have serious drawbacks that may, depending on the therapy chosen, include poor long-term outcome, donor site morbidity, or elevated costs because of a complicated two-stage intervention. Further, as always in cartilage healing, the cartilage tissue is repaired rather than restored, which means that the native articular cartilage is replaced by a predominantly fibrous tissue. Therefore, researchers world-wide investigate possible strategies for the improvement of current clinical practice in the treatment of (osteo) chondral defects.

In regenerative medicine, a combination of cells, materials and growth factors is used, in order to improve, restore or replace damaged tissues or organs. Finding the optimal proportions in the delicate balance of these three factors is a major challenge in the field. Biomaterials, as a temporary extracellular matrix, must provide a support structure for the cells and at the same time allow the cells to proliferate and/or differentiate (3). Apart from the materials used, the method of manufacturing of the matrix also determines functionality, and techniques such as stereolithography and bioprinting are recognized as promising innovative technologies in the emerging field of regenerative medicine (4). Bioprinting involves the organized and specific placement of cells and materials, with or without a carrier material, to recreate the complex (cellular) organization of tissues and organs (5-7). The possibility of combining different cell types makes this approach particularly interesting for cartilage tissue engineering, since it can aid in the replication of the native zonal differences of the tissue (8). The field is advancing, but a number of challenges still must be solved before this technology can be successfully translated to clinical practice.

Biomaterials used in bioprinting need to meet a number of requirements. First, the viscosity of the material must enable the deposition of strands. Second, the material must have adequate mechanical properties to allow the construct to retain its shape after printing. Third, the biomaterial must be cytocompatible and allow for differentiation of the encapsulated cells. Controlling the swelling characteristics of hydrogels is particularly important for bioprinting constructs with defined sizes and geometries. The final shape and size of a construct are only reached after swelling, so swelling characteristics are an important design parameter for printing hydrogel constructs.

A biomaterial that holds promise for bioprinting of cartilaginous tissue constructs is gelatin, a water-soluble protein obtained by the denaturation of animal collagen. In aqueous solutions, gelatin forms a thermoreversible hydrogel once it is below its upper critical solution temperature (UCST) (9). The UCST of gelatin ranges from approximately 25 - 35 °C, depending on the concentration, source, treatment, concentration and solvent (9, 10). Gelatin solutions form thermal gels within physiological temperature ranges, allowing cells to be encapsulated within printed constructs. Thanks to its biodegradability (11, 12) and biocompatibility (13), gelatin is a useful component for cell culture systems and tissue engineering. Functionalisation of gelatin with photosensitive groups allows preparation of covalently crosslinked hydrogels

under mild conditions, while crosslink densities can be tailored by tuning the degree of functionalisation (DoF) (14, 15). Gelatin methacrylamide (gelMA) gels have already been applied for cell encapsulation for a wide range of cell types (16-19). To match the mechanical properties of the surrounding tissue, the properties of cell-free GelMA hydrogels can be modulated in three ways: 1) the UV exposure duration can be varied, 2) the concentration of the gelMA precursor solutions (and thus the degree of crosslinking) can be varied, 3) the hydrogels can be either solely UV crosslinked, or both thermally and UV crosslinked.

For the treatment of articular cartilage defects, large stiffness (while retaining a certain degree of resilience) of implants is particularly relevant, since the material will be subjected to high contact pressures during movement in weight bearing joints (20, 21). Furthermore, in native cartilage tissue (mechanical) properties and functions of the tissue vary with distance from the surface; mechanical stiffness increases with depth to be more than an order of magnitude higher in the deep zone (22). The ability to regenerate articular cartilage with a zonal structure featuring different characteristics with changing depth would mark a significant advancement in the treatment of chondral defects.

The UCST-behaviour makes gelatin gels a suitable candidate for bioprinting. In addition to physical thermal gelation, gelatin can be chemically crosslinked in several ways to obtain an irreversible gel. Alternatively, a second crosslinkable component can be mixed in to create a stable printed structure, for example fibrin (23) or hyaluronic acid (HA) (24). The addition of HA can be specially beneficial for cartilage regenerative medicine since the compound has been shown to promote extracellular matrix synthesis (25, 26).

In this work, we characterize how the UV dose and macromer concentration influence the mechanical and swelling properties of gelMA hydrogels. Since bioprinting approaches utilize the thermoresponsive properties of gelMA to provide the temporary mechanical characteristics, we investigated the influence of cooling and thermal gel formation before photocrosslinking of the gelMA solutions. Subsequently, the suitability of GelMA for engineering of cartilaginous tissue was assessed through culturing of chondrocytes encapsulated in photocrosslinked gelMA gels. Lastly, the suitability of these gels for bioprinting was explored.

MATERIALS AND METHODS

Preparation of gelMA

GelMA was prepared by reaction of type A gelatin (Sigma-Aldrich, St. Louis, Missouri, USA) with methacrylic anhydride (Sigma-Aldrich) at 50 °C for one hour, as previously described (14). Briefly, methacrylic anhydride was added dropwise to a 10% solution of gelatin in phosphate-buffered saline (PBS Invitrogen, Carlsbad, California, USA) under constant stirring. To achieve a high degree of functionalisation, 0.6 g of methacrylic anhydride was added per gram of gelatin (27). The functionalised polymer was dialysed against distilled water for 3 days at 40 °C to remove methacrylic anhydride, neutralized with 10% sodium bicarbonate (Merck, Darmstadt, Germany), and freeze-dried before use. The addition of photocrosslinkable methacrylamide groups to gelatin was confirmed and quantified using proton nuclear magnetic resonance (1H NMR) (Bruker 400 MHz, Alexandria, NSW, Australia). The 1H NMR

spectrum for gelatin showed no peaks in the range δ 5-6, while the gelMA spectrum showed distinct peaks at δ 5.33 and 5.57, corresponding to the vinyl protons of the methacrylamide groups. The degree of functionalisation was determined as previously published (28) and using a composition of acid treated, porcine skin derived gelatin (29). The integral of the peaks for vinyl protons (δ 5.33, 5.57) was normalized to the integral of the aromatic side chains (δ 7.2), giving a degree of functionalisation of 53%.

Hydrogel precursor solutions were prepared in PBS, with a final concentration of the photoinitiator Irgacure 2959 (Ciba, BASF, Ludwigshafen am Rhein, Germany) of 0.05%. Cell-free gelMA hydrogels were crosslinked in a custom-built teflon mold in which gel discs with a height of approximately 10x4x2 mm (LxWxH) can be fabricated. Gels were photocrosslinked using 365 nm light at an intensity of 2.7 mW/cm² in a UVP CL-1000L crosslinker (UVP, Upland, California, USA). GelMA solutions were either crosslinked at 37 °C, or allowed to cool to room temperature and then UV crosslinked.

Physical properties

To assess the mass swelling ratio, swelled gels were weighed, then lyophilized to determine their dry mass, and the mass swelling ratio was determined by the ratio of equilibrium wet weight to dry weight. To determine the effective swelling, gels were weighed immediately after crosslinking and again after swelling overnight in PBS at 37 °C. The difference in wet weights was expressed as a percentage. The compressive moduli of swelled gelMA hydrogels were measured using an Instron 5848 microtester (Instron, Norwood, Massachusetts, USA) with a 5N load cell. The hydrogels were tested in an unconfined arrangement while submerged in PBS at 37 °C. The gels were compressed at a rate of 0.01 mm/s, and the Young's modulus was taken as the slope of the stress-strain curve from 10-15% strain.

Three-dimensional fiber deposition

Three-dimensional models for the constructs were designed using Rhino 3D software (McNeel, Seattle, Washington, USA). The Standard Tessellation Language (STL) files of these models were then loaded via computer-aided manufacturing (CAM) software (PrimCAM, Einsiedeln, Switzerland), and constructs were printed using the BioScaffolder dispensing system (SYS+ENG, Salzgitter-Bad, Germany). Briefly, the BioScaffolder is a three-axis dispensing machine, which can build three-dimensional (3D) constructs by coordinated motion of one or more pneumatic syringe dispensers (for dispensing hydrogel) and a polymer dispenser, which deposit on a stationary platform. To ensure sterile conditions the BioScaffolder is placed in a custom-built laminar cross flow cabinet (Clean Air, Woerden, the Netherlands). Manufacturing was performed at room temperature. To keep the hydrogel at a temperature of 37 °C, both pneumatic syringe dispenser heads were heated using warm water flow provided by a ThermoCube (Solid State Cooling Systems, New York, USA).

Two types of constructs were printed, one a hydrogel only construct, consisting of either 10% or 20% GelMA, combined with 2,4% hyaluronic acid sodium salt (Sigma-Aldrich), the other a hybrid construct consisting of 10% GelMA, 2,4% hyaluronic acid sodium salt, and the thermoplastic polymer Polycaprolactone (PCL, Mw 70,000–90,000, Sigma-Aldrich). For the hydrogel construct, scaffolds of 4 layers high (height approximately 1.2 mm width

x length 20 x 20 mm) were fabricated. Deposition was performed using alternating angles of 0° and 90°, a 27G needle (inner diameter 210 μm), an XY-plane speed of 1000 mm min^{-1} , a spindle speed of 1.5 (arbitrary units), a strand distance of 1.5 mm, and a layer thickness of 0.3 mm.

The fabrication of the hybrid construct (6 x 60 x 2 mm) consisted of alternating steps of thermoplastic polymer and hydrogel printing. The PCL was heated to 160°C and subsequently dispensed through a 23G metal needle (inner diameter 337 μm , DL Technology LLC, Haverhill, MA, USA) using a pressure of 0.5 MPa, and a deposition speed of 176 mm min^{-1} . Two pneumatic syringe dispenser heads were used to dispense GelMA/HA between the PCL fibers at an XY-plane speed of 60 mm min^{-1} , a spindle speed of 1.10 (arbitrary units), using an 18G needle (inner diameter 838 μm). To visualize the possibility of depositing separate hydrogel layers, GelMA/HA hydrogel was either stained using fast green, or basic fuchsin (pink, both from Sigma-Aldrich), or loaded with Dye-Trak 'F' fluorescent blue or lemon beads (Triton technology, San Diego, CA, USA). Subsequent layers were deposited at an angle (normally 90°, 0–90) with the underlying layer. After all layers had been printed, GelMA was crosslinked using UV light for 5 minutes with a Superlite S-UV 2001AV lamp (Lumatec). Printed constructs were cut to yield samples with sizes of approximately 6 x 5 x 2 mm, and analyzed using a light microscope, equipped with an epifluorescence setup and excitation/emission setting of 488/530nm to detect yellow fluorescent beads and 460/495 nm to detect blue fluorescent beads.

Cell isolation and culture

Full thickness healthy articular cartilage was harvested from the condyles and patellofemoral grooves of fresh equine cadavers (n=3 per condition, age 4–9 years) under aseptic conditions. After digestion of the tissue using 0.15% type II collagenase (Worthington Biochemical Corporation, Lakewood, New Jersey, USA) overnight at 37°C, the cell suspension was filtered (100 μm cell strainer, BD Falcon, Bedford, Massachusetts, USA) and washed three times in PBS). Cells were then resuspended in chondrocyte expansion medium (DMEM (Invitrogen) supplemented with 10% Fetal Bovine Serum (FBS, Biowhittaker, Walkersville, Maryland, USA), 100 units/mL penicillin and 100 $\mu\text{g/mL}$ streptomycin (both Invitrogen), 25 mM Hepes (Gibco, Invitrogen) and 10 ng/mL FGF-2 (R&D Systems, Minneapolis, Minnesota, USA)) and counted using a hemacytometer. Chondrocytes were expanded until 90% confluency in monolayer cultures (5,000 cells/ cm^2) in expansion medium.

Fabrication of cell-laden gelatin hydrogel constructs

After expansion, cells were detached using trypsin 0.25% (Invitrogen), washed with PBS, and resuspended in either a 10% gelMA solution or a solution of 10% gelMA and 2.4% HA methacrylamide acid solution (GelMA/HA). The GelMA hydrogel consisted of 10% (w/v) gelatin methacrylamide and 0.05% (w/v) Irgacure 2959 (Ciba). For the GelMA/HA, 2.4% hyaluronic acid sodium salt (from *Streptococcus equi*, Sigma-Aldrich) was added to the gelatin hydrogel. Cells were encapsulated at a density of 5.0×10^6 cells/ml for LIVE/DEAD assays and at a density of 2.0×10^7 cells/ml for differentiation assays. Constructs of 100 μl were fabricated using two sterilized glass slides and two PVC spacers of 2 mm height. The hydrogel-cell suspension was put on a glass, the spacers were placed, and the second glass was put on top of the gel, yielding a cylindrical construct. A Superlite S-UV 2001AV lamp (Lumatec, Munchen, Germany)

was used to cross-link the cell-laden hydrogel constructs for 5 minutes. Constructs were cultured in chondrogenic differentiation medium (DMEM supplemented with 0.2 mM ascorbic acid 2-phosphate (Sigma-Aldrich), 0.5% human serum albumin (Cealb, Sanquin, Utrecht, The Netherlands), 1% (v/v) insulin-transferrin-selenium mixture (ITS-X, Invitrogen), 100 units/mL penicillin and 100 µg/mL streptomycin, and 5 ng/mL TGF- β 2 (R&D Systems Abingdon, United Kingdom)). Samples for LIVE/DEAD assays were taken after 1 and 3 days. Samples for differentiation were cultured for 4 weeks, medium was refreshed twice a week. Samples (n=3 per donor) were cut in half, one half was processed for histology whilst the other half was used for quantitative assays.

Viability assay

To visualize cell viability, a LIVE/DEAD Viability Assay (Molecular Probes MP03224, Eugene, USA) was performed according to the manufacturer's recommendations. The samples were examined using a light microscope and photomicrographs taken with an Olympus DP70 camera (both Olympus, BX51, United States). The excitation/emission filters were set at 488/530 nm to observe living (green) cells and at 530/580 nm to detect dead (red) cells. Live and dead cells were counted for 3 samples per time point, at four locations within each construct.

Histological, immunohistochemical and biochemical analyses

For histology, samples were fixed in formalin, processed through graded alcohol series and embedded in paraffin. Embedded sections were cut to yield 5 µm sections. Sections were stained with Weigert's hematoxylin (Klinipath, Duiven, The Netherlands) and fast green (Merck) for cells and with Safranin-O (Merck) for proteoglycans. For immunolocalization of cartilage marker collagen type II, endogenous peroxidase was blocked using a 0.3% H₂O₂ solution for 10 minutes. Samples were washed with PBS/Tween (0.1%) and subsequently, hyaluronidase and pronase antigen retrieval was used. Samples were blocked with 5% BSA in PBS for 30 minutes and then incubated overnight with the monoclonal anti-collagen type II antibody (1:100, II-6B3II, Developmental Studies Hybridoma Bank, USA). Samples were then incubated for 60 minutes with goat anti-mouse HRP antibody. Staining was visualized using DAB solution (Sigma-Aldrich, USA) for 10 minutes. Counterstaining was performed with hematoxylin. The sections were examined using a light microscope. Isotype controls were performed by using mouse isotype IgG1 monoclonal antibody at concentrations similar to those used for the staining. For biochemical analysis, samples were digested overnight at 56°C in a solution containing 250 µg/mL papain (Sigma-Aldrich). Quantification of total DNA was performed by Quant-iT PicoGreen dsDNA kit (Molecular Probes, Invitrogen) using a spectrofluorometer (Biorad, Hercules, California, USA). The amount of GAGs was determined spectrophotometrically after reaction with dimethylmethylene blue dye (DMMB, Sigma-Aldrich)(30), pH=3.0. Intensity of color change was quantified immediately in a microplate reader (Biorad) by measuring absorbance at 540 and 595 nm. The amount of GAGs was calculated using a standard of chondroitin sulphate Cx(Sigma-Aldrich) and by calculating the ratio of absorbances. The tissue sections were examined using a light microscope (Olympus BX51, Hamburg, Germany) to assess the tissue thickness, the distribution of cells and GAGs. Photographs of all samples were then taken using an Olympus DP70 camera.

Statistics

All statistical analyses were performed using SPSS 15.0 software (IBM Corporation, Armonk, NY, USA). A one-way ANOVA was used for analysis of physical properties. To analyze viability between conditions, a one-way analysis of variance (ANOVA) was used, while for viability in time, a repeated measurements ANOVA was performed. For the comparison between GAG and GAG per DNA, an independent samples t-test was used. All data are shown as mean values \pm standard deviation.

RESULTS

Effect of UV exposure

Total UV exposure is a sensitive parameter for controlling the stiffness and swelling characteristics of gelMA hydrogels. The compressive moduli of GelMA hydrogels crosslinked for 30 minutes were over 10-fold greater than those crosslinked for 5 minutes (Figure 1). Gels which were crosslinked for 5 minutes had a compressive modulus of 13 kPa, an equilibrium mass swelling ratio of 11.5, and wet weight increased by over 60% after swelling in PBS at 37 °C. In comparison, gels crosslinked for 30 minutes had a compressive modulus of approximately 180 kPa, an equilibrium mass swelling ratio of 5.5, while the wet weight was unchanged after swelling in PBS.

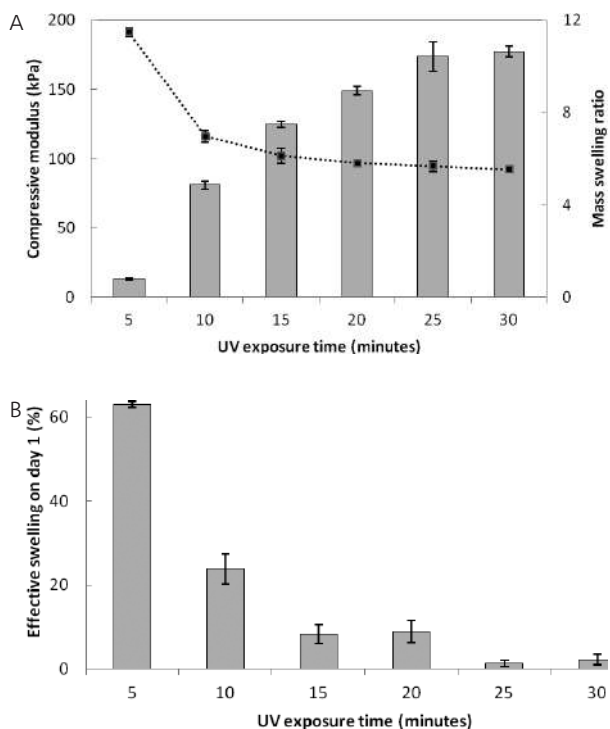


Figure 1. Effect of UV exposure on the mechanical and swelling properties of 20% (w/v) gelMA hydrogels. Stiffness of the hydrogels increases with UV exposure up to 25 minutes, and equilibrium mass swelling ratios decrease with increased UV exposure (A). Bars and lines represent compressive modulus and swelling, respectively. Effective swelling (B) decreases significantly with increased UV exposure.

The equilibrium mass swelling ratio (q) is a commonly used metric to gauge the water content of hydrogels. For applications in which the hydrogel geometry and size are important, the change in wet weight of the hydrogel during swelling is also important.

Effect of macromer concentration

To investigate the effect of macromer concentration on swelling and mechanical properties, gels were produced by photocrosslinking gelMA solutions with concentrations of 5, 10, 15 and 20% (w/v) (Figure 2). The photo initiator concentration was 0.05% (w/v) in all gels, and a UV exposure time of 30 minutes was selected to produce fully crosslinked gels. GelMA concentration had a significant impact on hydrogel stiffness, but only a minor influence on the effective swelling. For gels which were photocrosslinked for 30 minutes, gelMA precursor concentrations of 5, 10, 15 and 20% gave gels with compressive moduli of approximately 5, 33, 100 and 180 kPa, respectively, while effective swelling values were -11, -5, -1 and 1%, respectively.

Effect of temperature

The state of gelMA polymer chains during crosslinking, and the mechanical properties of the resulting gels, is dependent on crosslinking temperature (Figure 3).

Photocrosslinking gels at 37 °C produces gels that are solely crosslinked by covalent linkages, whereas photocrosslinking gels at room temperature utilizes the thermoresponsive

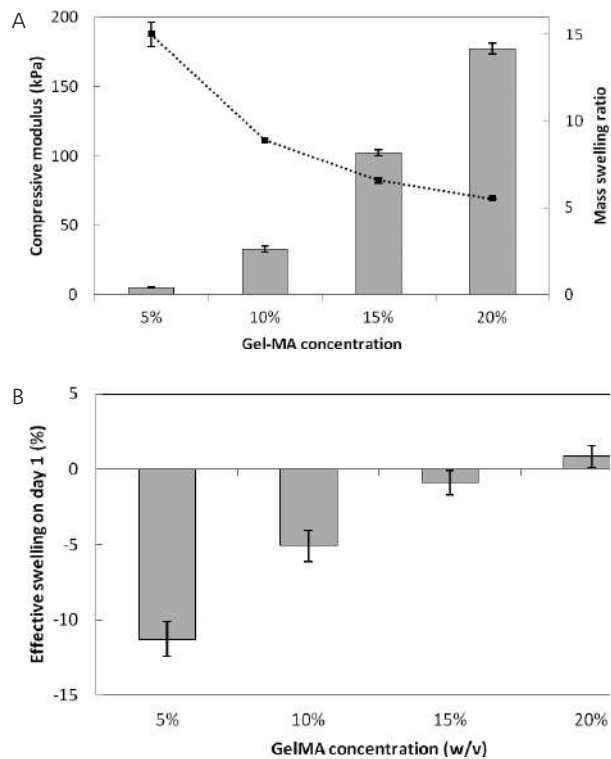


Figure 2. Mechanical and swelling properties of gel-MA hydrogels crosslinked 30 minutes. Bars and lines (A) represent compressive modulus and mass swelling ratio, respectively. Effective swelling (B) increases only moderately with gel-MA concentration.

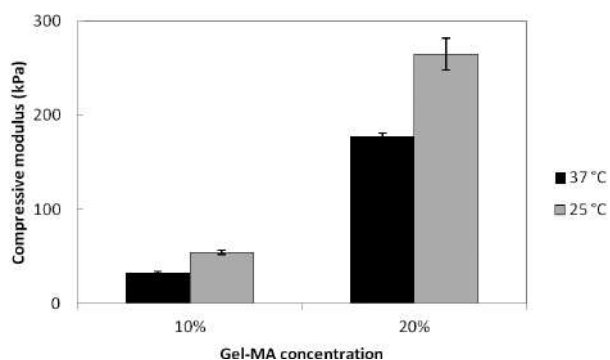


Figure 3. Effect of crosslinking temperature on the stiffness of 10 and 20% gelMA hydrogels. Gels were crosslinked at 37 °C, or allowed to cool to 25 °C then UV crosslinked.

property of gelatin to form a gel which is both physically and covalently crosslinked. The increased stiffness of gels which were crosslinked at room temperature was maintained when the gels were swelled and tested at 37 °C, suggesting that the physical crosslinks that arise from thermal gelation are no longer temperature responsive after covalent crosslinking.

Bioprinting of GelMA and GelMA/HA

Bioprinting of GelMA alone, without the addition of HA, was not feasible, because the hydrogel was not viscous enough to print. Likewise, the printing of 10% GelMA/2.4% HA did not result in defined constructs; the hydrogel was not viscous enough to retain shape (not shown). Increasing the concentration to 20%GelMA/2.4%HA, however, resulted in homogeneous deposition of the hydrogel, yielding porous constructs of four layers high, with predefined size and shape (Figure 4). For the fabrication of hybrid scaffolds, a lower percentage of GelMA/HA hydrogel (10% GelMA) could be used. These constructs consist of hydrogels which are reinforced with the thermoplastic polymer polycaprolactone (PCL), which made it feasible to print more layers on top of each other, creating rectangular scaffolds (W x L x H (mm): 6 x 60 x 1.98), with two separate GelMA/HA hydrogel parts (Figure 5).

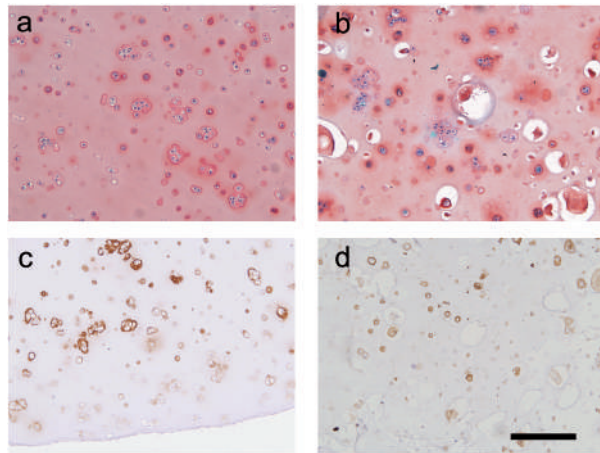
Cell-laden GelMA hydrogel constructs

The chondrocytes incorporated in GelMA showed a cell viability of 83% and 73% for 1 and 3 days, respectively. For GelMA/HA, these values were 79% and 82% (Table 1). No significant differences were observed between the 1 and 3 days time points for either of the hydrogels ($p=0.320$ for

Table 1. Cell viability, glycosaminoglycans, DNA per construct and glycosaminoglycans per DNA for Gelatin Methacrylamide (GelMA) and Gelatin Methacrylamide/Hyaluronic acid (GelMA/HA). * =significantly different from GelMA day 3 ($p=0.045$), ** =significantly different from GelMA ($p=0.026$).

	Viability day 1 (\pm SD)	Viability day 3 (\pm SD)	GAG/construct (\pm SD)	DNA/construct (\pm SD)	GAG/DNA (\pm SD)
GelMA	83 \pm 13%	73 \pm 2%	79.7 \pm 18.2 μ g	3.97 \pm 3.44 μ g	28.7 \pm 15.8
GelMA/HA	79 \pm 18%	82 \pm 8% *	42.8 \pm 38.3 μ g **	1.76 \pm 0.55 μ g ***	22.6 \pm 16

Figure 4. Histology and immunohistochemistry for GelMA and GelMA/HA hydrogels. Cells are stained blue in both stainings. Safranin O staining indicating glycosaminoglycan formation (red) in GelMA (a) and GelMA/HA (b) hydrogel. Collagen type II immunostainings (brown) showing cartilaginous differentiation in GelMA (c) and GelMA/HA (d) hydrogel. Scale bar represents 200 μ m.



GelMA, $p=0.662$ for GelMA/HA), nor between materials at day 1 ($p=0.946$), while there was a significantly higher cell viability in GelMA/HA for day 3 ($p=0.045$). Cartilaginous tissue formation was shown after 4 weeks in both materials by the presence of glycosaminoglycans, as shown by the safranin-O staining, and by the presence of cartilage marker collagen type II (Figure 4). The GAG production was quantified using a DMMB assay, which showed that considerable amounts of GAG were produced by chondrocytes in both hydrogel types (Table 1). In the GelMA hydrogel, significantly more GAGs were produced than in the GelMA/HA (79.7 versus 42.8 μ g), although high standard deviations occurred in the GelMA/HA hydrogels. The content of DNA did not significantly differ between groups (3.97 μ g for GelMA versus 1.76 μ g for GelMA/HA). When normalized for the amount of DNA, no significant difference for GAG incorporation was observed between GelMA and GelMA/HA hydrogels ($p=0.457$).

DISCUSSION

Preparation, mechanical characterization, swelling properties, effect of UV exposure

Cell-based approaches in which chondrocytes are encapsulated in hydrogels have shown promise for cartilage regeneration. The hydrogel scaffold must provide temporary mechanical support while promoting the production of new matrix. Whilst the stiffest gels may provide the greatest mechanical support, it remains to be tested how the stiffness influences matrix production. The crosslink density of polyethylene glycol gels affects the distribution and composition of matrix deposited by encapsulated chondrocytes [31]. In gelMA hydrogels, the viability of encapsulated 3T3 cells varied inversely to gelMA concentration, so selecting conditions which favor cell viability will also be a requirement for tissue engineering applications.

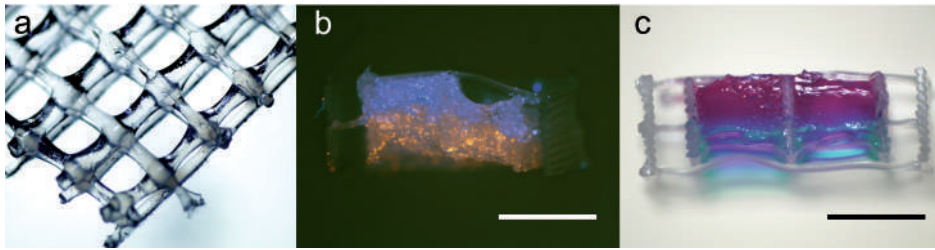


Figure 5. Bioprinting of GelMA/HA. GelMA/HA was printed on its own (a) or in a hybrid construct (b and c). Printing GelMA/HA alone (20%) was challenging and resulted in a construct of four layers, while printing of a lower percentage of GelMA/HA (10%) resulted in rectangular scaffolds (W x L x H (mm): 6 x 60 x 1.98), with two separate GelMA/HA hydrogel parts. In (b), a cross-section of such a construct is shown, with incorporated blue and orange fluorescent beads (b) or basic fuchsin (pink) and fast green (c) to visualize the two GelMA hydrogels. Scale bar represents 2 mm.

Effect of macromer concentration

UV exposure is a simple and sensitive way for controlling the physical properties of gelMA hydrogels, but has several limitations. Stiffness cannot be controlled independently of swelling, so it may be possible to produce gels with either the desired stiffness or swelling properties, but not both. To produce multi-layered constructs with different properties, it may not be possible to precisely control the UV exposure for each region, so controlling the gels properties by manipulating other parameters would be advantageous. In addition, for cell encapsulation, increasing UV exposure may affect cell viability unacceptably.

Effect of temperature

The thermo-responsive properties of gelMA are utilized during bioprinting to provide the structure with sufficient mechanical strength to retain its shape until it is photocrosslinked. By photocrosslinking the hydrogel in a thermal gel state, the gelMA polymer chains are in a triple helical conformation [28]. Photocrosslinking these structures results in reduced temperature sensitivity, and gels remain stiffer at 37 °C than those crosslinked in the solution state. Gels which were crosslinked at 37 °C had similar equilibrium swelling ratios to those crosslinked at room temperature.

Bioprinting of GelMA and GelMA/HA

The layered deposition of a GelMA/HA hydrogel of low weight percentage (10% GelMA) did not result in an organized, defined construct. The addition of HA to the GelMA makes the solution more viscous, and feasible to print, as has been previously shown [32]. This way, porosity could be introduced, which is especially important when larger scale constructs are to be manufactured [33-35]. Porosity can enhance nutrient transport and waste removal [36], and is suggested to promote vasculogenesis *in vivo* [37]. This in turn leads to more homogeneous cell differentiation [34] and extracellular matrix deposition.

GelMA/HA of lower viscosity could be used when cell-laden GelMA/HA strands were deposited in a network of thermoplastic polymer fibers. The advantages of these hybrid constructs are twofold: a wider range of hydrogels can be used for bioprinting, as we show here

with a lower percentage of GelMA, and the mechanical stiffness of the resulting fiber-reinforced hydrogel is higher [38] and hence better suited for musculoskeletal applications [38-41]. It has already been shown that the cell viability in hybrid constructs is similar to unprinted controls [38]. Alternatively, GelMA can be combined with another material to enhance the mechanical properties, for instance with gellan gum [42] or fibrin [23]. Bioprinting enables researchers to combine different materials and different cell types into one construct, thus facilitating the replication of the complex architecture of tissues. This can be of value both for *in vitro* models and for the engineering of neo-tissues for implantation.

Cell-laden GelMA hydrogel constructs

High viability was observed for both GelMA and GelMA/HA hydrogels. Viability was comparable to the values reported for the often used regular [43] or photocrosslinkable [44] alginate hydrogels. The addition of HA significantly enhanced the viability of the chondrocytes at the 3 days time point, although viability in GelMA without the addition of HA (73% after 3 days) still was acceptable. Furthermore, in both types of hydrogel cartilaginous tissue formation was evidenced by the formation of GAGs and the deposition of the cartilage-specific marker collagen type II. The amount of incorporated GAGs differed between GelMA and GelMA/HA, but the values corrected for DNA did not show a significant difference and hence productivity per cell was similar. The higher viscosity of the GelMA/HA does not hamper biosynthesis of GAGs. The characterization GelMA/HA will be subject of future investigation. Overall, the high cell viability and the formation of cartilaginous tissue confirm the suitability of both tested materials for cartilage tissue engineering purposes.

CONCLUSION

The physical properties of gelMA hydrogels can be controlled by manipulating the UV dose and percentage of gelMA in the precursor solution. Gels with compressive moduli in the range 5 – 180 kPa can be produced by varying the concentration of the precursor solution. By manipulating UV exposure time, gels can be produced which swell up to 60% of their initial mass, or gels where swelling is negligible.

The possibility to tune the mechanical and swelling properties of the material, combined with the high cell survival and the formation of cartilaginous tissue make gelatin methacrylamide into a suitable candidate for cartilage tissue engineering. When combined with HA, the biomaterial is also an interesting candidate for bioprinting.

REFERENCES

1. Saris DB, Vanlauwe J, Victor J, Haspl M, Bohnsack M, Fortems Y, Vandekerckhove B, Almqvist KF, Claes T, Handelberg F, Lagae K, *et al.*, Characterized chondrocyte implantation results in better structural repair when treating symptomatic cartilage defects of the knee in a randomized controlled trial versus microfracture. *Am J Sports Med*, 2008. **36**(2): p. 235-46.
2. Bentley G and Minas T, Treating joint damage in young people. *Bmj*, 2000. **320**(7249): p. 1585-8.
3. Hutmacher DW, Scaffolds in tissue engineering bone and cartilage. *Biomaterials*, 2000. **21**(24): p. 2529-43.
4. Melchels FPW, Domingos MAN, Klein TJ, Malda J, Bartolo PJ, and Hutmacher DW, Additive Manufacturing of Tissues and Organs. *Progress in Polymer Science*, 2011. **In press**.
5. Guillotin B, Souquet A, Catros S, Duocastella M, Pippenger B, Bellance S, Bareille R, Remy M, Bordenave L, Amedee J, and Guillemot F, Laser assisted bioprinting of engineered tissue with high cell density and microscale organization. *Biomaterials*, 2010. **31**(28): p. 7250-6.
6. Mironov V, Boland T, Trusk T, Forgacs G, and Markwald RR, Organ printing: computer-aided jet-based 3D tissue engineering. *Trends Biotechnol*, 2003. **21**(4): p. 157-61.
7. Fedorovich NE, Schuurman W, Wijnberg HM, Prins HJ, van Weeren PR, Malda J, Alblas J, and Dhert WJ, Biofabrication of Osteochondral Tissue Equivalents by Printing Topologically Defined, Cell-Laden Hydrogel Scaffolds. *Tissue Eng Part C Methods*, 2011.
8. Klein TJ, Rizzi SC, Reichert JC, Georgi N, Malda J, Schuurman W, Crawford RW, and Hutmacher DW, Strategies for zonal cartilage repair using hydrogels. *Macromol Biosci*, 2009. **9**(11): p. 1049-58.
9. Gupta A, Mohanty B, and Bohidar HB, Flory temperature and upper critical solution temperature of gelatin solutions. *Biomacromolecules*, 2005. **6**(3): p. 1623-7.
10. Mohanty B and Bohidar HB, Microscopic structure of gelatin coacervates. *Int J Biol Macromol*, 2005. **36**(1-2): p. 39-46.
11. Balakrishnan B and Jayakrishnan A, Self-cross-linking biopolymers as injectable in situ forming biodegradable scaffolds. *Biomaterials*, 2005. **26**(18): p. 3941-51.
12. Kawai K, Suzuki S, Tabata Y, Ikada Y, and Nishimura Y, Accelerated tissue regeneration through incorporation of basic fibroblast growth factor-impregnated gelatin microspheres into artificial dermis. *Biomaterials*, 2000. **21**(5): p. 489-99.
13. Kuijpers AJ, van Wachem PB, van Luyn MJ, Plantinga JA, Engbers GH, Krijgsveld J, Zaat SA, Dankert J, and Feijen J, In vivo compatibility and degradation of crosslinked gelatin gels incorporated in knitted Dacron. *J Biomed Mater Res*, 2000. **51**(1): p. 136-45.
14. Van den Bulcke AI, Bogdanov B, De Rooze N, Schacht EH, Cornelissen M, and Berghmans H, Structural and rheological properties of methacrylamide modified gelatin hydrogels. *Biomacromolecules*, 2000. **1**(1): p. 31-8.
15. Sutter M, Siepmann J, Hennink WE, and Jiskoot W, Recombinant gelatin hydrogels for the sustained release of proteins. *J Control Release*, 2007. **119**(3): p. 301-12.
16. Benton JA, DeForest CA, Vivekanandan V, and Anseth KS, Photocrosslinking of gelatin macromers to synthesize porous hydrogels that promote valvular interstitial cell function. *Tissue Eng Part A*, 2009. **15**(11): p. 3221-30.
17. Aubin H, Nichol JW, Hutson CB, Bae H, Sieminski AL, Crokek DM, Akhyari P, and Khademhosseini A, Directed 3D cell alignment and elongation in microengineered hydrogels. *Biomaterials*, 2010. **31**(27): p. 6941-6951.
18. Nichol JW, Koshy ST, Bae H, Hwang CM, Yamanlar S, and Khademhosseini A, Cell-laden microengineered gelatin methacrylate hydrogels. *Biomaterials*, 2010. **31**(21): p. 5536-44.
19. Qi H, Du Y, Wang L, Kaji H, Bae H, and Khademhosseini A, Patterned differentiation of individual embryoid bodies in spatially organized 3D hybrid microgels. *Adv Mater*, 2010. **22**(46): p. 5276-81.
20. Bergmann G, Graichen F, and Rohlmann A, Hip joint loading during walking and running, measured in two patients. *J Biomech*, 1993. **26**(8): p. 969-90.
21. Krebs DE, Robbins CE, Lavine L, and Mann RW, Hip biomechanics during gait. *J Orthop Sports Phys Ther*, 1998. **28**(1): p. 51-9.
22. Schinagl R, Gurskis D, Chen A, and Sah R, Depth-dependent confined compression modulus of full-thickness bovine articular cartilage. *Journal of Orthopaedic Research*, 1997. **15**(4): p. 499-506.
23. Xu WW, X; Yan, Y; Zheng, W; Xiong, Z; Lin, F; Wu, R; Zhang, R, Rapid Prototyping Three-Dimensional Cell/Gelatin/Fibrinogen Constructs for Medical Regeneration. *Journal of Bioactive and Biocompatible Polymers*, 2007. **22**: p. 363-377.
24. Skardal A, Zhang J, McCoard L, Xu X, Oottamasathien S, and Prestwich GD, Photocrosslinkable hyaluronan-gelatin hydrogels for two-step bioprinting. *Tissue Eng Part A*, 2010. **16**(8): p. 2675-85.
25. Chung C, Erickson IE, Mauck RL, and Burdick JA, Differential behavior of auricular and articular chondrocytes in hyaluronic acid hydrogels. *Tissue Eng Part A*, 2008. **14**(7): p. 1121-31.
26. Park SH, Park SR, Chung SI, Pai KS, and Min BH, Tissue-engineered cartilage using fibrin/hyaluronan composite gel and its in vivo implantation. *Artif Organs*, 2005. **29**(10): p. 838-45.

27. Shin H, Olsen BD, and Khademhosseini A, The mechanical properties and cytotoxicity of cell-laden double-network hydrogels based on photocrosslinkable gelatin and gellan gum biomacromolecules. *Biomaterials*, 2012.
28. Brinkman WT, Nagapudi K, Thomas BS, and Chaikof EL, Photo-cross-linking of type I collagen gels in the presence of smooth muscle cells: mechanical properties, cell viability, and function. *Biomacromolecules*, 2003. **4**(4): p. 890-5.
29. Eastoe JE, *Composition of collagen and allied proteins*, in *Treatise on collagen*, Ramachandran GN, Editor. 1967, London academic press: London. p. 27.
30. Farndale RW, Buttle DJ, and Barrett AJ, Improved quantitation and discrimination of sulphated glycosaminoglycans by use of dimethylmethylene blue. *Biochim Biophys Acta*, 1986. **883**(2): p. 173-7.
31. Bryant SJ and Anseth KS, Hydrogel properties influence ECM production by chondrocytes photoencapsulated in poly(ethylene glycol) hydrogels. *Journal of Biomedical Materials Research Part A*, 2002. **59**(1): p. 63-72.
32. Pescosolido L, Schuurman W, Malda J, Matricardi P, Alhaique F, Coviello T, van Weeren PR, Dhert WJ, Hennink WE, and Vermonden T, Hyaluronic acid and dextran-based semi-IPN hydrogels as biomaterials for bioprinting. *Biomacromolecules*, 2011. **12**(5): p. 1831-8.
33. Lewis MC, Macarthur BD, Malda J, Pettet G, and Please CP, Heterogeneous proliferation within engineered cartilaginous tissue: the role of oxygen tension. *Biotechnol Bioeng*, 2005. **91**(5): p. 607-15.
34. Carrier RL, Rupnick M, Langer R, Schoen FJ, Freed LE, and Vunjak-Novakovic G, Perfusion improves tissue architecture of engineered cardiac muscle. *Tissue Eng*, 2002. **8**(2): p. 175-88.
35. Obradovic B, Carrier RL, Vunjak-Novakovic G, and Freed LE, Gas exchange is essential for bioreactor cultivation of tissue engineered cartilage. *Biotechnol Bioeng*, 1999. **63**(2): p. 197-205.
36. Fedorovich NE, Kuipers E, Gawlitta D, Dhert WJ, and Alblas J, Scaffold porosity and oxygenation of printed hydrogel constructs affect functionality of embedded osteogenic progenitors. *Tissue Eng Part A*, 2011. **17**(19-20): p. 2473-86.
37. Stosich MS, Bastian B, Marion NW, Clark PA, Reilly G, and Mao JJ, Vascularized adipose tissue grafts from human mesenchymal stem cells with bioactive cues and microchannel conduits. *Tissue Eng*, 2007. **13**(12): p. 2881-90.
38. Schuurman W, Khristov V, Pot MW, van Weeren PR, Dhert WJ, and Malda J, Bioprinting of hybrid tissue constructs with tailorable mechanical properties. *Biofabrication*, 2011. **3**(2): p. 021001.
39. Endres M, Huttmacher DW, Salgado AJ, Kaps C, Ringe J, Reis RL, Sittinger M, Brandwood A, and Schantz JT, Osteogenic induction of human bone marrow-derived mesenchymal progenitor cells in novel synthetic polymer-hydrogel matrices. *Tissue Eng*, 2003. **9**(4): p. 689-702.
40. Holloway JL, Lowman AM, and Palmese GR, Mechanical evaluation of poly(vinyl alcohol)-based fibrous composites as biomaterials for meniscal tissue replacement. *Acta Biomater*, 2010. **6**(12): p. 4716-24.
41. Schagemann JC, Chung HW, Mrosek EH, Stone JJ, Fitzsimmons JS, O'Driscoll SW, and Reinholz GG, Poly-epsilon-caprolactone/gel hybrid scaffolds for cartilage tissue engineering. *J Biomed Mater Res A*, 2010. **93**(2): p. 454-63.
42. Shin H, Olsen BD, and Khademhosseini A, The mechanical properties and cytotoxicity of cell-laden double-network hydrogels based on photocrosslinkable gelatin and gellan gum biomacromolecules. *Biomaterials*, 2012. **33**(11): p. 3143-52.
43. Heiligenstein S, Cucchiari M, Laschke MW, Bohle RM, Kohn D, Menger MD, and Madry H, In vitro and in vivo characterization of nonbiomedical- and biomedical-grade alginates for articular chondrocyte transplantation. *Tissue Eng Part C Methods*, 2011. **17**(8): p. 829-42.
44. Rouillard AD, Berglund CM, Lee JY, Polacheck WJ, Tsui Y, Bonassar LJ, and Kirby BJ, Methods for photocrosslinking alginate hydrogel scaffolds with high cell viability. *Tissue Eng Part C Methods*, 2011. **17**(2): p. 173-9.



chapter **NINE**

BIOPRINTING OF HYBRID TISSUE CONSTRUCTS WITH TAILORABLE MECHANICAL PROPERTIES

Wouter Schuurman, Vladimir Khristov, Michiel W. Pot, P. René van Weeren,
Wouter J. A. Dhert, and Jos Malda

ABSTRACT

Tissue/organ printing aims to recapitulate the intrinsic complexity of native tissues. For a number of tissues, in particular those of musculoskeletal origin, adequate mechanical characteristics are an important prerequisite for their initial handling and stability, as well as long-lasting functioning. Hence, organized implants, possessing mechanical characteristics similar to the native tissue, may result in improved clinical outcomes of regenerative approaches. Using a bioprinter, grafts were constructed by alternate deposition of thermoplastic fibers and (cell-laden) hydrogels. Constructs of different shapes and sizes were manufactured and mechanical properties, as well as cell viability were assessed. This approach yields novel organized viable hybrid constructs, which possess favorable mechanical characteristics, within the same range as those of native tissues. Moreover, the approach allows the use of multiple hydrogels, and can thus produce constructs containing multiple cell types or bioactive factors. Furthermore, since the hydrogel is supported by the thermoplastic material, a broader range of hydrogel types can be used compared to bioprinting of hydrogels alone. In conclusion, we present an innovative and versatile approach for bioprinting, yielding constructs of which the mechanical stiffness provided by thermoplastic polymers can potentially be tailored and combined specific cell placement patterns of multiple cell types embedded in a wide range of hydrogels.

INTRODUCTION

Regenerative medicine aims to improve, restore or replace damaged tissues or organs using a combination of cells, materials and growth factors. The ultimate goal is to restore tissue functionality, preferably in a durable way. For a number of these tissues, especially those of musculoskeletal origin, adequate mechanical characteristics, matching the biomechanical challenges the tissues are exposed to, are crucial for their adequate long-term functioning. Hence, implants possessing mechanical characteristics similar to the native tissue, are likely to perform best in regenerative approaches.

Natural tissues with a biomechanical function are invariably multicomposite in structure. They are often composed of an acellular structural component characterized by a high degree of stiffness, which is surrounded by a much softer matrix with a varying amount of cells. To mimic this architecture, composite artificial (hybrid) constructs have been developed that typically consist of organized scaffolds to provide strength together with cell-seeded hydrogels (1-8). Organized scaffolds from thermoplastic materials can be fabricated using three-dimensional fiber deposition (3DF) technologies (9, 10). Mechanical properties of such scaffolds can be tailored by adopting different scaffold architectures (11), hence mechanical properties in the same order of magnitude as those of native tissues can be achieved (10). Combining cell-seeded hydrogels with such an organized scaffold, using for example combinations with woven thermoplastic materials or with electrospun meshes, or the infusion of a 3DF manufactured rigid scaffold structure, provides the construct with the possibility to remodel and, eventually, to replace itself by newly formed native tissue. A wide range of possible applications for this type of reinforced hydrogels has been suggested, varying from musculoskeletal tissues like intervertebral discs, cartilage, bone and ligaments, to large blood vessels (1, 4, 8, 12-14). However, these scaffolds have considerable disadvantages that affect clinical applicability. For example, the cell-seeding efficiency on polymer scaffolds is often low (15, 16). In addition, for both thermoplastic scaffolds and the hybrid scaffolds, specific spatial arrangements of multiple cell types that are pivotal to tissue functionality cannot be achieved, despite the fact that the distribution of the cells may be influenced by variations in the local scaffold porosity (17).

Bioprinting technologies, which apply the principles of rapid prototyping using layer by layer deposition of cells, matrix or both (18), allow for the development of porous 3D constructs with detailed specific spatial cellular arrangements (18-22). Although printing of living cells imposes strict requirements on the conditions during the printing process, viable 3D constructs can be obtained when using biocompatible hydrogels as a "bio-ink" (23-25). However, these constructs have disadvantages too. In order to obtain high shape-fidelity of the printed structures, these hydrogels have to meet very specific requirements with regards to viscosity and gelling speed, limiting the number of potential hydrogel formulations that can be applied in bioprinting approaches (24, 26, 27). Perhaps more importantly, the resulting hydrogel constructs will possess limited mechanical resistance and stiffness will always remain far below the values in most native musculoskeletal tissues, which may hamper clinical applicability constructs.

The objective of this study was to combine the advantages of both approaches, using state-of-the-art printing technology to create viable hybrid constructs by a layer-by-layer deposition of a stiff polymer (polycaprolactone; PCL) and cell-laden hydrogels (alginate). We demonstrate

that the physical (thermal) requirements for printing of the polymer can be made compatible with requirements for maintaining cell viability in the hydrogel and that in the resulting construct the mechanical stiffness provided by the polymer can be successfully combined with the specific cell placement patterns of multiple cell types.

MATERIALS AND METHODS

Hybrid three-dimensional fiber deposition

Models for the constructs were designed using Rhino 3D software (McNeel, Seattle, Washington, USA). The Standard Tessellation Language (STL) files of these models were then loaded via computer-aided manufacturing (CAM) software (PrimCAM, Einsiedeln, Switzerland), and constructs were printed using the BioScaffolder dispensing system (SYS+ENG, Salzgitter-Bad, Germany). Briefly, the BioScaffolder is a three-axis dispensing machine, which can build three-dimensional (3D) constructs by coordinated motion of both a pneumatic syringe dispenser (for dispensing hydrogel) and a polymer dispenser, which both deposit on a stationary platform. To ensure sterile conditions the BioScaffolder is placed in a custom-built laminar cross flow cabinet (Clean Air, Woerden, The Netherlands).

Manufacturing was performed at room temperature, and consisted of alternating steps of thermoplastic polymer and hydrogel printing. Polycaprolactone (PCL, Mw 70,000-90,000, Sigma-Aldrich, Zwijndrecht, The Netherlands) was heated to 160°C and subsequently dispensed through a 23G metal needle (DL Technology LLC, Haverhill Massachusetts, USA) using a pressure of 0.5 MPa, and a deposition speed of 176 mm/min. Medium viscosity sodium alginate (2%, Sigma-Aldrich, in phosphate buffered saline (PBS, Invitrogen, Carlsbad, California, USA) and subsequently autoclaved) was dispensed between the PCL strands, at room temperature, using a deposition speed of 100 mm/min, a spindle speed of 1.5 and a nozzle diameter of 210 µm. Subsequent layers were deposited at an angle (normally 90°, 0-90) with the underlying layer. After all layers had been printed, alginate was crosslinked with 102 mM calcium chloride (CaCl₂, Sigma-Aldrich) solution for 15 minutes.

To illustrate the versatility of this hybrid deposition technique, constructs of different shapes and sizes were fabricated: one rectangular construct containing PCL and two differently stained hydrogels, a construct combining round and rectangular shapes, and a construct in the shape of an intervertebral disc. For this purpose, alginate was left unstained or stained with fast green (Merck, Whitehouse Station, New Jersey, USA), methylene blue, basic fuchsin (pink), or ponceau xylidine (red) (all from Sigma-Aldrich) in order to be able to visually assess the fate of more complex scaffolds containing multiple hydrogels. To visualize the ability to create multiple layered constructs, hydrogel was stained as above, or loaded with Dye-Trak "F" fluorescent blue or lemon microspheres (Triton technology, San Diego, California, USA).

Mechanical characterization

For the determination of mechanical properties, 3 different construct types (n=3) were manufactured (w_xl_xh (mm): 15x15x3.3, fiber spacing 2 mm, 0-90), consisting of alginate alone, a combination of alginate and PCL, and PCL alone. The combined construct was manufactured

as described above; for the PCL alone scaffold, an analogous protocol was used, but without alginate. For the alginate construct, a mold was printed with the same outer dimensions as the other two constructs, which was then filled with alginate. The constructs containing alginate were treated with CaCl_2 as described above. After this, the alginate alone constructs were removed from their molds.

Samples were mechanically analyzed using a DMA 2980 dynamic analyzer (TA instruments, New Castle, Delaware, USA) in controlled force mode. Each sample was tested at 3 randomly chosen different sites. Scaffolds were placed between the parallel plates and a static force was applied. For alginate this force increased from 0 to 1 N at a rate of 0.2 N/min. For PCL and combined scaffolds, the applied force was between 0 and 18 N, with incremental steps of 3 N. Young's modulus (E) was determined by measuring the variation of apparent stress/strain ratio, as described previously (28).

Cells

C20A4 cells were a kind gift from Dr. Mary B. Goldring (29). Cells (passage 9-12) were cultured in DMEM (Invitrogen), supplemented with 10% FBS (Biowhittaker, Walkersville, Maryland, USA), 100 U/ml penicillin, and 100 $\mu\text{g}/\text{mL}$ streptomycin (Invitrogen).

Viability assay

For the evaluation of cell viability, cells were embedded in sterilized 2% alginate (Sigma-Aldrich) at a density of 5×10^6 cells/ml and rectangular constructs (6x60x2mm, fiber spacing 2 mm, 0-90) were printed and crosslinked as described above. Constructs were cut to yield approximately 6x6x2mm specimens; these were then cultured for up to 3 days in differentiation medium (DMEM (Invitrogen) supplemented with 0.2 mM ascorbic acid 2-phosphate (Sigma-Aldrich), 0.5% human serum albumin (Cealb, Sanquin, Utrecht, The Netherlands), 1% (v/v) insulin-transferrin-selenium mixture (ITS-X, Invitrogen), 100 U/ml penicillin, 100 $\mu\text{g}/\text{mL}$ streptomycin (Invitrogen) and 5 ng/ml $\text{TGF-}\beta_2$ (R&D Systems, Abingdon, United Kingdom)). Samples were taken for viability assays immediately after printing and after 1 and 3 days of culture (n=3 for each time point). A LIVE/DEAD Viability Assay (Molecular Probes MP03224, Eugene, USA) was performed according to the manufacturer's instructions. The samples were examined using a light microscope (Olympus, BX51, Center Valley, PA, United States) and photomicrographs were taken with an Olympus DP70 camera. The excitation/emission filters were set at 488/530 nm to observe living (green) cells and at 530/580 nm to detect dead (red) cells. Live and dead cells were counted for 3 samples per time point, at 4 locations within each construct.

Statistics

A one-way ANOVA with post-hoc Bonferroni correction was performed for the mechanical characterization experiments. For the viability assay, a two-sided independent samples t-test was performed. Young's modulus and viability data are shown \pm standard deviation.

RESULTS & DISCUSSION

Architecture and spatial arrangement

A schematic overview of the hybrid bioprinting process is shown in figure 1. Using a multi-head bioprinter, strands of the thermoplastic polymer are deposited first and subsequently, the “channels” formed by the thermoplastic are filled, either completely or partly, with hydrogel, which can be loaded with cells or bioactive components. These steps are repeated to yield a 3D construct with the desired architecture and spatial cell distributions.

As the presented hybrid bioprinting technique employs multiple cartridges that can contain different biomaterials, it is possible to specifically place multiple polymers, hydrogels (figures 1 and 2), or cell types into a single construct. The use of multiple hydrogels in one construct has

9

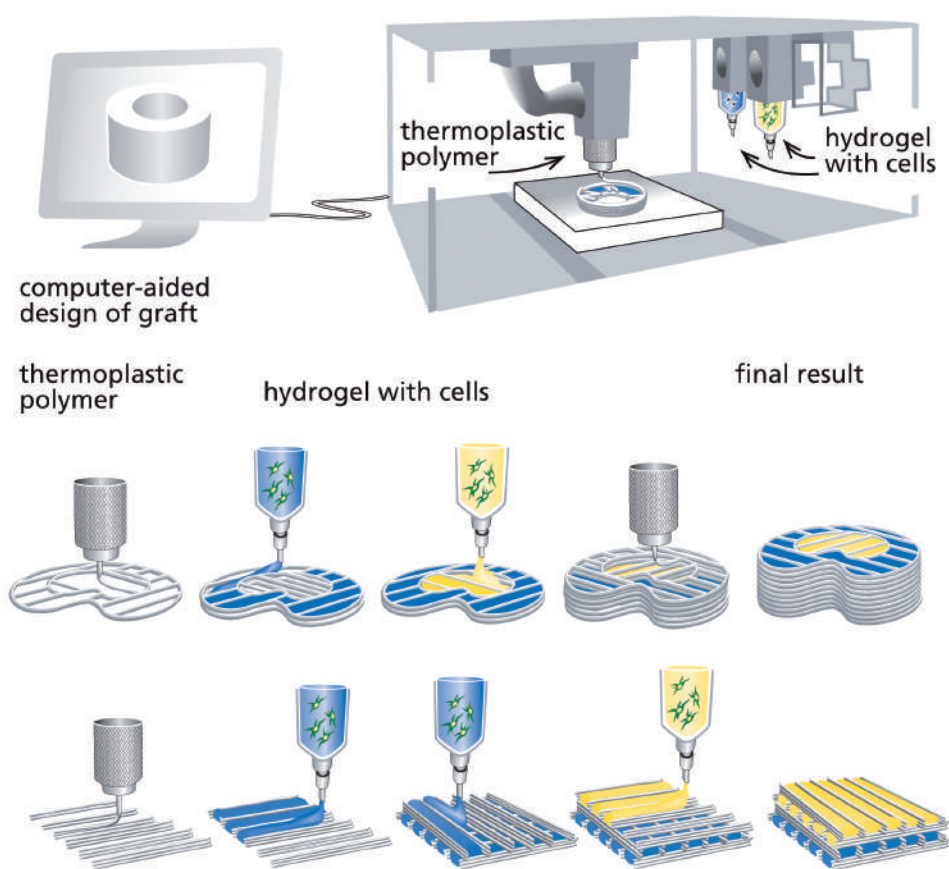


Figure 1. Schematic overview of the hybrid bioprinting process. A three-dimensional design is translated to a deposition protocol which uses thermoplastic polymer and different types of hydrogel (top panel). Alternating steps of printing polymer and cell-laden hydrogels are performed to yield hybrid constructs, combining multiple hydrogels in one layer (middle panel) or multiple hydrogels on top of each other (bottom panel).

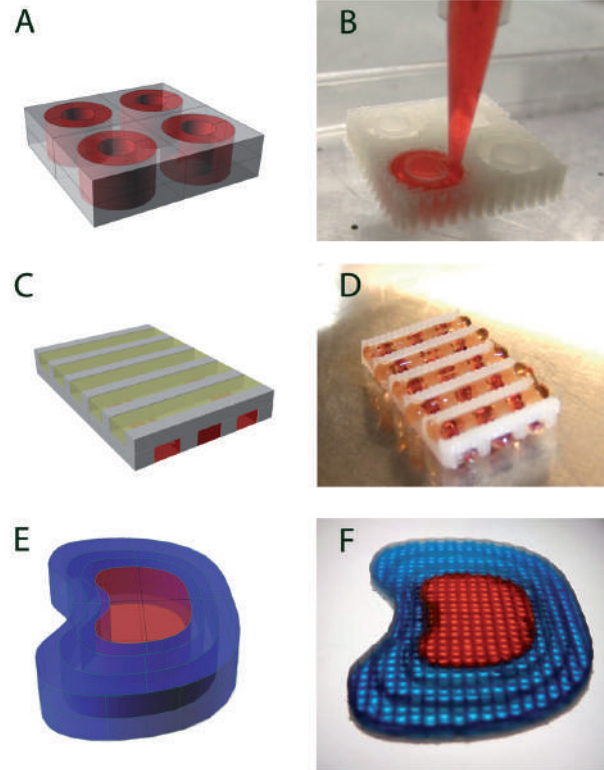


Figure 2. Versatility of the hybrid bioprinting system. Structures of different shapes and architectures can be designed (**A**, **C**, **E**) and printed using a combination of thermoplastic polymer and hydrogel (**B**, **D**, **F**). Constructs are manufactured, which combine rectangular and round shapes (**A** and **B**, WxLxH (mm): 12x12x3), with deposition layers of differently stained hydrogels on top of each other (**C** and **D**, WxLxH (mm): 8x5x1) and representing a model of an intervertebral disc (**E** and **F**, WxLxH (mm): 30x20x1.62).

been described previously (30-32). However, in the current study, we combined a commonly used hydrogel with a stiff thermoplastic polymer to demonstrate the feasibility and versatility of a novel approach to generate viable hybrid constructs. First, PCL was used as the thermoplastic component. PCL and its copolymers have been extensively studied in the biomedical field as drug delivery systems, in medical devices, as well as scaffolds for generation of a wide range of tissues, including bone, cartilage, ligament, blood vessels and skin (reviewed in Woodruff and Hutmacher 2010 (33)). In addition, alginate was used as the hydrogel phase for the hybrid printing, allowing the inclusion of encapsulated cells in the generated constructs. Alginate is a natural hydrogel, which has been described for use *in vitro*(33-37) and *in vivo* (38-40) for a broad range of applications, including drug delivery and tissue engineering of different tissues. Alginate is also used in a clinical setting for various purposes, including the treatment of cartilage defects and tympanic membrane perforations (41-43). Moreover, alginate was already identified as a suitable hydrogel for bioprinting purposes, although control over porosity characteristics of produced constructs was limited (20, 44).

The printing technique described in this paper, allows for the generation of organized 3D constructs with different controlled architectures and multiple cell populations (figures 2 and 3). Critically, no mixing of the different hydrogels was observed (figure 3) despite the low viscosity of the hydrogel used. Also, additional porosity could be introduced if desired (not shown),

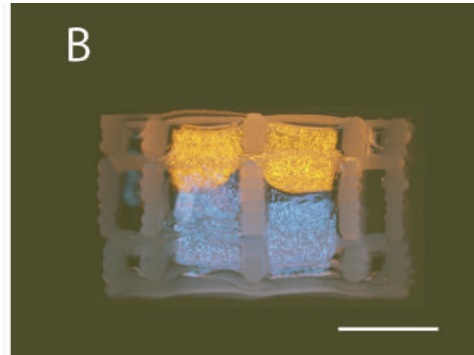
A**B**

Figure 3. Layering of the hydrogels results in specific confinement of the printed hydrogels. The layers are shown using differently stained hydrogels (**A**) and hydrogels containing fluorescent microspheres (size 15 μm , **B**). Scale bar represents 2 mm.

9

allowing perfusion of larger constructs and confirming the high degree of control over the architecture that can be achieved. Using this technique, a sheer infinite range of 3D constructs can be manufactured, varying from simple rectangular shapes to more complex structures that further mimic the organization of mammalian tissues, including those of cartilage, bone or the intervertebral disc (IVD, figure 3).

Mechanical characteristics

Printed hydrogel constructs based on alginate alone or other hydrogels (20, 27), possess a low mechanical stiffness (figure 4). Consequently, the thickness of printed hydrogel constructs is often limited, restricting the applicability of this technique. When combined with the PCL support structure, however, a significantly higher Young's modulus was measured. Interestingly, these fiber-reinforced hybrid hydrogel structures exhibited mechanical characteristics that are within the same range as those of the thermoplastic scaffolds without hydrogel (figure 4). As a consequence, by using the mechanical support of the thermoplastic material, hydrogels with a relatively low viscosity can be printed as well, whilst they would be challenging to print on their own. Clearly, this ability of printing lower viscosity hydrogels broadens the variety of possible hydrogels to be used in fiber deposition-based bioprinting approaches.

Since the mechanical properties of hybrid constructs strongly depend on the properties of PCL fibers, the overall mechanical stiffness can easily be tailored by changing fiber spacing, orientation and/or thickness (45). As a consequence, mechanical characteristics can be obtained within the same range as those of native tissues (e.g. Young's modulus of cartilage 4.1 MPa (10) and trachea 3.33 MPa (46)). Ultimately, the capability of the hybrid printed scaffolds to withstand the mechanical environment *in vivo* will still need to be assessed. However, a 3D printed PCL scaffold loaded with a growth factor-containing hydrogel, already showed promising results after implantation at an orthotopic location (47).

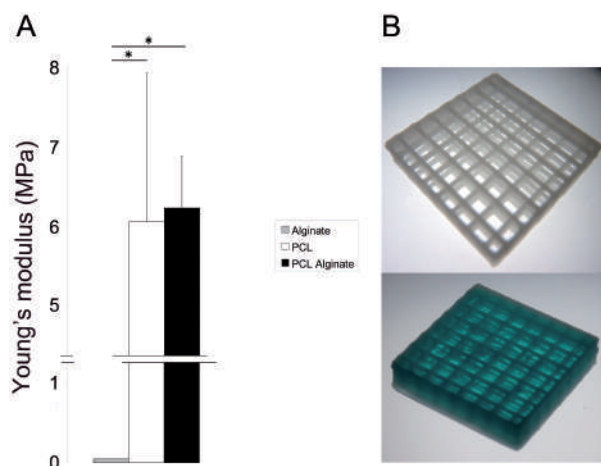


Figure 4. Mechanical properties of printed constructs. Young's modulus is shown for constructs composed of PCL, of PCL combined with alginate, and for the alginate controls (A). Data are presented as mean \pm standard deviation, * indicates $p < 0.05$. Examples of tested samples (WxLxH (mm): 15x15x3.3, fiber spacing 2 mm, 0–90) are shown in (B): an empty PCL scaffold (top) and a PCL scaffold filled with alginate (bottom).

Viability

Whilst the 3DF printing process of cell-laden hydrogels previously demonstrated to have negligible effects on viability of various cell types, including those from cartilage (20), liver (48), and bone marrow (27), the successful simultaneous deposition of thermoplastic polymers and cells has not been reported. Cell viability in the generated hybrid constructs was high immediately after printing, as well as after 1 and 3 days of *in vitro* culture. Although a small but significant difference was observed after 1 day, viability after 1 day was high. Immediately after printing and after 3 days, viability was within the same range as those of non-printed hydrogel-only constructs (figure 5). Most likely, the conditions in the laminar flow cabinet resulted in sufficient cooling of the deposited thermoplastic polymer to allow cell survival in the hydrogel strands, whilst maintaining proper conditions for integration of the thermoplastic fibers. Moreover, the slight evaporation of water from the hydrogel, induced by the laminar flow, may also have helped in accommodating the heat from the fibers. Nevertheless, additional studies focusing on heat shock protein expression (49) or cell differentiation, need to be carried out to investigate the protective mechanisms involved and the longer-term effects on cellular behavior.

CONCLUSION AND FUTURE OUTLOOK

We here demonstrate a novel approach for the generation of organized living grafts with improved mechanical stability, adding another level of controlled complexity to tissue-engineered constructs of clinically relevant dimensions. Besides yielding constructs with improved control over mechanical characteristics, this technique also allows the application of a wider range of hydrogel formulations in bioprinting, since requirements for viscosity and gelling speed are less stringent. The resolution of bioprinting could potentially be enhanced using higher printing speeds, smaller nozzle sizes and possible combination with technologies such as inkjet printing, although it is not yet clear what degree of resolution is required for optimal functioning of grafts *in vitro* and *in vivo*. The use of imaging techniques, such of CT or MRI, could

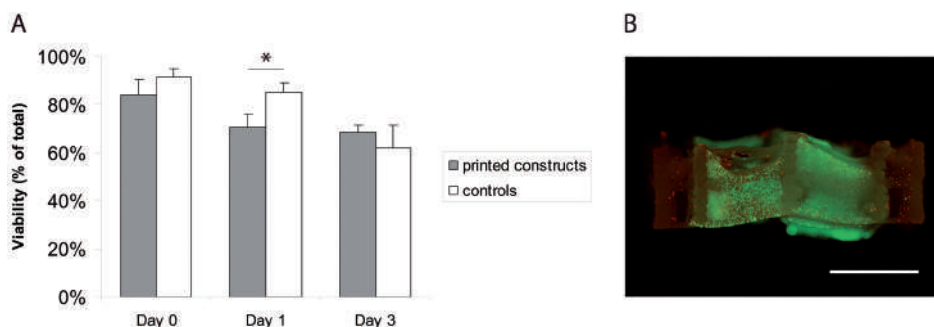


Figure 5. Cell viability of printed cells. At day 1, a significant difference was observed between printed constructs and controls (A). Data are presented as mean \pm standard deviation, * indicates $p < 0.05$. An example of an image for viability analysis (day 0) is shown in (B). Scale bar represents 2 mm.

9

in the future advance construct design, thus bringing individual custom-designed implants within reach. Furthermore, this process is not limited to the controlled deposition of cell laden hydrogels, but can also be applied for the targeted distribution of other bioactive components, such as growth factors, DNA or siRNA, or to generate sophisticated *in vitro* model systems, which more closely resemble *in vivo* environments, for testing pharmaceutical compounds.

ACKNOWLEDGEMENTS

The authors thank Dr. Tina Vermonden for her assistance with the mechanical analysis.

REFERENCES

- Endres M, Hutmacher DW, Salgado AJ, Kaps C, Ringe J, Reis RL, Sittinger M, Brandwood A, and Schantz JT, Osteogenic induction of human bone marrow-derived mesenchymal progenitor cells in novel synthetic polymer-hydrogel matrices. *Tissue Eng*, 2003. **9**(4): p. 689-702.
- Hayami JW, Surrao DC, Waldman SD, and Amsden BG, Design and characterization of a biodegradable composite scaffold for ligament tissue engineering. *J Biomed Mater Res A*, 2010. **92**(4): p. 1407-20.
- Nerurkar NL, Sen S, Huang AH, Elliott DM, and Mauck RL, Engineered disc-like angle-ply structures for intervertebral disc replacement. *Spine (Phila Pa 1976)*, 2010. **35**(8): p. 867-73.
- Schagemann JC, Chung HW, Mrosek EH, Stone JJ, Fitzsimmons JS, O'Driscoll SW, and Reinholz GG, Poly-epsilon-caprolactone/gel hybrid scaffolds for cartilage tissue engineering. *J Biomed Mater Res A*, 2010. **93**(2): p. 454-63.
- Xu W, Ma J, and Jabbari E, Material properties and osteogenic differentiation of marrow stromal cells on fiber-reinforced laminated hydrogel nanocomposites. *Acta Biomater*, 2010. **6**(6): p. 1992-2002.
- Yang Y, Wimpenny I, and Ahearne M, Portable nanofiber meshes dictate cell orientation throughout three dimensional hydrogels. *Nanomedicine*, 2011.
- Eyrich D, Wiese H, Maier G, Skodacek D, Appel B, Sarhan H, Tessmar J, Staudenmaier R, Wenzel MM, Goepferich A, and Blunk T, In vitro and in vivo cartilage engineering using a combination of chondrocyte-seeded long-term stable fibrin gels and polycaprolactone-based polyurethane scaffolds. *Tissue Eng*, 2007. **13**(9): p. 2207-18.
- McMahon RE, Qu X, Jimenez-Vergara AC, Bashur CA, Guelcher SA, Goldstein AS, and Hahn MS, Hydrogel-Electrospun Mesh Composites for Coronary Artery Bypass Grafts. *Tissue Eng Part C Methods*, 2011.
- Hutmacher DW, Sittinger M, and Risbud MV, Scaffold-based tissue engineering: rationale for computer-aided design and solid free-form fabrication systems. *Trends Biotechnol*, 2004. **22**(7): p. 354-62.

10. Woodfield TB, Malda J, de Wijn J, Peters F, Riesle J, and van Blitterswijk CA, Design of porous scaffolds for cartilage tissue engineering using a three-dimensional fiber-deposition technique. *Biomaterials*, 2004. **25**(18): p. 4149-61.
11. Moroni L, de Wijn JR, and van Blitterswijk CA, Three-dimensional fiber-deposited PEOT/PBT copolymer scaffolds for tissue engineering: influence of porosity, molecular network mesh size, and swelling in aqueous media on dynamic mechanical properties. *J Biomed Mater Res A*, 2005. **75**(4): p. 957-65.
12. Ambrosio L, De Santis R, Iannace S, Netti PA, and Nicolais L, Viscoelastic behavior of composite ligament prostheses. *J Biomed Mater Res*, 1998. **42**(1): p. 6-12.
13. Gloria A, Causa F, De Santis R, Netti PA, and Ambrosio L, Dynamic-mechanical properties of a novel composite intervertebral disc prosthesis. *J Mater Sci Mater Med*, 2007. **18**(11): p. 2159-65.
14. Holloway JL, Lowman AM, and Palmese GR, Mechanical evaluation of poly(vinyl alcohol)-based fibrous composites as biomaterials for meniscal tissue replacement. *Acta Biomater*, 2010. **6**(12): p. 4716-24.
15. Bruinink A, Siragusano D, Ettel G, Brandsberg T, Brandsberg F, Petitmermet M, Muller B, Mayer J, and Wintermantel E, The stiffness of bone marrow cell-knit composites is increased during mechanical load. *Biomaterials*, 2001. **22**(23): p. 3169-78.
16. Roh JD, Nelson GN, Udelsman BV, Brennan MP, Lockhart B, Fong PM, Lopez-Soler RI, Saltzman WM, and Breuer CK, Centrifugal seeding increases seeding efficiency and cellular distribution of bone marrow stromal cells in porous biodegradable scaffolds. *Tissue Eng*, 2007. **13**(11): p. 2743-9.
17. Woodfield TB, Van Blitterswijk CA, De Wijn J, Sims TJ, Hollander AP, and Riesle J, Polymer scaffolds fabricated with pore-size gradients as a model for studying the zonal organization within tissue-engineered cartilage constructs. *Tissue Eng*, 2005. **11**(9-10): p. 1297-311.
18. Mironov V, Boland T, Trusk T, Forgacs G, and Markwald RR, Organ printing: computer-aided jet-based 3D tissue engineering. *Trends Biotechnol*, 2003. **21**(4): p. 157-61.
19. Arcaute K, Mann BK, and Wicker RB, Stereolithography of three-dimensional bioactive poly(ethylene glycol) constructs with encapsulated cells. *Ann Biomed Eng*, 2006. **34**(9): p. 1429-41.
20. Cohen DL, Malone E, Lipson H, and Bonassar LJ, Direct freeform fabrication of seeded hydrogels in arbitrary geometries. *Tissue Eng*, 2006. **12**(5): p. 1325-35.
21. Lee W, Debasitis JC, Lee VK, Lee JH, Fischer K, Edminster K, Park JK, and Yoo SS, Multi-layered culture of human skin fibroblasts and keratinocytes through three-dimensional freeform fabrication. *Biomaterials*, 2009. **30**(8): p. 1587-95.
22. Ovsianikov A, Gruene M, Pflaum M, Koch L, Maiorana F, Wilhelm M, Haverich A, and Chichkov B, Laser printing of cells into 3D scaffolds. *Biofabrication*, 2010. **2**(1): p. 014104.
23. Guillotin B, Souquet A, Catros S, Duocastella M, Pippenger B, Bellance S, Bareille R, Remy M, Bordenave L, Amedee J, and Guillemot F, Laser assisted bioprinting of engineered tissue with high cell density and microscale organization. *Biomaterials*, 2010. **31**(28): p. 7250-6.
24. Khalil S and Sun W, Bioprinting endothelial cells with alginate for 3D tissue constructs. *J Biomech Eng*, 2009. **131**(11): p. 111002.
25. Nishiyama Y, Nakamura M, Henmi C, Yamaguchi K, Mochizuki S, Nakagawa H, and Takiura K, Development of a three-dimensional bioprinter: construction of cell supporting structures using hydrogel and state-of-the-art inkjet technology. *J Biomech Eng*, 2009. **131**(3): p. 035001.
26. Censi R, Schuurman W, di Dato G, Burgisser PE, Malda J, Dhert WJA, van Nostrum CF, di Martino P, Vermonden T, and Hennink WE, A Printable Photopolymerizable Thermosensitive p(HPMam-lactate)-PEG Hydrogel for Tissue Engineering. *Adv Funct Mater*, 2011. **21**(10): p. 1833-42.
27. Fedorovich NE, De Wijn JR, Verbout AJ, Alblas J, and Dhert WJ, Three-dimensional fiber deposition of cell-laden, viable, patterned constructs for bone tissue printing. *Tissue Eng Part A*, 2008. **14**(1): p. 127-33.
28. Meyvis TK, Stubbe BG, Van Steenberg MJ, Hennink WE, De Smedt SC, and Demeester J, A comparison between the use of dynamic mechanical analysis and oscillatory shear rheometry for the characterisation of hydrogels. *Int J Pharm*, 2002. **244**(1-2): p. 163-8.
29. Goldring MB, Birkhead JR, Suen LF, Yamin R, Mizuno S, Glowacki J, Arbiser JL, and Apperley JF, Interleukin-1 beta-modulated gene expression in immortalized human chondrocytes. *J Clin Invest*, 1994. **94**(6): p. 2307-16.
30. Koch L, Kuhn S, Sorg H, Gruene M, Schlie S, Gaebel R, Polchow B, Reimers K, Stoelting S, Ma N, Vogt PM, et al., Laser printing of skin cells and human stem cells. *Tissue Eng Part C Methods*, 2010. **16**(5): p. 847-54.
31. Norotte C, Marga FS, Niklason LE, and Forgacs G, Scaffold-free vascular tissue engineering using bioprinting. *Biomaterials*, 2009. **30**(30): p. 5910-7.
32. Skardal A, Zhang J, McCoard L, Xu X, Oottamasathien S, and Prestwich GD, Photocrosslinkable hyaluronan-gelatin hydrogels for two-step bioprinting. *Tissue Eng Part A*, 2010. **16**(8): p. 2675-85.
33. Woodruff MA and D.W. H, The return of a forgotten polymer: Polycaprolactone in the 21st century. *Progress in Polymer Science (In Press)*, 2010.
34. Hauselmann HJ, Fernandes RJ, Mok SS, Schmid TM, Block JA, Aydelotte MB, Kuettner KE, and Thonar EJ, Phenotypic stability of bovine articular chondrocytes after long-term culture in alginate beads. *J Cell Sci*, 1994. **107** (Pt 1): p. 17-27.
35. Hoesli CA, Raghuram K, Kiang RL, Mocinecova D, Hu X, Johnson JD, Lacic I, Kieffer TJ, and Piret JM, Pancreatic cell immobilization in alginate beads

- produced by emulsion and internal gelation. *Biotechnol Bioeng*, 2011. **108**(2): p. 424-34.
36. Hunt NC, Smith AM, Gbureck U, Shelton RM, and Grover LM, Encapsulation of fibroblasts causes accelerated alginate hydrogel degradation. *Acta Biomater*, 2010. **6**(9): p. 3649-56.
 37. Maguire T, Davidovich AE, Wallenstein EJ, Novik E, Sharma N, Pedersen H, Androulakis IP, Schloss R, and Yarmush M, Control of hepatic differentiation via cellular aggregation in an alginate microenvironment. *Biotechnol Bioeng*, 2007. **98**(3): p. 631-44.
 38. Alsberg E, Kong HJ, Hirano Y, Smith MK, Albeiruti A, and Mooney DJ, Regulating bone formation via controlled scaffold degradation. *J Dent Res*, 2003. **82**(11): p. 903-8.
 39. Grillo R, de Melo NF, de Araujo DR, de Paula E, Rosa AH, and Fraceto LF, Polymeric alginate nanoparticles containing the local anesthetic bupivacaine. *J Drug Target*, 2010. **18**(9): p. 688-99.
 40. Suzuki Y, Kitaura M, Wu S, Kataoka K, Suzuki K, Endo K, Nishimura Y, and Ide C, Electrophysiological and horseradish peroxidase-tracing studies of nerve regeneration through alginate-filled gap in adult rat spinal cord. *Neurosci Lett*, 2002. **318**(3): p. 121-4.
 41. Almqvist KF, Dhollander AA, Verdonk PC, Forsyth R, Verdonk R, and Verbruggen G, Treatment of cartilage defects in the knee using alginate beads containing human mature allogenic chondrocytes. *Am J Sports Med*, 2009. **37**(10): p. 1920-9.
 42. Selmi TA, Verdonk P, Chambat P, Dubrana F, Potel JF, Barnouin L, and Neyret P, Autologous chondrocyte implantation in a novel alginate-agarose hydrogel: outcome at two years. *J Bone Joint Surg Br*, 2008. **90**(5): p. 597-604.
 43. Weber DE, Semaan MT, Wasman JK, Beane R, Bonassar LJ, and Megerian CA, Tissue-engineered calcium alginate patches in the repair of chronic chinchilla tympanic membrane perforations. *Laryngoscope*, 2006. **116**(5): p. 700-4.
 44. Landers R, Hubner U, Schmelzeisen R, and Mulhaupt R, Rapid prototyping of scaffolds derived from thermoreversible hydrogels and tailored for applications in tissue engineering. *Biomaterials*, 2002. **23**(23): p. 4437-47.
 45. Moroni L, de Wijn JR, and van Blitterswijk CA, 3D fiber-deposited scaffolds for tissue engineering: influence of pores geometry and architecture on dynamic mechanical properties. *Biomaterials*, 2006. **27**(7): p. 974-85.
 46. Trabelsi O, del Palomar AP, Lopez-Villalobos JL, Ginel A, and Doblare M, Experimental characterization and constitutive modeling of the mechanical behavior of the human trachea. *Med Eng Phys*, 2010. **32**(1): p. 76-82.
 47. Lee CH, Cook JL, Mendelson A, Moiola EK, Yao H, and Mao JJ, Regeneration of the articular surface of the rabbit synovial joint by cell homing: a proof of concept study. *Lancet*, 2010. **376**(9739): p. 440-8.
 48. Wang X, Yan Y, Pan Y, Xiong Z, Liu H, Cheng J, Liu F, Lin F, Wu R, Zhang R, and Lu Q, Generation of three-dimensional hepatocyte/gelatin structures with rapid prototyping system. *Tissue Eng*, 2006. **12**(1): p. 83-90.
 49. Richter K, Haslbeck M, and Buchner J, The heat shock response: life on the verge of death. *Mol Cell*, 2010. **40**(2): p. 253-66.



chondrocytes
SZ
ECM
produce
PRG4
step
expression
however
different
tissue
phenotype
changes
combined
approaches
show
type
conditions
direction
enhance
redifferentiation
MZ
COMP
DZ
surface
lowest
limited
density
harvested
combination
formation
size
oxygen
amount
engineering
increasing
proteins
view
orientation
GAG
feasible
based
pure
challenge
leads
biomechanical
mechanical
immature
cultured
factors
growth
depth-dependent
part
disten
long-term
collagen
seen
proteins
subpopulations
promising
compressive
articular
isolated
layer
depth
may
differences
MSCs
research
one
difference
Table
using
morphology
cell
order
highest
present
thus
minute
scald-free
creating
composition
lead
fabrication
towards
culture
remains
need
methods
expansion
lead
composition
fabrication
towards
culture
remains
shows
constructs
superficial
chondrogenic
matrix
also
use
approach
populations
similar
characteristics
lose
simple
used
vivo
concept
shear
clinical
since
role
structure
defects
volume
zone
possible
However
forward
might
Cartilage
higher
development
results
Zones
higher
manufacturing
deep
stratified
specific

*SYNOPSIS, REVIEW
AND DISCUSSION*





SYNOPSIS

In this short section, the results of the previous chapters are summarized and interrelated with each other, but only briefly discussed. The overall outcome of the work reported in this thesis, put in the context of other research in the field, has served as the basis of a perspective paper, which expresses our evolving conceptions and ideas with respect to the possible merits and technical approaches of the zonal concept in cartilage engineering. That paper follows this short synopsis and concludes the thesis.

Zonal differences in vitro and the role of imposed organization

First, it was demonstrated that enriched populations of chondrocytes from the superficial, middle, and deep zones of articular cartilage can be harvested (**Chapter 2**). After expansion and subsequent re-differentiation, these enriched chondrocyte populations showed incorporation of different amounts of GAG, in a ratio comparable to native articular cartilage. Further, the expanded populations secreted zone-specific proteins. These phenomena were observed when the cells were cultured in alginate but in pellet culture no differences were seen. These observations support the use of alginate-based hydrogels for engineering zonal cartilage constructs.

As a next step, the effect of stratified combination of chondrocyte subpopulations was investigated (**Chapter 3**). To this end, pellets of deep zone and superficial zone cells were seeded and cultured in three-dimensional (3D) constructs. Zonal chondrocyte pellet culture in 3D scaffolds resulted in abundant cartilaginous tissue formation, as shown by the production of collagen type II and glycosaminoglycans (GAGs). Newly produced GAGs were better retained than in plain pellet cultures. However, maintenance or restoration of the original zonal phenotype was not observed, leading to the conclusion that neither the culture of expanded zonal chondrocytes in separate pellets, nor the layered combination of such pellets led to the desired zonal phenotype.

Insight in growth mechanisms

In the next experiment, a mathematical model was constructed to provide insight in the mechanisms of *in vitro* growth of cartilaginous tissue (**Chapter 4**). Experimental data were compared with the predictions of the simulation to refine the initial models. For this, expanded full thickness chondrocytes were seeded on collagen-coated filters and cultured for up to 7 weeks. The mathematical simulations correlated well with the experimentally obtained cell and matrix distributions. Glycosaminoglycan and cell distribution appeared to be highly dependent on the cell differentiation rate, and large regions of the tissue were inactive in terms of proliferation and growth of the layer. This implies that higher seeding densities will not significantly affect growth rate. A relatively simple mathematical model was developed that could predict the experimental data and thereby enabled interpretation of the principal underlying mechanisms controlling growth-related changes in tissue composition. The study proved that *in silico* results may provide insight in underlying mechanisms of observed cell behaviour and can possibly be used in designing and fine-tuning culture methods.



The development of the innovative concept of bioprinting

The novel technique of bioprinting obviously holds much promise for the fabrication of stratified cartilage constructs, but needs to be customised for this specific purpose. In **Chapter 5** we described the proof of principle of 3D printing of multiple cell types, using alginate hydrogel as a model biomaterial. Multipotent stromal cells and full-thickness chondrocytes were used to achieve osteogenic and chondrogenic differentiation, respectively. Changing fibre spacing or angle of fibre deposition appeared to affect porosity and elastic modulus markedly, while the architecture and cell placement were retained. Moreover, distinctive and cell-specific tissue formation was observed, both *in vitro* and *in vivo*, at different locations within one construct. These results demonstrate the aptness of the bioprinting technique to manufacture viable centimetre-scaled structured tissues, which can potentially be used for the repair of osteochondral defects.



Although bioprinting proved to be successful in the creation of multi-cellular constructs, featuring specific extracellular matrix formation at distinct sites, there was still a need for further improvement. The biomaterial that was used, alginate, allowed for the generation of constructs of a limited height only; besides, the tissue formed was specific, but not abundant. Furthermore, alginate is a mechanically very weak material. Since we believed these limitations of alginate could be alleviated by the use of thermo- and photo-curable hydrogels, we investigated three thermoresponsive and photo-crosslinkable biomaterials: hyaluronic acid/hydroxyethyl-methacrylate-derivatized dextran (HA/dex-HEMA), poly(*N*-(2-hydroxy-propyl) methacrylamide-lactate)-poly(ethylene-glycol)-poly(*N*-(2-hydroxypropyl) methacryl-amide lactate) (p(HPMAm-lactate)-PEG), and gelatine methacrylamide (gelMA) (**Chapters 6-8**). All biomaterials were analyzed for mechanical properties and swelling, cell viability of encapsulated chondrocytes and printability. All hydrogels had suitable mechanical properties for bioprinting, allowing subsequent layer-by-layer deposition of gel fibres. High cell viability was observed, and in general stable constructs were fabricated. The printing of GelMA proved to be challenging due to the low viscosity of the material, but the addition of HA to GelMA significantly improved handling and printability of the hydrogel. For GelMA, also differentiation of encapsulated chondrocytes was assessed, showing cartilaginous tissue formation. In conclusion, all three hydrogels are suitable candidates for bioprinting.

As an alternative for the use of a biomaterial with a higher viscosity and mechanical stiffness for bioprinting, a lower-viscosity hydrogel can also be combined with a stiffer thermoplastic polymer. In the final experimental chapter (**Chapter 9**), the development of this new concept is described: the bioprinting of hybrid scaffolds, constructed by alternate deposition of thermoplastic fibres and (cell-laden) hydrogels. This approach is particularly interesting for engineering of tissues that must withstand high mechanical loads. Furthermore, since the hydrogel is supported by the thermoplastic material, a broader range of hydrogel types can be used compared to bioprinting of hydrogels alone.

It can be concluded that bioprinting has shown to be a powerful tool for replication of tissue architecture. However, although much progress has been made, it must be realized that the bioprinting technique is still in its infancy. The translation of the *in vitro* results to large *in vivo* studies, let alone to routine clinical applications, has yet to be made.





chapter **TEN**

CARTILAGE REGENERATION USING ZONAL CHONDROCYTE SUBPOPULATIONS: A PROMISING APPROACH OR AN OVERCOMPLICATED STRATEGY?

Wouter Schuurman, Travis J. Klein, Wouter J. A. Dhert, P. René van Weeren,
Dietmar W. Hutmacher, and Jos Malda



INTRODUCTION

Cartilage impresses as a relatively simple tissue: it is aneural, avascular, and it contains few cells of supposedly only one cell type, the chondrocyte. Mature articular cartilage has limited healing capacity, and when a cartilage defect occurs, this eventually leads to the development of osteoarthritic changes (1). Current clinically applied strategies include autologous chondrocyte implantation (ACI) (2), microfracture (3), and mosaicplasty (4). Although short-term results of these treatment modalities are satisfactory, all of them have drawbacks such as less favorable long-term outcome with microfracture (5), donor site morbidity (4) and inferior longer-term results (6) with mosaicplasty, and high expenses (7) and the need for a two-stage procedure in the case of ACI. This means that there is room for improvement of current clinical practice. Creating cartilage constructs with a zonal organisation may be a viable alternative to current therapies for cartilage defects, which, notwithstanding reasonable clinical success, all have major drawbacks.

Despite its simple appearance, cartilage is a heterogeneous tissue with a composition that varies greatly with depth. Articular cartilage can be divided into three zones: the superficial (the top 10–20% of the cartilage), middle (the next 40–60%), and deep (the bottom 30–40%) zone. The superficial zone (SZ) has the highest cell density, the lowest amount of glycosaminoglycans (GAGs) (8), and the lowest biosynthetic activity (9). With increasing depth, the cell density decreases and the amount of GAGs increases (8), resulting in the highest amount of GAGs and the lowest cell density in the deep zone (DZ). With increasing GAG amount, the compressive modulus of the tissue also increases (10). The cells in the different zones differ in morphology and size. Cells in the SZ are small and flattened, while in the DZ cells are larger and round (11). Further, the collagen fiber alignment differs between zones. The collagen fibers have an arcade-like structure (12). They originate from the calcified cartilage and continue perpendicular to the surface, through the DZ to make a transition in the middle zone (MZ) towards an orientation parallel to the surface in the superficial layer. The specific orientation of the collagen fibers provides, together with the proteoglycan aggregates that are interspersed between these fibrils, provides the tissue with its unique biomechanical characteristics, combining compressive stiffness, resilience and shear resistance. Various proteins are preferentially secreted among zones: in the superficial zone, clusterin (13, 14), proteoglycan-4 (PRG4) also known as superficial zone protein (SZP) (15) and Del1 (16) are more prominent, while in the MZ the levels of cartilage intermediate layer protein (CILP) (17, 18) are highest. Cartilage oligomeric matrix protein (COMP) is mainly seen in the MZ and DZ (19, 20). These proteins most probably contribute to the zone-specific functionality of the cartilage. The exact specific functions of many of the zone-related proteins remain unclear, but some information about their function is known. Del1 acts as a regulator of vascularization (21), clusterin plays a role in cellular stress protection (22), COMP is a mediator in chondrocyte attachment and matrix assembly (23, 24). The presence of PRG4 in the SZ of cartilage ensures boundary lubrication and low-friction articulation (25), which has led to the hypothesis that transplanting or implanting cells or tissues that can secrete SZP may aid functional lubrication (26, 27).

The heterogeneity of articular cartilage is not explicitly addressed in current therapies for cartilage defects. Nevertheless, under the hypothesis that replicating the zonal hierarchy will

lead to better long-term function of cartilage constructs, attempts have been made to mimic the zonal architecture of the tissue using zonal chondrocyte subpopulations. The goal of this discussion paper is to give an overview and critical appraisal of tissue engineering approaches that have used zonal chondrocytes to mimic native cartilage and to present our view of the role the zonal concept may play in the future to optimize constructs for the regeneration of articular cartilage.

CURRENT STATUS OF RESEARCH

Isolation and culture of zonal chondrocytes

Experiments have been performed to elucidate the role of zonal cell populations in cartilage tissue formation *in vitro*. It has been demonstrated that cartilage tissue from the different zones can be harvested under sterile conditions. The zonal tissue can then be harvested directly manually using dissection (11, 28-31) or abrasion (32) with a surgical blade. Alternatively, (osteo) chondral cores can be obtained from which the cartilage is dissected using a microtome (26) or manually (33). SZ chondrocytes have also been isolated from mouse cartilage using sequential brief treatment with trypsin and collagenase (34). Although these methods do not yield “pure” zonal cell populations, the enriched populations of zonal chondrocytes harvested this way show clear differences both directly after isolation and in culture (27, 30, 33, 35-38). In the research focusing on the (stratified) combination of zonal chondrocytes, almost exclusively unexpanded, immature articular cartilage cells have thus far been used (27, 30, 33, 36) (Table 1). An important characteristic of immature chondrocyte subpopulations is their high metabolic activity and chondrogenic potential (39, 40), which makes them well-suited for this type of

10

Table 1. Overview of stratified approaches using zonal chondrocyte subpopulations. SZ: superficial zone cells, PEGDA: poly(ethylene glycol) diacrylate, PEODA: poly(ethylene oxide) diacrylate, DZ: deep zone cells, PO: primary cells, PI: cells expanded for 1 passage.

Cell types used	Material	Cell type	Key results	Reference
SZ, MZ, DZ	PEGDA	Immature, PO	Cell size and intensity safranin-O staining increasing with depth,	(33)
SZ, MZ	Scaffold-free (filter-culture)	Immature, PO	SZ/MZ constructs: matrix growth and compressive properties lie in between the values of SZ and MZ alone constructs	(27)
SZ, MZ	Scaffold-free (filter-culture)	Immature, PI	In vivo: Stratification of cells lost	(59)
SZ, DZ	PEODA	Immature, PO	Stratified constructs: lower proliferation and higher matrix synthesis DZ cells alone, and greater shear and compressive strength than SZ or DZ cells alone.	(30)
SZ, MDZ	Agarose	Immature, PO	GAG, collagen and mechanical properties higher for zonal constructs than non-zonal constructs. Zonal constructs: depth-dependent mechanical properties	(36)

research. However, it should be realized that immature DZ cells significantly differ from mature DZ zone cells, because the former originate from a zone that is vascularized and later becomes bone through the process of endochondral ossification (41). In this same line, it was shown in a direct comparison that SZ cells have a more stable phenotype during growth than DZ cells do (39). As differences between zonal populations are more prominent in immature cells, immature cells should be solely seen as a source for models and caution should be taken when translating outcomes to the human situation because of the limited clinical relevance.

Under clinical circumstances, only a limited number of chondrocytes is available, and in order to yield clinically relevant numbers, expansion of cells is necessary, which entails dedifferentiation. The general signs of dedifferentiation in cultured chondrocytes are the expression and secretion of collagen type I instead of collagen type II, and a lower synthesis of GAGs (42). This process can be reversed by using growth factors (43) and 3-dimensional culture methods (42, 44, 45). Zonal populations will also undergo general dedifferentiation and thus lose their chondrogenic phenotype during expansion. Additionally, they will lose their specific zonal phenotype characteristics as well (46). Zonal cells will entirely or partly lose their size differences (11) and the expression and secretion of specific zonal proteins, such as PRG4 (46), clusterin (14), COMP (38), and CILP (47). With the use of the growth factors basic fibroblast growth factor (basic FGF) and transforming growth factor- β (TGF- β) during expansion and redifferentiation (48), or when cultured under low oxygen conditions (37), chondrocytes can reacquire at least part of their specific zonal chondrogenic characteristics. Culturing cells in a 3-dimensional (3D) environment, either scaffold-free or in a hydrogel (32, 38) favors redifferentiation, although even this does not completely reverse the dedifferentiation process (46). Moreover, it has been suggested that growth factor use for re-inducing specific features of SZ and DZ cells should be differential, since growth factors affect zonal cells differently (48). Separately cultured chondrocytes from the DZ produce more GAGs than those from the SZ (11, 29, 35, 38, 49, 50) and during redifferentiation zonal cells will start producing (part of) their specific proteins (27, 38, 48). Altogether, it is possible to harvest enriched subpopulations of zonal chondrocytes and partially re-induce the zonal phenotype of these cells using 3D culture, growth factors and low oxygen tension. This makes the use of zonal chondrocytes for the fabrication of stratified cartilage constructs feasible.

An important challenge lies in isolating pure zonal chondrocyte populations. Whilst separation of zonal cartilage tissue is possible, there are no methods available to separate zonal chondrocyte subpopulations from a mixed population isolated from a cartilage biopsy. Various candidate markers, based on proteins present in the ECM of native cartilage, have been proposed to distinguish between zonal cells (13-17, 19), but, though preferentially secreted in native cartilage zones, they are not specific for a single chondrocyte subpopulation. Additionally, sorting cells based on secreted molecules is problematic, since both the secreted molecule must be retained in the cell and the antibody must be transported into the cell. Alternatively, zonal chondrocytes could theoretically be sorted based on their size using the forward scatter channel of a fluorescence-activated cell sorter. However, we have observed significant overlap in size with human chondrocytes isolated from different zones (unpublished data). Using a sorter with a volume analyzer (rather than forward scatter), may give better outcomes since the cell volume scales with the cube of the diameter. The difference of 124% of between SZ and DZ

in cell volume would translate to a difference of only 32% in diameter (51). Nonetheless, there remains a significant overlap in cell volume even between the most divergent populations. Therefore, size-based sorting is unlikely to result in pure populations from the different zones.

Moreover, there is currently no gold standard for the determination of the zonal phenotype of newly formed cartilage. The International Cartilage Repair Society histological grading scheme includes depth –dependent characteristics (52), however, this assessment and other assessments of tissue are only based on the resemblance of the neo-tissue to the native tissue with respect to GAG content, cell morphology, and a number of – not completely understood – native cartilage proteins. These observations raise the question to what extent the division of articular cartilage in three different zones reflects reality or is just the use of a simplified categorical scale to describe an underlying continuous phenotypic transition in cartilage characteristics from the surface to the calcified layer.

Mechanical loading to enhance zonal differences *in vitro*

Biomechanical loading experienced by native tissue *in vivo* stimulates ECM synthesis and remodeling and is responsible for the zonal differences in collagen fiber orientation (53-55). *In vitro*, mechanical loading protocols also promote ECM formation, as reviewed in (56), and can also be used to specifically influence the behaviour of zonal cells (Table 2). One of the effects of the loading regimes is a shift of DZ cells to a more SZ-like phenotype. This is an undesirable effect from a biomimetic point of view; DZ cells in native cartilage have specific properties and should retain these in tissue engineered cartilage. Maintenance of the phenotype of the DZ cells might benefit from more indirect exposure to pressure, as is present in native cartilage. A depth-dependent mechanical loading protocol, for instance as described by Kock *et al.* (57), might be a good step forward in (re)creating the desired anisotropic structure and composition in implants.

Stratification of zonal cells

Since zonal chondrocytes do not show self-organization (58), zonal subpopulations should be arranged in a stratified manner in order to mimic the native zonal stratification. A number of

Table 2. Overview of mechanical loading protocols for zonal subpopulations (SZ: superficial zone cells, DZ: deep zone cells) and their effect on zonal behaviour.

Loading type	Culture type	Effect SZ	Effect DZ	Reference
Cyclic compression	Agarose hydrogel	Decreased GAG synthesis, increased proliferation	Increased GAG synthesis	(49)
Compression and surface motion	3D polyurethane scaffolds	No change in PRG4 expression	Increased PRG4 expression	(83)
Tensile loading	Fibrin hydrogel	Increased GAG synthesis	Synthesis GAG unaffected, decreased collagen	(84)
Cyclic compression	Cells seeded on calcium poly phosphate discs	Increased collagen and GAG synthesis	Decreased collagen and GAG synthesis	(85)

studies describe such approaches (Table 1). For instance, in layered, heterogeneous constructs of chondrocyte subpopulations embedded in diacrylated poly(ethylene)-based materials (30, 33) or agarose hydrogels (36), the deep layer produces more GAGs (30, 33) and collagen (30), and has higher shear and compressive strength (30) than the superficial layer. Values for collagen, GAG and mechanical properties are comparable to, or higher than, non-zonal constructs consisting of full thickness chondrocytes (30, 36). Further, the amount of GAGs is significantly higher in the SZ part of combined constructs than in SZ only constructs (36). For the zonal proteins no difference is seen in COMP gene expression between zones (33), yet SZ cells secrete PRG4, while DZ cells do not (36). In stratified scaffold-free constructs combining SZ and MZ cells, intermediate properties can be observed for thickness, GAG and collagen content, when compared to SZ and MZ only constructs. Further, zonal protein PRG4 is mainly seen in parts containing SZ cells (27). In the only study assessing zonal chondrocytes constructs *in vivo*, scaffold-free implants in the patellofemoral groove of mini-pigs show limited matrix production, and loss of zonal organization (59).

In summary, stratification of zonal cells can lead to depth-dependent differences *in vitro*; however, the step towards (long-term) *in vivo* zonal performance remains a challenge. Possibly, the use of state-of-the-art techniques such as magnetically guided 3D cell patterning and additive manufacturing may play a role in this. Using the former, the manipulation of cells into multi-directional cell arrangements is possible, both *in vitro* and *in situ* (60). Additive manufacturing can also aid in further development of this strategy, since this technology permits the fabrication of multi-cell type, multi-layered and multi-material constructs (61-64) (Figure 1), which have mechanical properties similar to native tissues (62, 65). Also, porosity of the constructs can be controlled in detail (66), creating the possibility to optimize diffusion of nutrients and waste products (67), and thus to produce larger constructs.

FUTURE PERSPECTIVES

If zonal chondrocytes are to be used, apart from the previously mentioned issues, a number of general challenges need to be overcome in order to reach a clinical application. First, the challenge of obtaining sufficient cells for implantation needs to be addressed. Typically, only a limited amount of cells can be harvested from a patient, and these cells need to be expanded or combined with another cell source. Expansion of chondrocytes leads to dedifferentiation and loss of (zonal) phenotype. A promising approach is to combine primary chondrocytes with bone marrow-derived mesenchymal stromal cells (MSCs). For full-thickness chondrocytes, this method leads to MSC-induced chondrocyte proliferation (68) and chondrocyte-enhanced chondrogenesis by MSCs (68-70). In this way, not only the quantity problem is solved, it may also bring one-stage surgery for cartilage defects a step closer. Of course, for a zonal approach it will be necessary to investigate whether a co-culture of this kind also benefits zonal chondrocytes.

However, the arguments raised above urge open-minded consideration of the entire zonal concept. The idea that zonal neo-tissue or constructs reflecting the native structural depth-dependent differences may have advantages over homogeneous material is valid and still stands. However, most of the attempts to generate zonal tissue have used cells from zonal subpopulations to achieve this. This approach goes from the premise that the cells are leading

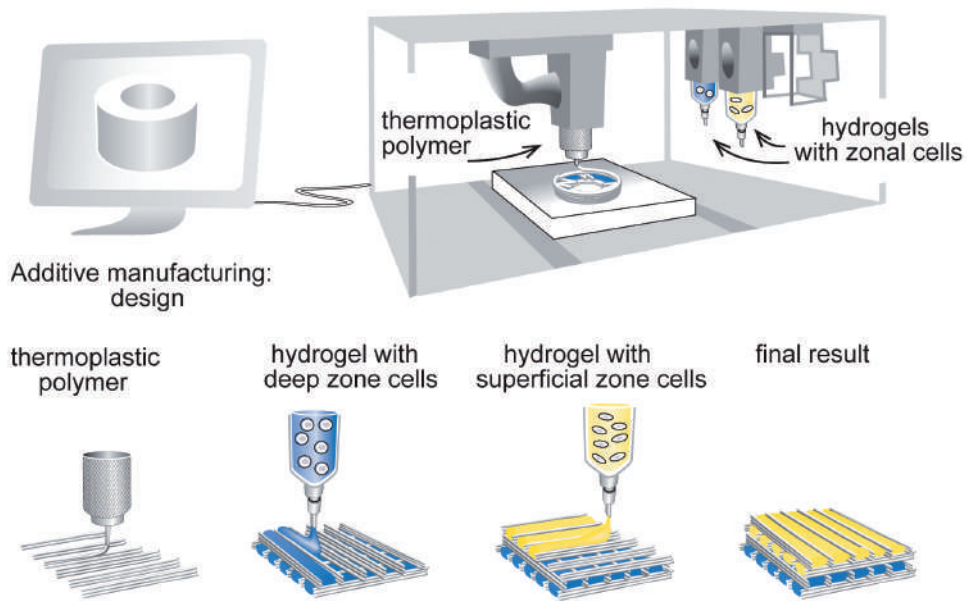


Figure 1. Possible combination of the use of additive manufacturing, smart materials, and (zonal) cells. A 3-dimensional (3D) design is loaded into the computer and converted to a 3D shape, using multiple cell types. Adapted from (62).

10

in determining zonal characteristics. This seems logical, as the cells produce the matrix and not *vice versa*. While this is true, another mechanistic option is that the cells are driven by the environmental (biomechanical and biochemical) conditions, which change with increasing depth. Load dissipation in cartilage is depth-dependent and non-linear (71); oxygen tension also changes rather dramatically with distance from the surface in an a-vascular tissue like cartilage (72). In this concept, the cells are programmed according to their depth-dependent location and adapt their morphology and expression patterns: they follow instead of lead. In fact, there are a number of studies advocating this concept. It has been shown in young, growing animals, that mechanical loading directs the formation of “horizontal” topographical heterogeneity and can affect the development of collagen orientation (53), and that also in vertical direction, *i.e.* depth-related, changes in the distribution of extracellular matrix components can be induced by exercise (73). This is direct *in vivo* evidence of the influence of loading on the zonal arrangement of cartilage. Experimental evidence from *in vitro* research on the effect of force direction on collagen formation in explants points in the same direction (57) and in this same line it was predicted in a numerical simulation that a combination of loading and shear stress holds promise to result in a physiological collagen structure (74). Of course, this replication of collagen fiber arcades needs to be confirmed experimentally, either *in vitro* using a mechanical loading system, or in an implant *in vivo* at an orthotopic location.

As an alternative for zonal chondrocytes, MSCs can be directed towards differentiation into zonal chondrogenic cells (75, 76) by the use of specific different biomaterials in one construct.

This method shows great promise, since it potentially could solve the problems of limited availability of zonal chondrocytes, donor site morbidity and chondrocyte dedifferentiation.

A promising approach for tissue engineering, that might lead to the formation of zonal cell populations, is the combination of a structure with biomechanical characteristics similar to the natural situation (hence creating a similar force dissipation pattern) with cells that resemble juvenile cells (e.g. MSCs). The realization of such an approach seems feasible. It has been shown that the combination of different biomaterials and smart scaffold design can affect the ECM deposition by influencing cell alignment (77). For the fabrication of complex multiple-material structures additive manufacturing techniques have already proven to be useful (61, 62, 78). To further enhance the desired anisotropic tissue formation, a depth-dependent, and maybe also a topography-dependent mechanical loading protocol could be employed. A mechanical loading regime can also be used to test whether a construct will be able to withstand the compressive loads and shear forces it will be subjected to *in vivo*.

In the future, complex shapes, based on actual patient images obtained by CT or MRI, may be fabricated using this technique. Possibly, zonal cartilage architecture could be combined with vascularized bone grafts to enhance vascularization and integration of the implant. When instructive biomaterials would be used, specific cell types can be attracted and cell behaviour such as proliferation and differentiation promoted (79, 80). In all cases, the creation of circumstances that allow the seeded cells to differentiate into zonal chondrocyte phenotypes, driven by their biomechanical and chemical microenvironment, seems the key to success.

We conclude from our literature review that the wide range of models and approaches used, and probably also the lack of success so far, reflect the lack of understanding of the requirements for zonal cartilage. It is striking, that while the first reports about zonal differences in cartilage tissue date from more than 20 years ago (35, 81) and a great deal of *in vitro* work has been performed non-zonal cartilage tissue engineering, only one short-term *in vivo* study relying on the zonal concept has been reported (59). There is reason to believe that the focus in research on the harvesting of zonal chondrocyte populations and on attempts to let these cells retain or regain their zonal phenotype has been too strong, and based on an overly simplistic conception of how the zonal characteristics of cartilage are generated and maintained *in vivo*. Alternatives for the use of zonal chondrocytes, like the use of mechanical loading regimes, instructive biomaterials and smart scaffold design that prompt the cells to develop a zonal phenotype exist and should be further investigated. The use of mesenchymal stromal cells in this context seems especially promising. In our view, the regeneration of zonal cartilage remains an important aim; however, an environment-driven cell differentiation approach is more feasible than one involving simple organization of zonal chondrocytes. The challenge of producing cartilaginous tissue with a zonal composition *in vivo* may even be greater than it seems, since negative results are not likely to be published (82). We therefore advocate that research groups publish also their negative results so they will not be repeated by others so we might gain the knowledge which was exhausted over the last twenty years.

REFERENCES

1. Prakash D and Learmonth D, Natural progression of osteo-chondral defect in the femoral condyle. *Knee*, 2002. **9**(1): p. 7-10.
2. Peterson L, Brittberg M, Kiviranta I, Akerlund EL, and Lindahl A, Autologous chondrocyte transplantation. Biomechanics and long-term durability. *Am J Sports Med*, 2002. **30**(1): p. 2-12.
3. Lane JG, Healey RM, Chen AC, Sah RL, and Amiel D, Can osteochondral grafting be augmented with microfracture in an extended-size lesion of articular cartilage? *Am J Sports Med*, 2010. **38**(7): p. 1316-23.
4. Hangody L, Vasarhelyi G, Hangody LR, Sukosd Z, Tibay G, Bartha L, and Bodo G, Autologous osteochondral grafting--technique and long-term results. *Injury*, 2008. **39 Suppl 1**: p. S32-9.
5. Saris DB, Vanlauwe J, Victor J, Almqvist KF, Verdonk R, Bellemans J, and Luyten FP, Treatment of symptomatic cartilage defects of the knee: characterized chondrocyte implantation results in better clinical outcome at 36 months in a randomized trial compared to microfracture. *Am J Sports Med*, 2009. **37 Suppl 1**: p. 10S-19S.
6. Bentley G, Biant LC, Carrington RW, Akmal M, Goldberg A, Williams AM, Skinner JA, and Pringle J, A prospective, randomised comparison of autologous chondrocyte implantation versus mosaicplasty for osteochondral defects in the knee. *J Bone Joint Surg Br*, 2003. **85**(2): p. 223-30.
7. Gerlier L, Lamotte M, Wille M, Kreuz PC, Vanlauwe J, Dubois D, and Meurgey FM, The cost utility of autologous chondrocytes implantation using ChondroSelect(R) in symptomatic knee cartilage lesions in Belgium. *Pharmacoeconomics*, 2010. **28**(12): p. 1129-46.
8. Buckwalter JA and Mankin HJ, Articular cartilage: tissue design and chondrocyte-matrix interactions. *Instr Course Lect*, 1998. **47**: p. 477-86.
9. Wong M, Wuethrich P, Egli P, and Hunziker E, Zone-specific cell biosynthetic activity in mature bovine articular cartilage: a new method using confocal microscopic stereology and quantitative autoradiography. *J Orthop Res*, 1996. **14**(3): p. 424-32.
10. Schinagl RM, Gurskis D, Chen AC, and Sah RL, Depth-dependent confined compression modulus of full-thickness bovine articular cartilage. *J Orthop Res*, 1997. **15**(4): p. 499-506.
11. Siczkowski M and Watt FM, Subpopulations of chondrocytes from different zones of pig articular cartilage. Isolation, growth and proteoglycan synthesis in culture. *J Cell Sci*, 1990. **97 (Pt 2)**: p. 349-60.
12. Benninghoff A, Form und Bau der Gelenkknorpel in Ihren Beziehungen zur Funktion. *Z Zellforsch*, 1925. **2**: p. 783-862.
13. Khan IM, Salter DM, Bayliss MT, Thomson BM, and Archer CW, Expression of clusterin in the superficial zone of bovine articular cartilage. *Arthritis Rheum*, 2001. **44**(8): p. 1795-9.
14. Malda J, ten Hoope W, Schuurman W, van Osch GJ, van Weeren PR, and Dhert WJ, Localization of the potential zonal marker clusterin in native cartilage and in tissue-engineered constructs. *Tissue Eng Part A*, 2010. **16**(3): p. 897-904.
15. Flannery CR, Hughes CE, Schumacher BL, Tudor D, Aydelotte MB, Kuettner KE, and Caterson B, Articular cartilage superficial zone protein (SZP) is homologous to megakaryocyte stimulating factor precursor and is a multifunctional proteoglycan with potential growth-promoting, cytoprotective, and lubricating properties in cartilage metabolism. *Biochem Biophys Res Commun*, 1999. **254**(3): p. 535-41.
16. Pfister BE, Aydelotte MB, Burkhart W, Kuettner KE, and Schmid TM, Del1: a new protein in the superficial layer of articular cartilage. *Biochem Biophys Res Commun*, 2001. **286**(2): p. 268-73.
17. Bernardo BC, Belluocchio D, Rowley L, Little CB, Hansen U, and Bateman JF, Cartilage intermediate layer protein 2 (CILP-2) is expressed in articular and meniscal cartilage and down-regulated in experimental osteoarthritis. *J Biol Chem*, 2011. **286**(43): p. 37758-67.
18. Lorenzo P, Bayliss MT, and Heinegard D, A novel cartilage protein (CILP) present in the mid-zone of human articular cartilage increases with age. *J Biol Chem*, 1998. **273**(36): p. 23463-8.
19. DiCesare PE, Morgelin M, Carlson CS, Pasmarti S, and Paulsson M, Cartilage oligomeric matrix protein: isolation and characterization from human articular cartilage. *J Orthop Res*, 1995. **13**(3): p. 422-8.
20. Murray RC, Smith RK, Henson FM, and Goodship A, The distribution of cartilage oligomeric matrix protein (COMP) in equine carpal articular cartilage and its variation with exercise and cartilage deterioration. *Vet J*, 2001. **162**(2): p. 121-8.
21. Penta K, Varner JA, Liaw L, Hidai C, Schatzman R, and Quertermous T, Del1 induces integrin signaling and angiogenesis by ligation of alphaVbeta3. *J Biol Chem*, 1999. **274**(16): p. 11101-9.
22. Rosenberg ME and Silikens J, Clusterin: physiologic and pathophysiologic considerations. *Int J Biochem Cell Biol*, 1995. **27**(7): p. 633-45.
23. DiCesare PE, Carlson CS, Stoleran ES, Hauser N, Tulli H, and Paulsson M, Increased degradation and altered tissue distribution of cartilage oligomeric matrix protein in human rheumatoid and osteoarthritic cartilage. *J Orthop Res*, 1996. **14**(6): p. 946-55.
24. Blumbach K, Bastiaansen-Jenniskens YM, DeGroot J, Paulsson M, van Osch GJ, and Zaucke F, Combined role of type IX collagen and cartilage oligomeric matrix protein in cartilage matrix assembly: cartilage oligomeric matrix protein counteracts type IX collagen-induced limitation of cartilage collagen

- fibril growth in mouse chondrocyte cultures. *Arthritis Rheum*, 2009. **60**(12): p. 3676-85.
25. Jay GD, Haberstroh K, and Cha CJ, Comparison of the boundary-lubricating ability of bovine synovial fluid, lubricin, and Healon. *J Biomed Mater Res*, 1998. **40**(3): p. 414-8.
 26. Schmidt TA, Schumacher BL, Klein TJ, Voegtline MS, and Sah RL, Synthesis of proteoglycan 4 by chondrocyte subpopulations in cartilage explants, monolayer cultures, and resurfaced cartilage cultures. *Arthritis Rheum*, 2004. **50**(9): p. 2849-57.
 27. Klein TJ, Schumacher BL, Schmidt TA, Li KW, Voegtline MS, Masuda K, Thonar EJ, and Sah RL, Tissue engineering of stratified articular cartilage from chondrocyte subpopulations. *Osteoarthritis Cartilage*, 2003. **11**(8): p. 595-602.
 28. Coates E and Fisher JP, Gene expression of alginate-embedded chondrocyte subpopulations and their response to exogenous IGF-1 delivery. *J Tissue Eng Regen Med*, 2011.
 29. Hwang NS, Varghese S, Lee HJ, Theprungsirikul P, Canver A, Sharma B, and Elisseff J, Response of zonal chondrocytes to extracellular matrix-hydrogels. *FEBS Lett*, 2007. **581**(22): p. 4172-8.
 30. Sharma B, Williams CG, Kim TK, Sun D, Malik A, Khan M, Leong K, and Elisseff JH, Designing zonal organization into tissue-engineered cartilage. *Tissue Eng*, 2007. **13**(2): p. 405-14.
 31. Waldman SD, Grynepas MD, Pilliar RM, and Kandel RA, The use of specific chondrocyte populations to modulate the properties of tissue-engineered cartilage. *J Orthop Res*, 2003. **21**(1): p. 132-8.
 32. Darling EM and Athanasiou KA, Retaining zonal chondrocyte phenotype by means of novel growth environments. *Tissue Eng*, 2005. **11**(3-4): p. 395-403.
 33. Kim TK, Sharma B, Williams CG, Ruffner MA, Malik A, McFarland EG, and Elisseff JH, Experimental model for cartilage tissue engineering to regenerate the zonal organization of articular cartilage. *Osteoarthritis Cartilage*, 2003. **11**(9): p. 653-64.
 34. Yasuhara R, Ohta Y, Yuasa T, Kondo N, Hoang T, Addya S, Fortina P, Pacifici M, Iwamoto M, and Enomoto-Iwamoto M, Roles of beta-catenin signaling in phenotypic expression and proliferation of articular cartilage superficial zone cells. *Lab Invest*, 2011. **91**(12): p. 1739-52.
 35. Aydelotte MB, Greenhill RR, and Kuettnner KE, Differences between sub-populations of cultured bovine articular chondrocytes. II. Proteoglycan metabolism. *Connect Tissue Res*, 1988. **18**(3): p. 223-34.
 36. Ng KW, Ateshian GA, and Hung CT, Zonal chondrocytes seeded in a layered agarose hydrogel create engineered cartilage with depth-dependent cellular and mechanical inhomogeneity. *Tissue Eng Part A*, 2009. **15**(9): p. 2315-24.
 37. Schrobback K, Klein TJ, Crawford R, Upton Z, Malda J, and Leavesley DI, Effects of oxygen and culture system on in vitro propagation and redifferentiation of osteoarthritic human articular chondrocytes. *Cell Tissue Res*, 2011. **[Epub ahead of print]**.
 38. Schuurman W, Gawlitta D, Klein TJ, ten Hoope W, van Rijen MH, Dhert WJ, van Weeren PR, and Malda J, Zonal chondrocyte subpopulations reacquire zone-specific characteristics during in vitro redifferentiation. *Am J Sports Med*, 2009. **37 Suppl 1**: p. 975-1045.
 39. Hidaka C, Cheng C, Alexandre D, Bhargava M, and Torzilli PA, Maturational differences in superficial and deep zone articular chondrocytes. *Cell Tissue Res*, 2006. **323**(1): p. 127-35.
 40. Pestka JM, Schmal H, Salzmann G, Hecky J, Sudkamp NP, and Niemeyer P, In vitro cell quality of articular chondrocytes assigned for autologous implantation in dependence of specific patient characteristics. *Arch Orthop Trauma Surg*, 2011. **131**(6): p. 779-89.
 41. Karaplis AC, 'Embryonic Development of Bone and Regulation of Intramembranous and Endochondral Bone Formation', in *Principles of bone biology*, Bilezikian JP, Raisz LG, and Martin TJ, Editors. 2008, Elsevier: San Diego.
 42. Benya PD and Shaffer JD, Dedifferentiated chondrocytes reexpress the differentiated collagen phenotype when cultured in agarose gels. *Cell*, 1982. **30**(1): p. 215-24.
 43. Jakob M, Demarteau O, Schafer D, Hintermann B, Dick W, Heberer M, and Martin I, Specific growth factors during the expansion and redifferentiation of adult human articular chondrocytes enhance chondrogenesis and cartilaginous tissue formation in vitro. *J Cell Biochem*, 2001. **81**(2): p. 368-77.
 44. Martin I, Vunjak-Novakovic G, Yang J, Langer R, and Freed LE, Mammalian chondrocytes expanded in the presence of fibroblast growth factor 2 maintain the ability to differentiate and regenerate three-dimensional cartilaginous tissue. *Exp Cell Res*, 1999. **253**(2): p. 681-8.
 45. Stewart MC, Saunders KM, Burton-Wurster N, and Macleod JN, Phenotypic stability of articular chondrocytes in vitro: the effects of culture models, bone morphogenetic protein 2, and serum supplementation. *J Bone Miner Res*, 2000. **15**(1): p. 166-74.
 46. Darling EM and Athanasiou KA, Rapid phenotypic changes in passaged articular chondrocyte subpopulations. *J Orthop Res*, 2005. **23**(2): p. 425-32.
 47. Schrobback K, Malda J, Crawford R, Upton Z, Leavesley D, and Klein TJ, Effects of Oxygen on Zonal Marker Expression in Human Articular Chondrocytes. *Tissue Eng Part A*, 2012. **[Epub ahead of print]**.
 48. Darling EM and Athanasiou KA, Growth factor impact on articular cartilage subpopulations. *Cell Tissue Res*, 2005. **322**(3): p. 463-73.
 49. Lee DA, Noguchi T, Knight MM, O'Donnell L, Bentley G, and Bader DL, Response of chondrocyte subpopulations cultured within unloaded and loaded agarose. *J Orthop Res*, 1998. **16**(6): p. 726-33.

50. Cheng C, Conte E, Pleshko-Camacho N, and Hidaka C, Differences in matrix accumulation and hypertrophy in superficial and deep zone chondrocytes are controlled by bone morphogenetic protein. *Matrix Biol*, 2007. **26**(7): p. 541-53.
51. Hunziker EB, Quinn TM, and Hauselmann HJ, Quantitative structural organization of normal adult human articular cartilage. *Osteoarthritis Cartilage*, 2002. **10**(7): p. 564-72.
52. Mainil-Varlet P, Van Damme B, Nestic D, Knutsen G, Kandel R, and Roberts S, A new histology scoring system for the assessment of the quality of human cartilage repair: ICRS II. *Am J Sports Med*, 2010. **38**(5): p. 880-90.
53. Brama PA, Holopainen J, van Weeren PR, Firth EC, Helminen HJ, and Hyttinen MM, Effect of loading on the organization of the collagen fibril network in juvenile equine articular cartilage. *J Orthop Res*, 2009. **27**(9): p. 1226-34.
54. Harada Y, Tomita N, Wakitani S, Mii Y, Oka M, and Tsutsumi S, Use of controlled mechanical stimulation in vivo to induce cartilage layer formation on the surface of osteotomized bone. *Tissue Eng*, 2002. **8**(6): p. 969-78.
55. Moger CJ, Barrett R, Bleuet P, Bradley DA, Ellis RE, Green EM, Knapp KM, Muthuvelu P, and Winlove CP, Regional variations of collagen orientation in normal and diseased articular cartilage and subchondral bone determined using small angle X-ray scattering (SAXS). *Osteoarthritis Cartilage*, 2007. **15**(6): p. 682-7.
56. Grad S, Eglin D, Alini M, and Stoddart MJ, Physical stimulation of chondrogenic cells in vitro: a review. *Clin Orthop Relat Res*, 2011. **469**(10): p. 2764-72.
57. Kock LM, Ravetto A, van Donkelaar CC, Foolen J, Emans PJ, and Ito K, Tuning the differentiation of periosteum-derived cartilage using biochemical and mechanical stimulations. *Osteoarthritis Cartilage*, 2011. **18**(11): p. 1528-35.
58. Hayes AJ, Hall A, Brown L, Tubo R, and Catterson B, Macromolecular organization and in vitro growth characteristics of scaffold-free neocartilage grafts. *J Histochem Cytochem*, 2007. **55**(8): p. 853-66.
59. Chawla K, Klein TJ, Schumacher BL, Jadin KD, Shah BH, Nakagawa K, Wong VW, Chen AC, Masuda K, and Sah RL, Short-term retention of labeled chondrocyte subpopulations in stratified tissue-engineered cartilaginous constructs implanted in vivo in minipigs. *Tissue Eng*, 2007. **13**(7): p. 1525-37.
60. Grogan SP, Pauli C, Chen P, Du J, Chung CB, Kong SD, Colwell CW, Jr., Lotz MK, Jin S, and D'Lima DD, In Situ Tissue Engineering Using Magnetically Guided Three-Dimensional Cell Patterning. *Tissue Eng Part C Methods*, 2012. **[Epub ahead of print]**.
61. Fedorovich NE, Schuurman W, Wijnberg HM, Prins HJ, van Weeren PR, Malda J, Alblas J, and Dhert WJ, Biofabrication of osteochondral tissue equivalents by printing topologically defined, cell-laden hydrogel scaffolds. *Tissue Eng Part C Methods*, 2012. **18**(1): p. 33-44.
62. Schuurman W, Khristov V, Pot MW, van Weeren PR, Dhert WJ, and Malda J, Bioprinting of hybrid tissue constructs with tailorable mechanical properties. *Biofabrication*, 2011. **3**(2): p. 021001.
63. Melchels FPW, Domingos MAN, Klein TJ, Malda J, Bartolo PJ, and Huttmacher DW, Additive Manufacturing of Tissues and Organs. *Progress in Polymer Science*, 2011. **In press**.
64. Klein TJ, Rizzi SC, Reichert JC, Georgi N, Malda J, Schuurman W, Crawford RW, and Huttmacher DW, Strategies for zonal cartilage repair using hydrogels. *Macromol Biosci*, 2009. **9**(11): p. 1049-58.
65. Cui X, Breitenkamp K, Finn MG, Lotz M, and D'Lima D, Direct Human Cartilage Repair Using 3D Bioprinting Technology. *Tissue Eng Part A*, 2012. **[Epub ahead of print]**.
66. Fedorovich NE, De Wijn JR, Verbout AJ, Alblas J, and Dhert WJ, Three-dimensional fiber deposition of cell-laden, viable, patterned constructs for bone tissue printing. *Tissue Eng Part A*, 2008. **14**(1): p. 127-33.
67. Shipley RJ, Jones CW, Dyson RJ, Sengers BG, Bailey CL, Catt CJ, Please CP, and Malda J, Design criteria for a printed tissue engineering construct: a mathematical homogenization approach. *J Theor Biol*, 2009. **259**(3): p. 489-502.
68. Acharya C, Adesida A, Zajac P, Mumme M, Riesle J, Martin I, and Barbero A, Enhanced chondrocyte proliferation and mesenchymal stromal cells chondrogenesis in coculture pellets mediate improved cartilage formation. *J Cell Physiol*, 2012. **227**(1): p. 88-97.
69. Mo XT, Guo SC, Xie HQ, Deng L, Zhi W, Xiang Z, Li XQ, and Yang ZM, Variations in the ratios of co-cultured mesenchymal stem cells and chondrocytes regulate the expression of cartilaginous and osseous phenotype in alginate constructs. *Bone*, 2009. **45**(1): p. 42-51.
70. Wu L, Leijten JC, Georgi N, Post JN, van Blitterswijk CA, and Karperien M, Trophic effects of mesenchymal stem cells increase chondrocyte proliferation and matrix formation. *Tissue Eng Part A*, 2011. **17**(9-10): p. 1425-36.
71. Koolstra JH and van Eijden TM, Prediction of volumetric strain in the human temporomandibular joint cartilage during jaw movement. *J Anat*, 2006. **209**(3): p. 369-80.
72. Zhou S, Cui Z, and Urban JP, Factors influencing the oxygen concentration gradient from the synovial surface of articular cartilage to the cartilage-bone interface: a modeling study. *Arthritis Rheum*, 2004. **50**(12): p. 3915-24.
73. van Weeren PR, Firth EC, Brommer B, Hyttinen MM, Helminen AE, Rogers CW, Degroot J, and Brama PA, Early exercise advances the maturation of glycosaminoglycans and collagen in the extracellular matrix of articular cartilage in the horse. *Equine Vet J*, 2008. **40**(2): p. 128-35.

74. Khoshgoftar M, van Donkelaar CC, and Ito K, Mechanical stimulation to stimulate formation of a physiological collagen architecture in tissue-engineered cartilage: a numerical study. *Comput Methods Biomech Biomed Engin*, 2011. **14**(2): p. 135-44.
75. Nguyen LH, Kudva AK, Saxena NS, and Roy K, Engineering articular cartilage with spatially-varying matrix composition and mechanical properties from a single stem cell population using a multi-layered hydrogel. *Biomaterials*, 2011. **32**(29): p. 6946-52.
76. Nguyen LH, Kudva AK, Guckert NL, Linse KD, and Roy K, Unique biomaterial compositions direct bone marrow stem cells into specific chondrocytic phenotypes corresponding to the various zones of articular cartilage. *Biomaterials*, 2011. **32**(5): p. 1327-38.
77. Wise JK, Yarin AL, Megaridis CM, and Cho M, Chondrogenic differentiation of human mesenchymal stem cells on oriented nanofibrous scaffolds: engineering the superficial zone of articular cartilage. *Tissue Eng Part A*, 2009. **15**(4): p. 913-21.
78. Mironov V, Boland T, Trusk T, Forgacs G, and Markwald RR, Organ printing: computer-aided jet-based 3D tissue engineering. *Trends Biotechnol*, 2003. **21**(4): p. 157-61.
79. Lutolf MP and Hubbell JA, Synthetic biomaterials as instructive extracellular microenvironments for morphogenesis in tissue engineering. *Nat Biotechnol*, 2005. **23**(1): p. 47-55.
80. Romano NH, Sengupta D, Chung C, and Heilshorn SC, Protein-engineered biomaterials: nanoscale mimics of the extracellular matrix. *Biochim Biophys Acta*, 2012. **1810**(3): p. 339-49.
81. Archer CW, McDowell J, Bayliss MT, Stephens MD, and Bentley G, Phenotypic modulation in subpopulations of human articular chondrocytes in vitro. *J Cell Sci*, 1990. **97** (Pt 2): p. 361-71.
82. Stern JM and Simes RJ, Publication bias: evidence of delayed publication in a cohort study of clinical research projects. *Bmj*, 1997. **315**(7109): p. 640-5.
83. Li Z, Yao S, Alini M, and Grad S, Different response of articular chondrocyte subpopulations to surface motion. *Osteoarthritis Cartilage*, 2007. **15**(9): p. 1034-41.
84. Vanderploeg EJ, Wilson CG, and Levenston ME, Articular chondrocytes derived from distinct tissue zones differentially respond to in vitro oscillatory tensile loading. *Osteoarthritis Cartilage*, 2008. **16**(10): p. 1228-36.
85. Raizman I, De Croos JN, St-Pierre JP, Pilliar RM, and Kandel RA, Articular cartilage subpopulations respond differently to cyclic compression in vitro. *Tissue Eng Part A*, 2009. **15**(12): p. 3789-98.



NEDERLANDSE SAMENVATTING

INTRODUCTIE

Defecten in gewrichtskraakbeen op traumatische basis komen veel voor en de aangedane populatie bestaat veelal uit jonge, actieve patiënten. Het ziektebeeld is niet beperkt tot mensen, maar is ook bij het paard een klinisch probleem. De klachten bestaan uit pijn en bewegingsbeperking, en leiden tot (hoge) kosten voor medische behandeling, bij mensen tot ziekteverzuim en bij paarden tot ongeschiktheid voor het doel waarvoor ze gebruikt worden (verschillende takken van paardensport). Aangezien volwassen kraakbeen weinig herstelvermogen heeft en onbehandeld laten van de defecten kan leiden tot chronische gewrichtsdegeneratie (osteoarthrose), is ingrijpen noodzakelijk. Bestaande therapieën, zoals microfractuur en autologe chondrocyten-transplantatie geven goede resultaten op korte en middellange termijn, maar hebben ook nadelen zoals hoge kosten en onvolledig herstel van het oorspronkelijke weefsel.

Gewrichtskraakbeen, waarvan één van de belangrijkste eigenschappen het schokabsorberende vermogen is, is geen homogeen weefsel maar verschilt in samenstelling en opbouw van de extracellulaire matrix, zowel per locatie in het gewricht als in de diepte. Deze heterogeniteit is waarschijnlijk het gevolg van en in ieder geval het antwoord op lokale verschillen in belastingen en schuifkrachten. Kraakbeen kan worden onderverdeeld in drie zones: de oppervlakkige zone (bovenste 10-20%), de middenlaag (volgende 40-60%), en de diepe zone (de onderste 30-40%). De zones verschillen van elkaar wat betreft celgrootte, -morfologie en -hoeveelheid, en wat betreft de hoeveelheid van glycosaminoglycanen (GAGs), één van de hoofdbestanddelen van de extracellulaire matrix van kraakbeen. Ook qua oriëntatie van de collageenvezels die samen het collageennetwerk vormen dat de glycosaminoglycanen op hun plaats houdt en dat het andere hoofdbestanddeel van de extracellulaire matrix van kraakbeen vormt, zijn er duidelijke verschillen. Ten slotte zijn er nog dieptever verschillen wat betreft de secretie van een aantal eiwitten. Clusterine en proteoglycaan-4 (PRG4) (ook bekend als *superficial zone protein* (SZP)) komen bijvoorbeeld voornamelijk voor in de oppervlakkige laag, terwijl in de middenzone de concentratie van *cartilage intermediate layer protein* (CILP) het hoogst is; *cartilage oligomeric matrix protein* (COMP) wordt vooral gevonden in de midden- en diepe zone.

Onze hypothese was dat het niet volledig herstellen van kraakbeen in de huidige behandelpraktijk gerelateerd is aan het gebrek aan zonale organisatie. In dat geval zal het duidelijk zijn dat, indien men kraakbeenconstructen die met behulp van *tissue engineering* worden gemaakt succesvol wil maken, er rekening moet worden gehouden met de natuurlijke zonale verschillen in kraakbeen.

ZONALE VERSCHILLEN EN DE ROL VAN AANGEBRACHTE ORGANISATIE IN VITRO

In **hoofdstuk 2** wordt aangetoond dat verrijkte celpopulaties van kraakbeencellen (chondrocyten) uit de oppervlakkige, midden- en de diepe zone kunnen worden geoogst. Na vermenigvuldiging en vervolgens redifferentiatie blijken deze celpopulaties van elkaar te verschillen wat betreft het inbouwen van GAGs, in een verhouding die vergelijkbaar is met die in natief kraakbeen. Verder scheiden de celpopulaties zone-specifieke eiwitten uit. Bovenstaande



observaties gelden voor cellen die gekweekt zijn in alginaat hydrogel; wanneer cellen in pellets worden gekweekt worden geen verschillen gezien. Deze bevindingen ondersteunen het gebruiken van (alginaat-) hydrogels voor zonale *tissue engineering* van kraakbeen.

De volgende stap was het onderzoeken van de invloed van het gelaagd combineren van celpopulaties (**hoofdstuk 3**). Pellets van oppervlakkige en diepe zone cellen werden laagsgewijs aangebracht in 3-dimensionale (3D) constructen. Dit resulteerde na enkele weken kweken in kraakbeenachtig weefsel dat rijk was aan GAGs en collageen type II. In geen van de gekweekte constructen werd echter behoud of terugkeer van het zonale fenotype gezien, wel werd waargenomen dat kweken in 3D constructen, vergeleken met pelletkweek, leidde tot een betere incorporatie van GAGs.

BEGRIJ VAN GROEIMECHANISMEN

In **hoofdstuk 4** wordt een wiskundig model beschreven dat inzicht verschaft in de mechanismen van *in vitro* groei. Experimentele gegevens werden vergeleken met voorspellingen op basis van wiskundige simulaties om het model te verfijnen. Hiertoe werden chondrocyten gezaaid op met collageen gecoate filters en tot 7 weken gekweekt. De wiskundige simulatie kwam goed overeen met de experimenteel verkregen cel- en matrixverdeling. De verdeling van GAGs en cellen bleek in hoge mate afhankelijk te zijn van de celdifferentiatiesnelheid. Grote delen van het weefsel bleken niet bij te dragen aan de proliferatie en groei van de lagen. Dit kan betekenen dat het gebruik van een hogere zaaidichtheid van cellen geen significant effect heeft op de groeisnelheid. Het bleek bij dit experiment dus mogelijk met behulp van een relatief eenvoudig wiskundig model de werkelijkheid te voorspellen, hetgeen de interpretatie van het mechanisme van *in vitro* weefselgroei mogelijk maakte. Met deze studie werd zo aangetoond dat *in silico* resultaten kunnen helpen inzicht te verschaffen in onderliggende mechanismen van het gedrag van cellen, en dus mogelijk gebruikt kunnen worden om kweekmethoden te ontwerpen en te ontwikkelen.

DE ONTWIKKELING VAN HET INNOVATIEVE CONCEPT VAN BIOPRINTEN

Bioprinten is een nieuwe, veelbelovende techniek voor het fabriceren van weefselconstructen. Bij deze techniek wordt een driedimensionale structuur gecreëerd die bestaat uit strengen van een –in eerste instantie dik vloeibaar- materiaal (veelal een hydrogel), al dan niet geladen met cellen. De techniek is ook bruikbaar voor het produceren van gelaagde (kraakbeen) constructen, maar dient nog wel te worden geoptimaliseerd voor dit specifieke doel. In **hoofdstuk 5** beschrijven we het *proof of principle* van het 3D printen van meerdere celtypes waarbij alginaat hydrogel als model-biomateriaal werd gebruikt. Multipotente stromale cellen en chondrocyten werden gebruikt om respectievelijk osteogene en chondrogene differentiatie te bewerkstelligen. Het veranderen van de afstand tussen de geprinte strengen en de richtingshoek waarmee deze op de vorige streng werden geprint bleek grote invloed te hebben op de porositeit en de elastische modulus van het construct. De architectuur van het construct en de lokalisering van de cellen bleven gedurende drie weken onveranderd, maar

er trad afzonderlijke en celspecifieke weefselvorming op in de verschillende delen van het construct, zowel *in vitro* als *in vivo*. Deze resultaten tonen aan dat bioprinten geschikt is om levensvatbare weefsels te fabriceren met een voldoende volume, die mogelijk kunnen worden gebruikt voor het herstellen van bot-kraakbeendefecten.

Bioprinten kan dus worden gebruikt om constructen met meerdere celtypes te maken, met specifieke extracellulaire matrixvorming op gespecificeerde plaatsen, maar het proces dient nog op een aantal punten verbeterd te worden. Door de zachte consistentie van het gebruikte biomateriaal, alginaat, kan slechts een construct van beperkte hoogte worden geproduceerd. Om dezelfde reden wordt het uiteindelijke construct mechanisch (te) zwak. Tenslotte, hoewel het gevormde weefsel specifiek was, werd het niet in voldoende mate aangemaakt.

Om te onderzoeken of deze beperkingen van alginaat konden worden ondervangen door het gebruik van thermosensitieve en fotosensitieve hydrogels, werden drie mogelijke biomaterialen getest: hyaluronzuur/hydroxyethyl-methacrylaat-gederivatiseerde dextraan (HA/dex-HEMA), poly(*N*-(2-hydroxy-propyl)methacrylamide-lactaat)-poly(ethyleen-glycol)-poly(*N*-(2-hydroxypropyl) methacryl-amide lactaat) (p(HPMAm-lactaat)-PEG), en gelatine methacrylamide (gelMA) (**hoofdstukken 6-8**). Deze biomaterialen werden getest op mechanische en zwellingeigenschappen, op de mate van overleving van cellen in de gel en op printbaarheid. De mechanische eigenschappen van de drie geteste biomaterialen maakten ze geschikt voor bioprinten; opeenvolgende lagen van gelstrengen konden op elkaar worden geprint. Verder was de biocompatibiliteit goed: de overlevingspercentages van de cellen waren hoog. Het printen van GelMA bleek uitdagend door de lage viscositeit van het materiaal, maar de toevoeging van hyaluronzuur (HA) verbeterde de hanteerbaarheid en de printbaarheid van deze gel aanzienlijk. Bij GelMA werd ook de differentiatie van de geïncorporeerde cellen onderzocht, waarbij kraakbeenachtige weefselvorming werd gevonden. Concluderend zijn alle drie onderzochte materialen geschikt voor bioprinten, maar alle drie zijn het mechanisch zwakke materialen.

Als alternatief voor het gebruik van een mechanisch sterker biomateriaal met een hogere viscositeit (dat vaak minder gunstige eigenschappen voor celoverleving heeft) kan ook de combinatie van een hydrogel met een stijver materiaal, zoals een thermoplastische polymeer, worden gebruikt. In het laatste experimentele hoofdstuk (**hoofdstuk 9**) wordt dit concept beschreven en uitgewerkt: het bioprinten van zogenaamde hybride constructen, vervaardigd door het afwisselend printen van strengen thermoplastische polymeer en hydrogel (met geïncorporeerde cellen). Deze benadering is vooral interessant voor weefsels die hoge mechanische krachten moeten kunnen weerstaan (zoals gewrichtskraakbeen). Omdat de thermoplastische polymeer zorgt voor ondersteuning van de hydrogel, kan voor het printen van hybride constructen een grotere verscheidenheid aan biomaterialen worden gebruikt dan met het printen van alleen hydrogel.

Geconcludeerd kan worden dat bioprinten een uitstekende techniek is om de replicatie van weefselarchitectuur te bewerkstelligen. Hoewel er veel vooruitgang is geboekt, is het wel belangrijk te realiseren dat de bioprint-techniek nog in de kinderschoenen staat. De vertaalslag van de *in vitro* resultaten naar uitgebreide *in vivo* studies in grote diermodellen, laat staan naar humane (of veterinaire) klinische toepassingen, moet nog worden gemaakt.





DANKWOORD

“The length of this document defends it well against the risk of being read”
Winston Churchill

En dan nu het gedeelte dat wel door iedereen wordt gelezen; dit proefschrift had niet tot stand kunnen komen zonder de inspanning, de invloed of de opvoeding van en door de onderstaande personen, aan wie ik bij deze mijn dank wil betuigen.

Prof. dr. van Weeren, beste René, met je brommende stemgeluid en met groot gevoel voor *common sense* wist je altijd de onderzoekszaken weer in hun perspectief te plaatsen. Af en toe moest ik even een paar seconden wachten voor ik verstond wat je had gezegd. Ik heb me zeer gewaardeerd en gesteund gevoeld door je de afgelopen jaren.

Prof. dr. Dhert, beste Wouter, of ook wel “grote” Wouter, ook door jou heb ik me zeer gesteund gevoeld, als je tijdens een bespreking weer eens aanvoerde dat ik toch écht hele leuke data had geproduceerd, écht aan een mooi proefschrift aan het werken was, en dat ik niet zo bescheiden hoefde te doen. Dank daarvoor.

Dr. ir. Malda, beste Jos, jij bent de motor achter dit proefschrift, de aanjager, de stok achter de deur. Je had altijd tijd om even de nieuwste resultaten door te nemen, nieuwe plannen te smeden of te brainstormen. Ik heb wel eens het idee dat jij meer ideeën hebt dan 30 promovendi kunnen uitvoeren. Ik heb in elk geval waanzinnig veel van je geleerd, en ik had geen betere begeleider kunnen wensen.

Dokter Willems, beste Jaap, eigenlijk begon mijn traject in het OLVG, waar ik onderzoek deed en coschappen liep. Onder andere door jouw aanbeveling kon ik in Utrecht aan de slag. Veel dank.

Dokter Smit, ek is baie bang my afrikaans laat te wense oor, maar ek wil dit tog probeer. Ek dink dokters het voorbeelde nodig, en dat ben jij seker vir my gewees in daardie half jaar in Suid-Afrika. Baie dankie.

En dan mijn paranimfen: Mattie en Kim. Ik ben er trots op dat jullie straks naast me staan tijdens mijn verdediging. Mattie, spil van het lab, welkomstcomité voor nieuwe studenten/promovendi/bezoekers, vraagbaak. Je hebt er vanaf het begin voor gezorgd dat ik me welkom voelde op het lab. Borrels, feesten, skiën en heel, heel, heel veel koffie drinken. Ik vind je een held.

En Kim, als student bij Jos kwam je het lab binnenwaaien, niet wetende dat er al een pad voor je was uitgestippeld in het UMC met een korte tussenstop in Brisbane. Je hebt het “zingen” op het lab tot kunst verheven. Over DMMB’s en studenten en bazen en wat niet. “Je bent een heel sterke vrouw”.

Laura en Daan, als bazen van de kraakbeengroep hebben jullie wat meer op de achtergrond bijgedragen aan dit proefschrift, maar ik heb veel van jullie mogen leren.

De collega’s van het UMC: Anika, Anneloes, Debby, Fiona, Henk-Jan, Hsiao Yin, Jacqueline, Jetze, Joost, Joris, Loek, Lucienne, Marijn, Michelle, Michiel en Michiel, Natalja, Rhandy, Ruth, Ruud, Tom, Tommy, Yvonne. Dank voor de fijne samenwerking, in het UMC en daarbuiten, en de mooie avonturen die we hebben beleefd.

De collega’s van het departement paard: room mates Esmée, Annemiek, (tijdelijk) Gerald, Jennifer, en verder Stefan, Janny en Everaldo. Dank voor het mogen zeuren, uitrazen, motorrijden, roddelen en borrelen.

Mijn studenten, soms nagel aan mijn doods-kist en redder in nood tegelijkertijd of in heel kort tijdsbestek, dank voor jullie inzet en werk: Werner, Petra, Hans, Eko, Vladimir, Michiel.

Dank voor de vruchtbare samenwerking aan de collega’s van de afdeling farmacie van de Universiteit Utrecht: Roberta en Laura, Tina, professor Wim Hennink.



De Grunneger dokters: Anina, Jet, Karin, Marijn, Remco, René, Tineke. Mogen we tot in lengte der dagen op onregelmatige basis met elkaar afspreken.

Ivo, oude vriend, ik vind het mooi dat we in Utrecht de draad van onze vriendschap weer hebben opgepakt en dat het eigenlijk voelt alsof het nooit anders is geweest.

Capreoli, Jan Jaap en Berend, de avonden in Loetje zijn me zeer dierbaar en vervelen nooit, ik hoop dat we dat nog lang zullen blijven doen.

Berend en Kicky, het was een geweldige eer om voor jullie ceremoniemeester te zijn. De rest heb ik toen al gezegd.

Dispuut Despinoza (en in het bijzonder de Utrechtenaren: Chris, Paul, Rutger, Sebas en Siebren): dispuutslid ben je voor het leven en dat blijkt: fietsen, oud en nieuw, koninginnedag of dispuutsweekend, Groningen, Tunesië of Alpe d'Huez, klussen of biertjes drinken, ik weet jullie te vinden en jullie mij.

Mijn lieve schoonfamilie, Kati en Janos, ik weet dat jullie trots op me zijn als was ik jullie eigen zoon. Juli en Jan, Dani en Mirjam, en kleine Benjamin. Jullie zijn met recht mijn tweede familie.

Lieve Toon, oom en onderdakverschaffer, doordat ik welkom was bij jou in Amsterdam heeft het hele proces van onderzoek en coschap orthopedie, en vervolgens de promotie zich in gang kunnen zetten vanaf juni 2007. Je bent heel belangrijk voor me.

Mijn ouders, mijn zusjes Crystal en Janneke, mijn broer Mattijs en zijn vriendin Lotte. Dank voor jullie steun, interesse en hulp de afgelopen jaren. Ik houd waanzinnig veel van jullie.

Mijn aller-allerliefste, -leukste, -mooiste, -grappigste, overal ergens altijd ooit. Anna, je bent er vanaf (bijna) het begin bij geweest, en hebt me altijd gesteund, moed ingesproken, en af en toe een flinke duw in de goede richting gegeven. Jij helpt me het beste uit mezelf te halen en me te blijven ontwikkelen, elke dag. Lieve Panka, ik hoop dat je voor altijd bij me blijft, ik blijf in ieder geval wel bij jou. Ik houd van je.

&

DANKWOORD



CURRICULUM VITAE
AND LIST OF PUBLICATIONS



The author of this thesis was born in the Hague, the Netherlands, on the 20th of September 1979. He graduated from high school (gymnasium, Haags Montessori Lyceum, the Hague) in 1997 and started studying Movement Sciences in 1999, and medicine in 2000 at the University of Groningen. In 2007, the author performed an elective internship in Pelonomi Hospital, Bloemfontein, South Africa, under supervision of dr. Kobus Smit. The author did his final internship at the Department of Orthopaedic Surgery in the Onze Lieve Vrouwe Gasthuis in Amsterdam (head: dr. Jaap Willems). At the end of 2007, he received his medical degree, and in March 2008, he started working as a Ph. D. candidate at the Department of Orthopaedics of the UMC Utrecht and the Department of Equine Sciences of the Faculty of Veterinary Science, Utrecht University. The research was performed under supervision of prof. dr. René van Weeren, prof. dr. Wouter Dhert, and dr. ir. Jos Malda. The research resulted in several publications, a number of presentations at international conferences, and this thesis. Currently, the author works as a non-training resident in Oudshoorn long stay hospital in Alphen aan de Rijn.

Wouter Schuurman lives with Anna Sarbo in Utrecht.



LIST OF PUBLICATIONS

This thesis was based on the following publications

W. Schuurman, D. Gawlitta, T.J. Klein, W. ten Hoop, M.H.P van Rijen, W.J.A. Dhert, P.R. van Weeren, and J. Malda
Zonal Chondrocyte Subpopulations Reacquire Zone-specific Characteristics During *in vitro* Redifferentiation.

American Journal of Sports Medicine 2009

W. Schuurman, E.B. Harimulyo, D. Gawlitta, T.B.F. Woodfield, W.J.A. Dhert, P.R. van Weeren, and J. Malda

Zonal Assembly of Chondrocyte Pellets in Tissue Engineered Constructs Results in Cartilaginous Tissue Formation without Retainment of Zonal Characteristics

Submitted for publication

C.J. Catt, **W. Schuurman**, B. Sengers, C.P. Please, W.J.A. Dhert and J. Malda

Mathematical modelling of tissue formation in chondrocyte filter cultures.

European Cells and Materials 2011.

W. Schuurman, N.E. Fedorovich, H.M. Wijnberg, H.J. Prins, P.R. van Weeren, J. Malda, J. Alblas, W.J.A. Dhert.

Biofabrication of Osteochondral Tissue Equivalents by Printing Topologically Defined, Cell-laden Hydrogel Scaffolds

Tissue Engineering part C 2012

L. Pescosolido, **W. Schuurman**, J. Malda, P. Matricardi, F. Alhaique, T. Coviello,

P.R. van Weeren, W.J.A. Dhert, W.E. Hennink, T. Vermonden.

Hyaluronic Acid and Dextran-Based Semi-IPN Hydrogels as Biomaterials for Bioprinting

Biomacromolecules 2011

R. Censi, **W. Schuurman**, J. Malda, G. di Dato, P.E. Burgisser, W.J.A. Dhert, C.F. van Nostrum,

P. di Martino, T. Vermonden, W.E. Hennink.

Printable Photopolymerizable Thermosensitive p(HPMA-lactate)-PEG Hydrogel as Scaffold for Tissue Engineering

Advanced functional materials 2011

W. Schuurman, P. Levett, M.W. Pot, P.R. van Weeren, W.J.A. Dhert, D.M. Hutmacher,

F. Melchels, T.J. Klein, and J. Malda,

Thermoresponsive Gelatin-Methacrylamide Hydrogels for Bioprinting of Cartilaginous Tissue

Engineering Constructs

W. Schuurman, V. Khristov, M.W. Pot, P.R. van Weeren, W.J.A. Dhert, and J. Malda.

Bioprinting of Hybrid Tissue Constructs with Tailorable Mechanical Properties.

Biofabrication 2011

W. Schuurman, T.J. Klein, W.J.A. Dhert, P.R. van Weeren, D.W. Hutmacher, and J. Malda

Cartilage regeneration using zonal chondrocyte subpopulations: a promising approach or an overcomplicated strategy?

Submitted for publication



SELECTED ABSTRACTS

W. Schuurman, W. ten Hoope, D. Gawlitta, P.R. van Weeren, W.J.A. Dhert and J. Malda.
Zonal Differences In Equine Chondrocytes In Vitro.

International Cartilage Research Society Conference 2009

W. Schuurman, N.E. Fedorovich, J. Malda, P.R. van Weeren, J. Alblas, W.J.A. Dhert.
3D-Fiber Deposition Of Cell-Laden Hydrogels To Construct Viable Osteochondral Grafts.

International Conference on Biofabrication 2009

W. Schuurman, N.E. Fedorovich, J. Malda, P.R. van Weeren, J. Alblas, W.J.A. Dhert.
3D-Printing of Cells In Gels: A New Concept For Constructing Osteochondral Grafts.

International Cartilage Research Society Conference 2010

C.J. Catt, **W. Schuurman**, B. Sengers, C.P. Please, W.J.A. Dhert and J. Malda.
Modelling Of Tissue Formation In Chondrocyte Filter Cultures.

International Cartilage Research Society Conference 2010

W. Schuurman, N.E. Fedorovich, J. Malda, P.R. van Weeren, J. Alblas, W.J.A. Dhert.
3D Fiber Deposition Of Cell-Laden Hydrogel To Form Heterogeneous Grafts In Vivo.

International Conference on Biofabrication 2010

OTHER PUBLICATIONS

W. Schuurman, W.J. Willems

Lateral ankle reconstruction using a patellar tendon graft: a case report.

Journal of Foot and Ankle Surgery 2009

T.J. Klein, S.C. Rizzi, J.C. Reichert, N. Georgi, J. Malda, **W. Schuurman**, R.W. Crawford,
D. W. Hutmacher.

Strategies for zonal cartilage repair using hydrogels.

Macromolecular Bioscience 2009

J. Malda, W. ten Hoope, **W. Schuurman**, G.J. van Osch, P.R. van Weeren, W.J.A. Dhert.
Localization of the potential zonal marker clusterin in native cartilage and in tissue-
engineered constructs.

Tissue Engineering part A 2010

H. Seyednejad, W. Ji, **W. Schuurman**, W.J.A. Dhert, J. Malda, F. Yang, J.A. Jansen,
C. van Nostrum, T. Vermonden, W.E. Hennink.

An electrospun degradable scaffold based on a novel hydrophilic polyester for tissue-
engineering applications.

Macromolecular Bioscience 2011



